APPLICATION OF ADAPTIVE EQUALISATION TO MICROWAVE DIGITAL RADIO

Michael C.S. Young

A thesis submitted for the degree
of Doctor of Philosophy to the
Faculty of Science,
University of Edinburgh.

April 1989

ABSTRACT

Fading due to multipath propagation remains one of the principle sources of signal loss or outage in microwave digital radio communications, introducing amplitude and phase distortion to the received signal. This thesis examines a number of adaptive equalisation techniques with the aim of reducing degradation due to fading. The chapters may be categorised into an examination of system performance, followed by details of practical equaliser implementation.

The requirement for bandwidth efficient modulation techniques has placed greater demands on the equalisation process, and more advanced structures are continually required. Two main types of adaptive equaliser are considered, linear transversal equalisers and nonlinear decision feedback equalisers. Linear equalisers are currently available in certain commercial digital radio systems, however results in chapter 3 indicate that during severe fading conditions, linear equalisation provides insufficient compensation, and system outage is likely. A number of suggestions are made for enhancing equaliser performance during deep fading.

Decision feedback equalisers offer considerable performance gain over linear equalisers, and one configuration is shown to have the capability of maintaining performance through a phase transition. Transitions between different phase types remain one of the fundamental problems for reliable microwave communications. To ensure a stable timing phase, a novel receiver structure is proposed, whereby timing information is obtained from an estimate of the received channel impulse response. The proposed structure is shown to be capable of dealing with the most severe fading conditions described by the simplified three-path channel model.

Equaliser implementation is the second main area of research. Recognising the relatively straightforward implementation of linear equaliser designs, results are presented for this structure. Similar techniques and analysis may be applied to other equaliser types. The least mean squares (LMS) algorithm is commonly used to adaptively update the equaliser tap weights, while the slightly less complex zero-forcing (ZF) algorithm has found favour for certain high speed designs. Chapter 5 provides a comparative study of various adaptive algorithms suitable for high speed implementation, including block least mean squares (BLMS) algorithms. The BLMS algorithm is shown to be a practical alternative when arithmetic resolution is limited by high speed digital operation. Finally, a novel 'off-line' adaptation technique is proposed where adaptation is performed by a digital signal processor. Results are presented from the implemented system.

ACKNOWLEDGEMENTS

The help, guidance and encouragement from my superviser, Professor P.M. Grant, is gratefully acknowledged. The contribution provided by Dr. C.F.N. Cowan is also acknowledged, both for his supervision during the first year of the project and for technical assistance on numerous occasions. Within the University, numerous individuals contributed to an enjoyable and productive three years, however Dr. B. Mulgrew and Dr. K. Manning merit special thanks for their technical expertise and help.

The funding of the Science and Engineering Research Council and Ferranti Industrial Electronics, Dalkeith, provided financial support for the project. I would like to thank Mr. H. Bell and Mr. M. Salvesen from Ferranti for their assistance and backing.

On a personal note, the support provided by my Parents and Rona cannot be underestimated, and this volume is dedicated to them.

Many thanks.

GLOSSARY

ABREVIATIONS

ADC	Analogue-to-Digital Converter
AGC	Automatic Gain Control
ALC	Automatic Level Control
AM	Amplitude Modulation
ARQ	Automatic Request Transmission
ASK	Amplitude Shift Keying
BBD	Bucket Brigade Device
BECM	Band Edge Component Maximisation
BER	Bit Error Rate
BLMS	Block Least Mean Squares (Algorithm)
BPF	Band Pass Filter
BT	British Telecom
CBLMS	Clipped Block Least Mean Squares (Algorithm)
CCD	Charge Coupled Device
CCIR	International Radio Consultative Committee
CCIT	International Telegraph Consultative Committee
CCITT	International Telegraph and Telephone Consultative Committee
CEPT	Conference of European Post and Telecommunication Administration
CLMS	Clipped Least Mean Squares (Algorithm)
CMOS	Complimentary Metal-Oxide Silicon (Transistor)
CNR	Carrier-to-Noise Ratio
DAC	Digital-to-Analogue Converter
DFE	Decision Feedback Equaliser
DPCM	Differential Pulse Code Moulation
DPLL	Digital Phase Locked Loop
DSP	Digital Signal Processor
ECC	Error Correcting Coding
ECL	Emitter Coupled Logic
EPROM	Erasable Programmable Read Only Mememory
FCC	Federal Communications Commission
FEC	Forward Error Correction

FM	Frequency Modulation
FDFE	Fractionally Spaced Decision Feedback Equaliser
FIR	Finite Impulse Response
FSE	Fractionally Spaced Equaliser
FSK	Frequency Shift Keying
FTE	Fractionally Spaced Transversal Equaliser
GaAS	Gallium Arsenide
HF	High Frequency
I/Q	In-phase/Quadrature Channels
IC	Integrated Circuit
IF	Intermediate Frequency
IIR	Infinite Impulse Response
ISI	Intersymbol Interference
ITU	International Telegraph Union
LMS	Least Mean Squares
LOS	Line-of-Sight
LPF	Low Pass Filter
LSB	Least Significant Bit
LSI	Large Scale Integration
MDAC	Multiplying Digital-to-Analogue Converter
MEO	Maximum Eye Opening
ML	Maximum Likelihood
MLSE	Maximum Likelihood Sequence Estimation
MMSE	Minimum Mean Square Error
MP	Minimum Phase
M-QAM	Multilevel Quadrature Amplitude Modulation
MSB	Most Significant Bit
MSE	Mean Square Error
NMP	Nonminimum Phase
PA	Power Amplifier
PAM	Pulse Amplitude Modulation
PCB	Printed Circuit Board
PCM	Pulse Code Modulation
PLA	Programmable Logic Array
PLL	Phase Locked Loop
PRBS	Pseudorandom Bit Sequence
PROM	Programmable Read Only Memory
QAM	Quadrature Amplitude Modulation

QPRS	Quadrature Partial Response Signalling
QPSK	Quaternary Phase Shift Keying
RAM	Random Access Memory
RBQPSK	Reduced Bandwidth QPSK
RF	Radio Frequency
RLS	Recursive Least Squares
RSL	Received Signal Level
RTP	Reference Tap Position
SAW	Surface Acoustic Wave
SNR	Signal-to-Noise Ratio
TE	Transversal Equaliser
TLA	Tap Leakage Algorithm
TTL	Transistor-Transistor Logic
VA	Viterbi Algorithm
VCC	Voltage Controlled Clock
VCO	Voltage Controlled Oscillator
VLSI	Very Large Scale Integration
XPD	Cross Polarisation Discrimination
ZF	Zero Forcing
μP	Microprocessor

PRINCIPAL SYMBOLS

a	Flat fade term in Rummler channel model
a_k, b_k	In-phase and quadrature data streams
$A_{\max}$	Flat fade margin
$B_{\max}$	Relative notch depth
b	Relative amplitude term in Rummler channel model
$\underline{b}(k)$	Backward DFE tap vector
$\underline{b}_{opt}(k)$	Optimum backward DFE tap vector
B	Bit length
$B(f)$	Backward filter response
B_C	Bit length for coefficient storage
$\underline{c}(k)$	Transversal equaliser tap vector
$\underline{c}_{opt}(k)$	Optimum transversal equaliser tap vector
$C(f)$	Forward filter response
$C_{opt}^*(f)$	Causal matched filter response
d	Delay through equaliser

D_{max}	Peak distortion
$e(k)$	Error sequence
f	Frequency
f_c	Carrier frequency
f_n	Highest frequency present in a signal
f_s	Sampling frequency
f_0	Notch offset frequency in Rummler channel model
$f(\tau_k)$	Timing phase function
$\underline{h}(k)$	General sampled channel response vector
$\underline{\hat{h}}(k)$	Estimated impulse response vector
$h_C(t)$	Channel impulse response
$h_N(t)$	Convolved response of transmit/receive filters and channel
$h_R(t)$	Receiver filter impulse response
$h_T(t)$	Transmitter filter impulse response
$hi(k)$	Imaginary sampled impulse response (estimated)
$hr(k)$	Real sampled impulse response (estimated)
$H_C(f)$	Multipath model transfer function
i	Equaliser coefficient index
I	Bit sequence length
$\underline{I}(k)$	Identity matrix
j	Square root of -1
J	Message length
k	Discrete vector time
K	Number of feedback taps in a DFE
l	Sampling factor
L	Block length
m	Sampling factor
M	Number of symbol states
n	Time index
$n(t)$	Gaussian noise
N	Number of forward taps in a transversal equaliser
N_0	Noise power
$P(\epsilon)$	Probablity of a symbol error
P_{ave}	Average power in an M-QAM constellation
$q(k)$	Convolved response of equaliser and $h_N(k)$
$S_N(f)$	Received signal power spectrum
t	Time
T	Symbol period

$U(k,\tau_k)$	Timing phase detection function
$x(t)$	Received data signal
$x'(t)$	Passband received data signal
$\ddot{x}(t)$	Received data signal in absence of fading
$x(k)$	Sampled received data signal
$\underline{x}(k)$	Received data vector
$X(k)$	Time varying process
$y(k)$	Decision device output
$\hat{y}(k)$	Equaliser output
$Z^{-\delta}$	Delay line of length δ
$\beta(k,B_{\max})$	Variable timing constant
γ	Decay factor
δ	Delay
$\delta(t)$	Delta dirac impulse response
$\underline{\epsilon}$	Coefficient error vector
θ_k	Carrier phase
$\hat{\theta}_k$	Estimated carrier phase
μ	LMS convergence factor
μ_L	BLMS convergence factor
ξ	Mean square error
ξ_{opt}	Optimum mean square error
ξ_{Total}	Total complex mean square error
σ_s	SNR
σ_x^2	Input signal variance
τ_k	Timing phase
$\hat{\tau}_k$	Estimated timing phase
υ	LSB amplitude
$\underline{\phi}_{xx}$	Autocorrelation matrix
$\underline{\phi}_{xy}$	Crosscorrelation vector
Δ	Increment
$\Delta(k)$	Increment of a time varying process
∇	Gradient of MSE cost function

OPERATORS

$E[.]$	Statistical expectation operator
z^{-1}	Unit sample delay
Σ	Summation
$\hat{\cdot}$	Denotes an estimate

VECTORS, MATRICES AND NOTATION

The adopted index notation is k for sampled data sequences and vectors/matrices, and t for analogue waveforms e.g. the received data signal may be described by $x(t)$, $x(k)$ or $\underline{x}(k)$.

All vectors are specified as column vectors. The transpose operation is denoted by the superscript T.

CONTENTS

Chapter 1

INTRODUCTION

1.1 MICROWAVE DIGITAL RADIO

Most countries have extensive microwave line-of-sight (LOS) radio systems as part of public and private communications networks, carrying data, television and up to 6000 telephone channels per carrier [1]. Microwave radio systems, in analogue form, have been deployed since the 1930's. Only in the past few years has digital technology proliferated, prompted by a number of factors and advantages, including the growth of data communications, advances in digital switching and terminal design, and importantly, economic reasons. It is interesting to note that historically digital radio is not a new communications application. Marconi's early work on radio telegraphy transmitted an on-off keyed 'binary' signal. Although means of increasing the transmission rate were developed, by the 1920's emphasis had shifted from 'digital' telegraphy to 'analogue' telephony [2].

Certain other advantages are inherent with digital radio systems notably that noise accumulation becomes an isolated problem between points of regeneration. Furthermore, network control and monitoring of great complexity are possible, in step with the development of all digital networks. Recognising the rise of the digital system, the relative efficiency should be highlighted. A nominal 3.2 kHz voice channel would occupy about 4 kHz bandwidth on an analogue radio link. In contrast, a conventional PCM baseband system allowing a bit/Hz efficiency and an 8 bit word, roughly requires 32 kHz of bandwidth [3]. This example illustrates the relative inefficiency of digital transmission and the requirement for spectrally efficient techniques.

Given that RF bandwidth is at a premium and that high-capacity digital microwave radio operates over a large bandwidth, digital radio design and planning requires spectrally efficient techniques for practical reasons, and often to satisfy regulatory conditions and agreements. The recommendations of the International Telegraph Union (ITU) have dominated bandwidth allocation and international standardisation. Commonly encountered in digital radio literature are recommendations from the CCIR and CCITT divisions of the ITU, covering technical/operating problems and standardisation, respectively. Within individual countries, other advisory and regulatory bodies exist e.g. the Conference of European Posts and Telecommunications (CEPT) in Europe and the Federal Communications Commission (FCC) in the USA.

Microwave radio systems currently supply around half the total transmission capacity in North America, Europe and Japan. Developing countries also have a 'backbone' network comprising of microwave radio relay links e.g. Indonesia, Central America and the PANAFTEL network in Africa. Often such networks are supplemented by satellite links for isolated areas. Optical fibre technology may be viewed as both competitor and compliment to microwave systems, due to their diverse characteristics and traffic handling capabilities. Over long-haul routes, requiring isolated repeaters, microwave digital radio systems would be unable to compete with fiber optic systems, however there are a number of strategic advantages. Where no infra-structure exists, digital radio systems offer flexible and rapid provision of service. Secondly, over rough terrain, fiber optic installation may be impractical. European digital radio systems were optimised mainly for national requirements and a number of incompatible systems evolved [4]. Under CEPT guidance, system designs are gradually converging to common operating standards. In Britain, the microwave network carries about one fifth of the total trunk traffic. British Telecom's (BT) network is extensive and varied, operating in the 2,4,6,11,19 and 24 GHz bands. BT's initially largely analogue network is gradually converting to digital, while Mercury, the Cable and Wireless subsidiary, adopted digital technology from it's onset [5].

Interest in spectrally efficient techniques has generally focussed on high level modulation. Modulation is discussed in chapter 2; at present it is sufficient to say that while practical spectral efficiencies of 4.5 bits/Hz are possible, the higher the modulation format, the greater the sensitivity to equipment imperfection and the greater the design difficulty. Dual-polarisation schemes are another technique, offering a potential doubling of spectral efficiency by transmitting two uncorrelated signals with vertical and horizontal polarisation [6]. Some technical problems remain unsolved with dual-polarisation and the system is not in widespread use, although

some countries are committed to it's use[4].

The dominating cause of outage conditions at the receiver is due to atmospheric anomalities i.e. multipath fading. This accounts for some 30% [7] of outage. High level modulation also reduces noise margins (and hence signal robustness), increasing demands on synchronisation and detection performance. Analogue FM systems are inherently less sensitive to multipath fading than their digital counterparts [3] and the transfer from analogue to digital technology has brought renewed interest in compensating for multipath fading, and prompted investigation into the use of adaptive equalisers to minimise multipath effects. A number of other technical problems arise, generally outwith the bounds of this work and are primarily due to system imperfections and nonlinearities, particularly at the transmitter power amplifier (PA). Considerable design effort has gone into allowing the PA to operate optimally without saturating [8].

1.2 MULTIPATH FADING

The examination of propagation effects on microwave LOS links began in the 1950's with studies on FM systems. While much early work focussed on multipath phenomena, the subject area encountered a rapid growth of interest with the introduction of digital radio systems. Digital radios are inherently sensitive to aspects of channel distortion having little effect on analogue FM systems, and considerable advances were required in the understanding of the multipath phenomena. A number of models have been proposed relating multipath occurrence and duration to physical (e.g. geographical and climatic) conditions [9, 10]. Such ideas have been extended to a mapping of the geographical distribution of multipath fading, for optimum radio system design and planning [11]. Studies on digital radio systems have led to the development of a number of models characterising the multipath fading channel [12]. In 1978, a system 'signature' [13] was proposed, based on system measurements, and is now widely used in assessing equipment performance during fading. In chapter 2 it is shown how the channel may be modelled for simulation purposes.

During many propagation conditions, the loss in signal power due to atmospheric conditions is flat across the entire radio channel bandwidth e.g. loss due to extreme rainfall rate [14]. An FM signal contains most of it's energy at the carrier frequency, and it's information is redundantly coded in it's sidebands. A spectrally efficient digital radio does not have any redundant sideband information and consequently the selective loss of frequency components can adversely effect the detection process at the receiver. When the signal loss imposed by the atmosphere

varies across the channel bandwidth, the channel is said to be experiencing frequency selective fading. Time variations of the channel response are generally much slower than the dynamic response of the radio. This is important, firstly because any circuit function employing feedback may suffer hysteresis effects. Secondly, the multipath fading channel may be considered to be wide-sense stationary for estimation theory applications.

Under normal (propagation) conditions, the decrease in atmospheric refractive index with height imparts a downward curve to the direction of the propagation path (figure 1.2.1).

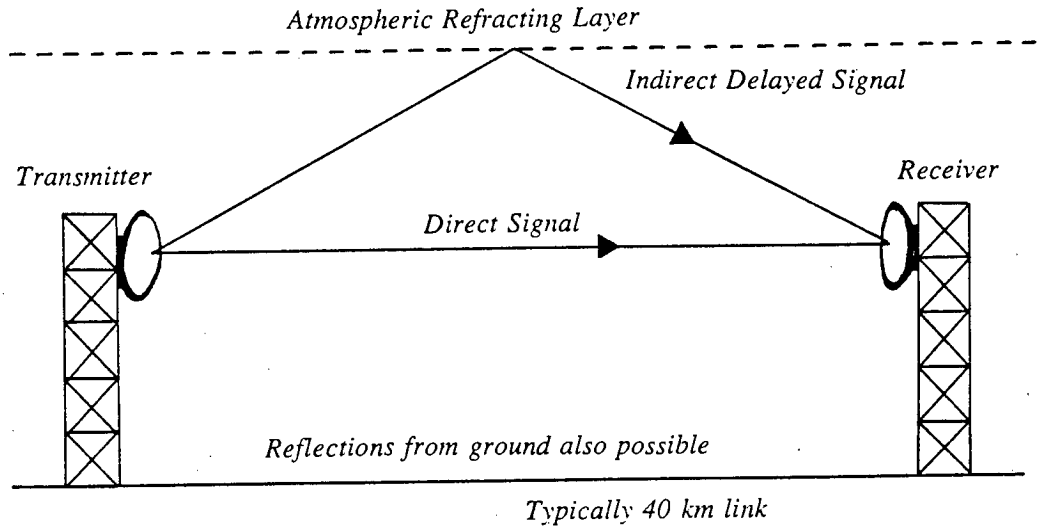

Figure 1.2.1 Simple Multipath Model

For a large fraction of time, propagation conditions are ideal, allowing essentially error free transmission in a high signal-to-noise ratio (SNR) environment. However, at other times certain atmospheric conditions induce atmospheric layering of different refractive indices in the propagation path [15]. Layering most commonly occurs during the summer months, particularly in the hot, humid conditions of temperate climates. In such a layered atmosphere, energy normally radiated into space may be refracted down to the receiving antenna by other paths, and a weighted sum of time shifted replicas of the transmitted signal is captured by the receiving antenna. Ground or sea [16] reflections may also arrive at the receiver, either separately or in combination with refractive paths.

Frequency selective multipath fading results in a reduction (attenuation) in the received signal power or amplitude distortion, around a given frequency. This attenuating factor in the power transfer function is known as the fade depth. Associated with amplitude distortion is group delay. A multipath fading channel with a positive group delay is generally said to be a minimum phase (MP) fade type. Conversely, a channel with a negative group delay is of non-minimum phase (NMP) type.

The most widely used methods for multipath compensation fall into the general categories of diversity and equalisation. Diversity techniques are based on introducing redundancy, whereby if a signal is received over different paths, the probability of all signal components fading simultaneously is reduced. Spectral efficiency requirements generally limit the use of frequency, however analogue systems often include a 'stand-by' channel [7]. Space diversity requires the vertical separation of two receive antenna. Typically this separation may be 10m, and while considerable performance improvements are possible [17], the installation of such a system may add considerably to the overall system cost.

Equaliser techniques may be sub-divided into amplitude and adaptive time-domain equalisation. Amplitude equalisers, unless coupled with space diversity [18], give only limited performance improvement and cannot compensate for group delay distortion. Often referred to as frequency domain equalisers, amplitude equalisers are generally implemented with analogue technology at IF. Adaptive time domain equalisers provide a solution to the overall compensation of amplitude and group delay. Time domain equalisation is the principle research topic in this thesis, and subsequent chapters will cover linear and non-linear structures and practical implementation. In the next section, adaptive equalisation is considered as an application of adaptive filtering.

1.3 ADAPTIVE FILTERING AND EQUALISATION

A linear discrete time filter operates such that the device output, $y(k)$, is a linear function of the input signal, $x(k)$. From a statistical approach, an optimum filter design may be obtained from minimisation of a given cost function. Wiener filter theory [19] provides an optimum design in a minimum mean-square error (MMSE) sense, in a known environment. Wiener filter theory is applicable to a stationary (non time-varying) environment. In nonstationary (time-varying) conditions, Kalman filter theory [20], optimal in a minimum variance sense, may be applicable. In an unknown or poorly defined environment, optimal filters cannot be designed and the use of

adaptive techniques may be required.

An adaptive filter may be thought of as 'self designing', operating satisfactorily where full knowledge of signal statistics is unknown, through the use of a recursive (adaptive) algorithm. The adaptive filter impulse response is changed as more information becomes available such that the filter output approximates the optimum filter output. Thus an adaptive filter is a time varying filter, whose impulse response is dependant on known signal statistics and the adaptive filter algorithm.

The adaptive filter response is adjusted to minimise a given cost function. In addition to an estimate of the input signal statistics, a secondary signal source (known also as the conditioning input or training sequence) is required to define the cost function. Adaptive filtering structures may be generalised into system modelling and prediction [21], illustrated by the three main operating configurations in figure 1.3.1. For a given input configuration, the adaptive filter may perform either linear prediction (figure 1.3.1(a)),direct system modelling (figure 1.3.1(b)) or inverse system modelling (figure 1.3.1(c)).

Linear prediction is the basic structure used in linear predictive coding of speech [22]. The input to the filter is a delayed version of the desired filter output i.e. the filter is required to predict future values. This is possible only if the input is sufficiently coloured, and the filter will acquire similar spectral characteristics [21].

In both cases of modelling, a spectrally white signal is connected directly to the adaptive filter input and indirectly through a system with impulse response $h(k)$. When configured for direct system modelling, the optimum adaptive filter impulse response is a direct model of the (unknown) system response $h(k)$. Applications of direct modelling (also known as system identification) may be found in interference cancellation e.g. echo and noise cancellation, fetal heartbeat monitoring [23].

The third configuration is inverse system modelling (or deconvolution), where the optimum filter response is the inverse of an unknown linearly distorted system. Adaptive equalisation of intersymbol interference in a digital communications channel is a classical example of inverse system modelling. An adaptive equaliser attempts to reconstruct the transmitted sequence prior to a final decision at the receiver output. The first truly adaptive equaliser is credited to Lucky [24], and used peak distortion (related to interference between adjacent symbols) as the cost function for minimisation.

Equalisation techniques form the basis of this work on reducing multipath induced degradation. Chapter 2 introduces equalisation techniques, while subsequent chapters examine equaliser performance, implementation and adaptive algorithms.

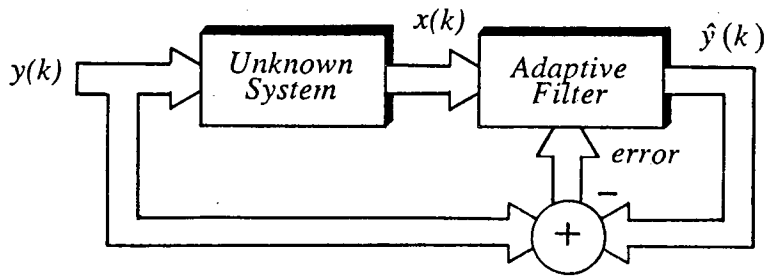

(a) Direct System Modeliing

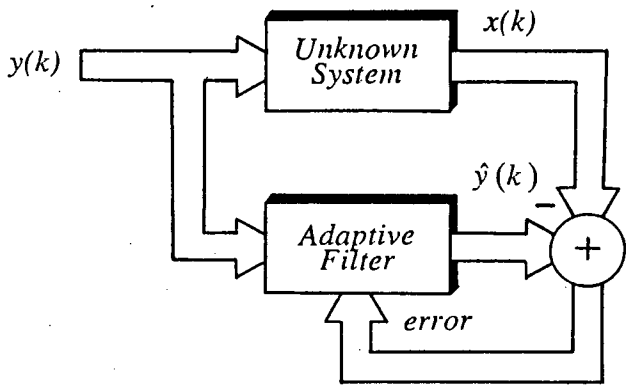

(b) Indirect System Modeliing

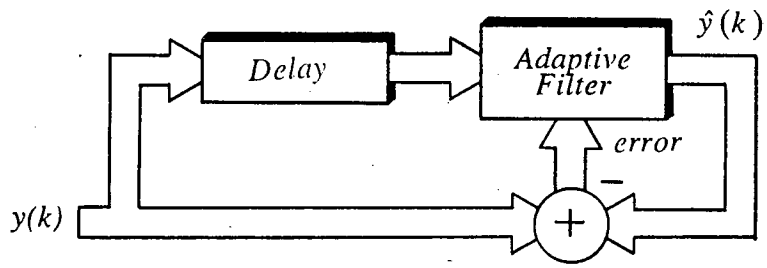

(c) Prediction

Figure 1.3.1 Adaptive Filter Operation

1.4 THESIS OUTLINE

The objective of this thesis is to examine the application of adaptive equalisation to microwave digital radio. Chapters 2 to 5 cover the relevant design aspects of adaptive equalisers, together with simulation and practical hardware results. Chapters 1 and 6 place this work within the context of current advances in microwave digital radio.

This introductory chapter provides an overview of microwave radio systems. Multipath fading is introduced as one of the main sources of degradation to reliable data transmission. Multipath fading is also slowly time varying in nature, therefore any countermeasures must be able to adapt to the current channel conditions. Frequency-domain adaptive equalisation offers limited performance improvement. Considerably superior performance may be obtained with adaptive time-domain equalisers.

Chapter 2 provides an introduction to equalisation techniques applied in later chapters. Important design issues related to microwave digital radio are also covered, notably with regard to modulation and synchronisation. Advances in higher level modulation, invariably place greater demands on compensation measures at the receiver. Means of modelling the channel during fading are also reviewed.

Chapters 3 and 4 examine linear and decision feedback equalisation. Emphasis is placed on maintaining the equaliser in lock during severe fading conditions, so reducing retraining requirements and associated hysteresis problems. A novel receiver structure is presented in chapter 4, based on channel equalisation and estimation techniques.

Results in chapters 3 and 4 were obtained with floating point arithmetic. Chapter 5 examines the effects of limited arithmetic precision on practical equaliser implementation. The equaliser adaptation process requires considerably longer word lengths for tap storage and calculation, so a considerable part of the chapter is devoted to implementation of adaptive algorithms. A comprehensive summary of algorithms is presented, and new conclusions are reached with regard to the viability of the BLMS algorithm for high speed implementation. Finally in chapter 5, a novel means of 'off-line' adaptation with a DSP is presented.

Chapter 6 closes with an overview of the new results presented in earlier chapters. This work is viewed with regard to future developments in microwave digital radio. Suggestions for further research work are then proposed.

Chapter 2

DIGITAL RECEIVER DESIGN

This chapter is intended as background to microwave digital radio systems and reception. A number of textbooks provide more general coverage of digital transmission theory [25-27]. Proceeding with a review of a complete digital radio system, subsequent sections review individual radio components, with an emphasis on receiver techniques and estimation theory for signal reconstruction and optimum reception. Means of representing the multipath channel with modelling functions and for simulation purposes is discussed. Finally, important definitions for measuring degradation and system outage are given.

2.1 A MICROWAVE DIGITAL RADIO SYSTEM

Figure 2.1.1 illustrates the general structure of a transmit-receive microwave digital radio system, subdivided into functional headings corresponding to a transformation from one signal space to another. Configurations will vary from system to system, and on whether transmission is over a multi-hop link requiring regenerative repeaters.

Formatting and source coding (section 2.2) renders the transmitted data sequence suitable for transmission and (optionally) introduces data compression. Modulation (section 2.3) may be thought of as the process whereby some waveform characteristic is varied in accordance with another. The transmitted data is up-converted to an radio frequency (RF) carrier, through an intermediate frequency (IF) stage.

Two fundamental concepts then apply at the receiver: demodulation/detection (section 2.4) and synchronisation (section 2.6). Equalisation (section 2.8) is generally

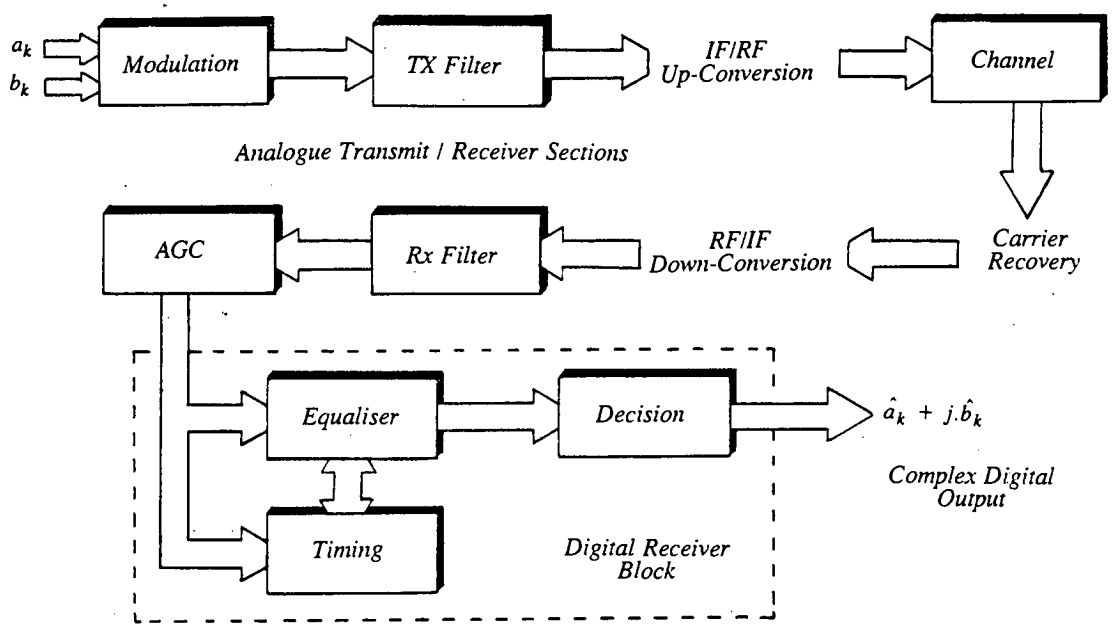

Figure 2.1.1 General Digital Radio Structure

performed at baseband prior to the final decision process and possibly jointly with other receiver functions.

2.2 FORMATTING AND SOURCE ENCODING

Formatting may be defined as any operation transforming data into digital symbols, while source coding generally refers to the manipulation of redundancy. If the data source is analogue, the waveform must be sampled at a rate of at least $2.f_n$ Hz (the Nyquist frequency, where f_n is the highest frequency present. Pulse amplitude modulation (PAM) systems transmit a train of constant width pulses, with amplitude in proportion to these sample values. Quantisation of the resultant samples allows each sample to be expressed as a level (digital symbol) from a finite number of pre-determined levels. Pulse code modulation (PCM) systems convert quantised samples into code groups of binary pulses. There are a number of PCM derivatives, each with certain advantages e.g. a compact spectral signature or self-clocking [28].

The transmitted data rate may be increased while maintaining the same symbol rate, by grouping incoming data in blocks of I bits, and assigning a weighting factor with one of $M=2^I$ equiprobable values or levels. This concept forms the basis for multilevel quadrature amplitude modulation (M-QAM) discussed in the next section. To minimise the error rate, the assignment of levels to each combination of bits is set according to a Gray code, ensuring that the crossing of one threshold level changes only one bit [29].

Conceptually, a data source may be split into two components: information and redundancy. Information has a well defined meaning within communications engineering, while transmission may be made more efficient by the selective minimising of redundancy, or more reliable by adding redundancy. Examples of source coding to reduce redundancy include differential PCM (DPCM), utilising differences between successive samples, rather than actual values. Another example, often used for voice coding and of interest from the adaptive systems viewpoint, is linear predictive coding [22].

Error correcting coding (ECC) involves the addition of redundancy as a means of data protection [30]. Automatic request transmission (ARQ) employs 'feedback' to request re-transmission when corrupt data is detected. The requirements for extra equipment and bandwidth limit it's use to outwith microwave systems. Forward error correction (FEC) involves adding sufficient redundant data such that the presence and position of data errors may be detected at the receiver. FEC has received extensive use in satellite and deep space applications [31], however technical and regulatory reasons have limited application in microwave digital links. To comply with European and North American standards, redundancy for FEC should not exceed 3-4% [32] of the total bandwidth. With the development of increasingly complex modulation formats, FEC and combined modulation/coding may well be key technologies. Future radio research may well see the further application of voice-band techniques, for example Reed-Solomon block codes [31] and the Viterbi algorithm to decode convolutional codes [33].

Finally, the addition of scrambling [34] helps minimise undesired signal characteristics, which would otherwise cause problems at the receiver synchronisation stage.

2.3 MODULATION

Modulation may be defined as the process whereby a carrier or subcarrier waveform is varied by a baseband signal. Phase, frequency and amplitude are varied by phase shift keying (PSK), frequency shift keying (FSK) and amplitude shift keying (ASK), respectively. Quadrature amplitude modulation (QAM) is a hybrid combination of ASK and PSK [35] . Numerous modulation formats exist, however microwave digital radio has generally employed QAM/QPSK and it's variants e.g. reduced bandwidth QPSK (RBQPSK) [36,37]. Trellis coding is a jointly optimised coding and modulation technique, and has recently received attention for microwave applications [38]. Spectrally efficient high-level modulation or M-ary signaling schemes process I bits at a time and instruct the modulator to produce one of an available $M = 2^I$ signal states e.g. multilevel QAM (M-ary QAM or M-QAM).

Modulation requirements for microwave digital radio may be characterised by a number of design features. Firstly, high transmission rates (2-400 Mbit/s) place serious limitations on hardware implementations. By contrast, voice-band modems operate at rates of less than 20 Kbit/s and realisation is considerably easier. Secondly, design emphasis is on spectral efficiency, with power efficiency a secondary factor. Thirdly, there is the susceptibility to multipath fading.

Development of microwave digital radio has evolved in three distinct stages, generally through the advancement of modulation technology. Many early systems used technically undemanding low level modulation techniques such as 4-QAM or 8-PSK. Existing analogue technology could often be used, and only with the introduction of second generation designs, were new technologies required. The operation of high-level modulation schemes brought the need for increased linearity in the RF transmitting amplifiers, and the necessity for adaptive equalisation. Third generation systems are currently in early development stages. Based on 256-QAM [39] and possibly 1024-QAM [40,41], the technical requirements are even more severe, placing further demands on compensation measures.

The principle of quadrature linear modulation is illustrated by figure 2.3.1. The I (in-phase) and Q (quadrature) inputs represent symbol spaced digital data values, subsequently converted into analogue sequences and low-pass filtered. A sinusoidal IF carrier $\cos 2\pi f_c t$ from a local oscillator is applied directly to the upper (balanced) modulator and with a 90° phase shift to the lower modulator. The modulator outputs are added and bandpass filtered to produce the IF signal:

$$x(t) = [\sum_{n=-\infty}^{\infty} a_n . h(t - nT)] \cos 2\pi f_c t - [\sum_{n=-\infty}^{\infty} b_n . h(t - nT)] \sin 2\pi f_c t \quad (2.3.1)$$

where $h(t)$ is the transmitted pulse shape. The equivalent complex received baseband

signal is

$$x(t) = \sum_{n=-\infty}^{\infty} a_n .h(t-nT) + j. \sum_{n=-\infty}^{\infty} b_n .h(t-nT) \qquad (2.3.2)$$

In the case of M-QAM modulation, a_n and b_n belong to the set of evenly distributed values $\{\pm 1, \pm 3, .., \pm \sqrt{M}-1\}$, where M is a perfect square.

2.4 DEMODULATION, DETECTION AND THE OPTIMUM RECEIVER

Demodulation at the receiver may be either coherent or noncoherent. Coherent schemes assume that the carrier phase is known at the receiver, while noncoherent demodulation operates in an essentially nonlinear fashion, making no attempt at carrier phase estimation. Noncoherent modulation methods trade simpler implementation against reduced performance. For microwave applications, coherent schemes predominate.

Figure 2.4.1 illustrates the process of demodulation in a QAM system. By multiplying or heterodyning with a local oscillator (derived from the carrier recovery circuit), the frequencies of the incoming signal may be translated down to baseband. The two demodulator outputs are low-pass filtered and digital output streams are produced by the ADC's†. The timing recovery circuit determines the control of the ADC sampling phase. It is apparent that synchronisation sub-systems (timing/carrier recovery) are of fundamental importance at the receiver, and will be discussed further in this chapter.

Usually detection is followed by a decision process, converting the recovered baseband signal into a sequence of digital bits. This process requires bit synchronisation under control of a timing recovery circuit. Decisions are made on a symbol-by-symbol basis, however some schemes gain improved performance by examining the signal over several symbols (the observation interval) prior to making a decision. Central to the discussion of coherent demodulation schemes is the concept of distance between an unknown received waveform and a set of known waveforms. Figure 2.4.2 illustrates a 16-QAM two-dimensional signal space (constellation diagram). After reception of the complex signal $x(t)$, the detector must determine which of the four possible signal states was transmitted. Minimisation of error probability is the usual decision criteria, however other schemes are possible. Since all signal states are equiprobable, it is possible to define decision boundaries as shown in

† In block diagrams, the term ADC generically refers to the complete sampling process e.g. analogue-to-digital conversion, sample-and-hold, and anti-aliasing filtering.

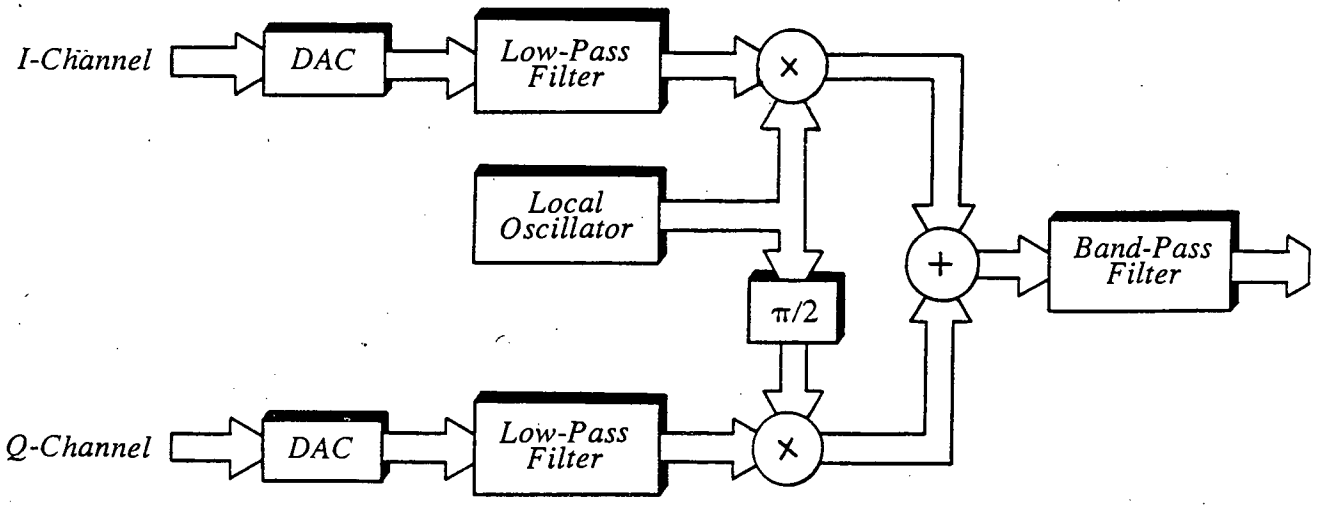

Figure 2.3.1 M-QAM Modulation

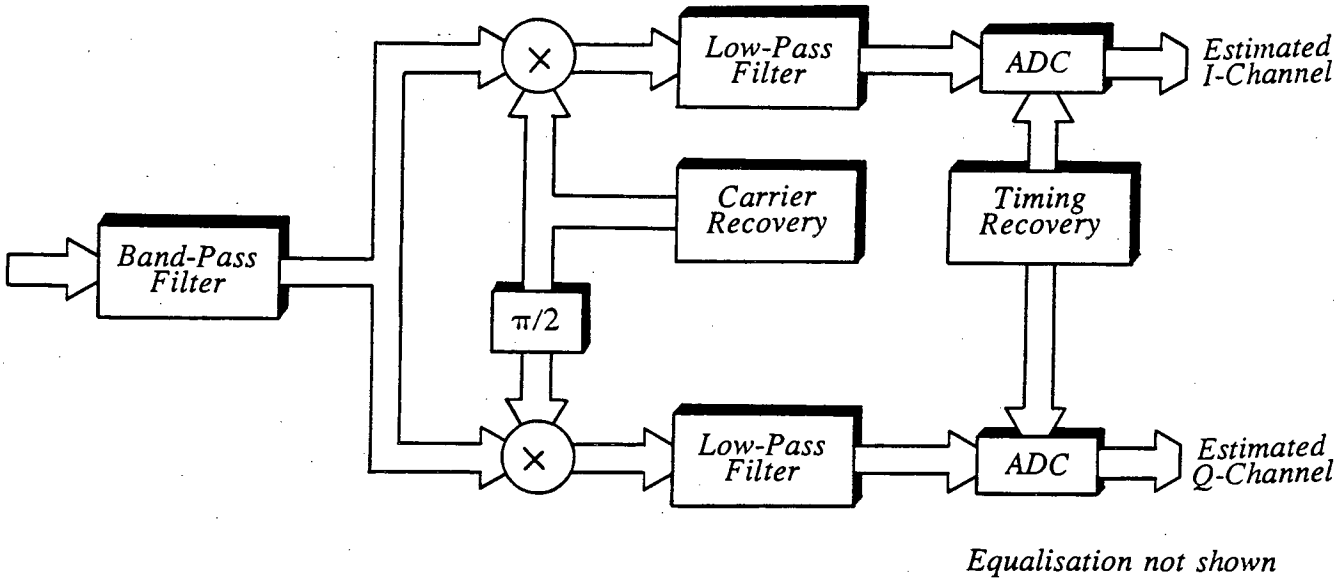

Figure 2.4.1 M-QAM Demodulation

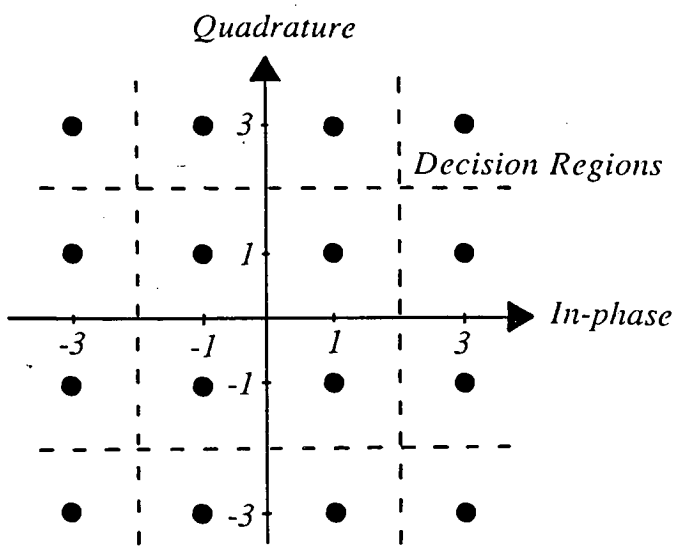

Figure 2.4.2 16-QAM Signal Space

figure 2.4.2.

In broad terms, the purpose of detection is to establish the presence or absence of a signal in noise. To enhance the signal power relative to that of the noise, and thereby facilitate the detection process, a detection system usually includes a predetection filter. When the additive noise is white, the optimum solution to the predetection filter is a matched filter, maximising the output SNR. An equivalent structure, derived from a probabalistic approach, is the correlation receiver. This involves correlation of the received wave with a stored replica of the transmitted signal.

A causal matched filter may be defined by [42]

$$c_{opt}^{*} = \begin{cases} 0 & t<0 \\ x(T-t) & t\geq 0 \end{cases} \qquad (2.4.1)$$

where $x(t)$ is the received analogue signal. Thus the matched filter response is a time reversed and delayed version of the input signal i.e. it is matched to the input. To be physically realisable, the system must be causal.

For an optimum digital receiver during ideal conditions, a sequence of symbol spaced samples, obtained at the correct timing phase, provides a sufficient set of statistics for estimation of the transmitted sequence at the output of a matched filter.

2.5 INTER-SYMBOL INTERFERENCE AND NYQUIST SIGNALING

In a channel suffering from multipath fading, the received signal over any symbol interval, will have contributions from a number of adjacent intervals. This smearing of the transmitted signal is known as inter-symbol interference (ISI). The received signal $x(t)$, is a superposition of the transmitted symbol impulse responses and additive white Gaussian noise $n(t)$. The complex received baseband waveform may be written

$$x(t) = \sum_{n=-\infty}^{\infty} (a_n + j.b_n).h_N(t - nT) + n(t) \tag{2.5.1}$$

where $h_N(t)$ is the overall channel impulse response. Sampling at instant $kT + \tau_k$, where τ_k represents the timing phase, equation (2.5.1) may be restated as

$$x(kT + \tau) = (a_k + j.b_k).h_N(\tau + kT) \tag{2.5.2}$$
$$+ \sum_{\substack{n=-\infty \\ n \neq k}}^{\infty} (a_n + j.b_n).h_N(\tau + kT - nT) + n(\tau + kT)$$

The first term on the right is the desired signal and the last term is additive noise. The middle term is due to the channel memory and is the ISI term. In the detection process, the ISI term may be viewed as a correlated random sequence or additive coloured noise.

The symbol pulse response may be designed with symbol spaced zero-crossings to satisfy Nyquist's first criteria, thereby eliminating ISI under ideal conditions. The most common Nyquist pulse shape is the raised cosine pulse [43], with impulse response

$$h(t) = \frac{\sin(\pi t/T)}{\pi t/T} \frac{cos(\pi \alpha t/T)}{(1-(2\alpha t/T))^2} \tag{2.5.3}$$

where $0.0 \leq \alpha \leq 1.0$, and is known as the rolloff factor. For microwave digital radio applications, the rolloff factor is usually close to 0.5 and this value was adopted for all simulation results. Selecting α near 1.0 compromises spectral efficiency, while values close to 0.0 make manufacturing difficult and increase sensitivity to impairments. For optimum performance, the overall raised cosine pulse shape is split equally between the transmit and receive filters [43].

The optimum digital receiver of section 2.4 comprised of a matched filter, symbol rate sampler and memoryless detector, applied to a white Gaussian noise channel. The effect of an additional ISI term due to multipath fading, is now equivalent to detection in coloured noise, and the optimum receiver structures so far considered are no longer applicable.

In the presence of ISI, an additional means of estimating the transmitted sequence is required. Equalisation techniques are the most practical approach for microwave digital radio, while Viterbi algorithm implementations of the maximum-likelihood sequence estimator (MLSE) offer another, considerably more complex solution [25]. If knowledge of the covariance matrix, $\underline{\phi}_{\alpha\alpha}$ (section 2.7), is available in a stationary coloured noise process with rational spectrum, another approach is to use a noise whitening filter derived from spectral factorisation of the noise spectrum [44].

2.6 RECEIVER SYNCHRONISATION

Prior to any form of symbol estimation or detection in a coherent digital communications system, two essential functions are required at the receiver: synchronisation of the carrier signal (carrier recovery) and symbol timing phase (timing recovery). Synchronisation may be generally defined as the alignment of time scales of spatially separated processes, and in the context of digital communications theory involves estimation of both time and frequency. A hierarchy of synchronisation levels is apparent in a digital receiver. In addition to carrier and timing recovery, frame and network synchronisation may be required [45], however neither will be considered further. A feature distinguishing the latter problems from those of carrier and symbol synchronisation, is the solution through the special design of the message format, involving the repetitive insertion of bits or words into the transmitted data stream. For maximum spectral efficiency, any synchronising signals should ideally be generated within the receiver.

Taken together, the carrier and timing problem is to obtain a good estimate of the carrier phase, θ_k, and the timing phase, τ_k, from the received signal

$$x(t) = \sum_{n=-\infty}^{\infty} (a_n + j.b_n).h_N(t - nT - \tau_k)e^{j\theta_k}.e^{j2\pi f_c t} + n(nT - \tau_k) \qquad (2.6.1)$$

where f_c denotes carrier frequency. While parameters θ_k and τ_k are considered stationary, both recovery circuits should be robust to avoid excessive outage through hysteresis effects during re-acquisition. Carrier and timing recovery is generally performed as a two stage process, however some performance advantages may be gained from the joint recovery of the two parameters [46, 47].

2.6.1. Carrier Recovery

A common means of carrier recovery, employing a non-linear square-law device, illustrates the process of carrier phase extraction. Considering the real part of the received signal

$$x(t) = x'(t).cos(2\pi f_c + \theta_k) \tag{2.6.2}$$

where $x'(t)$ is the passband received signal. The output of the square law device is

$$\begin{aligned} x(t) &= x'^2(t)\cos^2(2\pi f_c + \theta_k) \\ &= \tfrac{1}{2}x'^2(t) + \tfrac{1}{2}x'^2(t)cos(4\pi f_c + 2\theta_k) \end{aligned} \tag{2.6.3}$$

A frequency component is generated at $2f_c$, and this may be used to drive a PLL tuned to $2f_c$. The input to the PLL loop filter is approximately proportional to the phase error, $\theta_k - \hat{\theta}_k$, where $\hat{\theta}_k$ is local carrier phase estimate.

A crucial aspect of carrier recovery design is steady state performance. With increasing modulation complexity comes greater sensitivity to phase jitter and tighter demands on carrier recovery control. Any distortion introduced by multipath fading will increase the loop noise spectral density and reduce the phase detector gain. In microwave applications, a dominant factor in the frequency uncertainty of the recovered reference carrier is the stability of the microwave local oscillators [48]. To acquire lock over a relatively large frequency range, digital receivers may employ acquisition-aiding techniques such as frequency sweeping [36]. An additional periodic signal is applied to the VCO in the carrier recovery loop until the carrier is acquired. Acquisition time is determined by the frequency of the sweeping signal.

Carrier recovery techniques have evolved requiring decision-directed operation to improve robustness i.e. using knowledge of the receiver. In the design of baseband systems, care is however required to minimise any excessive delays due to the addition of any adaptive equalisation into the carrier recovery loop.

For assessing baseband equaliser performance, perfect coherent modulation is assumed at the receiver, implying ideal carrier recovery. A considerable reduction in computation time is possible, while the implications in assessing equaliser performance are discussed in chapters three and four.

2.6.2 Timing Recovery

The role of timing recovery is to generate a symbol rate signal to control sampling of the received signal such that detection of the received signal is optimal. Transmission of a tone at the sampling frequency, f_s is both power and bandwidth inefficient, since the synchronising signal contains no information. Spectrally efficient microwave digital radio receivers extract the timing information from the received symbol sequence through nonlinear processing to generate a spectral component at f_s, with correct timing phase, τ_k. Timing recovery and equaliser operation are closely linked when sampling the received signal at the symbol rate and any examination of equaliser techniques must also consider the problems of timing recovery during

conditions of channel distortion. This subsection introduces the general characteristics of timing recovery systems. Specific applications will depend on the type of equalisation employed, hence adaptive equaliser techniques are introduced in section 2.8 prior to the examination of a number of implemented timing recovery techniques in section 2.9.

Timing recovery may be performed at either passband or baseband, however the most straightforward approach is to demodulate first and then recover the timing phase, τ_k, from the baseband signal. Passband timing recovery may offer some performance gain since the timing and equaliser updating loops are decoupled [49]. In general terms, timing recovery may be accomplished through either data aided or non-data aided techniques. Data aided schemes may be regarded as 'bootstrap' approachs, assuming that knowledge of the data sequence is known at the receiver. Thus timing recovery may be performed during transmission of a training sequence or for microwave digital radio applications, continuously from the output of data detectors in place of true values. A number of timing recovery schemes are now discussed, each representative of a particular approach although no specific assumptions about equalisation requirements are made until chapters 3 and 4. With emphasis on an all digital receiver structure, there is a bias toward digital techniques.

Type A timing recovery is a symbol-rate scheme involving the derivation of the timing error estimate of the timing information for each symbol [50]. The type A timing function, $f(\tau_k)$, is

$$f(\tau_k) = \tfrac{1}{2}[h_N(T+\tau_k) - h_N(T-\tau_k)] \tag{2.6.4}$$

Timing based on this approach will be chosen to yield equal echoes $h_N(1)$ and $h_H(-1)$, and sampling instants will always be optimal if the impulse response is symmetrical. With symbol rate sampling, only samples at the receiver input and decisions at the output are available for an estimate with an expected value approximating $f(\tau_k)$. It may be shown that the estimate may be derived from a linear combination of available data, yielding the estimate

$$\hat{f}(\tau_k) = \frac{\tfrac{1}{2}(x(k).y(k-1) - x(k-1).y(k)}{E[y^2(k)]} \tag{2.6.5}$$

where $E[.]$ denotes the expectation operator A lower variance estimate of the timing function is possible by basing timing only on the reception of certain data sequences [51]. Implementation of both approaches is straightforward, while reduction in variance is obtained at the expense of convergence rate.

By correlating the signal derivative with the estimated data to produce updating information for a control loop, the resulting information is such that the mean square

error at the receiver output may be minimised. This may be written as

$$\tau_{k+1} = \tau_k - \frac{d[e(k)]^2}{d\tau_k} \tag{2.6.6}$$

where $e(k)$ is the difference or error between the detected input and output

$$e(k) = y(k) - x(k) \tag{2.6.7}$$

For implementation in a digital structure, an approximation is required to the derivative. MMSE timing was first proposed by Kobayashi [52], however the resultant structure was impractical, requiring duplication of equalisers. One proposal is the replacement of the MSE gradient with the polarity information of a first order approximation [53], thus

$$\tau_{k+1} = \tau_k - \delta.sgn\frac{[e(k+\tau_k+\Delta\tau_k)]^2 - [e(k+\tau_k)]^2}{\partial\tau_k} \tag{2.6.8}$$

where $sgn[]$ is the sign function. By using an unbalanced clock, (2.6.8) may be rewritten as

$$\tau_{k+1} = \tau_k - (-1)^k.\delta.sgn[e(k+\tau_k')]^2 - [e(k-1+\tau_{k-1}')]^2 \tag{2.6.9}$$

Consecutive sampling instants are obtained through the use of the modified clock phase, τ_k'

$$\tau_k' = \tau_k + (-1)^k\frac{\Delta\tau_k}{2} \tag{2.6.10}$$

To minimise excess jitter after convergence to a steady state value, δ must be chosen small enough to minimise degradation, but at the expense of convergence rate. By modifying the cost function, interaction between timing and carrier recovery loops may be decoupled.

Many analogue timing recovery approaches are based on the extraction of a spectral line at the clock frequency and filtering with a narrowband loop. Such lines are normally unavailable, and generation requires non-linear processing, typically with a square-law device [54].

2.7 OPTIMUM LINEAR ESTIMATION

Chapter 1 introduced adaptive filtering or equalisation as a means of reducing inter-symbol interference (ISI) at a receiver. Central to any discussion of adaptive filtering is optimum estimation theory. The following optimum Wiener filter provides a goal for adaptive algorithm convergence, and the LMS algorithm is an iterative, unbiased approximation to this solution. A linear FIR structure is considered initially,

while chapter four extends this solution to the case of a nonlinear decision-feedback equaliser.

A typical linear estimation problem is illustrated in figure 2.7.1(a), where a linear filter operates on an observed random sequence, $x(k)$, to yield an estimate $\hat{y}(k)$. A critical aspect of estimation theory is the definition of a cost function, based on the difference between the estimator output and the desired response $y(k)$

$$e(k) = y(k) - \hat{y}(k) \tag{2.7.1}$$

The cost function, $e(n)$, assigns a loss where the estimate is incorrect. The most commonly used cost function, and the one of relevance is mean square error (MSE), $\xi(k)$

$$\xi(k) = E[e^2(k)] = E[(y(k) - \hat{y}(k))^2] \tag{2.7.2}$$

The error surface is illustrated in figure 2.7.1(b). It is apparent that smaller errors have less emphasis than larger errors due to the nonlinear square function. Alternative cost functions include the error modulus (figure 2.7.1(c)) and non-linear threshold functions (figure 2.7.1(d))

The output of a FIR filter of order $N-1$ may be written as a finite sum of products

$$\hat{y}(k) = \sum_{i=0}^{N-1} c_i x(k-i) \tag{2.7.3}$$

A more compact notation is obtained with a vector inner product

$$\underline{\hat{y}}(k) = \underline{c}^T(k)\underline{x}(k) \tag{2.7.4}$$

where $\underline{c}(k)$ is a column vector containing the N elements of the equaliser impulse response.

$$\underline{c}(k) = [\, c_0\, c_1\, \cdots\, c_N]^T \tag{2.7.5}$$

and $[\,]^T$ denotes vector/matrix transposition. The last N elements of the input sequence are contained in $\underline{x}(k)$

$$\underline{x}(k) = [\, x(k)\, x(k-1)\, \cdots\, x(k-N+1)]^T \tag{2.7.6}$$

Substitution of (2.7.4) into (2.7.2) yields

$$\xi(k) = E[(y(k) - \underline{c}^T{}_i\underline{x}(k))^2] \tag{2.7.7}$$

Differentiating (2.7.7) with respect to $\underline{c}^T(k)$ and equating to zero gives

$$E[(y(k) - \underline{c}^T(k)\underline{\hat{y}}^T(k))\underline{\hat{y}}^T(k)] = 0 \tag{2.7.8}$$

Re-arranging, and assuming the weight vector $\underline{c}^T(k)$ and the signal vector are

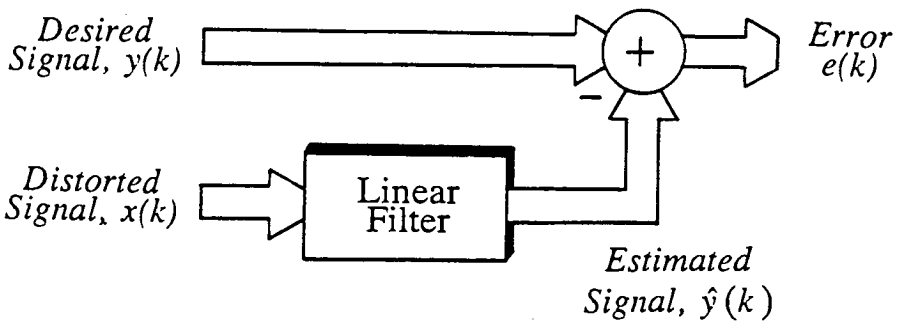

(a) The Optimum Linear Estimation Problem

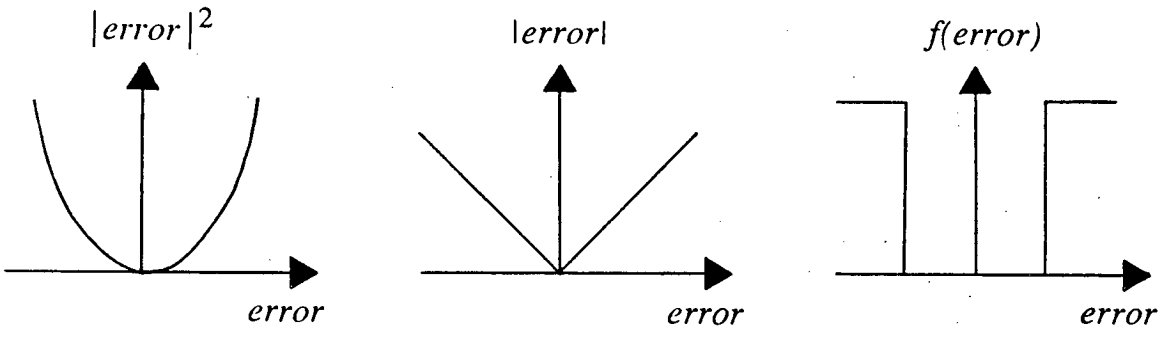

(b) MSE Cost Function (c) Modulus Cost Function (d) Nonlinear Cost Function

Figure 2.7.1 Optimum Linear Estimation and Cost Functions

uncorrelated

$$E[x(k)\underline{\hat{y}}^T(k)] = \underline{c}_{opt}{}^T(k).E[\underline{\hat{y}}(k)\underline{\hat{y}}^T(k)] \tag{2.7.9}$$

or

$$\underline{c}_{opt} = \underline{\phi}_{xx}{}^{-1}.\underline{\phi}_{xy} \tag{2.7.10}$$

where $\underline{\phi}_{xx}$ is the symmetrical N times N autocorrelation matrix defined by

$$\underline{\phi}_{xx} = E[\underline{x}(k).\underline{x}^T(k)] \tag{2.7.11}$$

and $\underline{\phi}_{xy}$ is the N element cross-correlation vector defined by

$$\underline{\phi}_{xy} = E[\underline{x}(k).y(k)] \tag{2.7.12}$$

The filter described by (2.7.10) is the Wiener FIR filter [19], and provides a means of designing optimum solutions. Direct application of Wiener filter theory requires a priori knowledge of the second order data statistics. An adaptive filter derives a time-varying impulse response, with a goal of converging to the Wiener solution.

2.8 ADAPTIVE EQUALISATION

Adaptive time domain equalisers comprise one of the most promising means of multipath compensation, and are the principle research topic of this thesis. This section provides an introduction to subsequent chapters.

Adaptive equalisation techniques may be categorised into time and frequency domain approaches. While both share a common aim in the reduction of multipath induced outage, problem definitions and performance are quite different. Frequency domain equalisers attempt to maintain desired characteristics in their frequency-domain specification, correcting only amplitude distortion. However, the primary cause of system outage is ISI, characterised by both amplitude and group delay. This is a time domain effect, and intuitively, time domain techniques are the most natural solution.

Frequency-domain, or more commonly called amplitude equalisers, are generally considered to be a simple low cost countermeasure, with variable results. Generally implemented at IF, amplitude equalisers adaptively compensate for slope or notches in the received signal spectrum [55, 56]. 'Slope' equalisers are only able to compensate for notches lying outside the passband and subsequently, performance is limited relative to time domain techniques. Some improvement is gained with 'notch' equalisers, which attempt to approximate the inverse of the channel characteristics through a variable resonator. Considerable performance may be gained when amplitude equalisers are operated in conjunction with space diversity [17]. While

performance may be acceptable for low level modulation schemes, for more complex systems, amplitude equalisation generally forms a pre-equalisation stage before adaptive time domain equalisation [57]. Throughout the remainder of the thesis, adaptive time domain equalisation will simply be referred to as adaptive equalisation.

2.8.1 Adaptive Equaliser Structures

The most common linear adaptive equaliser is the non-recursive transversal equaliser (figure 2.8.1). Recursive linear, with infinite impulse response (IIR), equaliser designs are possible, however performance over non-recursive types may be marginal [25], and in practice they are rarely used due to stability problems [29]. Recent work suggests a solution may ultimately be possible, thus implementing a structure requiring a lower order than a FIR design [21]. The output of a transversal equaliser is the summation of linearly weighted current and past values of the sampled input and this may be written from (2.7.3) as

$$\hat{y}(k) = \sum_{i=0}^{N-1} c_i . x(k-i) \tag{2.8.1}$$

where N is the number of equaliser coefficients. Coefficient adaptation is possible by a number of methods shortly to be discussed. The capability of a linear equaliser to reduce ISI is determined by the number of coefficients and the position of the reference tap (the location in the delay line of the symbol currently being detected). For microwave digital radio applications, typically 5-7 taps have been found to give an acceptable compromise between performance and complexity [58].

Deep spectral nulls in channels suffering particularly severe multipath fading reveal fundamental limitations in linear equaliser performance (chapter 3) and have prompted the examination of nonlinear equalisation techniques (chapter 4). Two main nonlinear types are decision feedback equalisers (DFEs) and maximum-likelihood sequence estimation (MLSE). MLSE techniques have received some investigation for use in voice-band modems, however complexity considerations currently limit extensive applications. While MLSE tecniques are currently impractical for microwave applications, the trend should be noted of equalisation techniques being initially applied to low data rate voice-band systems and later applied to higher data rate radio [59].

Decision feedback equalisers are a nonlinear equalisation technique based on the direct cancellation of ISI from previously detected symbols. The DFE depicted in figure (2.8.2) consists of a feedforward section similar to a transversal equaliser. Decisions made on the equalised signal are fedback through a second transversal filter, with the aim of removing that part of the ISI from previously detected symbols, from

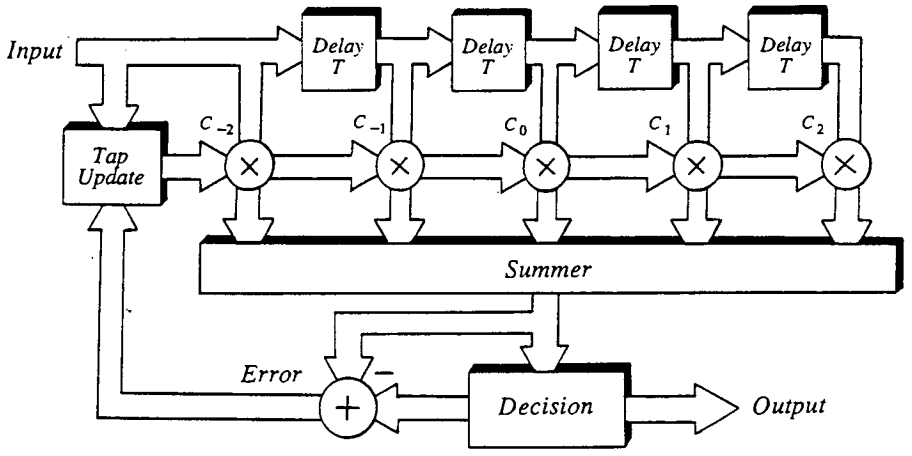

Figure 2.8.1 Linear Transversal Equaliser

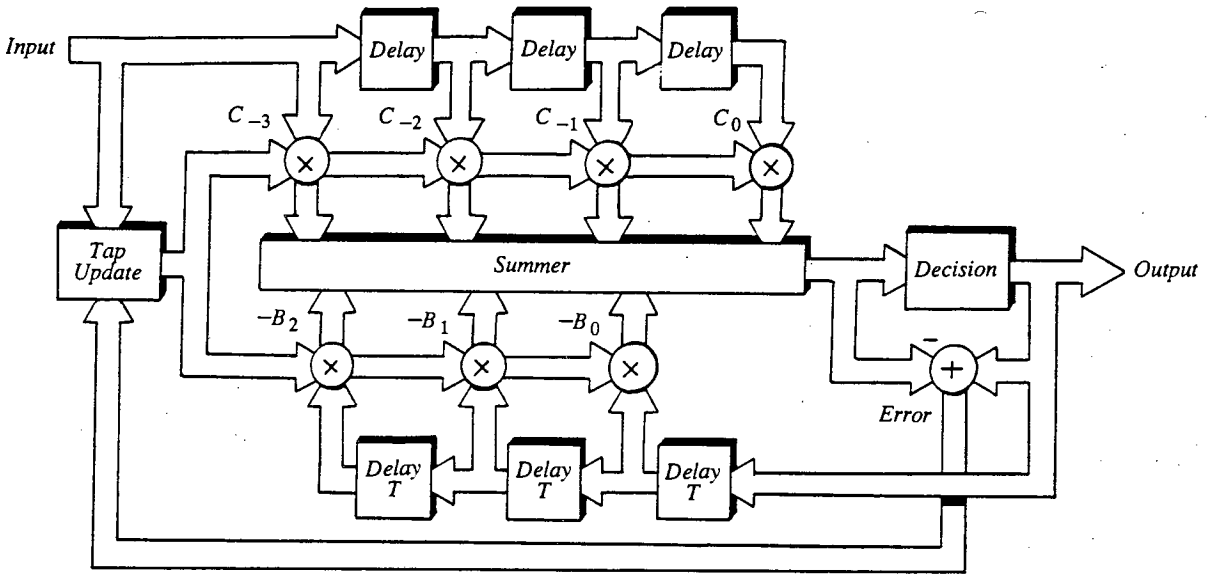

Figure 2.8.2 Decision Feedback Equaliser

the current estimate. The DFE output may be written as

$$\hat{y}(k) = \sum_{i=0}^{N-1} c_i . x(k-i) - \sum_{i=1}^{K} b_i . y(k-i) \qquad (2.8.2)$$

Tap lengths are typically 5-7 (3/4 forward, 2/3 feedback).

Increasing interest is being directed towards fractionally spaced equalisers (FSEs). FSEs operate at the Nyquist frequency or higher, compared with the symbol rate operation of conventional equalisers. The equaliser outputs are then decimated at the symbol rate. Such an approach is applicable to both transversal equalisers and DFE's. In a digital receiver sampling at rate T/m, equation (2.8.1) may be rewritten for the fractionally spaced transversal equaliser (FTE) as

$$\hat{y}(k) = \sum_{i=0}^{N-1} c_i . x(k/m-i) \qquad (2.8.3)$$

and for the fractionally spaced DFE (FDFE)

$$\hat{y}(k) = \sum_{i=0}^{N-1} c_i . x(k/M-i) - \sum_{i=1}^{K} b_i . y(k-i) \qquad (2.8.4)$$

FSEs have a number of inherent advantages over symbol spaced structures. A FSE can, with sufficient taps, shape the entire bandwidth of the received signal in contrast to a symbol spaced structure effectively operating on the aliased received spectrum. Thus FSEs may have superior performance for an equivalent number of taps, particularly for severe delay distortion at band edges. A further important advantage is that FSEs are largely insensitive to choice of timing phase.

For multilevel M-QAM systems, where two two separate data streams are transmitted on orthogonal channels, multipath fading introduces not only ISI but cross-rail interference or crosstalk between the two signal streams (figure (2.8.3(a)). A convenient description of equalisation against crosstalk may be achieved through the use of complex notation. By using complex signals, suitable complex adaptive equalisation structures may be designed for M-QAM systems incorporating additional equalisation against crosstalk. In practice, a complex equaliser would be implemented as a set of four real equaliser structures (figure 2.8.3(b)).

2.8.2 Equaliser Adaptation

Section (2.8.1) concentrated on the equaliser configuration as determining theoretical performance. How far this may be realised in practice will depend on the means of adapting the equalisers characteristics to match those appropriate to the channel. An important factor in adaptation design is that time variations in the channel occur slowly and may be based on simple adaptation techniques. The two

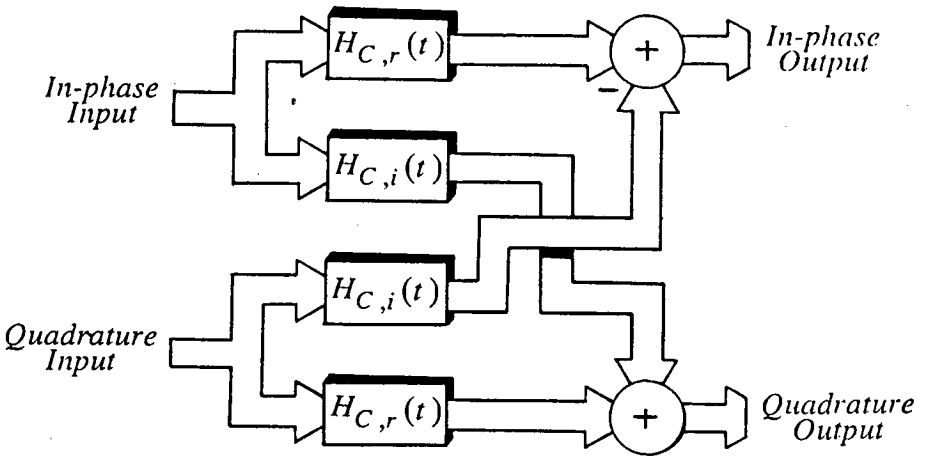

Figure 2.8.3 Complex Channel Structure

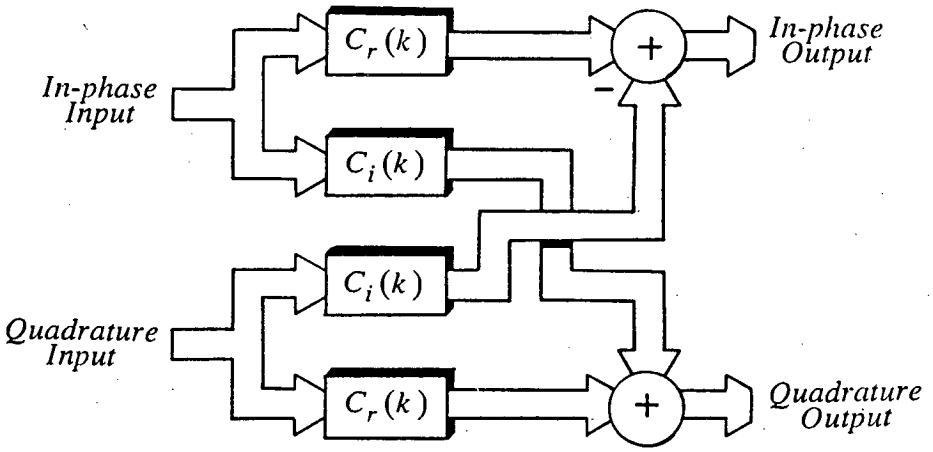

Figure 2.8.4 Complex Equaliser Structure

main adaptation techniques currently applied to microwave digital radio receivers are the zero-forcing (ZF) and least mean squares (LMS) algorithms. Both will be considered, however it will become apparent that the LMS algorithm has certain performance advantages and will be used for subsequent study.

ZF techniques are based on the cancellation of ISI, and originated with Lucky's original equaliser design [24]. In order to satisfy Nyquist's first criterion for zero ISI, the combined channel/equaliser response should be chosen such that an infinite length ZF equaliser is simply an inverse filter, inverting the folded channel spectrum. The peak distortion cost function [24] has a global minima, and adaptation may be carried out with the method of steepest decent according to

$$c_i(k+1) = c_i(k) + e(k).y(k-i) \tag{2.8.5}$$

where $e(n)$ is the equaliser output error at time k.

ZF equalisers have been implemented in many of microwave digital radio systems [60] due to implementation simplicity, inspite of performance limitations [29]. No account is taken of noise, and this may be excessively enhanced at frequencies where the folded channel spectrum has high attenuation. Secondly, convergence is not guaranteed if the eye pattern is closed.

Better performance is achievable if the equaliser taps are adjusted to minimise both ISI and noise error terms. This is the basis for the least mean squares (LMS) algorithm. The LMS algorithm is a recursive unbiased estimate of the Wiener filter discussed in section 2.7. Knowledge of the second order statistics is not required, and tap adaptation is performed by the time recursion

$$\underline{c}(k+1) = \underline{c}(k) - 2.\mu.\underline{x}(k).e(k) \tag{2.8.6}$$

where $\underline{c}(k)$ is an estimate of the Wiener filter $\underline{c}_{opt}$ at sample k. Derivation in vector notation of the LMS or stochastic gradient algorithm is from

$$\underline{c}(k+1) = \underline{c}(k) - \mu\hat{\underline{\nabla}}E[e^2(k)] \tag{2.8.7}$$

where $\hat{\underline{\nabla}}E[e^2(k)]$ is an estimate of the MSE cost function gradient, when the impulse response is $\underline{c}(k)$. The estimate normally used is

$$\hat{\underline{\nabla}}E[e^2(k)] = \hat{\underline{\nabla}}e^2(k) \tag{2.8.8}$$

i.e. the gradient is calculated for a single value of squared error. This is an unbiased estimate and may be shown to yield [23]

$$\hat{\underline{\nabla}}e^2(k) = 2.\underline{x}(k).\underline{e}(k) \tag{2.8.8}$$

Equation (2.8.6) may be proved stable given certain bounds on the convergence factor, while the convergence rate of the LMS algorithm is dependant on the spectral

colouring of the equaliser input, $\underline{x}(k)$. If the autocorrelation matrix $\underline{\phi}_{xx}$, is known, a stability bound based on the maximum eigenvalue maybe derived, and convergence rate may be shown to be dependant on the ratio of maximum to minimum eigenvalues [61]. A more practical bound is given in terms of the average signal power in the windowed input sequence [62]

$$0 < \mu < \frac{1}{3N.E[x^2(k)]} \tag{2.8.10}$$

where N is the number of taps. A number of variations on the basis LMS algorithm are discussed in chapter 5, generally based on reducing complexity by using only sign information. Chapter 5 also describes the block LMS (BLMS) algorithm. By holding the estimated impulse response constant over a block of L data points, the gradient estimate of (2.8.6) may be improved by replacing the 'ensemble' average by a time average over L values. The optimum set of block Wiener filter weights is equivalent to that for a conventional Wiener filter, and indeed the LMS algorithm may be viewed as a special case of the BLMS algorithm, with block length equal to one [63]. For applications requiring rapid convergence in a stationary environment, recursive least squares (RLS) techniques may be applied [64]. RLS algorithms operate by minimising a weighted or windowed sum of past squared errors. Other than for possibly 'off-line' adaptation, RLS techniques are not required for microwave digital radio applications. Two problems also exist with RLS algorithms: numerical instability and complexity of order N^2, compared with $2N$ for the LMS algorithm [65].

For application in a complex equaliser structure, the LMS algorithm should also be complex. The complex error surface in the MSE cost function is now

$$\xi(k) = E[e^{*2}(k)] = E[(\underline{y}_I(k) - \hat{\underline{y}}_I(k))^2 + (\underline{y}_Q(k) - \hat{\underline{y}}_Q(k))^2] \tag{2.8.11}$$

where $.^*$ denotes a complex variable and subscripts I and Q denote In-phase and Quadrature components. The complex LMS algorithm may be defined by [66]

$$\underline{c}^*(k+1) = \underline{c}^*(k) - 2\mu\underline{\tilde{x}}^*(k)\underline{e}^*(k) \tag{2.8.12}$$

with $\tilde{}$ denoting complex conjugate. Convergence properties are similar to the real case, (2.8.5).

2.9 FADING CHANNEL REPRESENTATION

To assess the impact of multipath fading, some means of characterising the channel is required. Two topics are now discussed: multipath modelling functions and modelling the overall system response in a suitable format for simulation.

2.9.1 Multipath Models

A multipath fading model is a means of characterising a microwave radio channel during fading. The complex frequency response, $H(j\omega)$ of the channel, may be written as

$$H(j2\pi f) = \begin{cases} 1+j0 & \textit{Normal Conditions} \\ H_C(j2\pi f) & \textit{During Fading} \end{cases} \tag{2.9.1}$$

The multipath transfer function $H_C(j\omega)$, may be described in amplitude-phase form as

$$H_C(j2\pi f) = |H(j\omega)|e^{j\Phi(2\pi f)} \tag{2.9.2}$$

from which the attenuation, $A(\omega)$ may be measured as

$$A(2\pi f) = -20.log|H(j2\pi f)| \tag{2.9.3}$$

A function modelling such a channel has three principle components. Firstly, a modelling function approximating $H(j2\pi f)$ over a finite frequency interval with suitable parameter functions, and the joint probability of these parameters must be known. Finally, a scale factor may be required to represent the probability of multipath fading on a particular radio path. This is applied to the conditional probability of the function parameters, and usually results are scaled to an annual or worst month basis [67].

One of the most common approaches to modelling nondiversity single polarisation channels is through the use of three ray models. The general three path or atmospheric model attempts to characterise the physical effects of an actual multipath fading channel [68]. Alternatively, channel models attempt to mathematically fit the measured channel response. The most commonly used channel model is the simplified three path model developed by Rummler [12] (often known simply as the Rummler model). This has the following transfer function

$$H_C(j2\pi f) = a.[1 - b.e^{-j2\pi(f-f_0)\tau}] \tag{2.9.4}$$

where a is a constant loss term or flat fade margin. The bracketed term suggests interference between two rays with relative amplitude, b, and relative delay, τ, and introducing a minimum or notch in the frequency response at f_0. While this approach has the appearance of a two path model, the response arises from three paths: a direct unfaded path; a second path, similar in strength to the first and close enough in delay such that the composite response is constant (the parameter a); and a third path with delay τ providing the frequency shaping of $H_C(j2\pi f)$.

A practical problem exists with the simplified three path model in that there are too many variable parameters to be determined from a given channel response measurement. This may be overcome by fixing τ at any convenient value. In

Rummler's original development [12], τ was set at the reciprocal of six times the measured bandwidth (6.3 ns). This value has subsequently been taken as standard in some work [69].

The two other main types of multipath model are the two path model and the polynomial model. The two path model is superficially similar to the simplified three path model, however it is a direct physical representation of a direct path with a single interfering signal. The two path model has been used in a number of studies to represent the dispersive component of fading [70].

Where measurements of individual paths in a multipath fading channel are difficult, any alternative characterisation is through modelling with mathematical functions. One studied approach is to use polynomial functions of frequency to describe the attenuation and group delay responses [71].

2.9.2 Phase Types

Frequency induced minima in the channel power transfer function are accompanied by maxima and minima in the delay distortion. A delay distortion plot with a frequency selective minima corresponds to a minimum phase (MP) fade, while a frequency selective maxima corresponds to a nonminimum phase (NMP) fade. During a transition between MP and NMP fading, an exact physical description of a microwave LOS channel is unclear, although three ray models provide a convincing description [72] and this approach was taken for simulating the fading channel.

A minimum phase transfer function may be defined more generally as one whose phase shift at each frequency is a minimum for a given overall amplitude response. In the z-domain, a MP function has no zeros outside the unit circle, while in the s-domain this corresponds to all the zeros in the left hand plane. A NMP function occurs if the transfer function has one or more zeros outside the unit circle. A transfer function with no zeros inside the unit circle is said to be 'maximum' phase.

In terms of the simplified three path channel model with a single zero in the transfer function, a MP fade occurs if the value for the relative amplitude, b, is in the range $0<b\leq 1.0$ and the relative delay, $\tau>0.0$. The response is NMP if the sign of the delay is reversed, or $b>1.0$ i.e. phase type is dependant on the relationship between interfering paths. Figure 2.9.1 illustrates the effect of 20 dB MP and NMP notches on the amplitude (power transfer function) and group delay responses of $H_C(j2\pi f)$. The NMP channel impulse response therefore has a dominant post-echo after the main sample.† The channel model loss term (equivalent to the flat fade margin) in the

† While true for the simplified three path model, this definition is not entirely consistent with the circuit theory definition of MP/NMP responses. A so-called 'MP' response may only have the dominant zeros inside the unit circle,

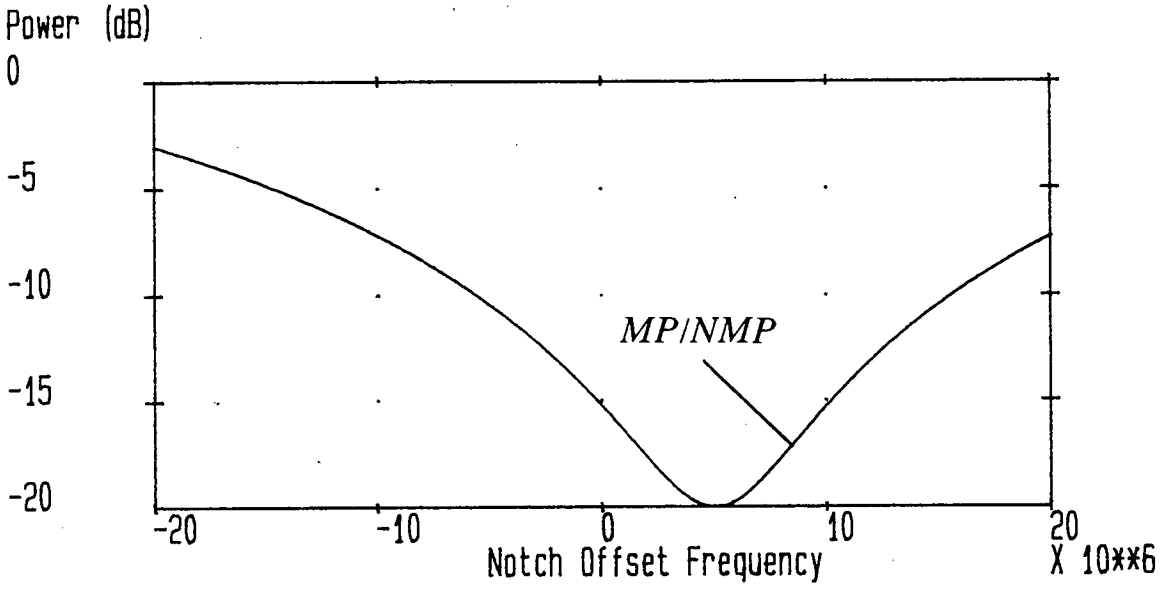

(a) Power Transfer Function (Amplitude Response)

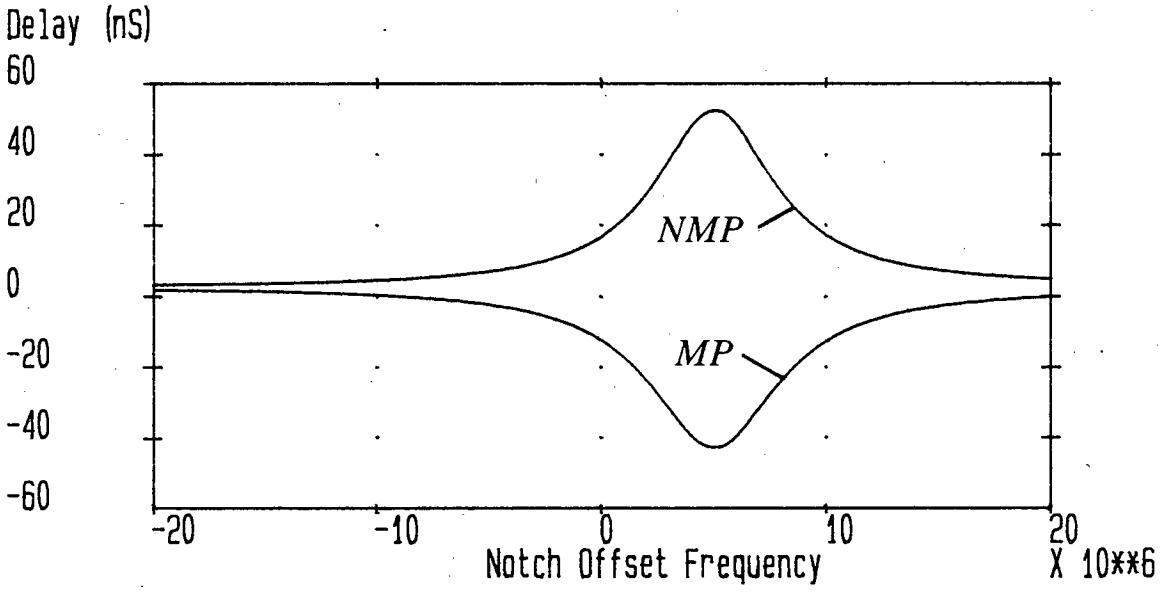

(b) Group Delay Response

Figure 2.9.1 Transfer Characteristics of the Rummler Model

simplified three path model is measured in dBs as

$$A_{\max} = -20.log\,|a| \tag{2.9.5}$$

and the relative notch depth for MP fading as $(0.0 \leq b \leq 1.0)$

$$B_{\max} = -20.log\,|1.0-b| \tag{2.9.6}$$

and for NMP fading $(1.0 \leq b \leq \infty)$

$$B_{\max} = -20.log\,|b-1.0| \tag{2.9.7}$$

The total fade depth at the response minima is $A_{\max}+B_{\max}$ dB.

2.9.3 An Equivalent Complex Baseband Model

A transmitter sends out discrete time symbols at a rate $1/T$ symbols/s and the sampled receiver output is also at rate $1/T$ symbols/s. It follows that the cascade of the analogue transmitter filter with impulse response $h_T(t)$, the channel with impulse response $h_C(t)$, the receiver filter $h_R(t)$ and the sampler, may be represented by an equivalent discrete-time FIR filter (Appendix A). The overall received impulse response is given by

$$h_N(t) = h_T(t)*h_C(t)*h_R(t) \tag{2.9.8}$$

Considering $h_C(t)$ in (2.9.8). This may be derived through the inverse Fourier transform of $H_C(f)$ given by (2.9.5). Thus

$$h_C(t) = F^{-1}[H_C(f)] \tag{2.9.9}$$

Rearranging (2.9.4)

$$H_C(f) = a[1 - b.e^{j2\pi f_0\tau}.e^{-j2\pi f\tau}] \tag{2.9.10}$$

The equivalent time domain response may be derived directly from this

$$h_C = a[\delta(t) - b.e^{j2\pi f_0\tau}.\delta(t-\tau)] \tag{2.9.11}$$

Multiplication of the transmitter and receiver filters results in the overall raised cosine response given by (2.5.3). If $\ddot{x}(t)$ is the baseband convolution of the transmitted data sequence in the absence of fading, such that

$$\ddot{x}(t) = a(t)*h_T(t)*h_R(t) \tag{2.9.12}$$

Further convolution with (2.9.11) results only in a time shift in the relative impulse responses. Thus the complex received baseband signal is

---

and is consequently not strictly MP [29].

$$x(t) = \ddot{x}(t) * h_C(t) \tag{2.9.13}$$

$$= a[\ddot{x}(t) - b.e^{j2\pi f_0 \tau}.\ddot{x}(t-\tau)]$$

2.10 PERFORMANCE ASSESSMENT AND OUTAGE CALCULATION

To increase the reliability of a microwave link, outage time and unavailability should be minimised. An outage event is said to occur if the the bit error rate (BER) exceeds a given value, typically 10^{-3}. If an outage period exceeds ten seconds, the link is said to be unavailable due to the fact that digital radio links loose framing if high BER's persist longer than ten seconds [73]. Radio unavailability tends to associated with longer lasting events e.g. rain attenuation, system failure. Multipath fading is the dominant source of system outages, consequently multipath countermeasures are principally concerned with the minimisation of outage time.

Although providing standard performance evaluation, BER measurements are time consuming and provide only limited information with regard to the receiver performance. Microwave digital radio systems are effectively error free during normal operating conditions (no fading), with a mean time between errors of around 500 hours [74]. One way round this is to specify the carrier to noise power ratio (CNR) or the received signal level (RSL) in dBm required to produce a BER of 10^{-3}. The CNR measurement at RF or IF is also equivalent to the baseband signal-to-noise ratio (SNR). For an M-QAM system, BER may be related to the SNR by [25]

$$P(\epsilon) = 1 - (1-P_m)^2 \tag{2.10.1}$$

where

$$P_m = [1-1/\sqrt{M}\,]erfc[\frac{3}{2(M-1)}\sigma_S] \tag{2.10.2}$$

where σ_S is the SNR and *erfc*[] is the complimentary error function. Such a solution is valuable for simulation purposes. Alternatively, Monte Carlo simulations provide a numeric solution to BER calculation [75], however direct application of Monte Carlo methods is only practical down to a BER of 10^{-4}.

The majority of simulation results are presented in terms of mean square error (MSE), defined in equation (2.7.2). Error distances are normalised such that the distance between adjacent symbol values is 2.0 e.g. for 16-QAM, values for $a(t)$ are taken from the set {-3,-1,1,3}. Complex quantities require the definition of an appropriate complex MSE term

$$\xi_{total} = \sqrt{(e_I^2)^2 + (e_Q^2)^2} \tag{2.10.3}$$

where e_I and e_Q are the in-phase and quadrature error components.

The average power in an M-QAM constellation is given by

$$P_{ave} = \frac{2(M-1)}{3} \tag{2.10.4}$$

The additive noise level for a given SNR (60 dB in most simulations) was then set by normalising P_{ave}. In practice, receiver performance is dependant on the transmitted power level [76], however this is constrained by amplifier nonlinearity. A SNR based on the normalised P_{ave} permits appropriate comparison between different modulation formats for a constant transmitter power.

2.11 SUMMARY

Chapter 2 has provided background information relevant to the main body of the text on equaliser performance and design. Emphasis has been on general receiver components, although system components are interdependant, and a single function cannot be treated in isolation. Within the receiver, synchronisation systems form a critical part of the demodulation process. The effectiveness of any adaptive equalisation may depend on suitably accurate timing recovery, unless the equaliser operates at greater than the symbol rate. The basic equalisation function and structures have been introduced, while the following chapters provide greater detail where required. To perform simulation results, a modelling function provides a description of the channel during different fading conditions. The commonly used, simplified three path model was selected. Finally, suitable performance measures for assessing the effects of fading were described, including BER and MSE, and the concepts of outage and unavailability.

Chapter 3

LINEAR EQUALISATION

3.1 INTRODUCTION

In the following chapter, results will be presented for linear equalisation techniques and the associated problems of timing recovery for microwave digital radio systems. Linear transversal equalisers are currently available (often only optionally) in many commercial radio systems, however many designs are a cost/performance compromise and much work remains to assess potential performance in certain key areas. In particular this chapter will examine receiver performance during dynamic fading conditions, timing recovery problems connected with multipath fading, retraining during non-ideal conditions, and the relative merits of different equaliser structures. Implementation issues will be considered in chapter 5. Some of the proposed approaches would currently prove impractical for present day techniques, however with rapidly advancing technology, this situation may soon change [41] and new ideas should be considered.

3.2 LINEAR OPTIMUM RECEIVERS

During multipath fading conditions, the received signal contains ISI in addition to noise. At any sampling instant, the current symbol is correlated with past and future symbols, and hence the matched filter receiver of section 2.4 is no longer optimal. For non-ideal channels, a linear receiver conventionally consists of a matched filter, symbol rate sampler and a memoryless symbol rate detector. Viewed in more general terms, this structure may be considered as a special case of a fractionally spaced transversal equaliser plus detector. For practical purposes, equalisers have historically been implemented mainly as symbol spaced structures for microwave

digital radio applications.

3.2.1 Symbol Spaced Optimum Receivers

If symbol rate sampling is employed, the equaliser effectively operates on the aliased signal spectrum. The received convolved signal impulse response, $h_N(t)$, defined by (2.9.8), may be transformed to the frequency domain as

$$H_N(f) = H_T(f)H_C(f)H_R(f) \tag{3.2.1}$$

The aliased received spectrum may be defined through Parseval's theorem as [28, 77]

$$S_N(f) = \sum_{n=-\infty}^{\infty} |H_N(f - n/T)|^2 \qquad 0 \leq f \leq 1/T \tag{3.2.2}$$

where T_0 is the symbol time period. The transversal equaliser has response $C(f)$, hence the equalised signal response is $S_N(f)C(f)$ for $0.0 \leq f \leq 1/T$. The symbol spaced equaliser effectively operates on the aliased spectrum and is unable to exercise independent control over both sides of the roll-off region. Assuming transmission of an ideal signal spectrum of unity power, the optimum MSE equaliser performance is derived by first summing ISI and noise power terms. Thus the MSE is given by [65]

$$\xi(f) = T\int_0^{1/T} [1 - S_N(f)C(f)]^2 + N_0 S_N(f)|C(f)|^2]\, df \tag{3.2.3}$$

where the noise power spectrum is $N_0 S_N(f)$. The optimum response to minimise the MSE at the equaliser output is obtained through differentiating (3.2.3) with respect to $C(f)$ and equating to zero, hence

$$C_{opt}(f) = \frac{1}{N_0 + S_N(f)} \tag{3.2.4}$$

Substituting (3.2.4) into (3.2.3) yields the minimum achievable MSE

$$\xi_{opt}(f) = T\int_0^{1/T} \frac{N_0}{N_0 + S_N(f)}\, df \tag{3.2.5}$$

3.2.2 Fractionally Spaced Optimum Receivers

If the order of the transversal equaliser and symbol-rate sampler are interchanged (permissible due to linearity), the composite response of the matched filter and equaliser may be realised by a single continuous time filter, consisting of a transversal equaliser with N (fractionally) spaced taps. The received signal spectrum is thus bandlimited within $|f| \leq 1/2NT$. The resulting frequency response, $H_N^*(f)C(f)$, is periodic about the sampling frequency $1/2NT$, and this may be sampled at the symbol rate without loss in optimality [65].

The fractionally spaced transversal equaliser (FTE) output spectrum may be written as

$$H_N(f)H_N^*(f)C(f) \tag{3.2.6}$$

This is equivalent to the conventional symbol spaced equaliser where $C_{opt}(f)$ is defined by (3.2.4), however the FTE is now performing the functions of both matched filter and symbol spaced equaliser. Derivation of the optimum response $C_{opt}(f)$ for minimisation of the MSE, may be derived with a similar approach to section 3.2.1.

3.3 OPTIMUM TRANSVERSAL EQUALISER REALISATION

Section 3.2 assumed the availability of infinite length continuous time nonadaptive equalisers in the receiver. Calculated performance is obviously ideal, and for practical design, the constraints of finite length and limited precision arithmetic must be imposed. Secondly, the receiver cannot be designed to match all spectral conditions encountered during multipath fading, and hence is required to be adaptive. The following subsections examine theoretical digital equaliser performance through the application of discrete time Wiener filter theory [19] (from chapter 2) to a finite length FIR filter of order $N-1$.

3.3.1 Finite Length Symbol Spaced Equalisers

From (2.6.1), the output of a FIR filter of length N is restated as

$$\hat{y}(k) = \sum_{i=0}^{N-1} c_i x(k-i) \tag{3.3.1}$$

or in vector inner product notation as

$$\hat{\underline{y}}(k) = \underline{c}^T \underline{x}(k) \tag{3.3.2}$$

where the superscript T denotes transpose and $\underline{x}(k)$ is the sampled received signal derived in subsection 2.9.2. Application of Wiener theory defines the set of optimum equaliser coefficients sufficient to minimise the MSE at the equaliser output. The optimum solution to (3.3.1) was defined by (2.7.10) and this is restated as

$$\underline{c}_{opt} = \underline{\phi}_{xx}^{-1} \underline{\phi}_{xy} \tag{3.3.3}$$

where $\underline{\phi}_{xx}$ is the N times N Hermitian autocorrelation matrix (2.7.11) and $\underline{\phi}_{xy}$ is the N element cross-correlation vector (2.7.12). The minimum MSE achievable by the conventional finite length linear receiver is given by

$$\xi_{opt} = E[x(k)] - \underline{\phi}_{xy}^* \underline{\phi}_{xx}^{-1} \underline{\phi}_{xy} \tag{3.3.4}$$

In practice, the LMS algorithm (section 2.8.2) provides an unbiased approximation to c_{opt} using a stochastic gradient search technique.

3.3.2 Finite Length Fractionally Spaced Equalisers

Considering a digitally implemented fractionally spaced equaliser with tap spacing T/M, the sampled received signal is derived by modifying equation A.8 in appendix A.

$$x(kT/m) = \sum_{i=0}^{N-1} h_N(kT/m).a(kT/m - i) + n(kT/m) \qquad (3.3.5)$$

In each symbol interval the FTE produces an output

$$y(k) = \sum_{i=0}^{N-1} c_i.x(k - ki/m) \qquad (3.3.6)$$

A common tap spacing is at half the symbol interval ($T/2$). With this arrangement, the FTE may be modelled (and implemented as two symbol spaced filters, with one incorporating a delay of $T/2$ (figure 3.3.1) [78].

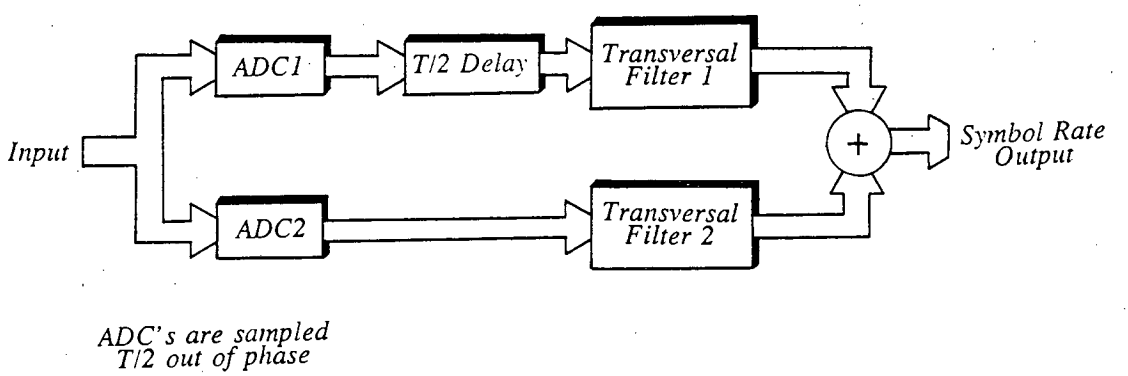

Figure 3.3.1 T/2 Spaced Linear Equaliser

The disadvantage with this arrangement is the duplication of ADCs or the alternatively high sampling rate. For a $T/2$ equaliser, equation (3.3.6) reduces to

$$y(k) = \sum_{i=0}^{N-1} c_i.x(k - i/2) \qquad (3.3.7)$$

In a similar manner to section 3.3.1, a set of filter coefficients may be derived to minimise the MSE at the equaliser output. Superficially the FTE optimum solution is very similar to that for the conventional symbol spaced transversal equaliser, however there are a number of significant differences. Firstly the FTE does not require a fixed receiver filter (although for simulation purposes, this is incorporated to give an overall raised cosine response). Secondly, while the FTE autocorrelation matrix is Hermitian, it is no longer Toeplitz [79]. Gitlin and Weinstein [79] showed that for a channel with an excess bandwidth of less than 100%, the resulting autocorrelation matrix is nonsingular and provides a unique optimum tap setting, even when additive noise becomes vanishingly small. Analysis of the eigenstructure of the autocorrelation matrix through singular value decomposition also reveals that the excess MSE is proportional to the number of nontrivial eigenvalues [80] .

3.4 TIMING RECOVERY CONSIDERATIONS

An important consideration in this chapter are timing recovery requirements during multipath fading. Simulation results will be presented illustrating important points, however some background information provides greater understanding of the equaliser performance with respect to timing phase, where taps are symbol and fractionally spaced.

Sensitivity due to poor choice of timing phase is one of the main differences between symbol and fractionally spaced transversal equalisers. Symbol rate sampling introduces aliasing. For a distortionless channel with properly designed bandlimiting filters and correct choice of timing phase, aliasing will result in the spectral components lying outside the bandedge, folding over to produce a flat response over the range $\pm 1/T$ Hz. For a microwave channel during multipath fading, the spectral components outside the bandedge will fold over and add constructively and destructively to the spectrum bounded by this bandedge. The minimum mean square error achievable by a symbol spaced transversal equaliser is thus a function of timing phase. Correct choice of timing phase is unimportant only when there is no excess bandwidth and consequently no aliasing. With sampling at greater than the symbol rate (e.g. a $T/2$ FTE), there is no spectral overlap at the equaliser input. Aliasing due to symbol rate decimation at the output takes place after the equaliser has compensated for the timing phase offset [81].

3.5 STATIC SYSTEM PERFORMANCE

Considerable research work has examined the theoretical and practical aspects of symbol spaced transversal equalisers, and to a lesser extent fractionally spaced equalisers during static channel conditions [54, 58]. Consequently one of the main aims of this section will be to illustrate the effects of multipath fading on a transmitted symbol sequence and digital radio performance. Examples from different M-QAM formats are chosen to highlight particular points. Appendix B provides an overview of the simulation approach, together with some examples of functions simulating adaptation and equalisation techniques. All simulation results for this chapter were performed with floating point arithmetic. Previous research indicated that around 7 taps provided the best compromise between performance and complexity [58] and this number was adopted for simulations.

The degradation due to multipath fading on a microwave digital radio channel is illustrated by the windowed time series in figure 3.5.1. Sampling four times per symbol allows sufficient resolution to observe a sequence of multilevel data on the In-phase channel of a 140 Mbit/s 16-QAM system. Comparison between 3.5.1(a) and 3.5.1(b) illustrates the introduction of ISI and the reduction in received signal power due to a 20 dB MP bandcentred fade. Two principle means of illustrating channel degradation at the receiver are with eye and constellation diagrams [7]. Both approaches provide an immediate visual means of examining decision thresholds to assess receiver performance. Figure 3.5.2 illustrates eye diagrams for a 16-QAM system during ideal conditions and a 15 dB MP bandcentred fade. The time scales are normalised to the symbol period for convenience.

One of the most common means of assessing equaliser performance during static channel conditions is with the signature plot. The signature plots in figure 3.5.3 indicate one aspect of the potential performance gain from fractionally spaced taps. Each point on the signature curve corresponds to the maximum tolerable fade depth before performance becomes unacceptable, for a given frequency. Unacceptable performance is defined where the BER exceeds 10^{-3}. Linear equalisers are transparent to phase type, thus NMP signatures are identical to those for MP fading [82]. Calculation of the signature is from knowledge of the MSE at the receiver output corresponding to a BER of 10^{-3} [83]. Performance between the two equaliser types is comparable at the bandcentre, while the fractionally spaced equaliser offers improvement at the bandedges. Results were obtained from a 140 Mbit/s 64-QAM digital radio system with MEO timing. Equalisation was from 7-tap symbol spaced and 8-tap fractionally spaced transversal equalisers.

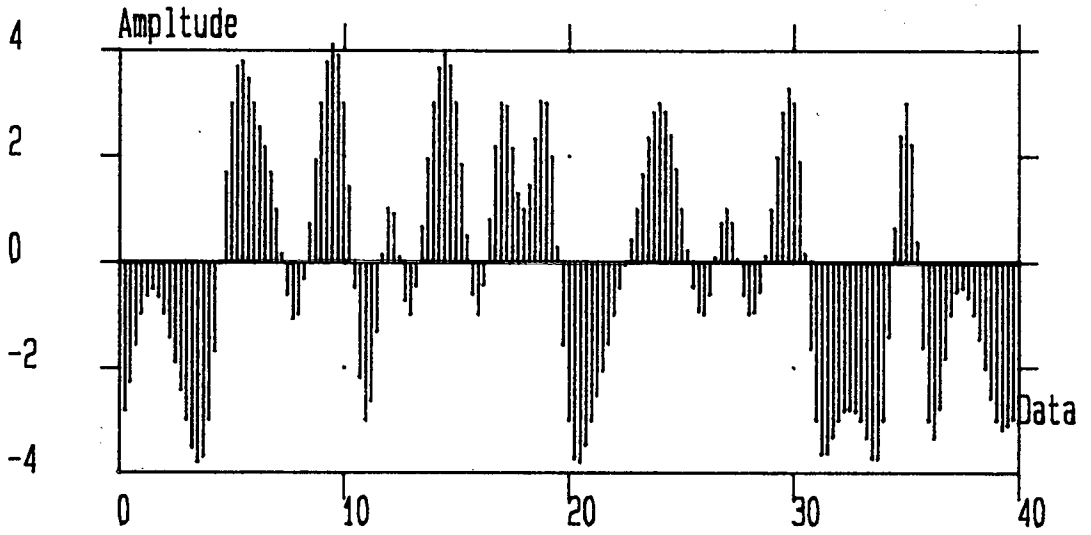

(a) Undistorted Channel

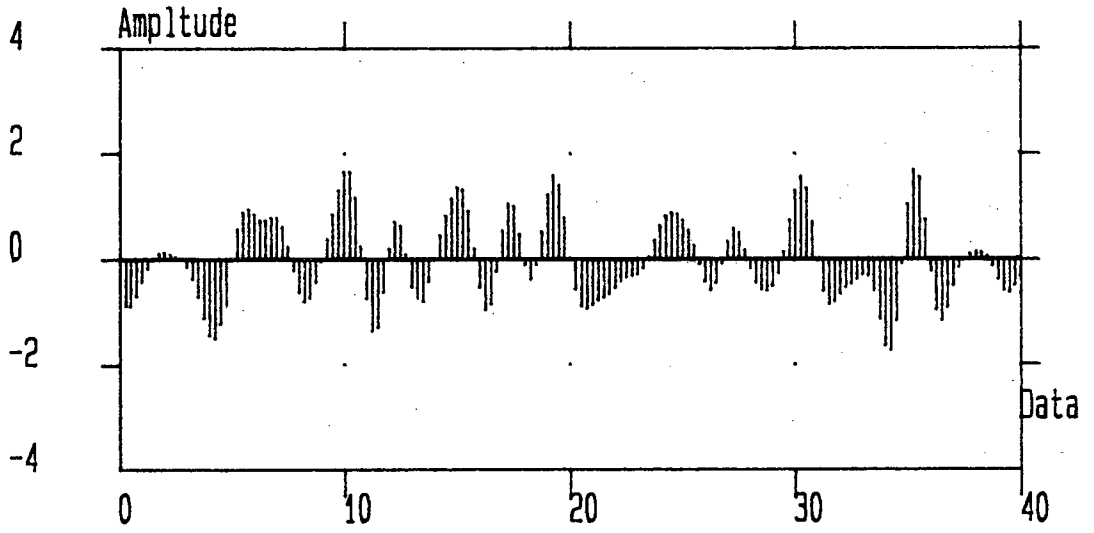

(b) 15 dB MP Fade

Figure 3.5.1 Effect of Fading on a Received Data Sequence

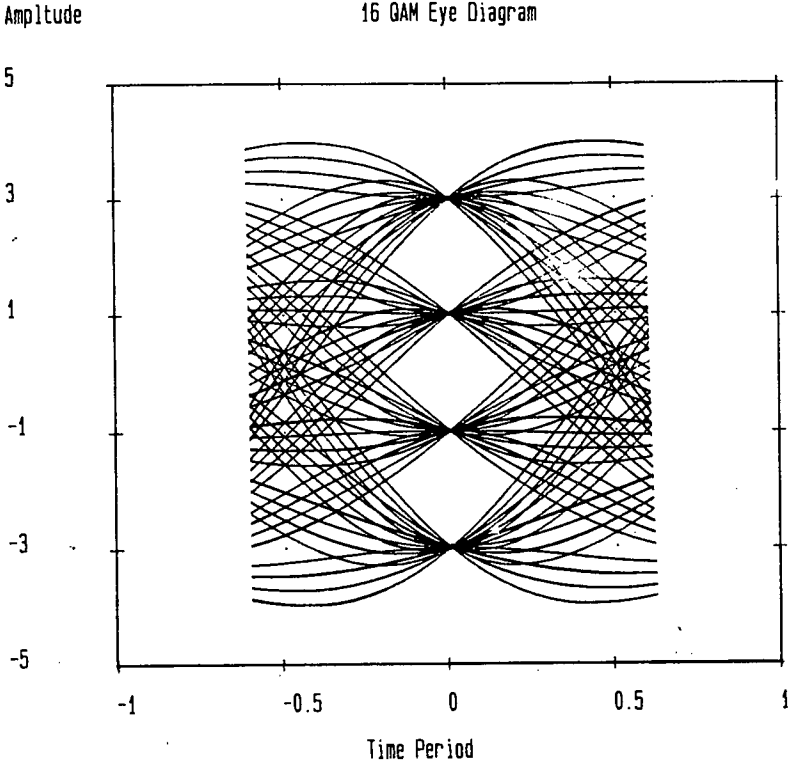

(a) Undistorted Channel

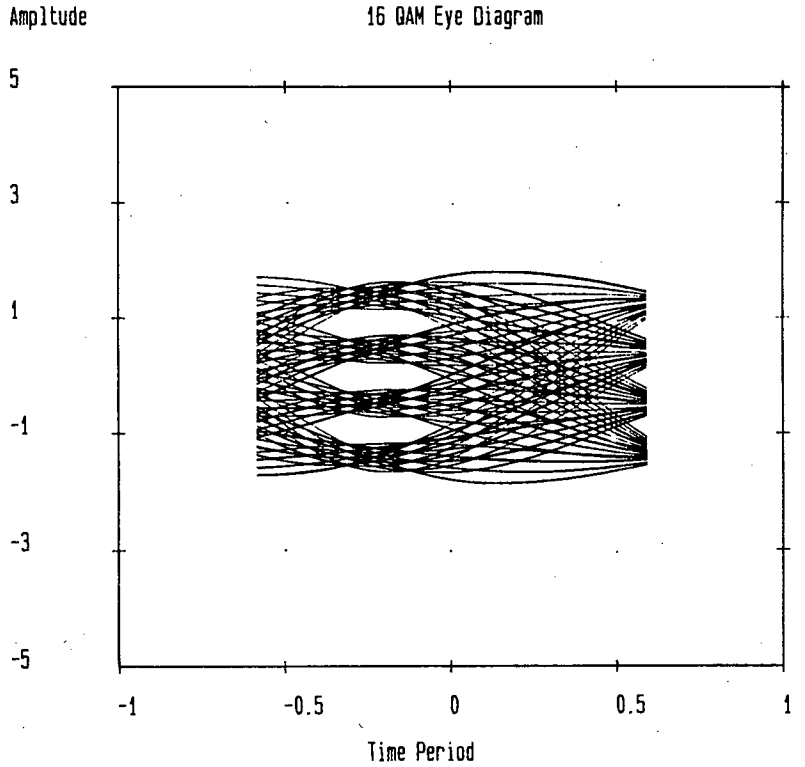

(b) 15 dB MP Fade

Figure 3.5.2 16-QAM Eye Diagrams

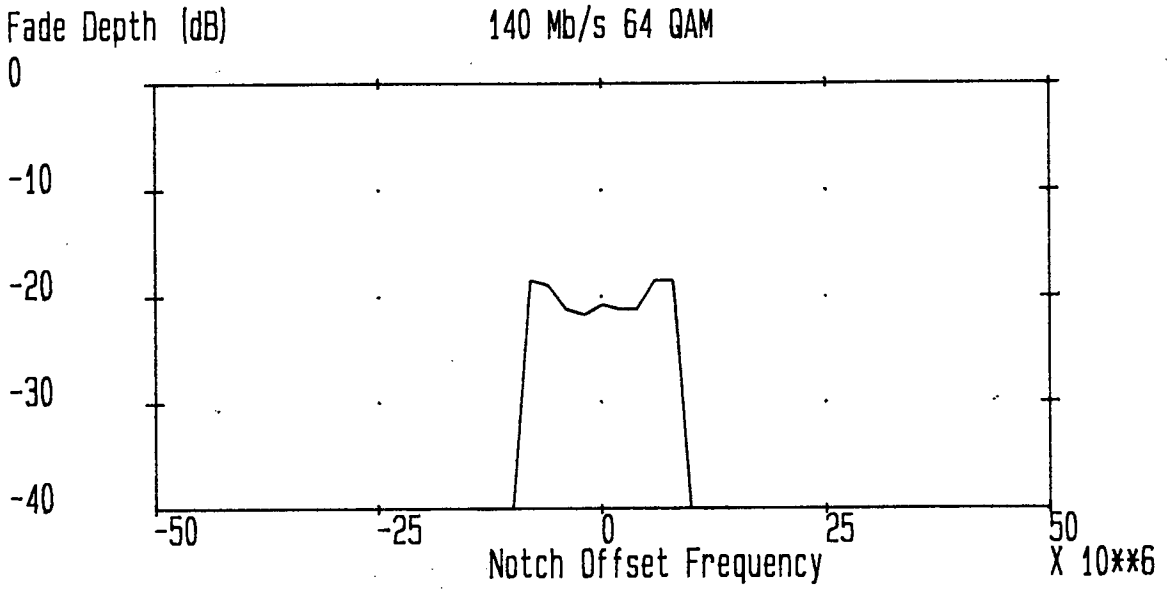

(a) Symbol Spaced Linear Transversal Equaliser

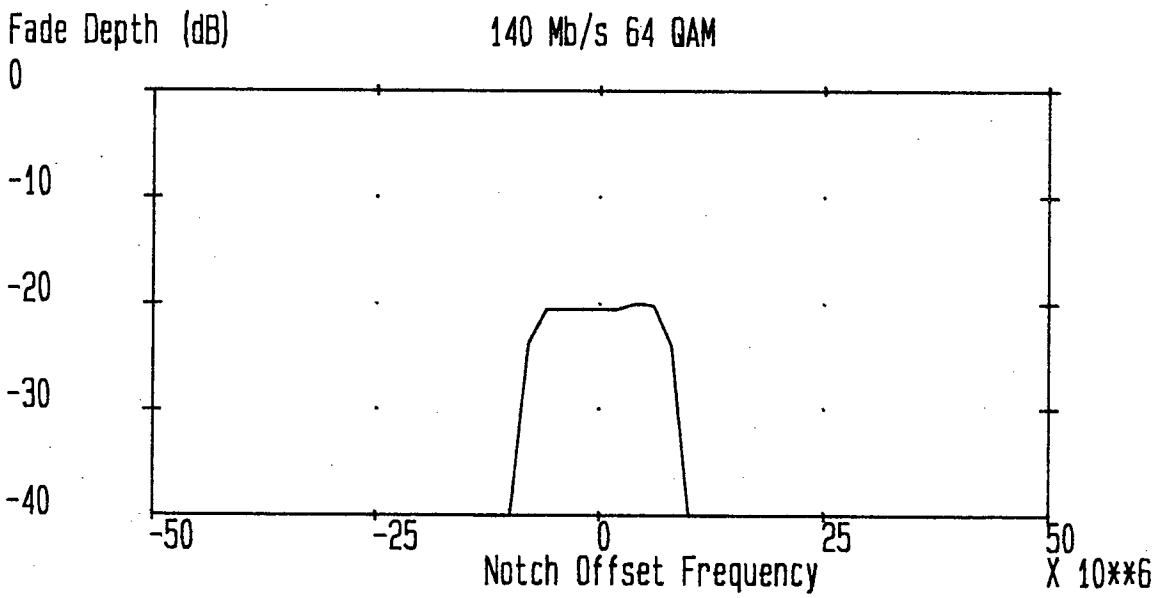

(b) Fractionally Spaced Linear Equaliser

Figure 3.5.3 64-QAM Signature Plots with MEO Timing

During static conditions, an ensemble averaged convergence curve indicates the ability and speed of the LMS (or any other adaptive algorithm) to converge to a steady state solution. Figure 3.5.4 illustrates that with a 34 Mbit/s 4-QAM system, LMS convergence is relatively rapid during near ideal conditions. Convergence rate is however dependant on the second order statistics of the received equaliser input, and with increased colouration (deepening fade), the convergence rate decreases to a poorer MSE value.

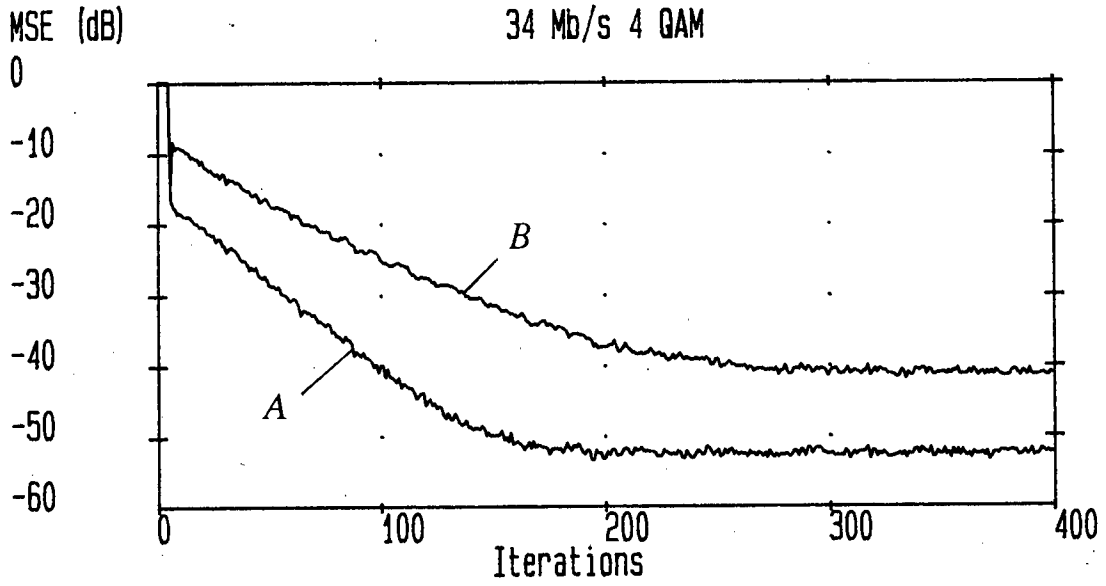

Figure 3.5.4 LMS Convergence Curves

Channel conditions are defined by channels **A** and **B** in table 5.5.3 in chapter 5.† It would appear that increased degradation will impede tracking ability during changing channel conditions, however it should be noted that changes in the fading channel are slow with respect to the data rate. In general during static or stationary conditions, near optimum MSE performance is obtained with small values for μ in equation (2.8.6) i.e. slow adaptation. Where the channel statistics are time varying, the best MSE performance is a compromise between fast adaptation to track time variations, and slow adaptation, yielding lower misadjustment noise [84]. For finite precision digital implementations, this statement no longer holds. The resulting effects on performance will be investigated in chapter 5.

† The exact channel characteristics are more relevant to later analysis and results, hence the location of the table in chapter 5.

3.6 DYNAMIC SYSTEMS (1): TRACKING DURING FADING

Discussion of channel characteristics and conditions has so far had two underlying assumptions. Firstly, time variations in the channel response are slower than the dynamic response of the digital radio equipment. The second requirement, very much related to the first, is that the performance of the radio is uniquely related to the current state of the channel i.e. there is minimal hysteresis in the receiver. Hysteresis problems encountered during re-acquisition will be examined in section 3.7

Channel dynamics may be assessed through measures of the speed of variation in the appropriate channel model parameters. Two obvious variations in the characteristics of a frequency selective fade are the rate of change in notch depth and the speed at which the notch moves across the transmitted signal bandwidth. Reported measurements have indicated worst case conditions of the notch depth changing at 100 dB/s and sweeping across the spectrum at 100 MHz/s. Reported results have indicated that in terms of notches sweeping across the transmitted bandwidth, a symbol spaced linear transversal equaliser only experiences dynamic limitations above rates of 1000 MHz/s [85]. Typically, practical measurements indicated slower channel variations to be prevalent [86, 87]. An additional important concept is that of trajectory [88]. The trajectory of a fading event describes the frequency and time characteristics of a fade at a given instant.

During nonstationary conditions, the autocorrelation matrix $\underline{\phi}_{xx}$, and the cross-correlation vector $\underline{\phi}_{xy}$, are time varying in nature, and the adaptive algorithm must not only converge to a minima in the error performance surface, but also track this changing optimum solution. A number of analysis have been reported into the performance of the LMS algorithm during non-stationary conditions [84, 89, 90]. Insight into nonstationary behaviour may be gained by defining a coefficient error vector

$$\underline{\epsilon}(k) = \hat{\underline{c}}(k) - \underline{c}(k) \tag{3.6.1}$$

where $\underline{\epsilon}(k)$ is the difference between the (time varying) estimated coefficient and the optimum Wiener solution. Equation (3.6.1) may be redefined as

$$\underline{\epsilon}(k) = (\hat{\underline{c}}(k) - E[\hat{\underline{c}}(k)]) + (E[\hat{\underline{c}}(k)] - \underline{c}(k)) \tag{3.6.2}$$

The first term on the right hand side of (3.6.2) is gradient noise due to any difference between individual coefficients and their ensemble averaged value. The second term is due to weight vector lag (delay in the adaptive process), and is the difference between the ensemble averaged coefficient value and the desired value. Selection of an appropriate convergence factor, μ, will be a function of these two error terms, and is in general selected to compromise between tracking ability (high μ) and excessive

residual MSE (low μ). This concept heuristically assumed that channel variations were slow. Later work by Macchi attempted to qualify this by defining a degree of variability [89], however insufficient data exists on the dynamic behaviour of microwave channels, particularly during deep fading when phase transitions are likely.

For simulation purposes, the channel transfer function has been modelled as having stationary increments [91]. Consider an increment of a time varying process $X(k)$, defined by

$$\Delta(k) = X(k+\delta) - X(k) \tag{3.6.3}$$

A process is said to have stationary increments if $\Delta(k)$ is stationary over δ. Changes in the channel parameters have been chosen to match those encountered from actual measurements. This approach has been followed with simulations illustrating equaliser MSE performance during changing fading conditions. To save computation time, steady state MSE values were obtained by time averaging over a short period where chanel conditions were held fixed. Time averaging is thus used to approximate ensemble averaging, although the the channel is not assumed ergodic.

'Maximum eye opening' (MEO) timing provides a benchmark for comparing equaliser performance. MEO timing is used in 34 Mbit/s 4-QAM and 140 Mbit/s 64-QAM receivers to produce figures 3.6.1 to 3.6.3, comparing the tracking performance of 7-tap symbol and 8-tap fractionally spaced transversal equalisers. The application of low (4-QAM) and high (64-QAM) level modulation formats illustrates the addition performance degradation suffered in high level systems. Tracking performance has been calculated with both MP and NMP fade types as the notch depth (defined by equation (2.9.7)) varies from 0 to 40 dB at a constant notch frequency. As the fade deepens, so the MSE value increases for both symbol and fractionally spaced equalisers, consistent with poorer BER performance at the receiver. Already, it would appear that linear equalisation alone will be insufficient to provide acceptable BER performance under all fading conditions. The remainder of this chapter progesses accepting this observation and certain measures will be proposed to provide as near optimum performance as possible. While the use of linear equalisers would thus appear to be limited, the occurrence of very deep fades should be a consideration during network planning. On many links the relative proportion of fades producing unacceptable performance with a linear equaliser is likely to be small. Encouraging results have been reported where a linear equaliser has operated in conjunction with diversity protection [17, 88], particularly using aperture diversity [92]. A further consideration when installing linear equalisation should be the ability of the equaliser to recover from a deep fade i.e. an outage condition may exist, however a situation of unavailability could be avoided if recovery were possible.

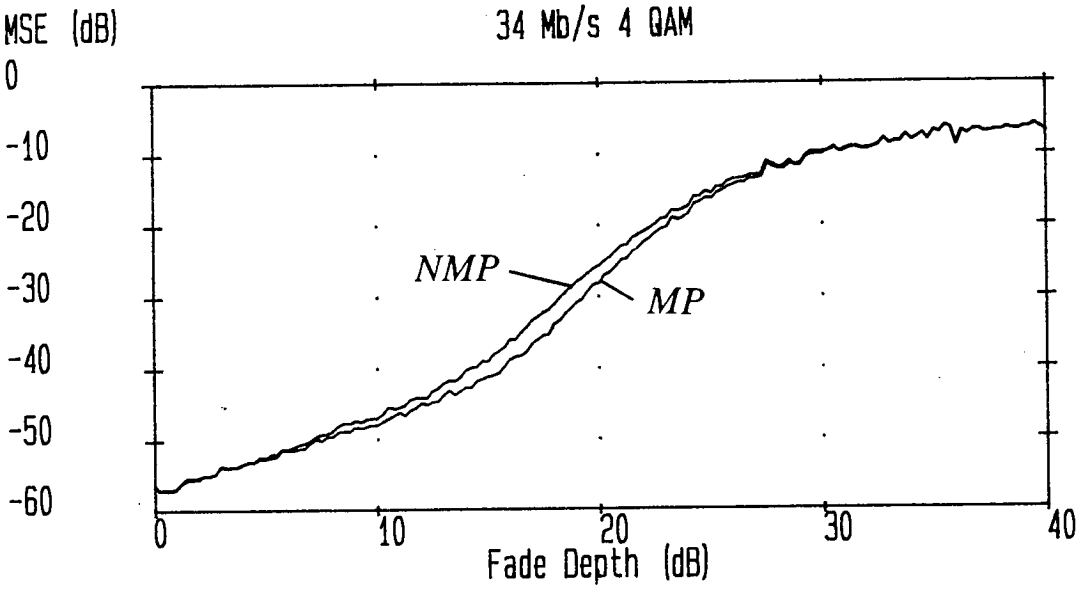

(a) 4-QAM

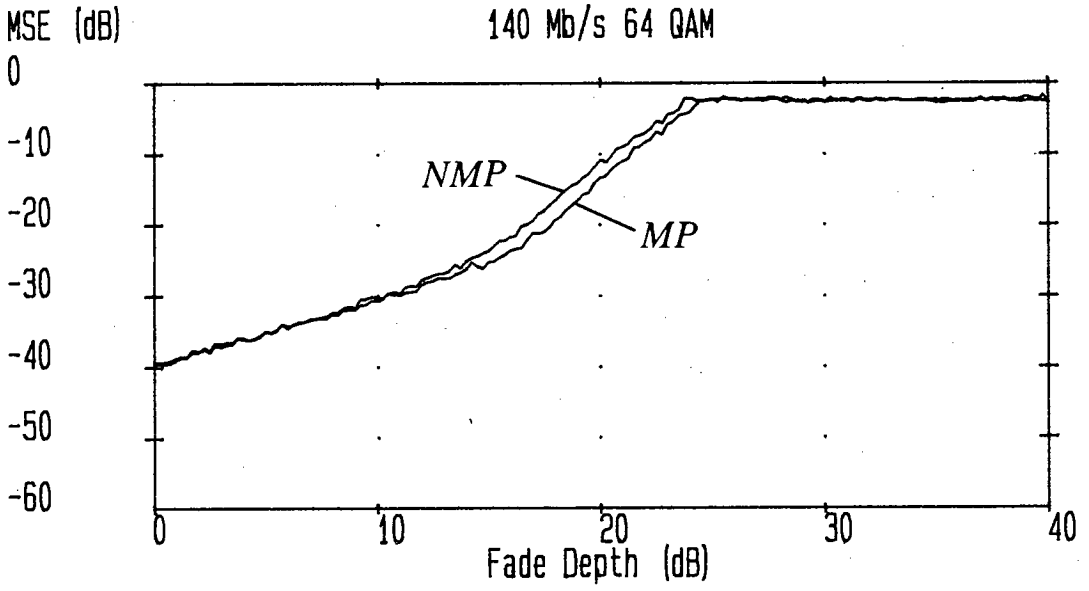

(b) 64-QAM

Figure 3.6.1 Symbol Spaced TE Tracking with MEO Timing

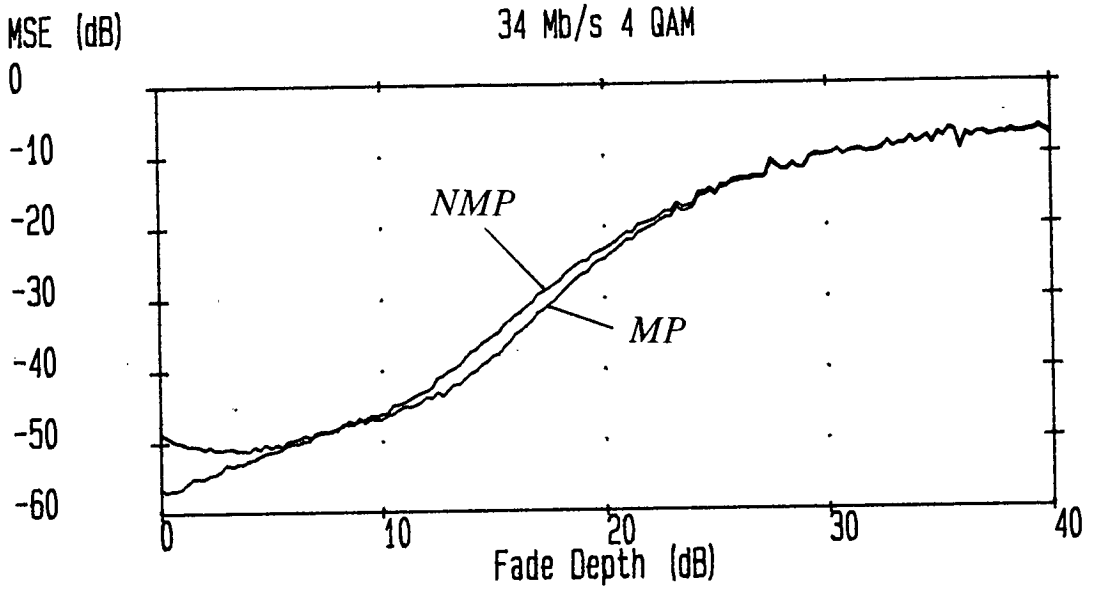

(a) 4-QAM

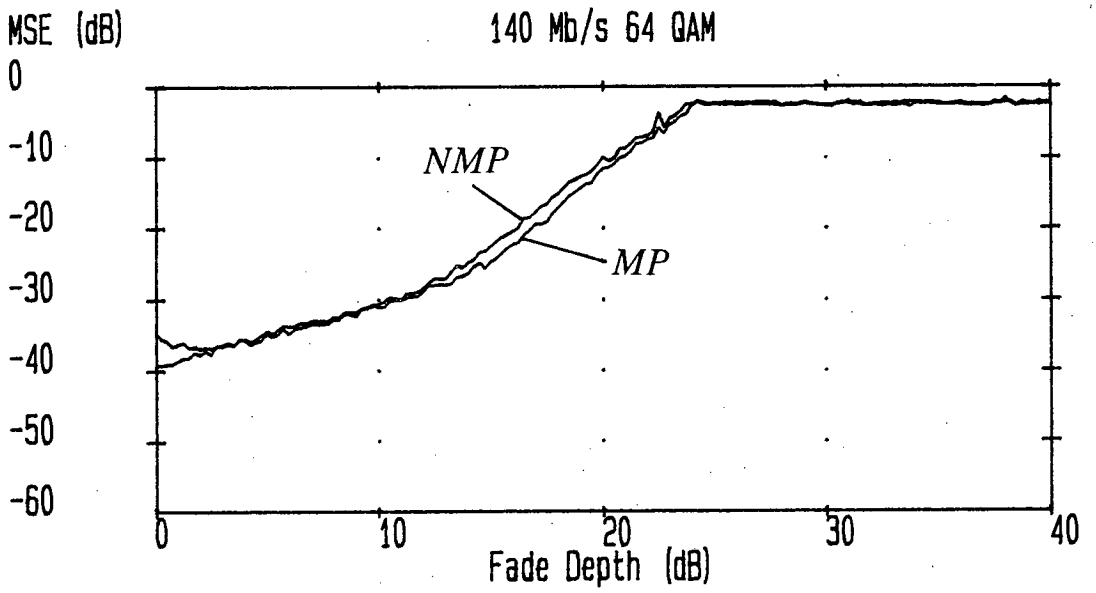

(b) 64-QAM

Figure 3.6.2 Fractionally Spaced Linear Equaliser Tracking with MEO Timing

With figure 3.6.1 for reference, figure 3.6.3 compares performance during a deepening MP fade with the 'MMSE' and 'type A' timing recovery schemes described in chapter 2. Selection of the timing recovery implementation placed emphasis on an all digital receiver, in keeping with current technology trends. Results are given for only the symbol spaced equaliser in a 34 Mbit/s 4-QAM receiver. Assuming suboptimum timing, better results would be expected with fractionally spaced equaliser taps due to time phase insensitivity. In theory, the fractionally spaced equaliser requires only to be frequency locked at the receiver, however the resulting phase roll where timing drifts over a number of symbol periods, increases the overall nonstationarity present within the equaliser loop. Given that MEO timing recovery is based on maximising the eye opening at the decision instant and not on any measure of receiver performance, it might be expected that MMSE timing would have performance at least equal to that of the MEO approach.

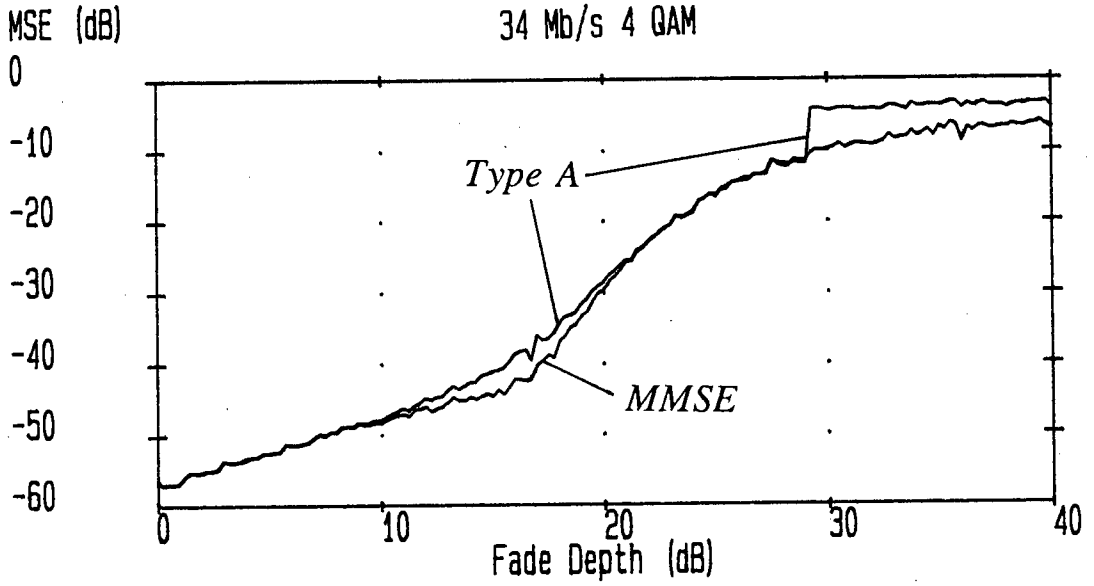

Figure 3.6.3 Symbol Spaced Equaliser Tracking a Deepening Fade with Various Timing Methods: 4-QAM

Simulated results would suggest that further work is required to bound MMSE timing recovery performance, and possibly this technique may not be suitable for use with a high level 64-QAM system. Type A timing had poorest performance, however it's operation assumes symmetrical pulse characteristics. During ideal conditions, type A performance will be near optimal, degradation only occurring as the fade deepens and

the pulse shape becomes asymmetrical.

3.7 DYNAMIC SYSTEMS (2): PHASE TRANSITIONS

The discussion in section 3.6 explored linear equaliser performance during a deepening fade for a single phase type. Measurements from microwave digital radio links have indicated that a channel experiencing a deep fade will have a probability of around 50% of changing from MP to NMP states or vice versa [87]. A worst case situation is now assumed where the channel changes phase state. Once in an NMP state, the notch depth may decrease before retracking back to the MP state.

The effect of a phase transition on real channel impulse response of a 34 Mbit/s 4-QAM signal are illustrated in figures 3.7.1 and 3.7.2. A changing fade condition is represented by a change in the variable b, corresponding to the relative amplitude parameter in the Rummler model (equation (2.9.5)). Values of b range from 0.0 (no fading) through 0.5 (MP fade), with a transition between MP and NMP fades occurring at $b=1.0$. Values of $b>1.0$ correspond to the NMP state. Two effects due to multipath fading are immediately obvious: the reduction in signal power and the shift in the maximum peak position. For correct detection, it is assumed that sampling will occur at the peak eye opening (i.e. MEO timing†). This instant is marked on figure 3.7.1(a), and is dependant on the state of the channel. During a deepening MP fade, the symbol maxima shifts forward in time until the transition point between MP and NMP fades. The timing phase shift is now 180° or $T/2$ from the timing phase calculated under optimum conditions. At the transition point there are now two peaks with similar power levels. A shift back in time of 360° or one symbol period would now be required to continue tracking the symbol peak (assuming that such tracking would ensure optimum performance). Figure 3.7.1(a) was obtained with a bandcentred notch while similar, if less pronounced, effects are observed in figures 3.7.1(b), where the notch is offset at 20 MHz from the bandcentre. This weakening dependance on the offset frequency is illustrated in figure 3.7.2, where the effect of a 20 dB notch (MP or NMP) is examined. As the notch moves away from bandcentre, the effect of the fading on the real channel impulse response diminishes. Distortion increases as the fade sweeps towards the bandcentre, and is symmetrical about this position. One consequence of the fading channel model is that the imaginary component of the overall impulse response increases towards the bandedges. This type of fading situation is examined further in chapter 4 where phase transitions are

† MEO timing takes into account the full complex channel response.

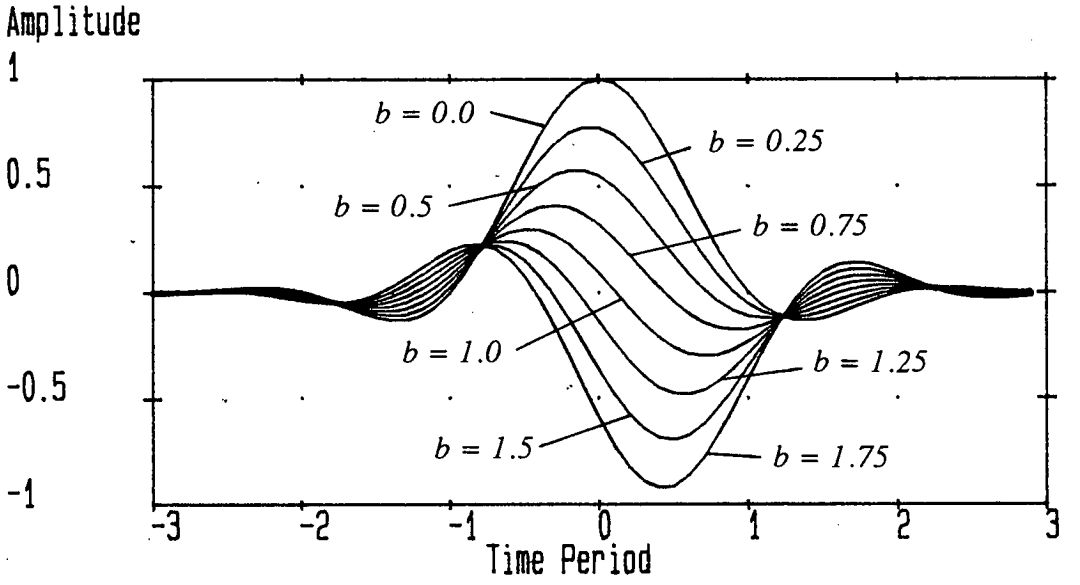

(a) Offset = 0 MHz

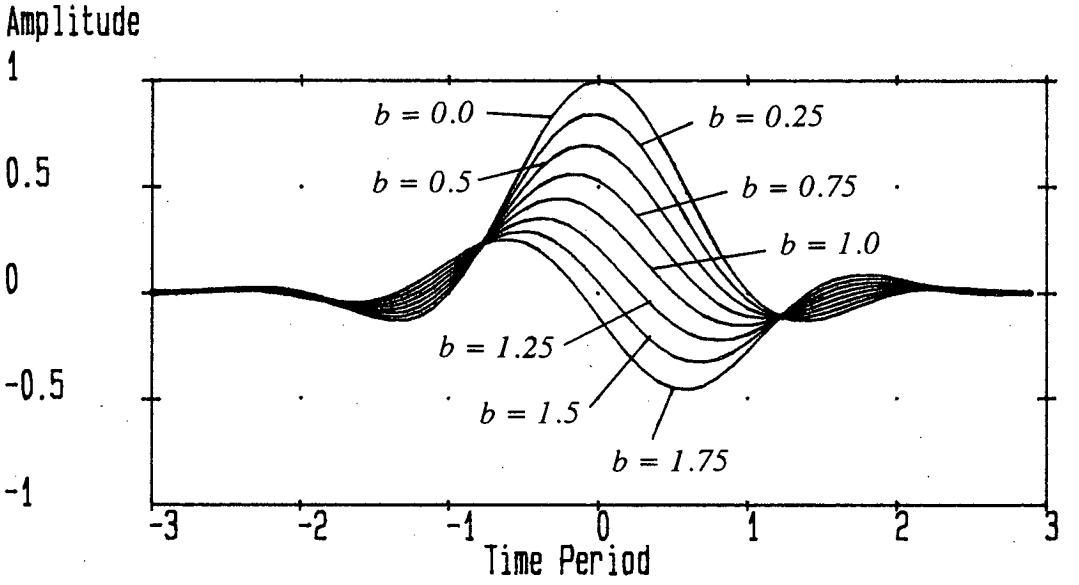

(b) Offset = 20 MHz

Figure 3.7.1 The Effect of Fading on the Real Channel Impulse Response

addressed as a nonlinear equalisation problem.

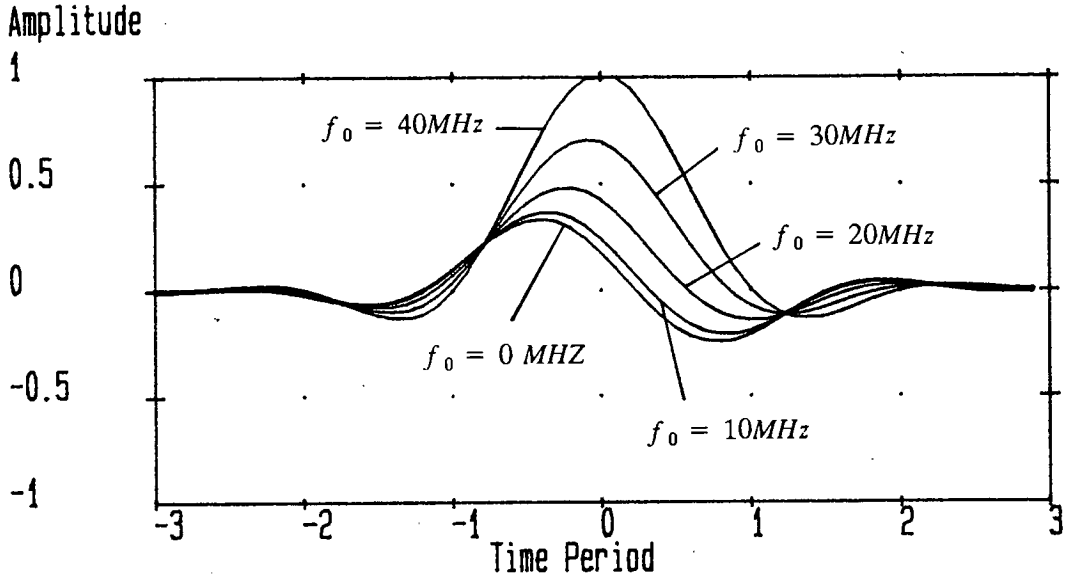

Figure 3.7.2 The Effect of Fading on the Real Channel Impulse Response: Offset = Variable, 20 dB Notch

In practice the jump in timing phase at a phase transition corresponds to a shift in the reference tap position. This approach has been examined by a number of authors, and will be assessed shortly, and again in chapter 4. Such a nonstationarity is untrackable with a real system, and phase transitions remain a fundamental problem. Another investigated solution to the transition problem employed the joint adaptation of equaliser coefficients, timing phase and carrier phase [93]. While some success was reported, the resulting highly complex hardware required nonlinear decision feedback equalisation, and could not be guaranteed to track back from a NMP state.

Figures 3.7.3 to 3.7.5 illustrate the performance of 34 Mbit/s 4-QAM and 140 Mbit/s 64-QAM systems as a bandcentred notch sweeps from MP to NMP states. Equalisation is with 7-tap symbol spaced and 8-tap fractionally spaced transversal equalisers. Timing recovery is implemented by the MEO and 'fixed' techniques. Fixed timing assumes that no attempt is made to track any change in timing phase due to fading, and the phase remains locked to that obtained under ideal transmission conditions. Such a scheme would be difficult to implement, where the timing would be required to be fixed for a period of perhaps seconds. The availability of accurate timing references and suitable damping in the PLL would help rectify this situation.

A novel solution to this problem will be presented in chapter 4. It should be apparent from figures 3.7.3 and 3.7.4 that maximum MSE degradation occurs well before the phase transition at $b = 1.0$, and the receiver performance would be unacceptable. Once in this outage condition, the 64-QAM system cannot recover and retraining would be required when channel conditions had improved. By contrast, the 4-QAM system exhibited ability to regain lock and acceptable performance. An outage condition would still exist during deep fading, however system unavailability may be avoided. To check the validity of results, the optimum Wiener filter solution was calculated for the 34 Mbit/s 4-QAM radio system. General agreement is illustrated by comparing the examples in figures 3.7.3(a) and 3.7.4(a) with figure 3.7.5. As expected, in both instances simulated performance was marginally worse than the theoretical value. With regard to timing recovery, it is interesting to note that during MP fading the use of fixed timing resulted in only marginal performance reduction relative to MEO timing as the fade deepened. Even if accurate timing is maintained, the receiver eye effectively is effectively closed at notch depths greater than 15 dB† [94]. This would suggest that once initial synchronisation has been established, accurate tracking of the pulse peak may not be necessary. When the shift in timing phase has become sufficiently pronounced, distortion is generally too great for the linear equaliser to counter.

It is clear so far that during very deep fading conditions, linear equalisation alone will provide insufficient compensation and other measures will be required. Chapter 4 examines decision feedback equalisation, and results will be presented suggesting that the performance problems encountered during deep fading may be overcome. Recognising the relative implementation simplicity of linear transversal equalisers and their current commercial use, two suggestions arising from this work may go some way to improving linear equaliser performance.

During the course of the work, it was noted that during deep fading, simulated timing recovery circuits provided a poor estimate of the required timing phase and synchronisation could be lost at a phase transition. Where a symbol spaced equaliser is used, one means of limiting (or damping) the tracking ability of the timing recovery circuit is to update phase information according to the following recursion

$$\tau_{k+1} = \beta(k, B_{\max})[\tau_k + \alpha U(k, \tau_k)] \qquad (3.7.1)$$

where $U(k, \tau_k)$ is the timing phase detection algorithm, and $\beta(k, B_{\max})$ is a variable convergence factor, inversely proportional to the notch depth, $B_{\max}$. Approximate knowledge of the channel conditions is required to realise equation (3.7.1), however

† Assuming that timing recovery is performed prior to the equalisation process.

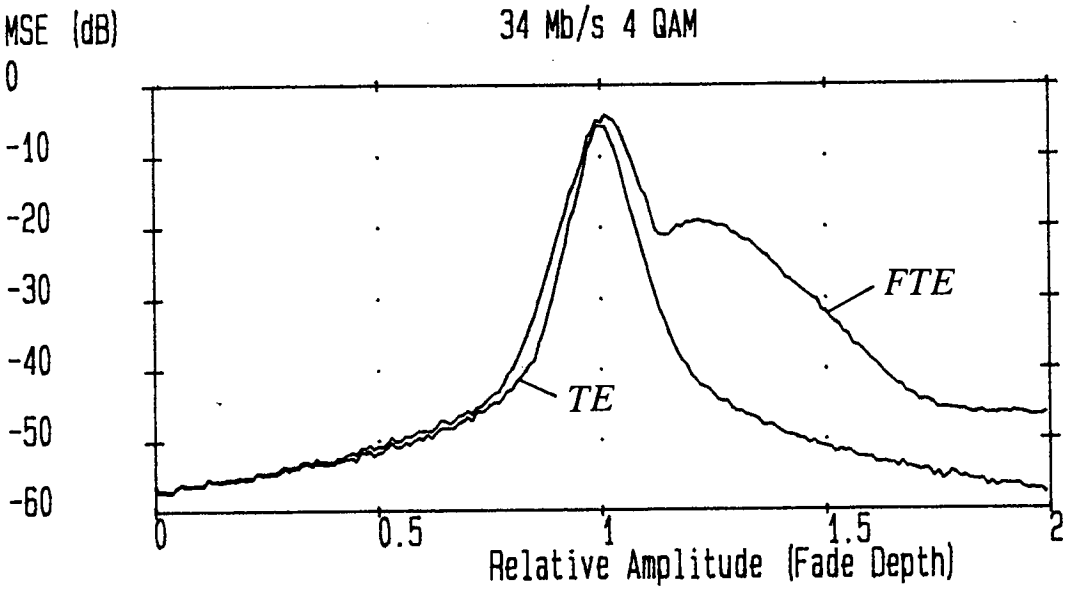

(a) 4-QAM

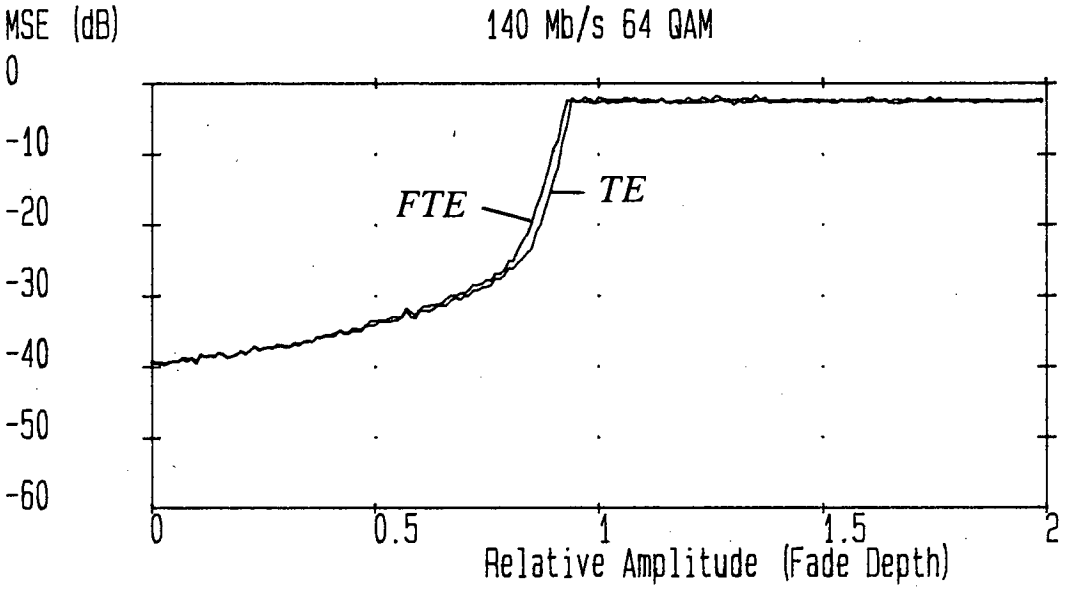

(b) 64-QAM

Figure 3.7.3 Tracking a Phase Transition with MEO Timing

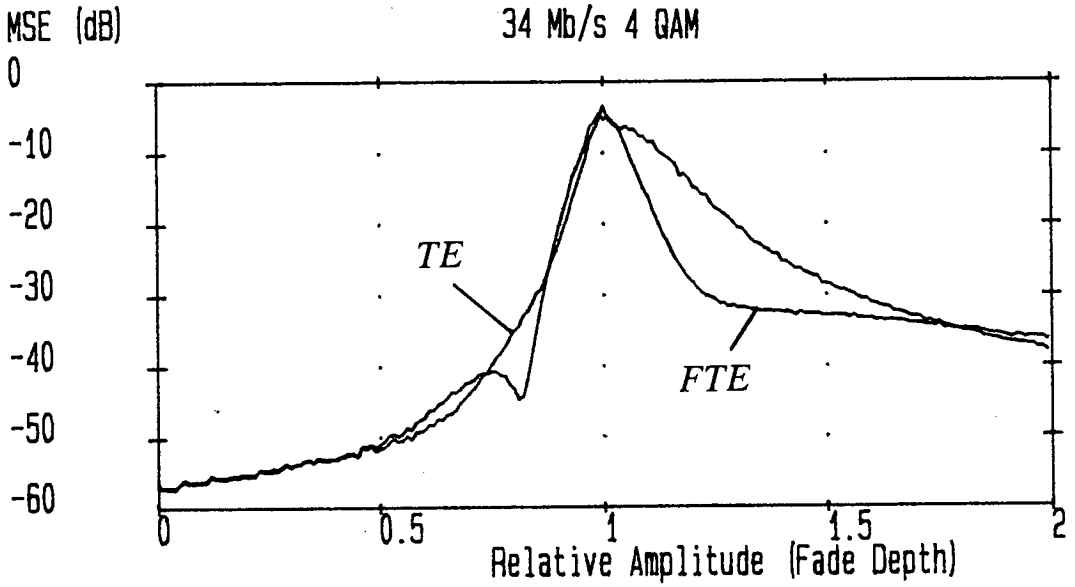

(a) 4-QAM

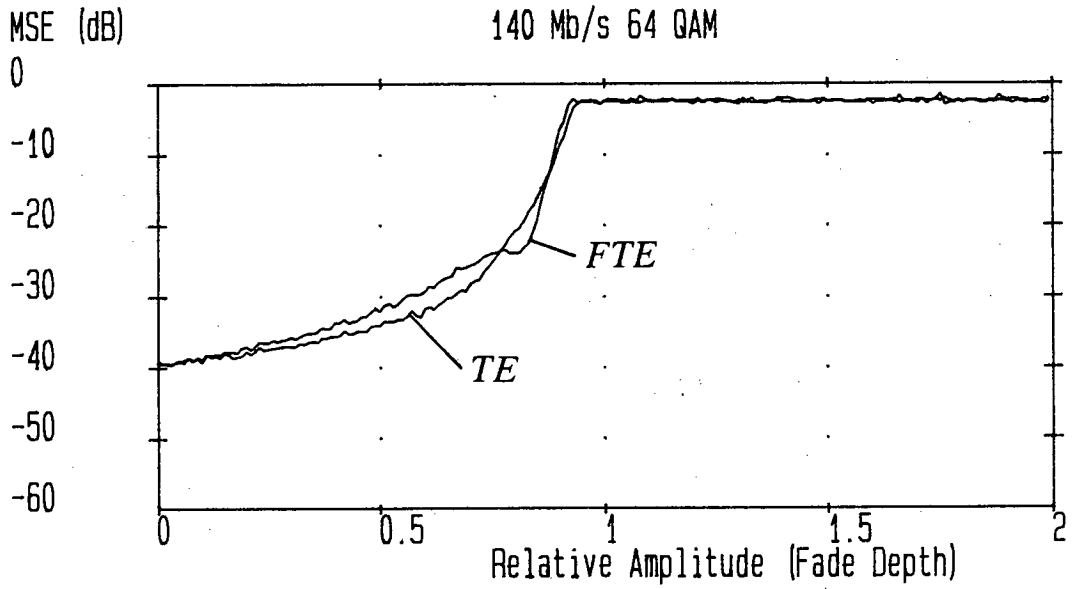

(b) 64-QAM

Figure 3.7.4 Tracking a Phase Transition with Fixed Timing

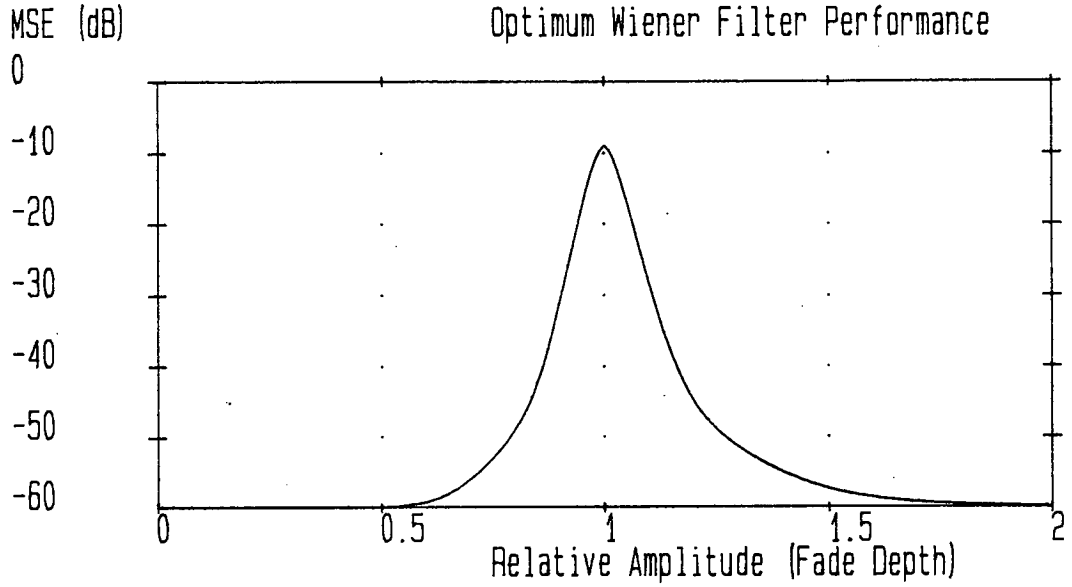

(a) MEO Timing

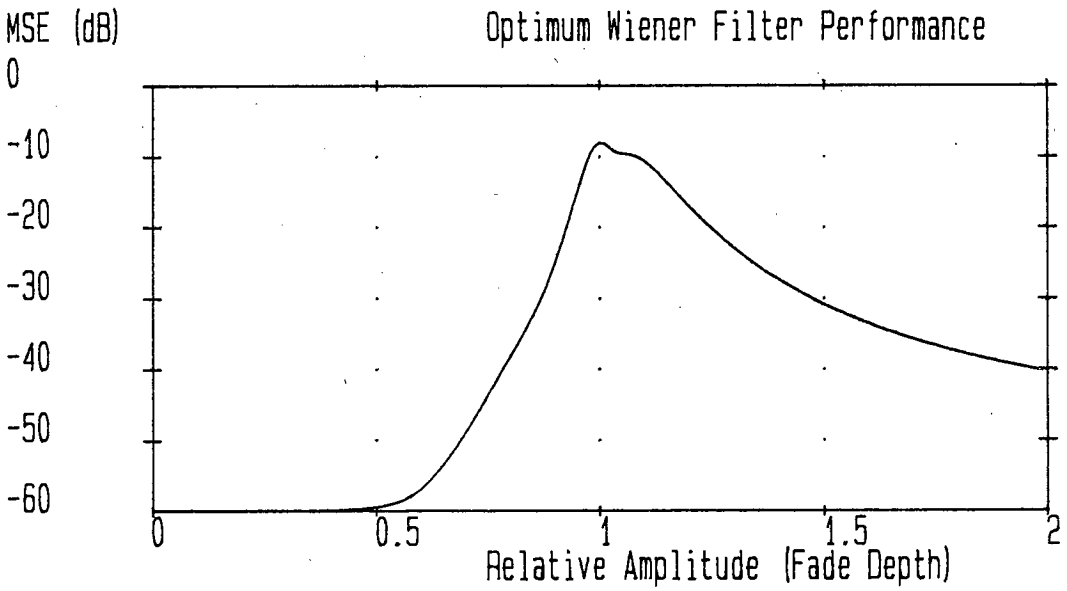

(b) Fixed Timing

Figure 3.7.5 Optimum Wiener Filter Tracking a Phase Transition

amplitude information would be available either from the AGC or at baseband from the equaliser coefficients. Results are presented in chapter 4 where channel information is obtained from a separate channel estimator utilising decisions from the equaliser output.

A second suggestion for further improved performance known as a 'dual-equaliser', still accepts the performance limitations of linear equalisation and would be of primary use to low-level modulation receivers with symbol spaced equalisers. The dual-equaliser is a double equaliser structure exploiting the symmetry of the channel impulse response between fade types about the transition region i.e an MP fade is equivalent to a time reversed NMP fade (figure 3.7.6). The ideal of the dual-equaliser is to have one equaliser configured to track an initial MP fade, the second equaliser would utilise the time reversed coefficients of the first and would be configured for an NMP fade. During a particularly severe MP fade (assumed to predominate), the coefficients of the NMP configured equaliser would be 'frozen'. If a transition from MP to NMP fades occurred, this second equaliser would be available for use. The potential performance of this technique is illustrated in figure 3.7.7 where a transition from MP to NMP fades occurs during the operation of a 34 Mbit/s 4-QAM system. Similar ideas apply to the transition from NMP to MP fades. Operation of the dual-equaliser would require both a certain amount of 'intelligent' decision-making based on the current channel conditions. Figure 3.7.7 was obtained with *a priori* information on the phase transition.

3.8 RETRAINING, HYSTERESIS AND BLIND EQUALISATION

The preceding sections of this chapter have emphasised maintaining the equaliser in lock even if BER performance is poor, providing there is the possibility of regaining acceptable performance and so reduce outage time. The situation is now discussed where retraining is inevitable due to the equaliser loosing lock under very severe fading conditions. Channel conditions will generally have to improve to some extent before reacquisition is possible, introducing a delay or hysteresis into the retraining process. Ideally hysteresis effects should be minimal, otherwise a state of unavailability will persist for possibly a number of seconds.

The conventional decision-directed LMS algorithm exhibits some self learning capabilities. Analysis has shown that in decision-directed operation, the LMS algorithm converges to the optimum tap setting for the noiseless case whenever the eye diagram at the receiver input is open [95]. Otherwise convergence may be towards local minima with subsequent poor BER performance [95].

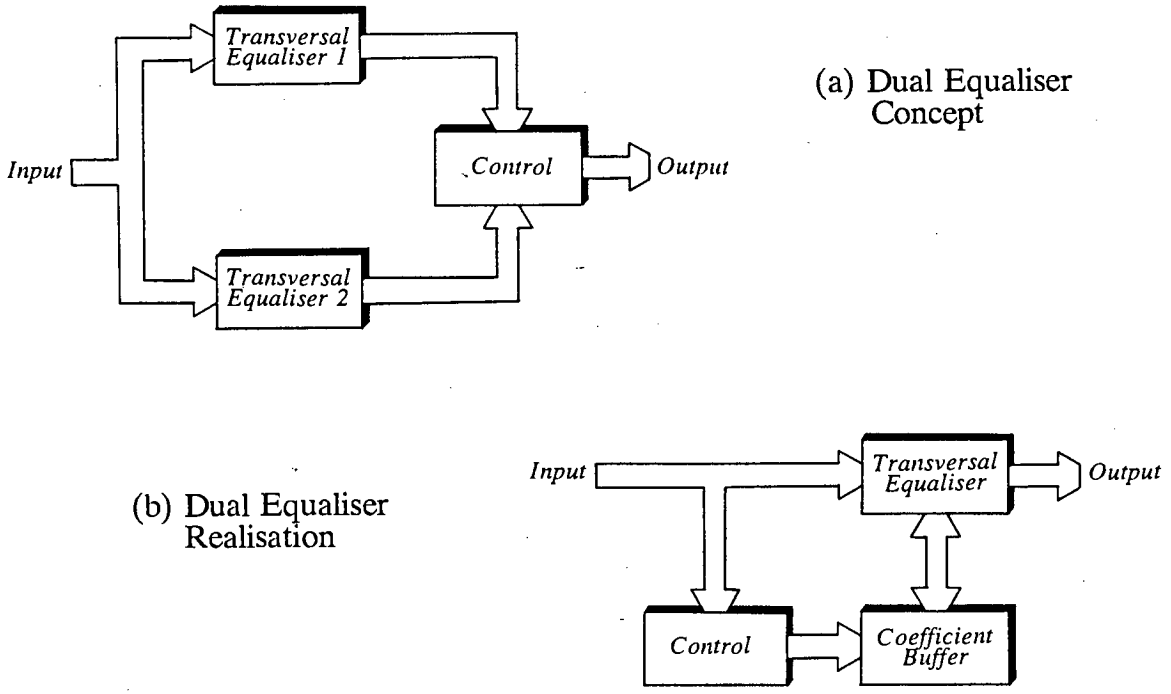

Figure 3.7.6 Dual Equaliser Implementation

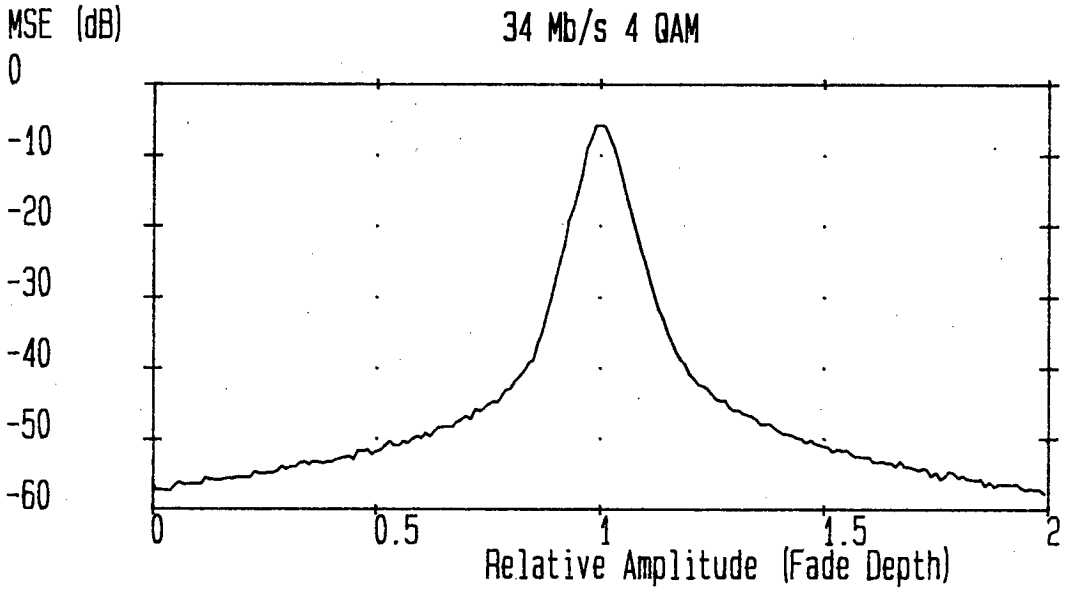

Figure 3.7.7 Dual Equaliser Performance

Figure 3.8.1 highlights a number of problems encountered with decision-directed equaliser startup with the LMS algorithm. Under normal operating conditions, when distortion due to multipath fading is too severe for the equaliser, synchronisation is lost and the equaliser is reset. Equaliser retraining is only possible once channel conditions have improved and the receiver has resynchronised. For the following figures, 34 Mbit/s 4-QAM and 140 Mbit/s 64-QAM receivers are resynchronised with MEO timing and symbol spaced transversal equalisation (7 taps). Results from section 3.7 may be compared with figure 3.8.1, where retraining has been initiated over discrete intervals as channel conditions deteriorate. The unfaded SNR was set to 60 dB in figure 3.8.1. The effect of decreasing the SNR is illustrated by comparing figure 3.8.1(b) with figures 3.8.2(a) and (b), where the SNR was set at 50 dB and 40 dB, respectively. When the equaliser is in lock, the MSE level is generally proportional to the SNR. Interestingly, the region of equaliser failure occurs during the same channel conditions. This would indicate that for typical microwave digital radio receiver SNRs, successful retraining is dependant primarily on the characteristics of the input autocorrelation matrix, $\underline{\phi}_{xx}$. This observation neglects the effect of noise on the receiver synchronisation components, and was made with the assumption that MEO timing had already been correctly derived.

Figures 3.8.1 and 3.8.2 were obtained with decision-directed operation, i.e. no training signal is available at the receiver and decisions made on the equaliser output are assumed to be correct. The time lag between a receiver loosing lock during a deep multipath fade and being able to retrain in decision-directed operation is known as hysteresis. In practice, hysteresis results in increased system unavailability. Blind equalisation techniques are one approach to reducing this unavailability by retraining the equaliser during conditions where channel distortion still persists.

Blind equalisation was originally proposed for voiceband modems [96-98], however such ideas have potential for inclusion in digital microwave radio systems [99, 100]. Techniques have generally evolved by (1) introducing nonconvex cost functions [96-98] and (2) retraining only during certain favourable conditions [100]. The former approach suffers from poor steady state performance in addition to increased convergence times suffered by both approaches. Improvement may be gained by switching back to the conventional decision-directed algorithm after an initial training period [100].

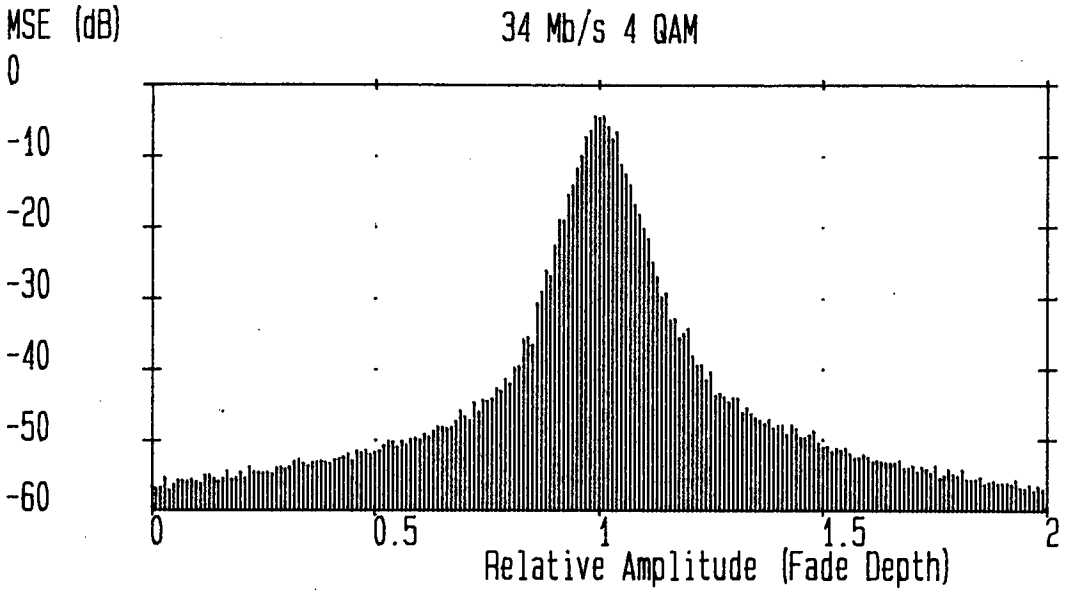

(a) 4-QAM

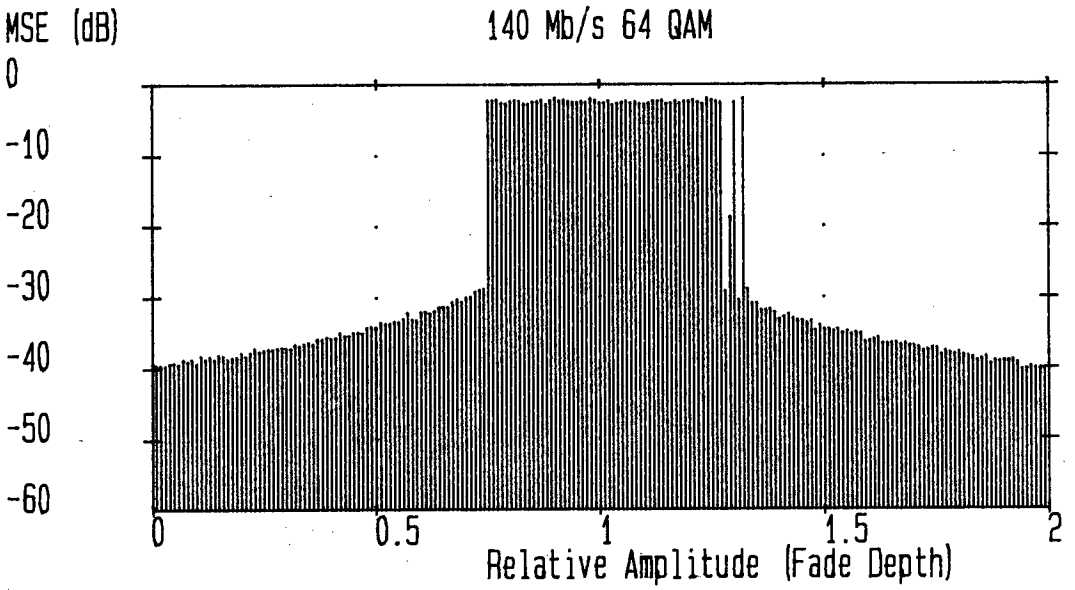

(b) 64-QAM

Figure 3.8.1 Decision-Directed Equaliser Performance

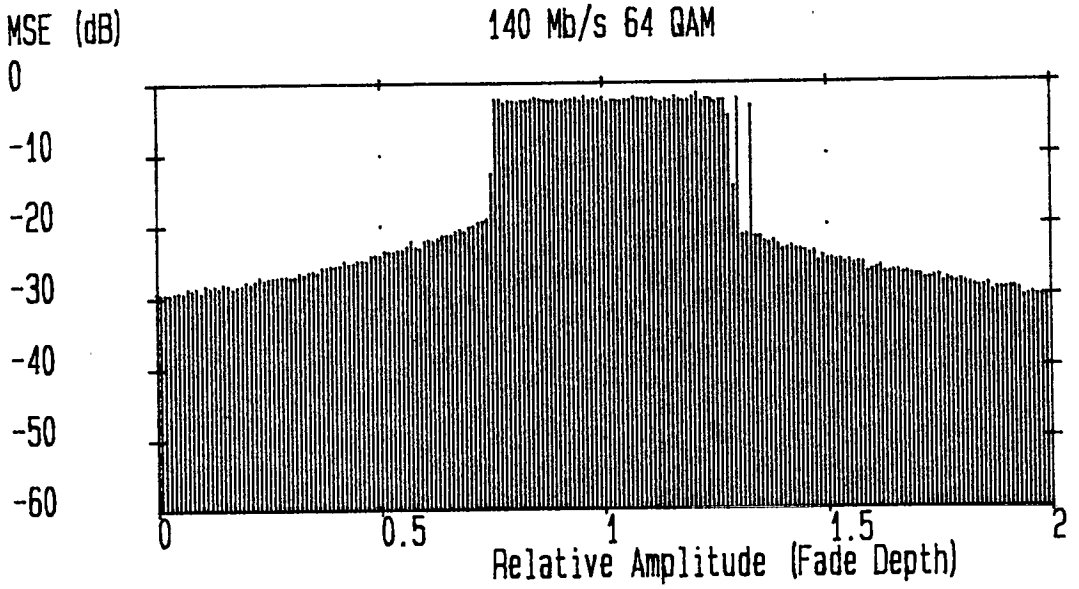

(a) 50 dB SNR

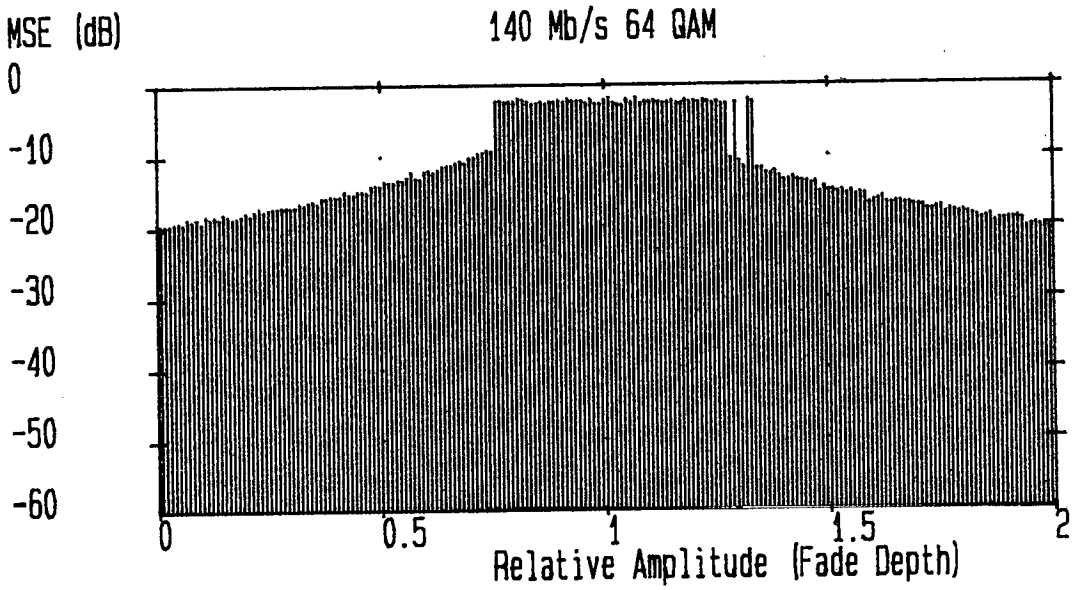

(b) 40 dB SNR

Figure 3.8.2 Effect of SNR on Decision-Directed Retraining

3.9 SUMMARY

In connection with this examination of linear equalisation, a number of conclusions may be drawn, together with suggestions for performance improvement. For network planning in general, linear equalisation alone will be sufficient only for certain routes not prone to very deep fades, typically short overland paths. One of the principle findings of this work is that linear equalisation without other compensation measures, will not provide adequate performance during very deep fades and more advanced techniques are required. Chapter 4 extends the work from this chapter to nonlinear equalisers. Other compensation measures may also be necessary e.g. diversity and coding. While a condition of outage may exist at the receiver, a situation of unavailability may still be avoided.

From simulation results, it would appear that for high level modulation, the MMSE timing algorithm would not justify the relative implementation complexity involved. The most practical approach still appears to be the commonly used 'square-law' method (section 2.6 in chapter 2). The use of fractionally spaced taps increases insensitivity to a poor choice of timing phase. During deep fading, it may be desirable to limit the tracking ability of the timing recovery circuit. An algorithm has been proposed for this purpose.

A dual-equaliser was proposed for low level modulation systems to deal with the problem of phase transitions. For high level modulation formats, the problems of very deep fades and phase transitions still exist and are considered further in the next chapter.

Chapter 4

NONLINEAR EQUALISATION

4.1 INTRODUCTION

Chapter 3 concluded that for high level modulation systems, linear equalisation alone is insufficient to counter very deep fades and phase transitions. Increased performance on links prone to severe fading is available with compensation measures such as diversity or coding (chapter 2). These techniques tend to be inefficient, and hence there are good economic/bandwidth justifications for obtaining greater performance from the adaptive equaliser. To maintain link reliability and reduce outage time, it is essential that the equaliser should maintain good BER performance and not require retraining. The following chapter investigates nonlinear equalisation, in particular the decision feedback equaliser.

Decision feedback equalisers (DFEs) provide the simplest and most common nonlinear equalisation technique. Other nonlinear methods†, currently applied to voiceband modems [59], offer improved performance at the expense of increased implementation complexity. Such techniques may eventually find application to very high modulation systems e.g. 256-QAM. Results based on a 64-QAM DFE receiver indicate that decision feedback equalisation may track the most severe channel conditions, and consequently DFEs are emphasised in this chapter.

† Not necessarily equalisation in the true sense, however the objectives are the same.

4.2 DECISION FEEDBACK EQUALISATION

A pure decision feedback equaliser (DFE) consists only of a feedback filter (figure 4.2.1), where the memoryless detector output is used by the feedback filter to cancel ISI from future outputs on the basis of past decisions.

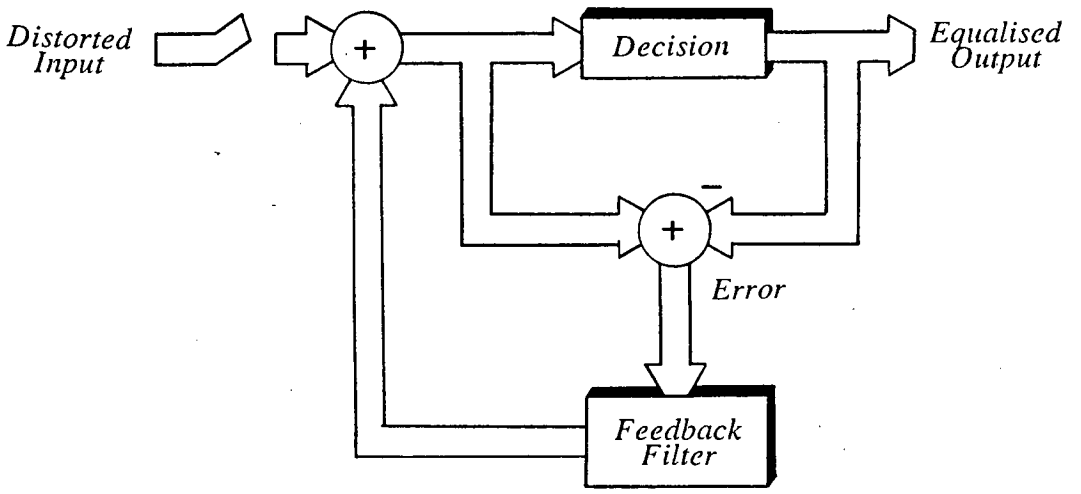

Figure 4.2.1 Pure Decision Feedback Equalisation

The term DFE is generically referred to as the structure consisting of forward and feedback filters as shown in figure 4.2.2. The additional forward filter may be thought of as a prefilter to the pure DFE. An equivalent DFE configuration, known as a predictor DFE, is depicted in figure 4.2.3. For infinite length filters, both structures are equivalent [101].

In the absence of fading, the minimum MSE obtained with an infinite length DFE is equivalent to that obtained with the linear matched filter receiver (equation (3.2.5) in chapter 3). With the addition of ISI, analysis yields a nontrivial expression for the minimum MSE in terms of the channel spectral characteristics [102]. Optimum DFE structures may also be derived by minimising the ZF criteria and BER [101]. When the constraints of finite length are applied to the DFE filters, the optimum DFE solution may be found as an extension of the optimum linear Wiener filter. Appendix C derives this optimum solution by assuming that decisions from the equaliser output are correct. From appendix C, the optimum set of feedback coefficients may be expressed as

$$\underline{b}_{opt} = -E[\underline{y}(k-d-1)\,\underline{x}^T(k)]\underline{c}_{opt} \qquad (4.2.1)$$

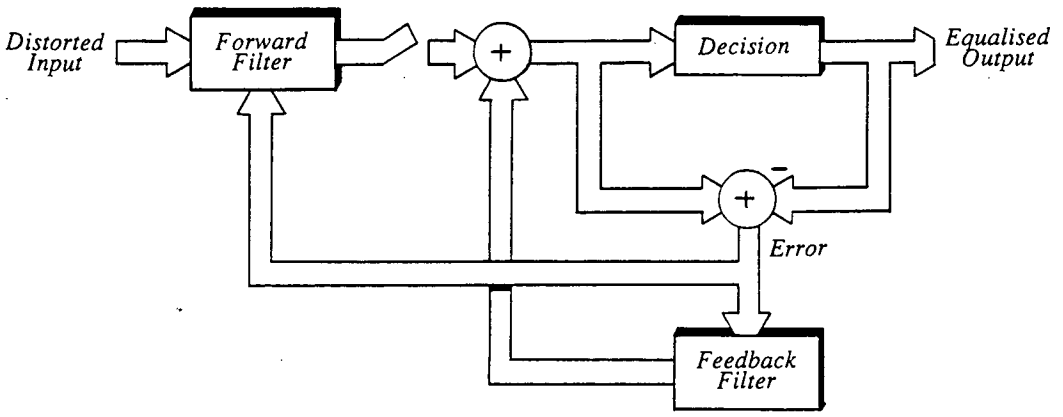

Figure 4.2.2 Conventional DFE

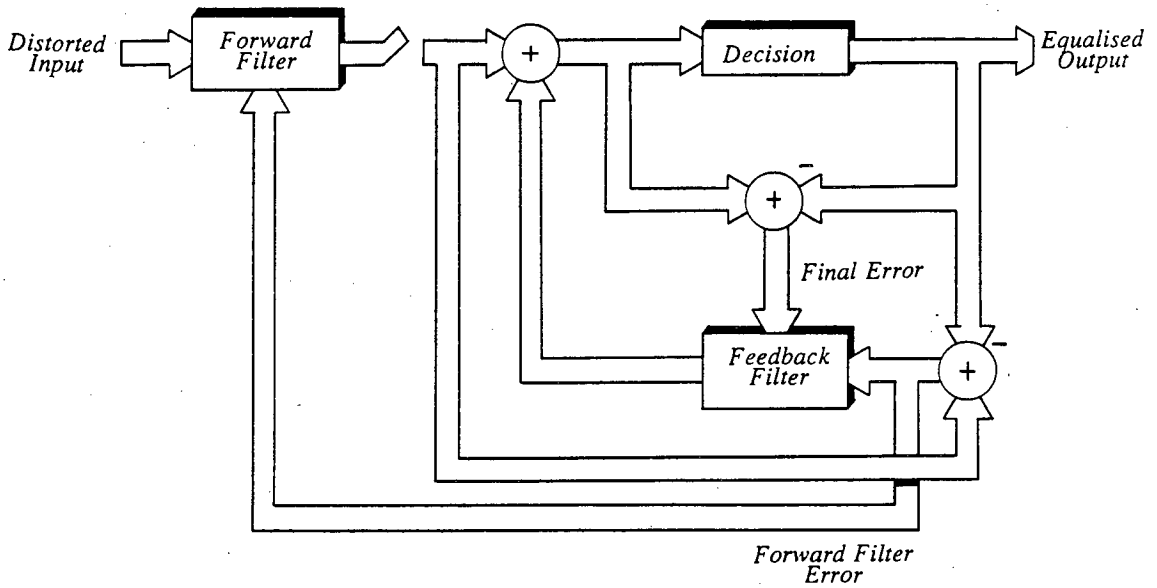

Figure 4.2.3 Predictor DFE

The solution to the feedforward coefficients is similar to section 2.7, except that the autocorrelation matrix, $\underline{\phi}_{xx}$, excludes the span of the feedback filter

$$\underline{\phi}_{xx} = E[\underline{x}(k)\underline{x}^T(k)] - E[\underline{x}(k)\underline{y}^T(k-d-1)].E[\underline{y}(k-d-1)\underline{x}^T(k)] \qquad (4.2.2)$$

where d is the delay through the equaliser. The cross-correlation vector is now defined by

$$\underline{\phi}_{xy} = E[\underline{x}(k)y(k-d)] \qquad (4.2.3)$$

The normal DFE configuration is with the last forward tap as the reference position. When retraining a DFE with, for example, 5 forward taps, the forward coefficient vector would therefore be $[0\ 0\ 0\ 0\ 1]^T$. In terms of the received impulse response, the feedforward filter equalises leading echoes (future terms in the received impulse response), while trailing ones (past terms) are largely cancelled by the feedback filter. A DFE with a reference tap taken at the centre of the forward filter would effectively result in a combination of a linear transversal equaliser and a pure feedback equaliser. No obvious advantage was found from this configuration and it is considered no further. The last forward tap is generally taken as the reference position for simulations. A number of authors have also considered the reference tap position (RTP) as the second last feedforward tap [103, 104]. A degree of freedom is then allowed should the RTP be required to shift during a phase change.

One 'favourable' aspect of the microwave radio channel during fading is that the received impulse response is not widely dispersed in time. Correspondingly few taps are sufficient for forward and feedback filters (voiceband modems might typically require 8-20 feedback taps [105]). Typical overall tap lengths for microwave digital radio are from 5-10 taps, configured as, for example, 3 forward and 2 feedback taps [103], (a (3,2) DFE)† or 5 forward and 5 feedback taps (a (5,5) DFE) [93]. The forward taps of the DFE may also be fractionally spaced in a similar manner to the linear fractionally spaced transversal equaliser (FTE), and tap spacing is taken as $T/2$ during simulations. Again, the set of optimum coefficients excludes the span of the feedback filter. Results from a $3T/4$ spaced DFE may be found in work by Shafi and Moore [69], and Herbig [106].

A potential problem with decision feedback equalisation is the error propagation effect induced by feeding back wrong decisions. A few authors have derived bounds on the error recovery time required for the DFE to resume correct operation [107, 108], however it has also been suggested that these bounds may be pessimistic [109]. Certainly results presented in this chapter indicate considerable performance

† This notation is used from now on to describe the DFE tap configuration.

gain with DFEs compared with linear equalisation. If the MSE remains sufficiently low, the likelihood of a wrong decision at the equaliser output is minimised. Errors do occur during deep fading, however the effects should not be regarded as catastrophic for single errors. This observation is consistent with work by Taylor and Shafi who reported error bursts in the performance of a (3,3) DFE while attempting to correct a 40 dB MP notch [110].

4.3 OTHER NONLINEAR RECEIVER STRUCTURES

Decision feedback equalisation provides the simplest nonlinear compensation against multipath fading for microwave digital radio applications. Other, more complex methods are possible and two are now briefly reviewed. Neither are pursued any further in this work, however it should become apparent that a wider performance perspective may be taken when considering equalisation systems.

ISI cancellers may be considered as an extension to the concept of cancelling ISI using past symbols (the idea behind decision feedback equalisation) to future symbols as well. Mueller and Salz [111] actually considered optimum linear and decision feedback equalisation within the general framework of an ISI canceller aided by past/future values. An ideal ISI canceller preceded by an adaptive matched filter, may achieve the optimum MSE bound for no distortion. A fundamental assumption/problem with this ideal situation is that tentative (future) decisions are correct. If this were always true, there would be little need for the ISI canceller.

Two problems exist for high speed microwave digital radio applications: (1) the additional hardware requirements and (2) the effect of wrong decisions on the final BER is still unclear [29, 65]. An intuitive solution to the requirement for correct decisions is with 'soft' decisions i.e. a decision based not just on a single data symbol. This leads to the concept of maximum-likelihood sequence estimation.

True maximum likelihood sequence estimation (MLSE) is based on correlating a complete received data sequence with all possible transmitted messages and selecting the greatest correlation. The classical maximum likelihood receiver consists of M^J matched filters, where J is the message length and symbols may take one of M possible values. Clearly, computation increases exponentially with with message length, and the method is generally impractical. The Viterbi (VA) algorithm provides a reduced state means of implementing marginally suboptimum MLSE. Complexity is now exponentially dependant on the duration of the impulse response i.e. the problem has now reduced to symbol-by-symbol detection, however implementation is still prohibitively complex for high speed applications. Intuitively, MLSE techniques should

provide improved performance over simpler nonlinear equalisation (DFEs). Results from Proakis [25] agree with this proposition, however work by Falconer [112] favours adoption of DFEs in preference to MLSE for HF channel applications. This may in part reflect the nonstationarity associated with the HF channel.

4.4 TIMING RECOVERY CONSIDERATIONS

In general, symbol spaced decision feedback structures are less sensitive to changes in timing phase relative to conventional, symbol spaced, linear equalisers. Salz [113] demonstrated that the DFE is more able to compensate for destructive nulling due to aliasing in the Nyquist band. In terms of ultimate BER performance, this timing insensitivity may not translate into actual performance gain because of increased error propagation in the feedback filter[65]. To cancel a spectral null resulting from inaccurate timing, the feedback filter requires a relatively long number of taps with potentially large magnitudes [65]. Timing recovery techniques discussed in chapters 2 and 3 may be applied to symbol spaced DFEs. An additional technique proposed for DFEs, is to obtain timing information from the first feedback tap [105]. Early sampling forces the first feedback tap positive, while late sampling forces the tap negative. The resulting control signal then drives a DPLL.‡

4.5 GENERAL DFE DYNAMIC TRACKING CHARACTERISTICS

This brief section presents results illustrating DFE performance during a deepening fade. Comparison with results in section 3.6 immediately conveys the superiority of DFEs for the simulated channel conditions. An initial observation is that DFE convergence is generally faster when compared with linear equalisation, as illustrated in figure 4.5.1. A 7-tap symbol spaced transversal equaliser and a (4,3) DFE are retrained on channel **B** defined in table 5.5.3† for a 34 Mbit/s 4-QAM digital receiver with MEO timing. The receiver is assumed to have been correctly resynchronised prior to equaliser retraining, a reasonable assumption for the degree of fading present. In theory, faster convergence should result in improved tracking performance, although this argument should not be regarded as rigorous and no assumptions of this nature were made when obtaining the simulation results.

‡ An initial timing phase is still required during initial retraining from an alternative source e.g. a square law device.
† As pointed out in chapter 3, the exact channel characteristics in table 5.5.3 are of more direct relevance to the analysis in chapter 5.

Figure 4.5.2 compares receiver performance during a bandcentred MP fade, deepening at 100 dB/s. An unequalised system is compared with a (4,3) DFE and a 7-tap symbol spaced transversal equaliser. Results are for a 140 Mbit/s, 64-QAM receiver with MEO timing. From this direct comparison, the DFE offers considerable performance gain over the the other systems and were the channel to remain in an MP state, the DFE would provide near a near optimum solution. Figure 4.5.2 is rather misleading, for with the advent of a phase transition, a catastrophic error condition occurs, decision feedback equalisation collapses, and the receiver would require retraining once channel conditions had improved. Results such as figure 4.5.2 provided early encouragement to further examine the DFE structure as a means of obtaining acceptable performance during deep fading. Section 4.6 now examines in detail the effects of phase transitions on various DFE structures.

4.6 DFE PERFORMANCE DURING SEVERE FADING CONDITIONS

Decision feedback equalisers are now considered according to the tap spacing in the forward filter i.e. symbol and fractionally spaced. Symbol spaced DFEs are simpler to implement, however it will become apparent that considerable benefits arise from fractionally spaced taps.

4.6.1 Symbol Spaced DFEs

One conclusion reached in chapter 3 was that phase transitions still remain a fundamental problem for high level modulation microwave digital radio systems. In fact, the linear equaliser performance had already degraded to such an extent that the effect of the phase transition on the 64-QAM system was indiscernible. The 'dual equaliser' and shifting the RTP provided a potential means of overcoming the transition for low level modulation formats, however for higher levels, a more powerful equalisation measure is required.

Figure 4.6.1 illustrates for 34 Mbit/s 4-QAM and 140 Mbit/s 64-QAM systems, a (4,3) DFE tracking from unfaded conditions ($b=0.0$), through the transition region ($b=1.0$) to a relatively shallow NMP fade ($b=2.0$).

Some deterioration in NMP performance occurs, relative to the equivalent MP fade depth. Comparison with figure 3.7.3(a) reveals some performance gain with a linear transversal equaliser in the shallow NMP region, however this is not large. A less desirable result was obtained for the 64-QAM system, where a catastrophic error condition occurs at the transition

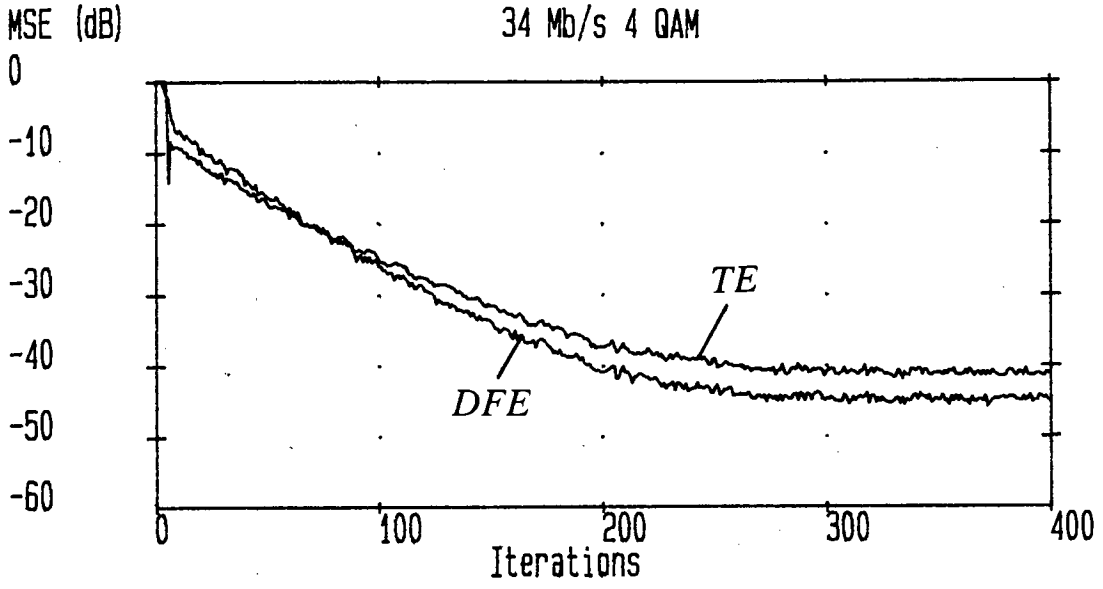

Figure 4.5.1 Comparison of Equaliser Convergence

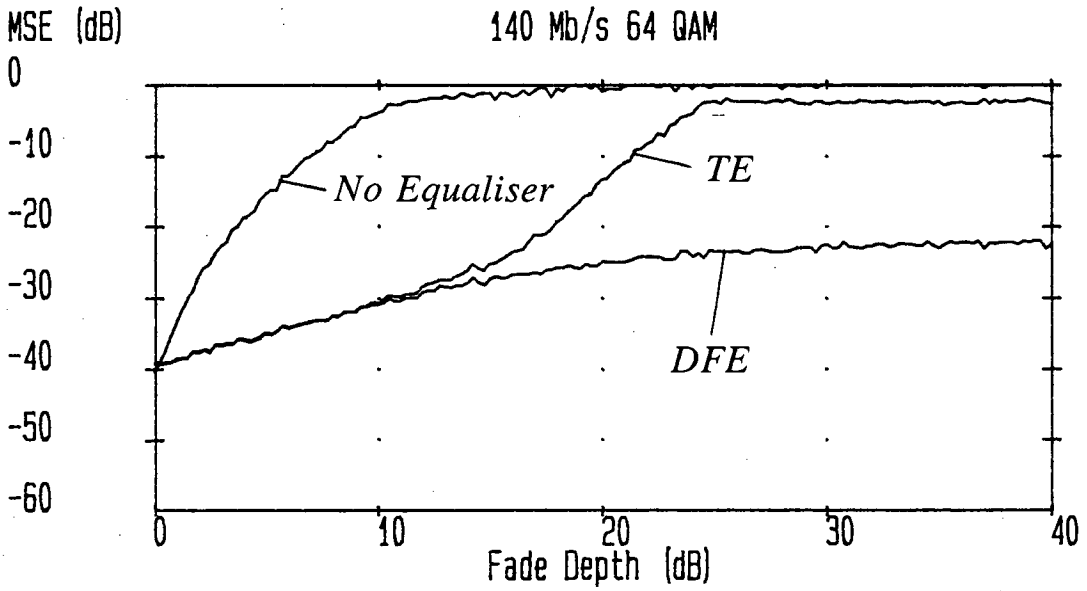

Figure 4.5.2 Comparison of Tracking Performance

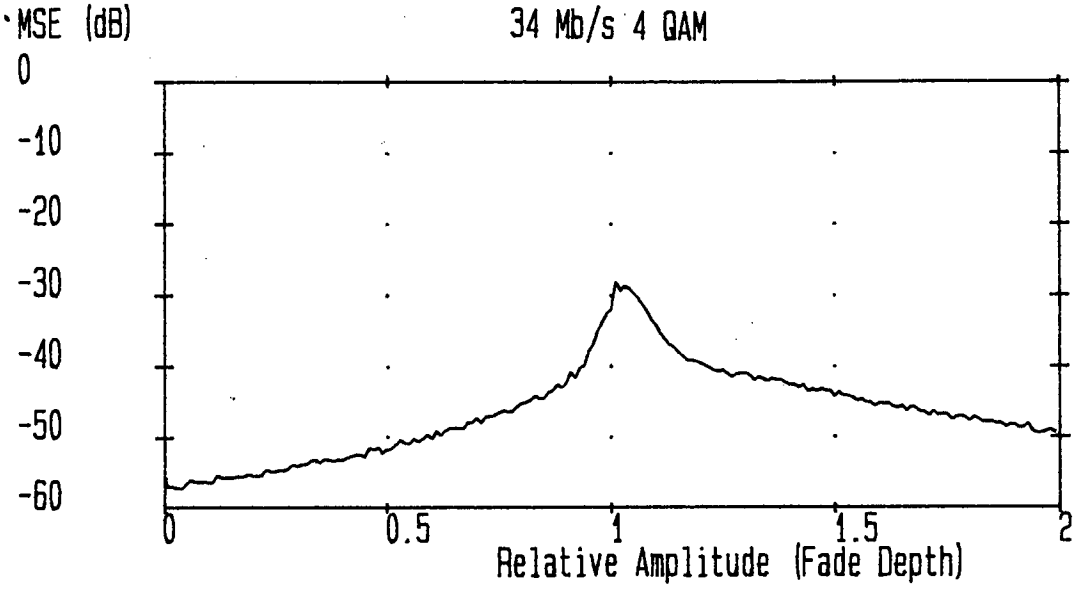

(a) 4-QAM

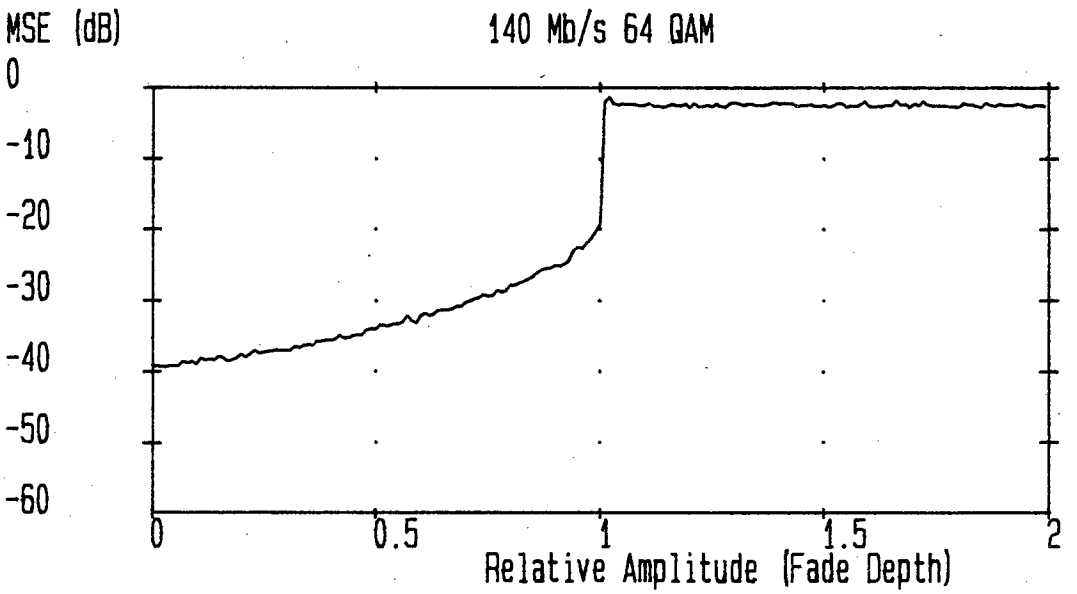

(b) 64-QAM

Figure 4.6.1 DFE Tracking a Phase Transition with MEO Timing

point and the equaliser is unable to recover.

At the transition between phase types, the timing phase derived with MEO timing undergoes a shift of approximately one symbol period or 360°, so that the equaliser is now synchronised to the first precursor [69]. This change may either be viewed as a shift in timing phase or a shift in RTP without the jump in timing. Neither situation is desirable, for any sudden change in either RTP or timing phase will appear nonstationary relative to the prevailing channel conditions. Severe demands will be placed on the adaptive equaliser; too severe in the case of the 64-QAM system. Should a shift in RTP be required the RTP should be set as the second last forward tap to accommodate the shift. Simulation results (not included) indicated that some degradation was introduced during MP tracking, and that phase transitions still remain a problem.

One recent proposal for improving DFE performance (applied to mobile radio channels) is superficially similar to the 'dual equaliser' in chapter 3, and is based on making 'soft' decisions at the DFE output [114]. The resulting structure provides an interesting link with (near) maximum-likelihood detection methods and might have received greater consideration for microwave digital radio applications, but for the potential of fractionally spaced DFEs discussed in the following subsection. The 'soft decision' DFE (figure 4.6.2) consists of a common forward filter providing an input to two parallel feedback filters. The feedback loops are identical, except for the possibility of inverting the decision of the second if the output of the forward filter is close to a decision threshold and therefore possibly wrong. If the second decision is inverted, the two feedback loops run independently for a period δ, and by summing the error magnitude over δ, an estimate of the most accurate configuration is obtained. Should the second feedback filter provide the lowest error, the feedback coefficients and the contents of the delay line $Z^{-\delta}$, are copied across to the first feedback section and the final decisions are taken as the output from the first loop. Results from the 'soft' decision DFE indicate slightly improved results over a conventional DFE operating in reference directed mode [114]. The major disadvantage of this structure are the uncertain effects of successive errors and the additional hardware requirements, although all operations are implemented at the symbol rate.

4.6.2 Fractionally Spaced DFEs

Results from using symbol spaced DFEs and MEO timing in section 4.6.1 were mixed, as the problem of phase transitions still remain for high level modulation systems. Application of a fixed timing phase is a different approach to the problem for

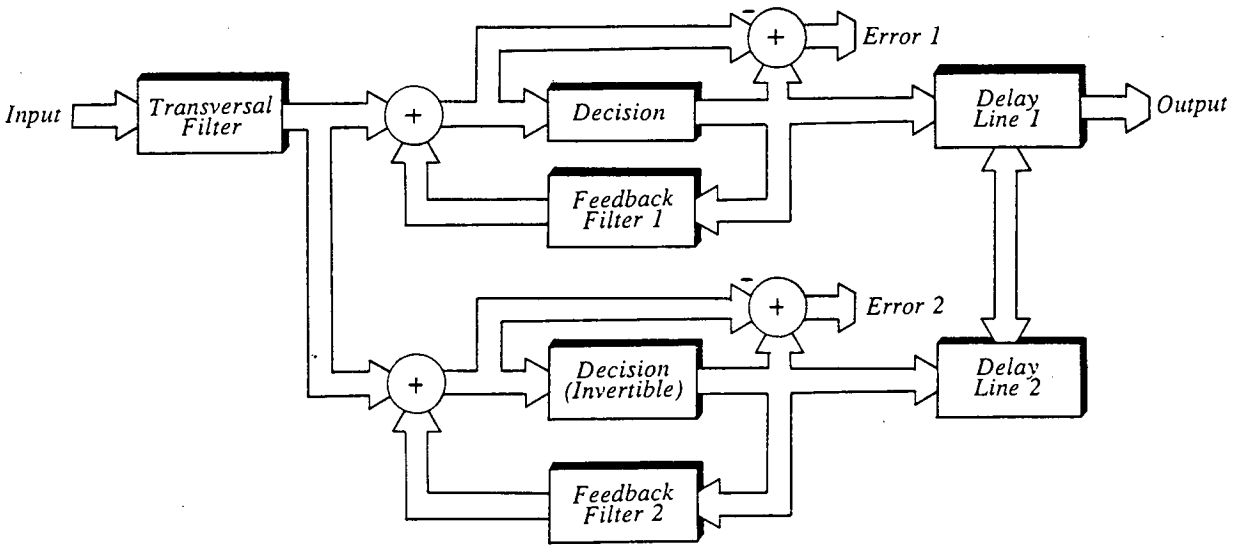

Figure 4.6.2 'Soft Decision' DFE

no attempt is now made to track changes in the timing phase due to multipath fading. The apparent suboptimum timing is countered by sampling and processing at greater than the symbol rate and exploiting the timing phase insensitivity of equalisers with fractionally spaced taps. Heuristically, the equaliser now has greater ability to manipulate a channel not widely dispersed in time.

Results are now presented for a fractionally spaced DFE, with forward taps spaced by $T/2$ and the same overall time span as the symbol spaced DFE. An equivalent structure consists of two symbol spaced forward filters offset by $T/2$, each with 5 taps, and a 3 tap feedback filter. In the adopted notation, this may be written as a (5,5,3) FDFE. A longer forward filter produces diminishing returns in terms of performance gain, while a short filter may be insufficient to track severe fades. The relatively short feedback filter helps reduce potential error propagation problems. Should MEO timing be employed, FDFE performance is acceptable until the transition region where performance, like the symbol spaced DFE, collapses (figure 4.6.3(a)). Figure 4.6.3(b) is a more promising result, for now the FDFE with fixed timing tracks continuously through the fade transition. MSE performance degrades to a maximum of approximately -15dB, and while some errors may occur, the equaliser remains in lock. Interestingly, the maximum MSE occurs on the NMP side of the

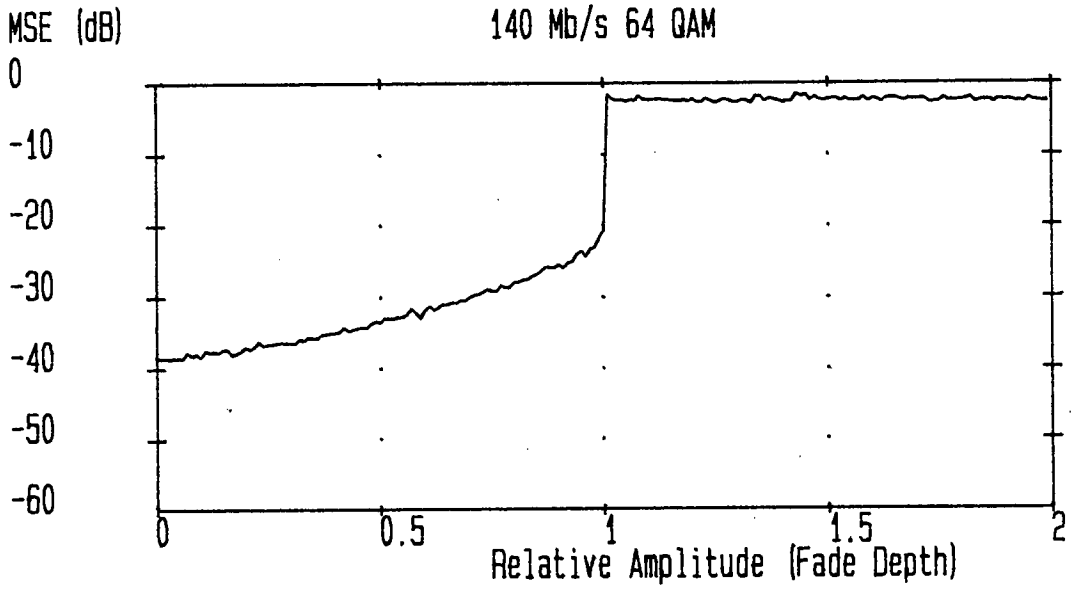

(a) MEO Timing

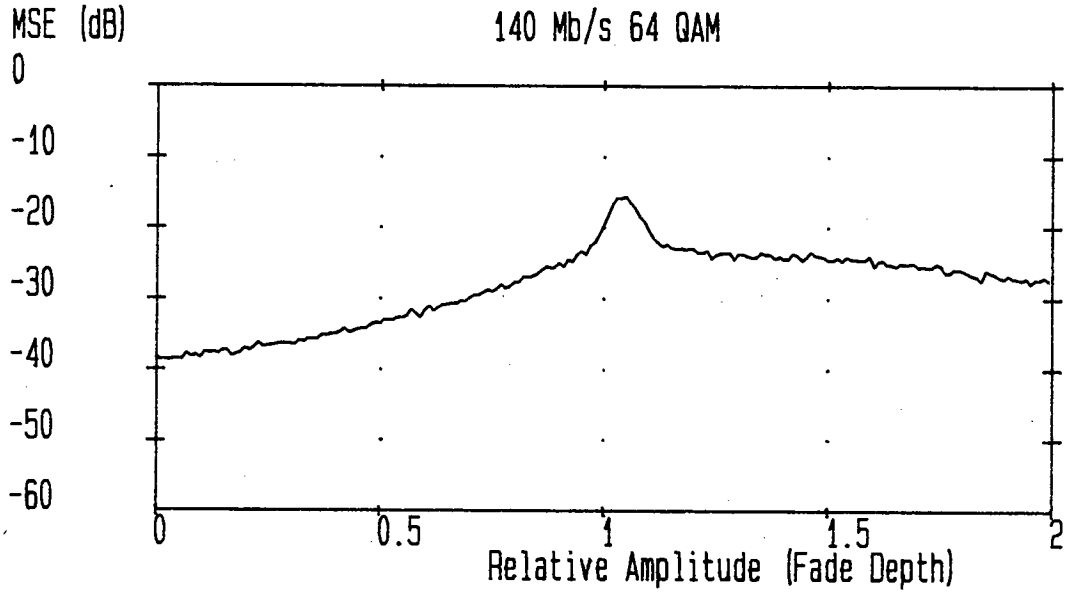

(b) Fixed Timing

Figure 4.6.3 FDFE Tracking a Phase Transition (RTP=0)

transition region, an observation also noted by Olmos et al [104]. Results in figure 4.6.3 were obtained with the reference tap set as the last forward filter tap. Similar performance trends were noted when the second last forward tap was taken as the RTP, although overall performance was slightly inferior around the transition region. The fractionally spaced DFE configuration adopted by Herbig [106] employed the second last forward tap as the RTP, however the overall approach taken was slightly different to that adopted here. Tap spacing was set as $3T/4$, while timing was based on an IF square law method. A jump in timing phase is still necessary at the transition instant, with the associated nonstationarity problems this entails.

The encouraging tracking performance in figure 4.6.3(b) was obtained with a fade changing from MP to NMP states. A more realistic situation would be to consider the fade changing back to an MP state prior to normal unfaded propagation conditions. Results from this scenario are illustrated in figure 4.6.4, for notches occurring at 5 and 10 MHz offset from the bandcentre. As also noted by Olmos [104], a fade slightly offset from bandcentre represents a potentially more severe fading condition than a bandcentred fade, as the overall channel impulse response now consists of real and imaginary components. Horizontal axis in figure 4.6.4 are in terms of relative amplitude, b, and range in magnitude from $b=0.0$ (no fading) to $b=1.5$ (6 dB NMP notch). With both channel conditions, the equaliser is able to track through the phase transitions without excessive MSE. Greater MSE degradation at the transition regions is present in figure 4.6.4(a), indicating that the effect of phase transitions diminishes as the notch moves away from the bandcentre. Examination of the (dominant) equaliser tap values for the channel conditions in figure 4.6.4(a), reveals that greatest change occurs between $1.0 \leq b \leq 1.1$ (figure 4.6.5). The change in dominant tap weights, as the initial RTP changes, also corresponds to the critical (maximum) MSE occurring approximately at a 30 dB NMP fade depth. Results were obtained with an unfaded SNR of 60 dB. At lower, SNRs the equaliser had difficulty tracking back from a NMP fading condition. While appearing to be a limitation, the unfaded SNR adopted is realistic for microwave digital radio [115].

Preceeding results have examined changes in a notch at a fixed frequency (offset from bandcentre). In practice the notch would likely be changing in frequency and depth. Results from a notch sweeping across the transmission bandwidth are illustrated in figure 4.6.6. Fading commences with a notch appearing at an offset frequency of -20 MHz and deepening to a 20 dB MP notch ($b=0.9$) in figure 4.6.6(a). In figure 4.6.6(b), the notch changes phase state to a 20 dB NMP notch ($b=1.1$). Figures 4.6.6 (a) and (b) then illustrate MSE performance as the notch sweeps from -20 to 20 MHz offset frequencies and disappears. A noticeable lack of symmetry is present about the

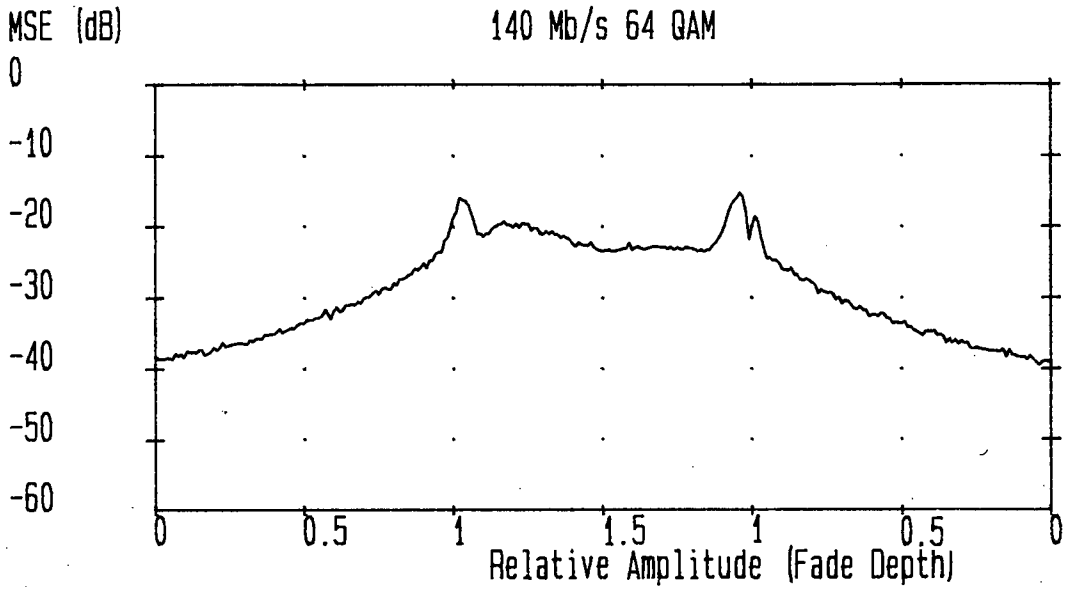

(a) f_0 = 5 MHz

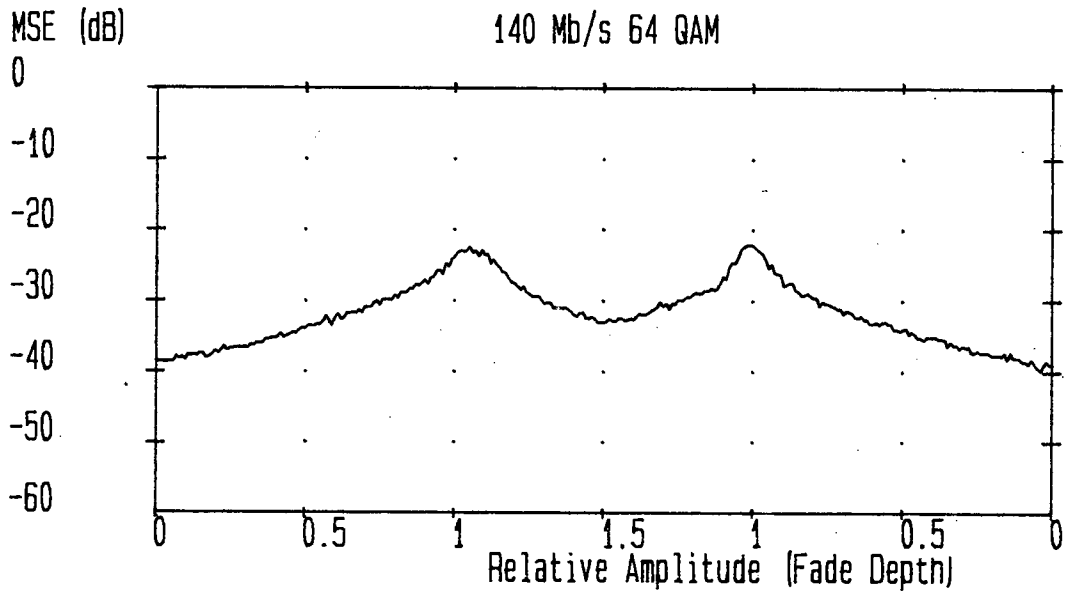

(b) f_0 = 10 MHz

Figure 4.6.4 FDFE Tracking in and out of NMP fade. Fixed Timing

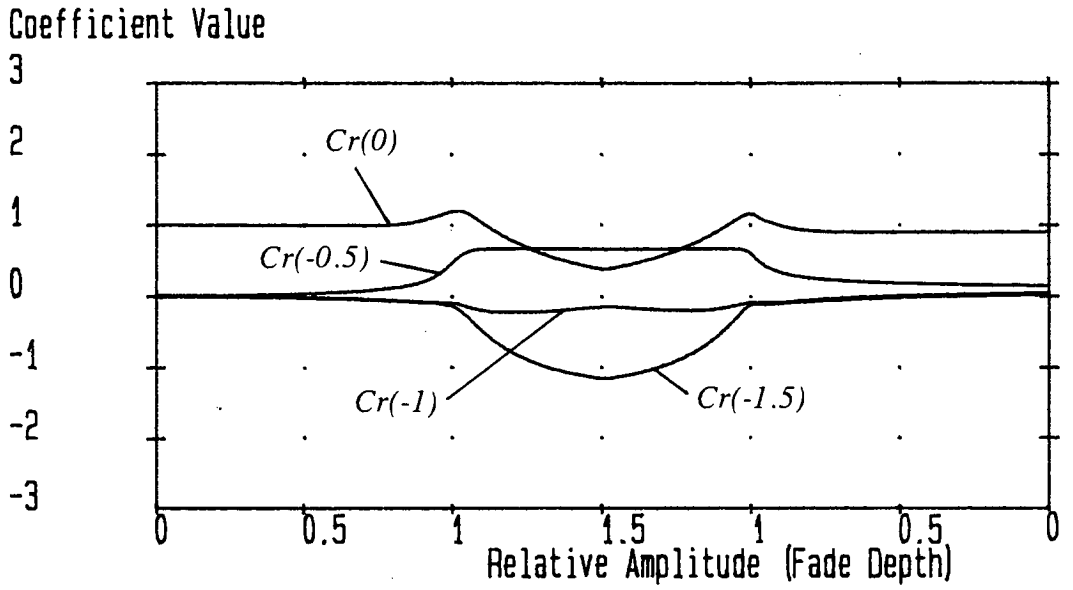

(a) Forward Coefficients

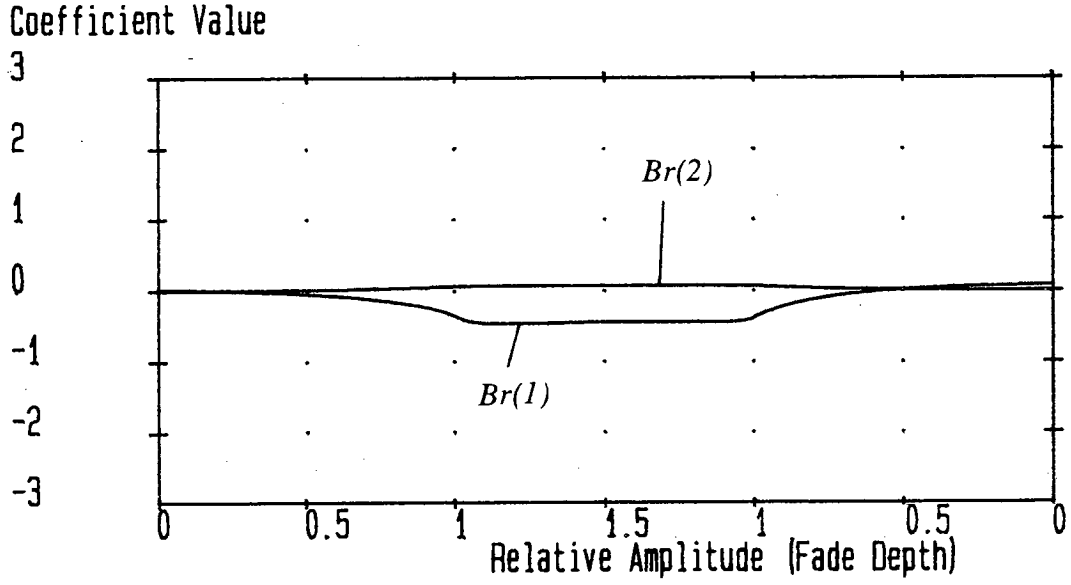

(b) Backward Coefficients

Figure 4.6.5 FDFE Real Coefficients

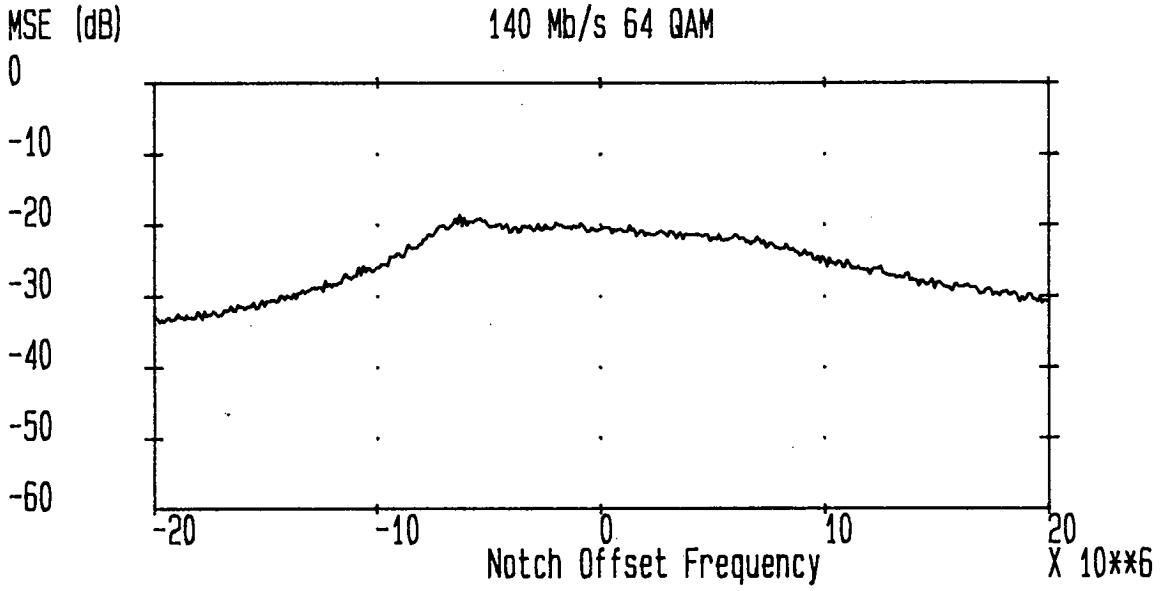

(a) MP Fade

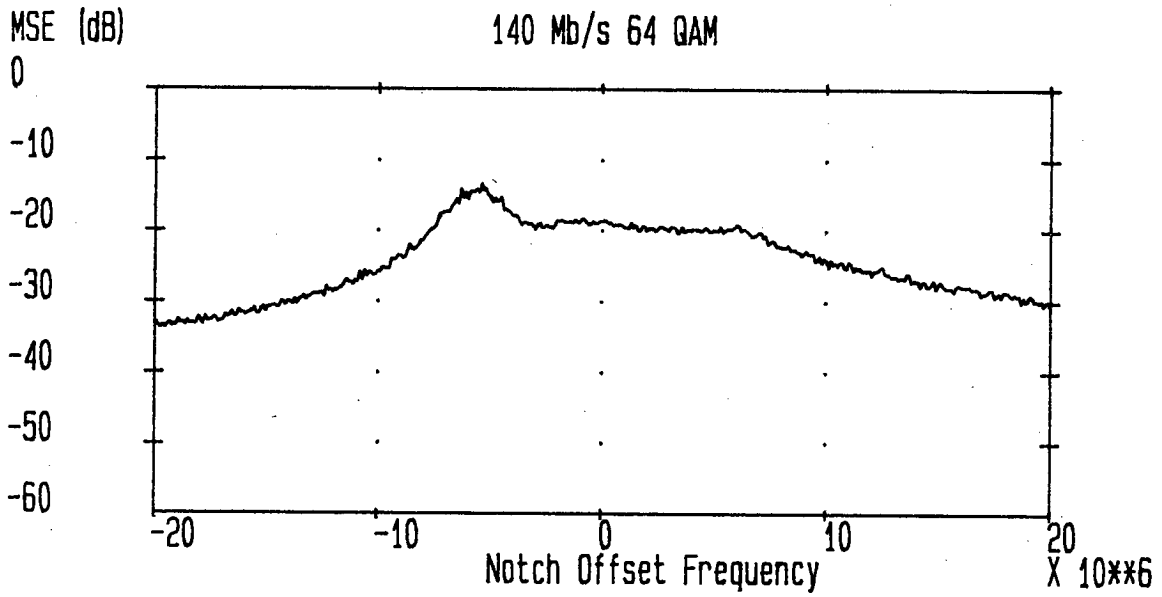

(b) NMP Fade

Figure 4.6.6 FDFE Tracking Frequency Selective Notch

bandcentre. This may be attributable to the equaliser operating in decision-directed mode and the changes in the equaliser taps values as the effects of the NMP fade diminish.

Inspite of encouraging results, implementation of fixed timing would be difficult. Some timing phase estimate is required for correct operation of a fractionally spaced equaliser to prevent phase roll and increasing nonstationarity. Obtaining the correct timing phase for a channel uncorrupted by ISI is relatively straightforward e.g. a 'square law' analogue implementation (chapter 2). If fading were detected by for example, monitoring the AGC gain, the timing phase would then be locked to the current setting. Stable timing references (i.e. the VCO) would help perpetuate this 'locked' situation, however due to drift in the fixed timing phase and any jitter present in the received signal, the timing phase would have to be updated at discrete intervals during a fading event of any duration. A practical means of decorrelating the calculated timing phase from the channel conditions is at first sight difficult to implement and was obtained for simulation results only with *a priori* knowledge of the channel impulse response. Since 'optimum' fixed timing was based on a known distorted impulse response, an investigation was performed to see if a similar idea could be applied to an estimate of the channel impulse response. Sections 4.8 and 4.9 examine channel estimation and performance, and present a DFE receiver based on this approach. Prior to this, in section 4.7 some issues regarding DFE retraining are examined.

4.7 DFE RETRAINING

The following section highlights the importance of maintaining the equaliser in lock during fading conditions. Figure 4.7.1 is similar in style to figure 3.8.1 in chapter 3, and illustrates the decision-directed performance of a (5,5,3) fractionally spaced DFE and fixed timing. Retraining is at discrete intervals throughout the relative amplitude range $0.0 \leq b \leq 2.0$ during a bandcentred fade. Results from section 4.6 indicated that this receiver combination had the ability to track particularly severe fading conditions, even for 64-QAM modulation. Should the equaliser loose lock for any reason and require retraining, channel conditions would have to be relatively good before performance is acceptable. This hysteresis effect is less severe for the 34 Mbit/s 4-QAM system, although in terms of fade depth, reconvergence is possible for fade depths of less than 14 dB. With the 140 Mbit/s 64-QAM system (figure 4.7.1(b)), retraining is possible for notch depths of around 6 dB or less.

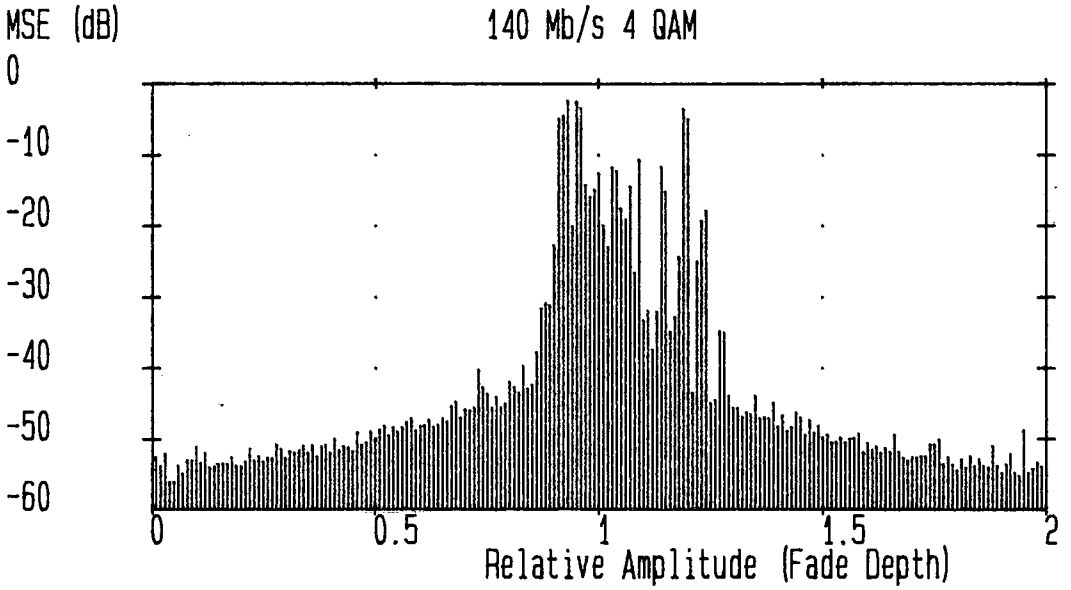

(a) 4-QAM

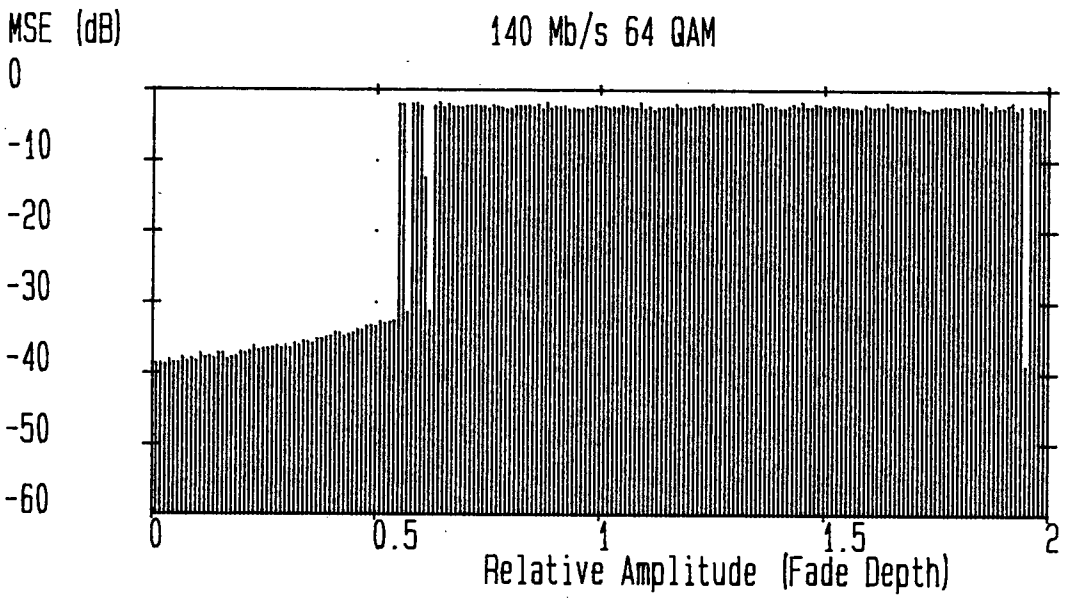

(b) 64-QAM

Figure 4.7.1 FDFE Retraining at Discrete Intervals. Fixed Timing

A certain degree of randomness may be associated with the likelihood of successful convergence during moderately deep fades. This may be attributed to decision-directed operation and a smoother MSE trend would be expected if ensemble averaging were performed (at the expense of increased computation time).

During a reset condition the DFE reset vector, $\{\underline{c}(k)\ \underline{b}(k)\}$, is initialised by setting the RTP to 1.0, and resetting all other taps. This configuration is obviously ideal only for unfaded channel conditions and is clearly suboptimum where ISI persists. When compared with the transversal equaliser and MEO timing (figure 3.8.1(b)), the increased degradation in figure 4.7.1(b) is due to a poor initial choice of tap settings for the fixed timing receiver. Blind equalisation techniques (section 3.8, chapter 3) may be applied to reduce retraining hysteresis, however a simpler solution is with a lookup approach postulated in figure 4.7.2. Assuming the presence of an RF/IF AGC outwith the demodulation/baseband loop, the reset vector is initialised from a PROM addressed by the sampled AGC gain crossing appropriate thresholds. Obviously the choice of settings is limited, however the technique is only attempting to provide a set of tap values allowing the equaliser to subsequently converge. No phase information is available from the AGC, therefore the channel must be assumed to be in a MP state. Given the relative ratio of MP to NMP fades at shallow to moderate fade depths [87], this is not an unreasonable assumption. A second disadvantage would be the difficulty in distinguishing between flat and frequency selective fades. A measure of inband distortion, similar to that used by amplitude equalisers (chapter 1), would give some indication of this aspect of the channel conditions.

4.8 CHANNEL ESTIMATION

Section 4.6 suggested obtaining timing information from an estimate of the received channel impulse response. Channel estimation may be practically implemented by an adaptive filter configured to perform FIR system identification or direct system modelling (chapter 1). A fundamental assumption is that the channel is modelled as a FIR filter (appendix A). Channel estimation may also find application in a number of other areas already mentioned in chapters 3 and 4. An estimated channel impulse response is required for ML/VA implementations (section 4.3.2) [25], as does the adaptive matched filter receiver (section 3.4, chapter 3) [116]. The 'dual equaliser' discussed in chapter 3 requires some indication of channel conditions, although the second equaliser structure effectively provides an indication of fading conditions and the addition of a separate estimator may not be justified in terms of

overall complexity.

A basic adaptive filter performing direct system modelling was illustrated by figure 1.3.1(a) in chapter 1. The data sequence, $a(k)$, is input to the unknown system (channel) and the adaptive filter. The channel output is now the desired output, $x(k)$, of the adaptive filter. By defining a suitable cost function, the adaptive filter may converge such that the filter output, $\hat{x}(k)$, approximates the channel output, providing that the orders of the two systems are equivalent. Ideally, the sequence $a(k)$ is white and the input autocorrelation matrix is diagonal with equal eigenvalues ensuring optimum convergence if the estimator taps are updated with the LMS algorithm. Adaptation is faster still with the RLS algorithm [21], however this is not required for microwave digital radio applications and the added complexity would be prohibitive. In a real system, the transmitted sequence is unknown at the receiver and the output from the decision device is employed. A decision-directed channel estimator is illustrated in figure 4.8.1. Channel estimator performance is now linked to that of the equaliser. Should the equaliser fail, so will the channel estimator. The relatively good performance of the FDFE/fixed timing combination proves an attractive solution to this problem and channel estimator performance with this overall structure is examined shortly.

The LMS algorithm performing system identification is summarised by the following equations. All quantities are complex.

$$\hat{\underline{h}}(k+1) = \hat{\underline{h}}(k) + 2\mu \underline{y}(k) e(k) \tag{4.8.1}$$

where the error signal is given by

$$e(k) = x(k) - \hat{\underline{h}}^T(k) \underline{y}(k) \tag{4.8.2}$$

and $\hat{\underline{h}}(k)$ is the estimate of the overall complex received impulse response $\underline{h}_N(k)$. For a stationary channel and white input, analysis of the LMS algorithm provides a bound on the convergence factor, μ, in terms of the input signal variance, σ_x^2 [21]

$$0 \leq \mu \leq \frac{1}{N_C \sigma_x^2} \tag{4.8.3}$$

where N_C is the length of the estimated impulse response. Prior knowledge of the characteristics of the raised cosine pulse shape during fading should help minimise uncertainty in the estimated model order.

The performance measure most useful for system identification is the norm, determining the accuracy of the estimated impulse response relative to the true value in vector space [21]. A more visual performance assessment is by directly comparing estimated and actual impulse responses (figure 4.8.2). Channel conditions in figure 4.8.2 are the same as in figure 4.6.8, where a bandcentred MP fade deepens and

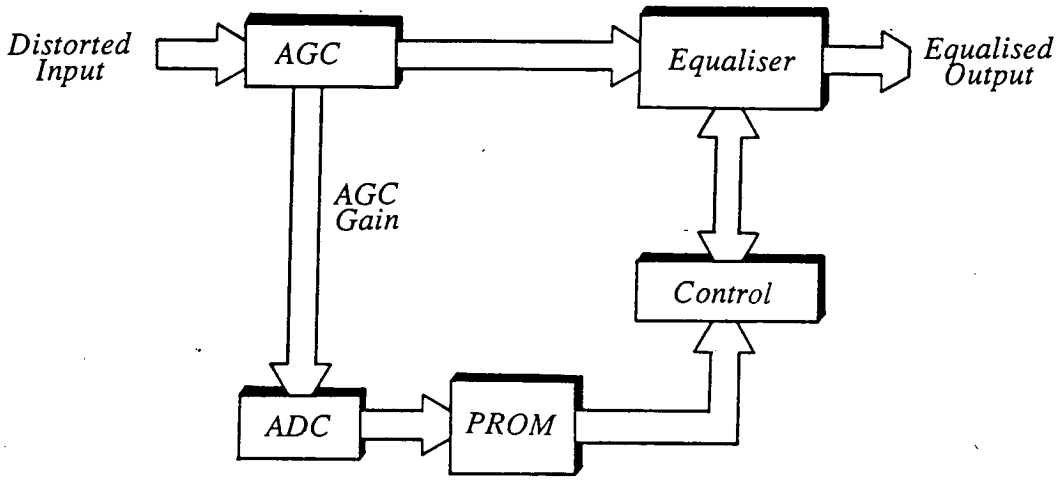

Figure 4.7.2 DFE Retaining System

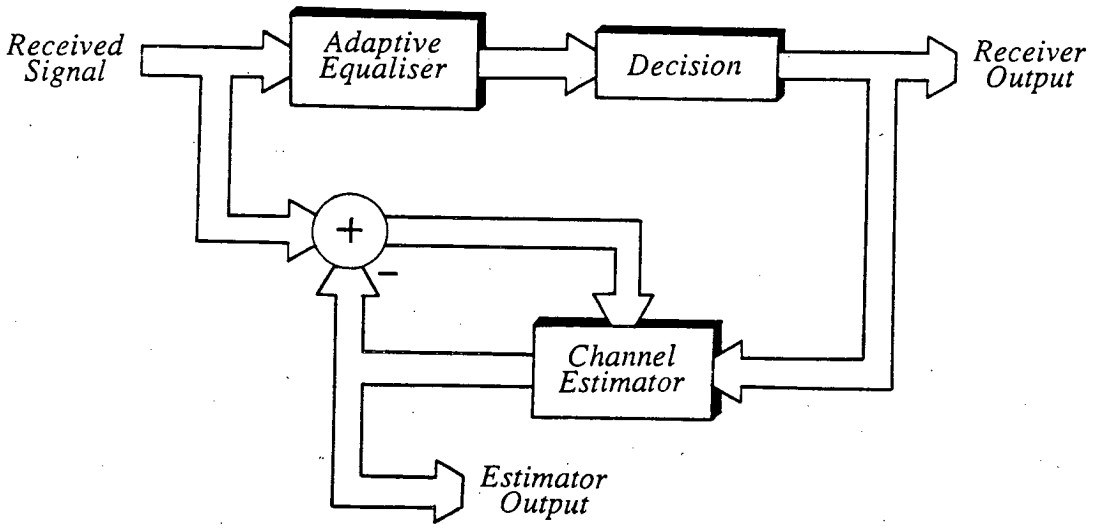

Figure 4.8.1 Channel Estimator

changes phase state to a NMP fade. It is obvious from figure 4.8.2 that the channel estimator is able to track successfully through the fade transition, based on the output of the FDFE with fixed timing. The estimated response is that obtained at the AGC input i.e. prior to any additional gain at the receiver. Results in the next section illustrate that the channel estimator will operate correctly on the AGC output, although the overall impulse response appears slightly different. Figure 4.8.2 is also interesting for a means of obtaining the 'fixed' timing phase is now apparent. During the phase transition, considerable change occurs in the value of the real centre tap, $hr(0)$, however, the magnitudes of the taps $hr(-1)$ and $hr(1)$ remain approximately similar in magnitude. Implementation of a timing recovery technique based on maintaining an equal balance in the power of the estimated response about the centre tap is described in the next section.

4.9 AN ADAPTIVE DFE RECEIVER

The potential of fractionally spaced DFEs for dealing with severe fading conditions was illustrated in section 4.6, however results were obtained with the timing phase locked to the optimum obtained during unfaded conditions. This fixed timing phase may be difficult to obtain in practice. Results from section 4.8 developed this idea, illustrating that only the centre tap of the estimated channel impulse response changes to any degree during fading conditions described by the simplified three path model. A technique for obtaining timing information from the estimated impulse response is now presented, followed by a description and results from a DFE receiver incorporating this timing technique.

4.9.1 Timing Phase Control

From figure 4.8.2, it was noted in section 4.8 that taps either side of the centre tap or pulse peak of the estimated real channel, remained approximately similar in magnitude throughout a phase transition. An initial step might be to ensure that the real tap values, $hr(-1)$ and $hr(1)$ maintain equal magnitudes. A unique value for the timing phase is not guaranteed with this arrangement during deep fading, and at notches offset from bandcentre, the imaginary components should also be considered.

A workable, if more involved solution is to base the timing phase estimate on the power in the complex channel response estimate. By maintaining equal power in the estimated response about the response peak, the timing recovery phase may be held relatively fixed, independent of the channel conditions and phase state. Implementation of the algorithm is illustrated in table 4.9.1, with a section of 'C'

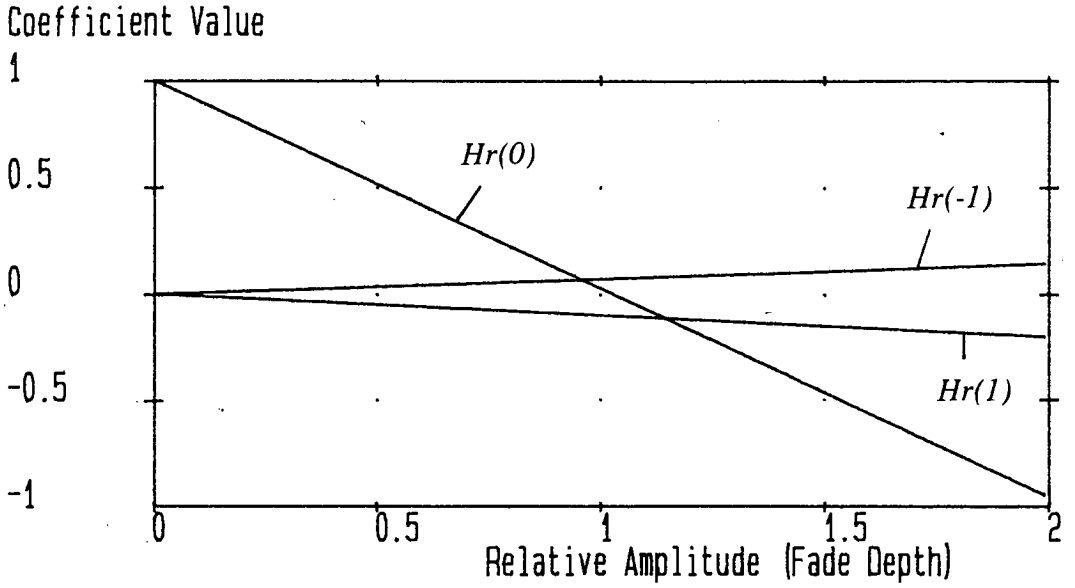

(a) Actual

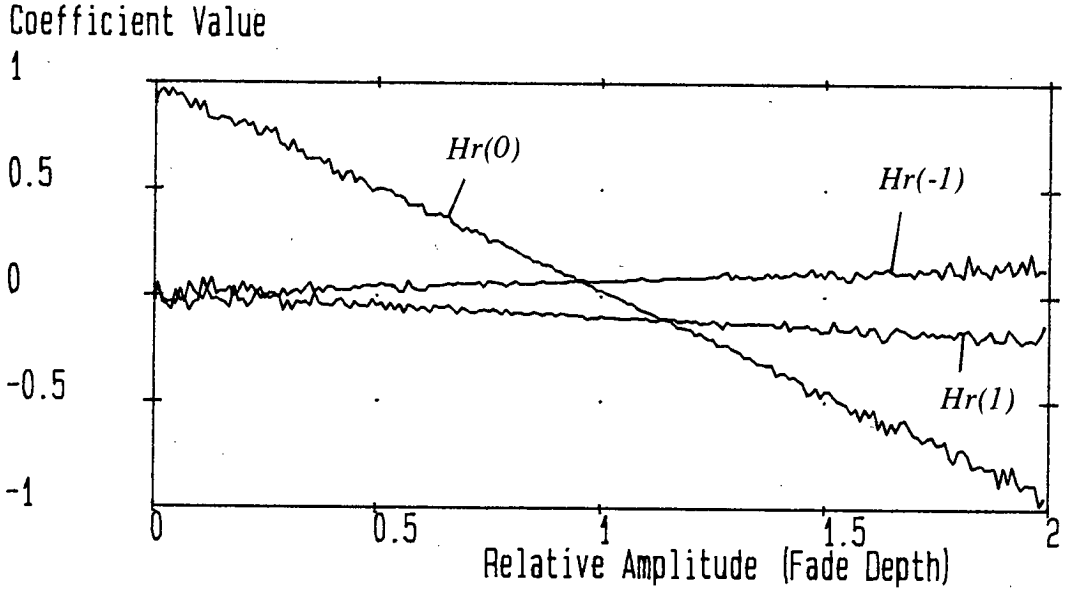

(b) Estimated

Figure 4.8.2 Channel Estimator Output from 64-QAM Real Channel

program taken from the simulation software.

```
alpha=0.001;

power1 = (Hr[-2]*Hr[-2] + Hi[-2]*Hi[-2]) + (Hr[-1]*Hr[-1] + Hi[-1]*Hi[-1]);
power2 = (Hr[1]*Hr[1] + Hi[1]*Hi[1]) + (Hr[2]*Hr[2] + Hi[2]*Hi[2]);
power3 = (Hr[0]*Hr[0] + Hi[0]*Hi[0]);

if ((power3 > power1) && (power3 > power2)) {
   if (power1 > power2)
        *tau = *tau + alpha;
   if (power2 > power1)
        *tau = *tau - alpha;
}
```

Table 4.9.1 Implementation of Timing Recovery from the Channel Estimator

Declarations have been omitted, and array addressing is slightly modified†, to illustrate the main points of the algorithm. Arrays $Hr[]$ and $Hi[]$ are equivalent to sampled values of the estimated real and imaginary impulse responses, $\underline{hr}(k)$, $\underline{hi}(k)$. Variables *power1* and *power2* correspond to the power in the impulse response either side of $Hr[0]+jHi[0]$ ($=power3$). Providing *power3* is sufficiently large, the timing phase is incremented/decremented by a constant term, *alpha*, according to the relative values of *power1* and *power2* . Overall robustness is improved by time averaging the estimated power components. Time averaging also helps reduce the effects of any jitter present in the received signal. Simplification to the algorithm is possible by considering magnitudes rather than power terms, thereby eliminating multiplication operations.

Some similarity exists between obtaining timing from the estimated channel impulse response and a technique proposed by Gitlin and Meadors [117]. This idea is applied to fractionally spaced linear equalisers to prevent the reference tap drifting over time from the centre of equaliser delay line. Timing recovery is consequently based on monitoring tap weight distribution about the centre tap. It is also noted that the idea of limiting changes in the timing phase is not original, only the application and realisation. Clark and McVerry [118] and Hodgkiss and Turner [119] independently proposed that for HF channels, receiver synchronisation is best achieved by limiting changes in the recovered timing phase.

† Strictly array addressing begins from 0 e.g. Hr[0].

4.9.2 The Receiver Configuration

Based on preceeding discussion and results, figure 4.9.1 illustrates the proposed receiver structure. All components of interest are implemented at baseband. Accurate carrier recovery is assumed prior to the baseband stage, although a loop involving the DFE output may enhance performance [104, 120]. Simulation results were obtained with an AGC normalising the received signal power (and enhancing noise at the same time). AGC implementation may be at IF or baseband, although IF implementation may be required for correct operation of the carrier recovery circuit [29].

In theory, the fractionally spaced DFE may be locked to any timing phase during retraining, however optimum performance was obtained with fixed timing such that one of sampling instants (assuming that the forward filter taps are spaced by $T/2$) occurs at the pulse peak during unfaded conditions. During normal conditions, relatively simple timing recovery methods e.g. square law timing, may provide a near optimum sampling phase [49]. An inconsistency is now apparent. The timing recovery technique discussed in section 4.9.1 and square law timing are based on sampling at the symbol rate. The problem may be resolved by considering the fractionally spaced DFE implementation. Figure 3.3.1 in chapter 3 illustrated how a linear fractionally spaced transversal equaliser sampling at twice the symbol rate, could be considered as two separate symbol spaced filters offset by $T/2$. A similar technique may be applied to the fractionally spaced DFE (figure 4.9.2). This arrangement has the advantage that all operations are performed at the symbol rate; the requirement to sample and operate at greater than the symbol rate has currently limited application of fractionally spaced equalisers in microwave radio to theoretical studies. Two ADCs are required, *ADC1* and *ADC2*. *ADC1* would be under the control of the timing signal already discussed. *ADC2* is required to sample $T/2$ or 180° from *ADC1* i.e. with inverse of the (periodic) sampling signal required for *ADC1*. Additional system cost is added by the requirement for 2 ADCs per equaliser, however the whole system may be realised with VLSI technology.

Figures 4.9.1 and 4.9.2 suggest that the overall structure is considerably more complex than a transversal equaliser or even a conventional DFE. A number of important issues regarding implementation should be noted. Firstly, the proposed receiver offers considerable performance gain over current equalisation systems. Emphasis on other, more costly, compensation measures may therefore be reduced, or else higher modulation formats accommodated e.g. 256-QAM. Secondly, the channel

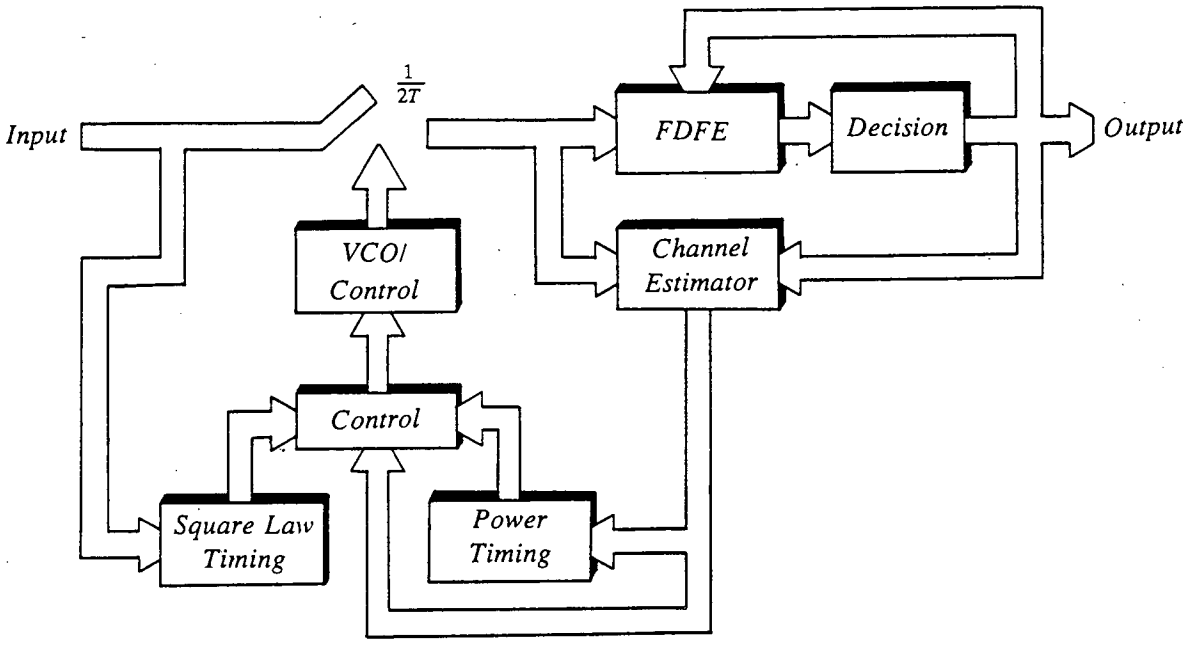

Figure 4.9.1 DFE - Channel Estimator Receiver

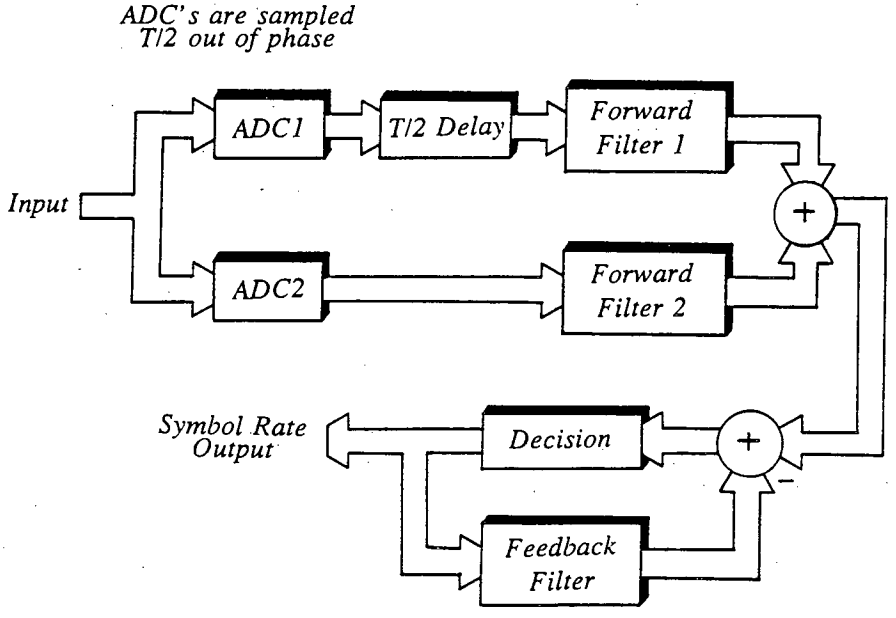

Figure 4.9.2 Fractionally Spaced ($T/2$) DFE

estimator has a similar structure to a linear transversal equaliser, thereby reducing design effort. Finally, timing based on the estimated channel response does not have to be updated at the symbol rate. Updating may be with an 'off-line' approach similar to that described in chapter 5. The timing algorithm summarised by table 4.9.1 is ideally suited to digital signal processor (DSP) implementation and control. Time averaging the estimated power terms simply requires additional memory to store the summations and at the end of every averaging interval, perform division to obtain the average. If the time averaged interval is an integer power of 2, division is simply by right shifting, requiring one DSP† instruction cycle.

4.9.3 Receiver Performance

Figures 4.9.3 to 4.9.7 illustrate certain key aspects of the proposed receiver performance. The fractionally spaced (5,5,3) DFE is operated in conjunction with timing based on the channel estimator output in a 140 Mbit/s 64-QAM receiver. Simulation results are calculated with floating point arithmetic.

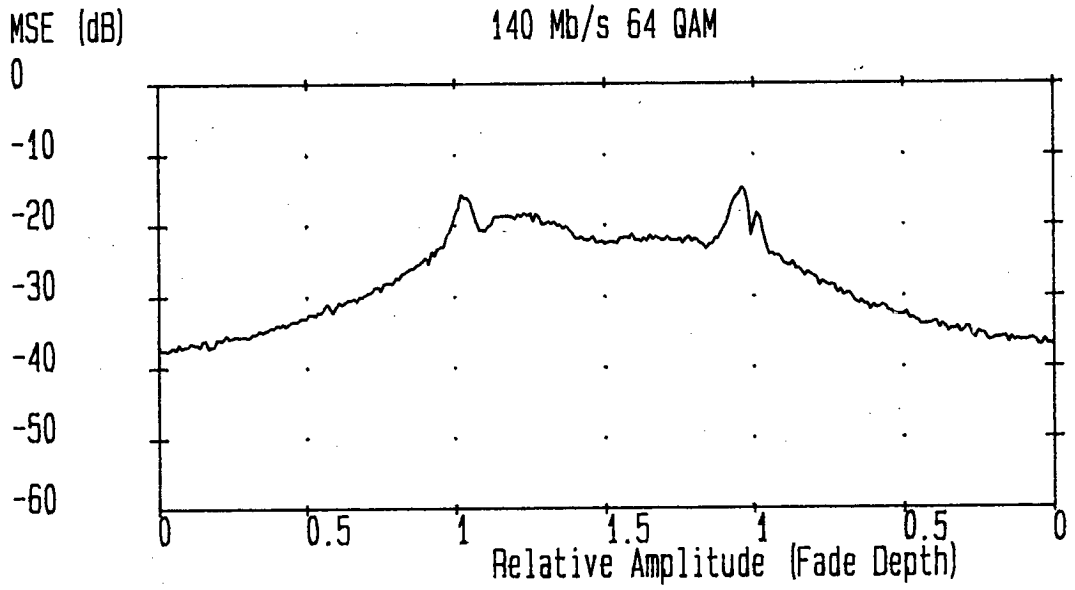

Figure 4.9.3 Receiver Tracking in and out of NMP Fade

Results may be compared with section 4.6, except timing is no longer determined *a priori*, but from the received signal. Tracking ability through phase transitions is

† TMS32010, as discussed in chapter 5.

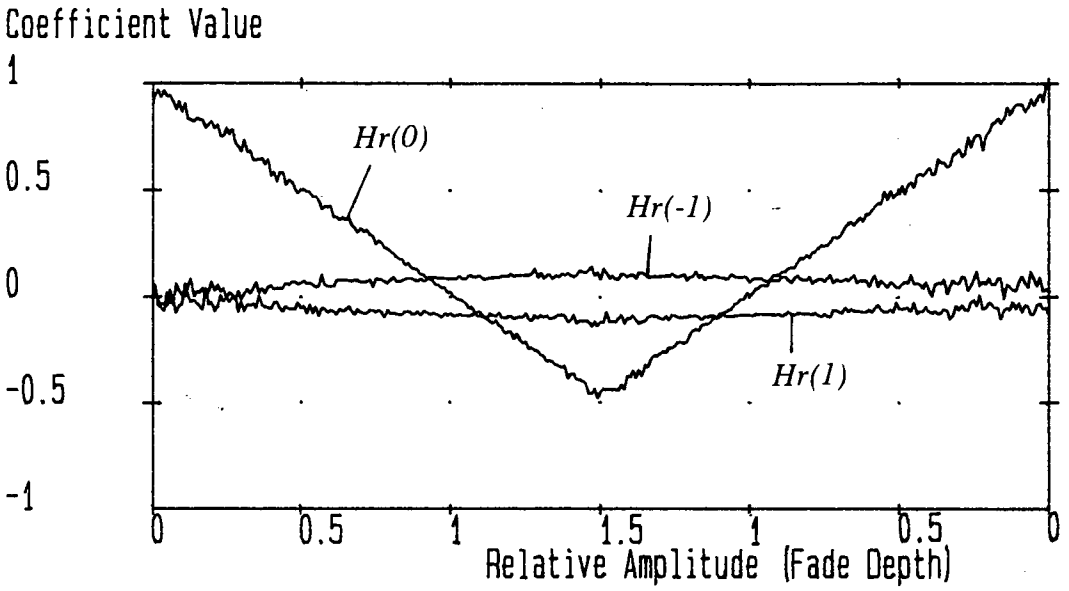

(a) Real

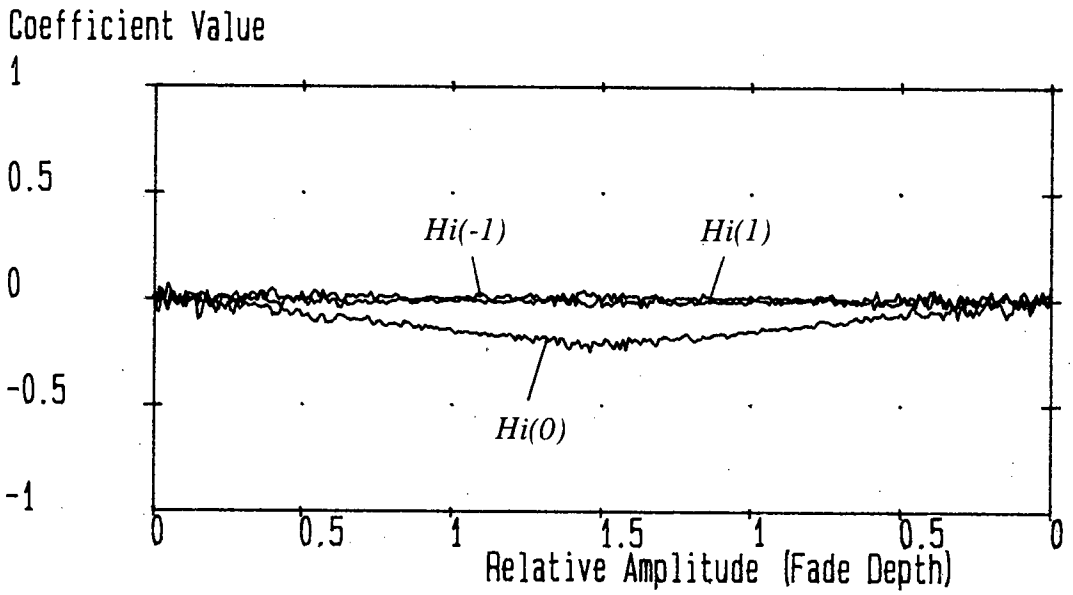

(b) Imaginary

Figure 4.9.4 Channel Estimator Output. Requires AGC Input

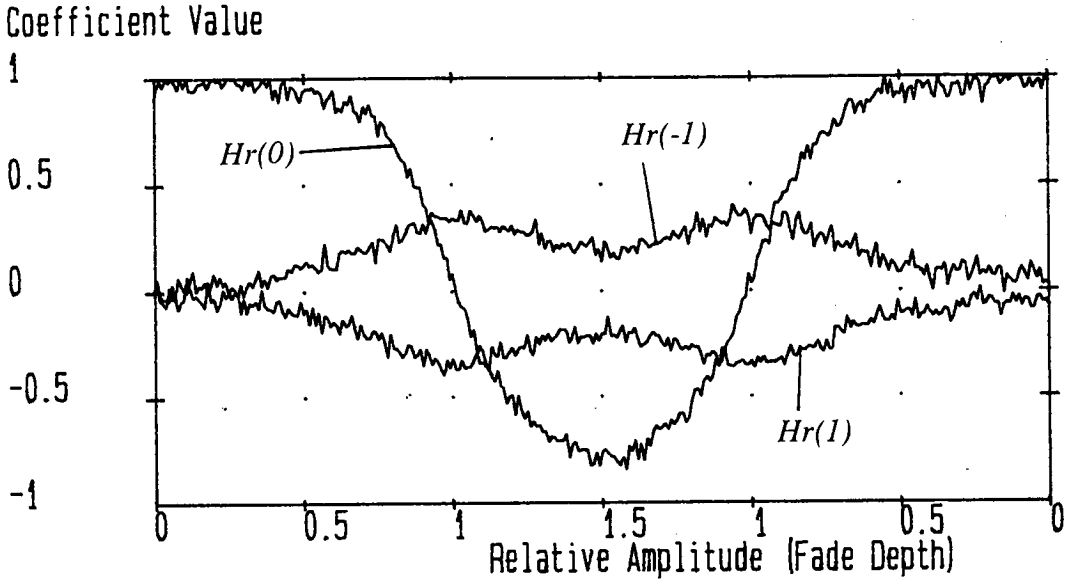

(a) Real

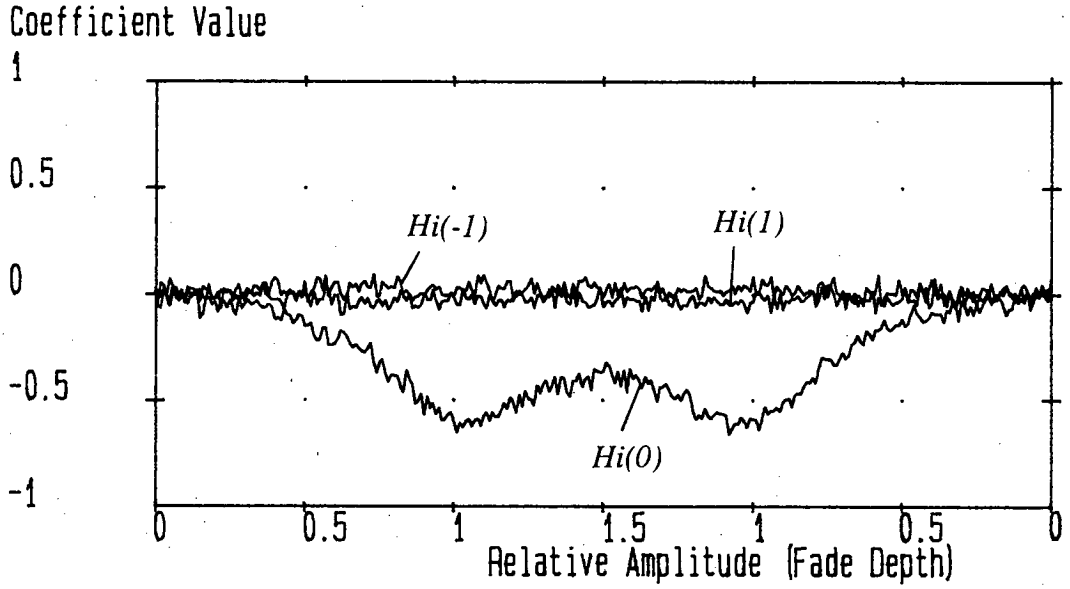

(b) Imaginary

Figure 4.9.5 Channel Estimator Output. Requires AGC Output

illustrated in figure 4.9.3 as a notch, 5 MHz offset from bandcentre, changes from MP to NMP states and back. Performance is effectively the same as if the timing phase were fixed (figure 4.6.4(a)). Throughout the fade, the channel estimator maintains an accurate estimate of the real and imaginary components of the channel response. Results were obtained with timing averaging over 8 symbols. The effectiveness of the timing recovery technique is noted from the similar magnitudes of $hr(-1)$ and $hr(1)$. The bias toward $|hr(1)|$ in figure 4.8.2(b), obtained with ideal fixed timing, no longer exists, indicating that sampled power in the estimated impulse response is symmetrical about the centre (reference) tap position. A corresponding bias would be expected in the estimated timing phase, and this is shown in figure 4.9.6. A certain amount of 'wander' is present in the calculated timing phase, however due to the timing phase insensitivity of the fractionally spaced equaliser, this is not critical and made no observable difference in equaliser performance or stability. When the receiver attempts to track a 20 dB NMP notch sweeping across the passband (figure 4.9.7), identical results to figure 4.6.6 were obtained. Again, the channel estimator maintains correct operation.

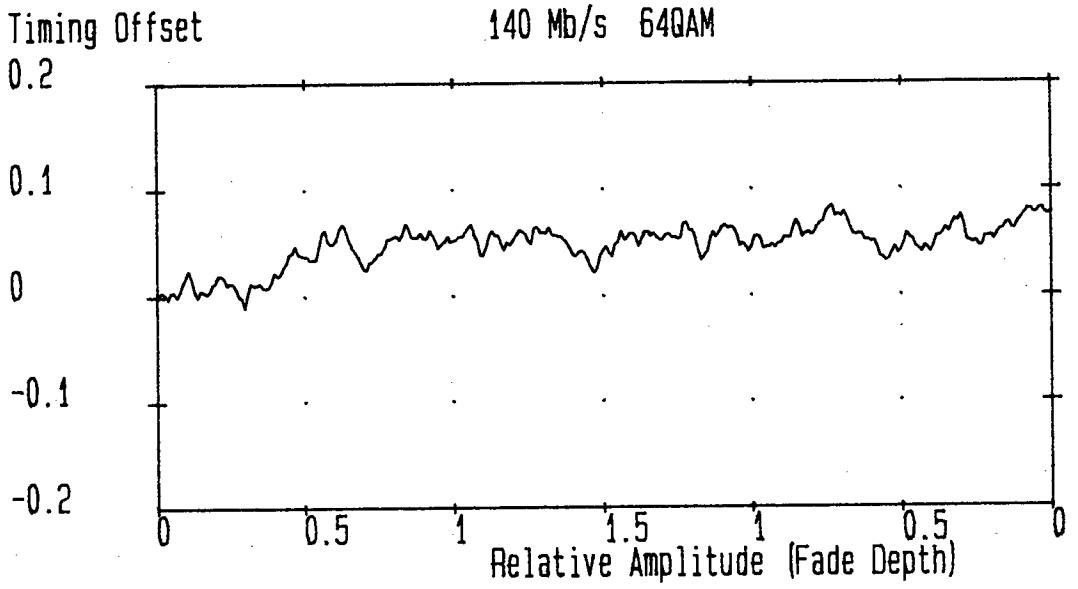

Figure 4.9.6 Timing Phase Calculated from Channel Estimator

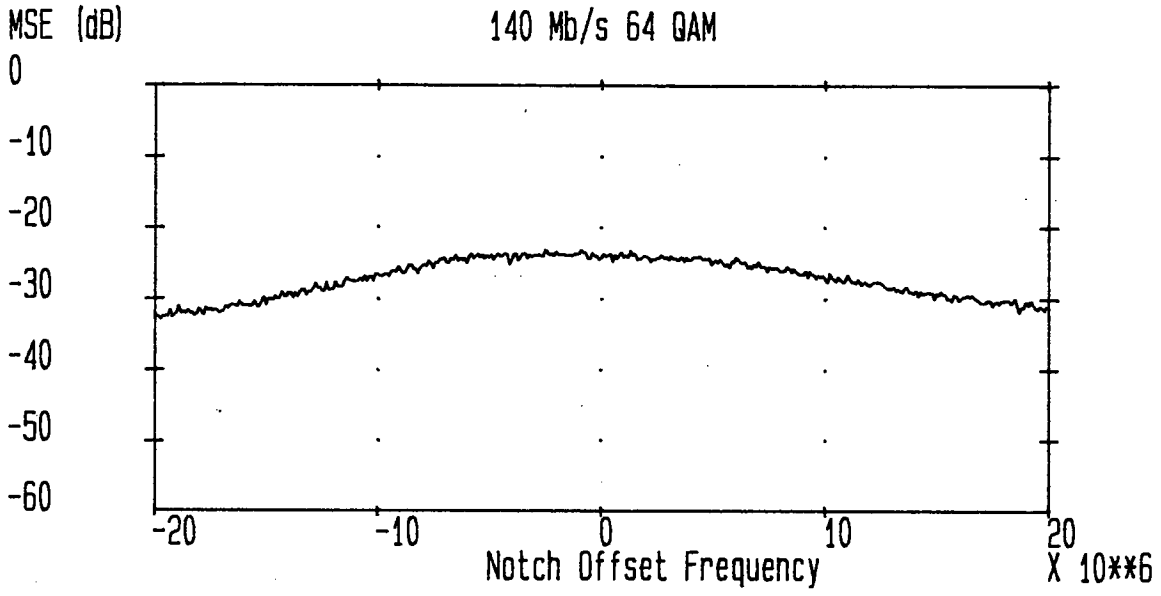

(a) 20 dB MP Notch

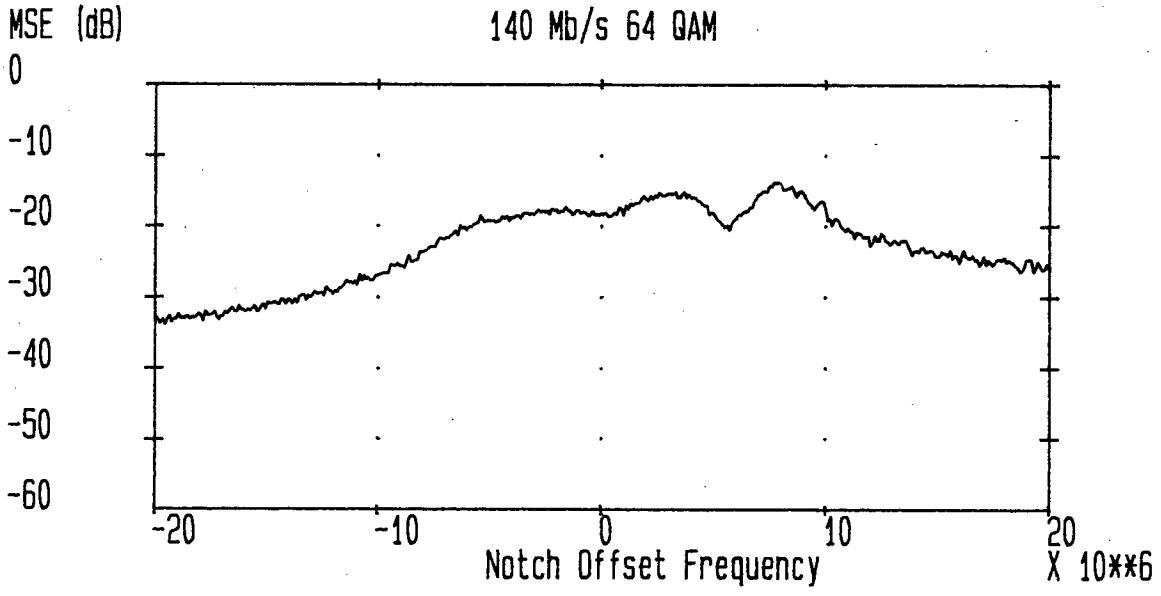

(b) 20 dB NMP Notch

Figure 4.9.7 Receiver Performance Tracking Frequency Selective Notch

4.10 SUMMARY

Chapter 4 has examined the performance of decision feedback equalisation during severe fading conditions. The two main DFE configurations adopted were with forward filter taps spaced by the symbol period (T), and spaced by a fraction of a symbol period ($T/2$). Fractionally spaced DFEs potentially offer greater insensitivity to timing phase selection and improved performance at bandedges (chapter 3). Against the use of fractionally spaced taps are the increased computation requirements and the potential for convergence to nonglobal minima if implemented digitally (chapter 5).

Symbol spaced DFE performance was found to be unsatisfactory during phase transitions, even when the NMP signal is sampled/'processed' to appear 'pseudo-MP'. Attention was focussed on fractionally spaced DFE structures with no attempt made to track any change in timing phase due to multipath fading. Results indicated that this combination of equaliser and timing was successfully able to maintain lock while tracking severe fading conditions. This timing recovery method would be difficult to implement in practice, for some means of calculating timing information must exist at the receiver. A novel timing recovery technique was proposed, based on an estimate of the channel impulse response. Unlike most timing recovery methods, the proposed technique is not attempting to track any change in the relative timing phase due to the effects of fading. Instead timing is held approximately fixed to that obtained during unfaded conditions. Jitter in the received signal would be countered in part, by the time averaging in the timing recovery process and through the timing phase insensitivity of the fractionally spaced DFE. The proposed receiver structure was shown to have similar performance to the fractionally spaced DFE operating with the timing phase fixed *a priori* .

Chapter 5

DIGITAL EQUALISER DESIGN

5.1 INTRODUCTION

Equaliser results derived from floating point simulations, approximately equivalent to analogue implementation, are discussed in chapters three and four. High precision is not available with practical digital hardware and quantisation error will inevitably result in some performance degradation. This chapter on digital equaliser implementation has two main objectives. Firstly, equaliser performance is assessed with differing word lengths to present, together with the preceeding chapters, a unified examination of potential equaliser performance for microwave digital radio. For comparative purposes, implementation is restricted mainly to a 4-QAM system operating at 8/34 Mbit/s, in conjunction with symbol spaced transversal equalisation. Essentially, the adaptive equaliser design is broken into two main components: a programmable FIR filter and the adaptive algorithm implementation (figure 5.1.1). Results and discussion are mainly from a 4-QAM transversal equaliser, although the techniques and ideas presented may be applied to higher level modulation formats and decision feedback equalisers.

From simulation results, it will become apparent that sufficient bit length is critical to the performance of the conventional LMS algorithm. Simplifications to the basic LMS algorithm, and the zero-forcing solution, are subsequently examined with a view to reducing word length requirements. The block LMS (BLMS) algorithm and a simplified version, the clipped BLMS (CBLMS) algorithm, are examined as other potential means of adaptation. Simulation results indicate that the finite precision BLMS algorithm has performance advantages over the finite precision LMS algorithm, at the expense of slightly increased convergence time and hardware requirements. This is a unique solution to equaliser adaptation for microwave digital radio, and the

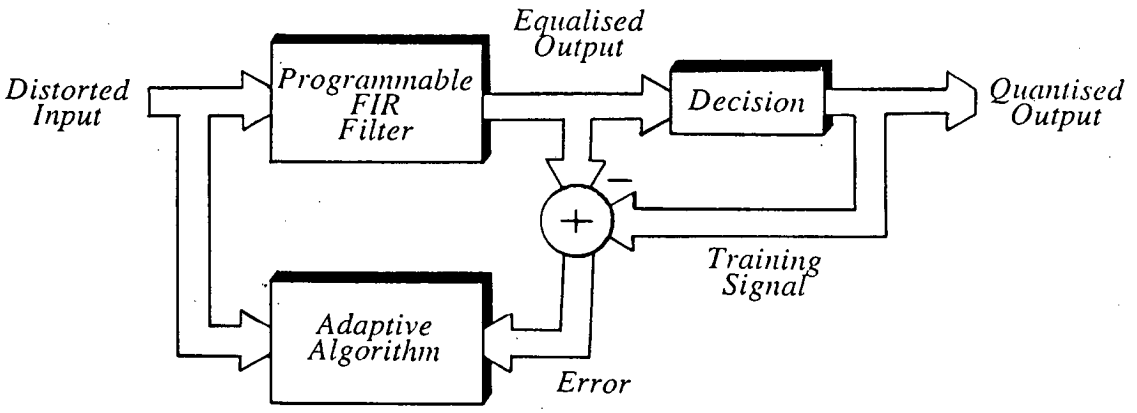

Figure 5.1.1 A General Adaptive Equaliser

additional hardware implementation should be straightforward.

The second main objective of this chapter is to describe a hardware implementation performed as part of this work. A literature survey reveals few published details of practical equaliser designs for microwave digital radio (or BLMS algorithm implementations) and nothing on the proposed 'off-line' adaptation approach. This novel solution to the equaliser adaptation problem exploits the relative channel stationarity to allow updating at less than the symbol rate with a digital signal processor (DSP).

5.2 DIGITAL SIGNAL REPRESENTATION AND OPERATIONS

Prior to any description of digital equaliser design and implementation, it is important to briefly define and discuss the means of digital signal representation and the operation of arithmetic functions. The principle source of error in a digital structure is due to quantisation. Word growth will inevitably be accompanied by quantisation error due to truncation/rounding. Section 5.4 examines the effect of coefficient quantisation on the adaptive algorithm, while section 5.5 examines the performance implications on the overall equaliser design. The initial error source is due to data quantisation at the ADC stage, where an error is generated with a mean

square value of $v/12$, with v corresponding to the least significant bit (LSB) amplitude. This error is inversely proportional to the word length and is reduced by 6 dB for each additional bit used. An 8 bit ADC would thus have a dynamic range of 48 dB. The digital ADC output is now assumed to be manipulated in fixed point two's compliment notation for ease of implementation [77]. Greater dynamic range is possible with floating point numbers but at the expense of greater complexity, and the extra dynamic range may not be essential. For positive numbers, two's complement representation is equivalent to sign and magnitude notation, however negative two's compliment numbers are given by

$$2^B - |x| \tag{5.2.1}$$

where B is the number of bits (including sign) and $|x|$ is the magnitude of the represented number.

When operating with fixed point two's compliment numbers and the result lies outside the allowed value range, an overflow condition occurs. Overflow from multiplication may be avoided with suitable scaling to represent all inputs in fractional two's compliment notation. Thus the quantised value of x is given by

$$[x] = -r_0 + \sum_{i=1}^{B-1} r_i 2^{-i} \tag{5.2.2}$$

where r_i denotes the weighting associated with each bit. Multiplication of say, two 8 bit numbers results in a 16 bit fractional product i.e. word growth occurs. Truncation or rounding of the product introduces roundoff error, however the potential for overflow is eliminated. The addition of two 8 bit numbers is a 9 bit sum, thus the potential for overflow still remains. Similarly, overflow may occur during left shifting of a two's compliment number. If overflow occurs, an incorrect in-range number is produced with value dependant on the arithmetic operation. For example, the output of a two's compliment adder has the 'wrap-around' characteristics illustrated in figure 5.2.1(a) [121]. The addition of MSB guard bits is a costly and inefficient solution. A more effective solution is to saturate the output characteristics (figure 5.2.1(b)). Detection is possible if two positive inputs produce a negative number or vice versa. The most practical solution is identification at the design stage of possible overflow states through computer simulations, followed by suitable scaling.

Appendix D lists examples of source code for the arithmetic functions used in the finite precision simulations. The functions, written in '*C*', perform multiplication, division, addition, subtraction, left shifting and right shifting. If any arithmetic overflow occurs, the output is saturated and sign extension is implemented during right shifting. Bit lengths are set according to the design.

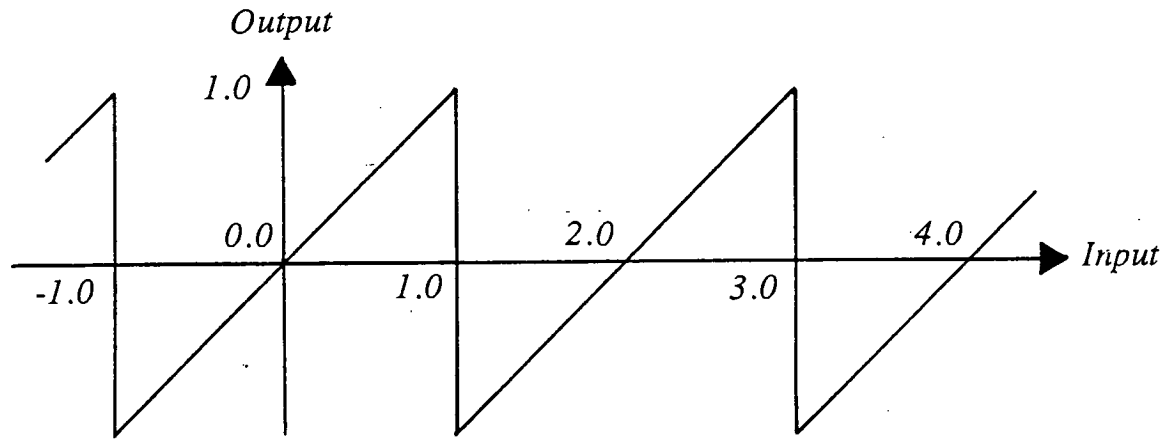

(a) 'Wraparound'

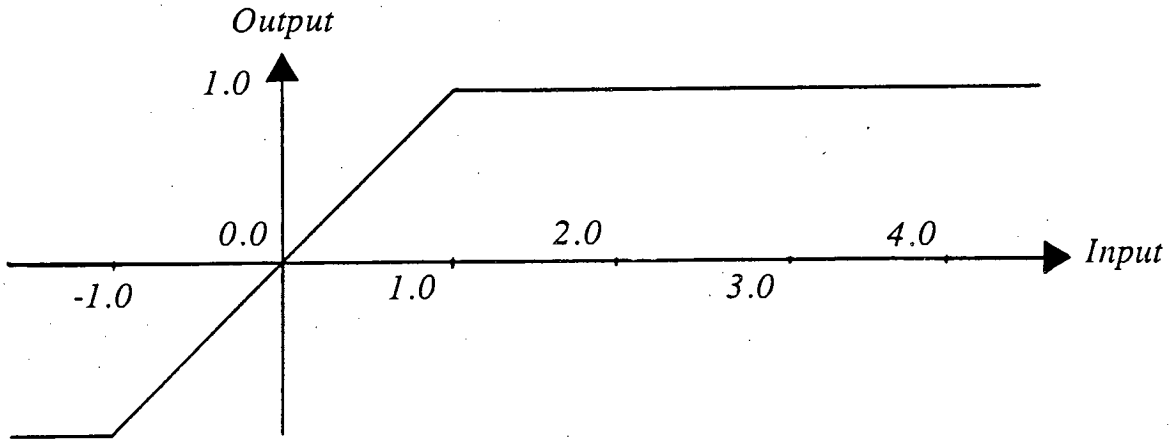

(b) Saturation

Figure 5.2.1 Two's Compliment Overflow Characteristics

5.3 PROGRAMMABLE FIR FILTER IMPLEMENTATION

The two principal equaliser structures considered in this work may both be considered as an arrangement of programmable FIR filters. A linear transversal equaliser, with symbol or fractionally spaced taps, consists of a single programmable FIR filter. The addition of a second FIR structure feeding back the equalised symbol decision for ISI cancellation, results in a simple decision feedback equaliser (DFE). The following section examines equaliser implementation, with emphasis mainly on FIR filter construction and technology. The additional hardware design to perform adaptation is examined in section 5.4, however the same analogue and digital technologies required for the FIR filter, would be similarly applied to the adaptation circuitry.

A nonadaptive FIR filter may be broken down into a tapped delay line, a multiplication array to weight the delay line outputs, and a final summation to form the equaliser output. Two main FIR filter structures arise from re-arranging the functional blocks. Firstly, the FIR filter may be implemented directly (figure 5.3.1(a)), where the signal is accessible from the delay line for weighting and summation. A pipelined time delay and integrate structure (figure 5.3.1(b)) is typical of commercial integrated filters. Signal weighting is now performed prior to input on the delay line. A third approach consists of separate delay elements for each weighted term. The resulting structure offers high speed at the expense of considerable additional hardware.

Numerous means of adaptive equaliser implementation exist, employing both analogue and digital technology. Techniques range from standard digital signal processors (DSPs) to individually designed analogue/hybrid hardwired solutions to programmable logic arrays (PLAs). The high data rates involved with microwave radio place particularly severe bounds on complexity and technology, and hence many varied solutions have evolved. As the basis for further research work, a review of current and potential designs is essential. The section now proceeds by examining analogue and digital FIR filter implementations, where the filter forms part of an overall adaptive equaliser design. Traditionally, analogue techniques have prevailed. Only with the advent of high speed VLSI and simultaneous conversion ADCs has digital equaliser implementation become viable. Existing designs are typically based on symbol spaced transversal structures. DFEs, while desirable, are difficult to implement in practice [60]. Careful design is required such that the feedback term is calculated at less than the symbol period.

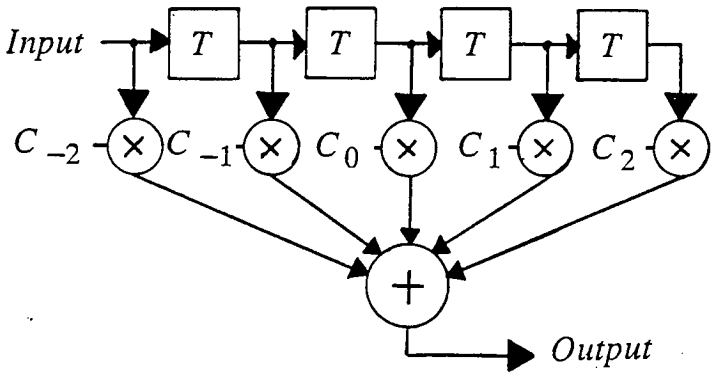

(a) Tapped Delay Line

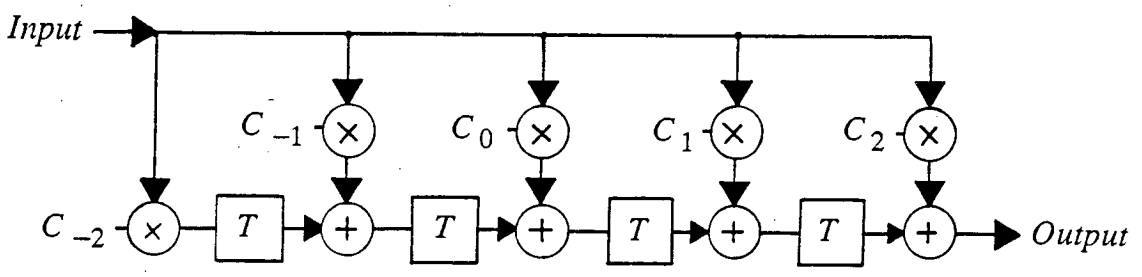

(b) Time Delay and Integrate

Figure 5.3.1 FIR Filter Configurations

5.3.1 Analogue Technology

Analogue and sampled-data analogue adaptive filters provided the earliest means of baseband transversal equaliser construction for microwave digital radio applications. IF pre-equalisation is by necessity performed by analogue means [57]. Baseband equaliser implementation is based around construction of the tapped delay line with individual lumped delay elements e.g. 100Ω wound transmission lines [60], or switched ladder attenuators/FETs [65]. Isolation between individual elements on the delay line and the coefficient weighting taps may be provided by buffer amplifiers [122]. Relatively recent results have been reported with such techniques [123, 124], including the feedback term in a DFE [60]. Digital techniques are commonly employed for coefficient updating, possibly in conjunction with multiplying DACs (MDACs) performing the multiplication operation.

At lower data rates, charge-coupled devices (CCDs) and bucket-brigade devices (BBDs) have been successfully used for delay line construction [125]. Weighting is possible by either direct analogue multiplication or if the equaliser coefficients are stored digitally, with an analogue/digital hybrid using MDACs [125]. Again at lower data rates, adaptive equalisers employing analogue sampled data switched-capacitor LSI technology are also possible. Here the input is sampled but not quantised, and the stored analogue values are transferred as charge packets.

SAW filter construction offers realistic data rates for both baseband and IF microwave digital radio equalisers. Simple IF slope equalisers have been reported [57], as well as fully adaptive transversal equalisers [125, 126]. Another important and developing use for SAW filters in microwave digital radio, is in the construction of IF spectral shaping filters [127, 128], i.e. formation of the raised cosine pulse shape.

5.3.2 Digital Technology

Fully digital adaptive equaliser designs have generally been achieved by hardwired and programmable approaches. For microwave digital radio, hardwired designs are currently the only practical solution. Programmable designs, while relatively simple and flexible, have generally been limited to voiceband modem equalisers [65]. Certain receiver applications may however benefit from microprocessor/DSP control, for example in chapter 4, the proposed timing recovery technique may be implemented off-line under programmable control. Later in this chapter, a novel means of DSP equaliser adaptation is presented.

Digital microwave radio transmission rates test the limits of current digital technology. Again, digital designs are primarily based on transversal filters, however a digital DFE for a 100 Mbit/s 16-QAM system has been reported [120]. Only with the

development of monolithic simultaneous conversion ADCs has sufficiently high sampling become available for the digital processing of microwave channels. Resolution of 6-8 bits is currently possible [129], although 8-bit ADCs tend to be specialised and expensive. GaAs IC technology [130] may eventually allow the very high sampling rates required for fractionally spaced equalisers. Early voiceband digital equalisers employed MOS shift registers and TTL circuits. All recent microwave digital radio designs are based on LSI fabrication with 2.0 μm [131] and 1.5 μm [132] high speed semicustom CMOS gate array technology allowing potentially 50,000 transistor functions per circuit [4]. Importantly, this also facilitates the merging of earlier functional units employing ECL gate array technology, reducing redundancy [4].

For high data rates and short equaliser span, the distributed structure in figure 5.3.1(b) provides a practical implementation of the conventional tapped delay line structure. The output is now a cascade of multiply-accumulate products with fewer critical delays than the conventional structure. The conventional tapped delay line may be implemented directly with a single multiplexed multiply-accumulate product [125], however throughput is unlikely to be sufficiently high, for all but the lowest microwave data rates.

5.4 TAP ADAPTATION DESIGN

Section 5.3 concentrates mainly on general implementation techniques applicable to FIR filter implementation. The same implementation techniques are applicable to the implementation of the adaptive algorithm, however even with an analogue FIR, the adaptive algorithm will invariably be digitally implemented. Quantisation effects consequently become one of the main design issues for digital implementation, and the effects of employing finite word lengths on a number of adaptive algorithms will now be examined. The following discussion precedes the evaluation of a number of adaptive algorithms in section 5.5.

5.4.1 Design of Digitally Implemented Gradient Algorithms

Prior to considering specific algorithms, it is useful to briefly consider the general characteristics of finite precision adaptive algorithms. Section 5.2 introduced the finite precision digital number format and the associated errors due to quantisation. Such errors have an important bearing on numerical stability and accuracy. A numerically unstable algorithm allows errors to accumulate without bound, potentially resulting in an overflow condition. Computationally efficient forms of the recursive least squares

(RLS) are particularly prone to numerical problems [21], fortunately the LMS algorithm is more robust under finite precision constraints [58]. If error accumulation does result in LMS overflow, a technique known as leakage, may prevent overflow at the expense of some increase in computational burden. Leakage will be discussed shortly. The second important finite precision aspect is the effect on accuracy of the adaptive algorithm. Accuracy is highly dependant on the implemented word lengths. Infinite precision accuracy may be approached with longer word lengths.

In general terms, accuracy is highly dependent on the conditioning of the input, $x(k)$, i.e. the ratio between smallest and largest eigenvalues of the autocorrelation matrix, $\underline{\phi}_{xx}$. Accuracy is also a function of the convergence factor, μ, in the adaptive algorithm. Under stationary channel conditions, optimum infinite precision performance is obtained as $\mu \to 0$. Paradoxically, with finite precision implementation, performance actually degrades as $\mu \to 0$. Selection of an appropriate finite precision convergence factor will be discussed at various points throughout the remainder of this chapter.

5.4.2 The LMS and ZF Algorithms

Emphasis will now mainly be on the LMS algorithm and derivatives, in preference to the ZF algorithm for the reasons mentioned in chapter 2. Briefly, these were that noise effects are neglected in an optimum ZF solution, and ZF convergence is not guaranteed if the eye is initially closed. The zero forcing (ZF) algorithm has found implementation in a number of microwave digital radio systems [60, 131] due to it's relative simplicity. Under normal propagations and shallow fades, noise levels are low and the ZF algorithm will suffice, however it should be noted that noise will be enhanced due to the reduction in received power during deep fading. A limited number of finite precision analysis of the LMS algorithm are available and where necessary, key results are stated and taken into account during the the equaliser design. Results from the simulated finite precision equaliser design are discussed in section 5.5.

The basic LMS algorithm is now restated from equation (2.8.11) in chapter 2,

$$\underline{c}(k+1) = \underline{c}(k) - 2\mu \underline{x}(k) e(k) \tag{5.4.1}$$

where $\underline{c}(k+1)$ is the new unbiased estimate of the optimum Wiener solution and $e(k)$ is the error term, obtained as the difference between desired and estimated output states. Adaptation with the LMS algorithm will start to fail (stall) when the update product, $\mu \underline{x}(k) e(k)$, falls in magnitude below half the LSB value. This corresponds to satisfying the following condition to ensure convergence

$$|\mu \underline{x}(k)e(k)| \geq 2^{-B_c} \tag{5.4.2}$$

where B_c is the [illegible] length used for coefficient storage. Fractional number representation is assumed. It has been shown that the mean square arithmetic error value is in fact approximately inversely proportional to the convergence factor, μ [133]. In terms of the overall equaliser design, a practical solution to this problem is to increase the operating bit lengths for coefficient storage and updating [125].

Convergence to nonglobal minima may result if the input autocorrelation matrix, $\underline{\phi}_{xx}$, contains small eigenvalues. This corresponds to an input with little or no energy over certain frequency bands. This is of particular relevance to fractionally spaced equalisers. During operation, errors may accumulate over time, however in such a way that the error output is unaffected. Word growth is hidden from the LMS algorithm, and eventually overflow may occur due to the finite precision numeric bounds. Saturation arithmetic may reduce the subsequent requirement for retraining [134], or alternatively 'leakage' may be introduced, increasing numerical performance at the expense of slight increases in performance degradation and complexity. Leakage methods augment the performance criteria by a term bounding or containing the energy in the equaliser response. The 'tap leakage algorithm' (TLA) [135] modifies (5.4.1) to

$$\underline{c}(k+1) = (1-\gamma)\underline{c}(k) - 2\mu \underline{x}(k)e(k) \tag{5.4.3}$$

where a decay factor, γ, is introduced into the usual algorithm. The TLA thus attempts to find a compromise setting between minimising the MSE and containing the energy of the coefficient settings in a finite precision implementation, according to the modified cost function [65]

$$\mu \underline{c}^*(k)\underline{c}^T(k) + \xi(k) \tag{5.4.4}$$

with $\xi(k)$ denoting MSE, as defined by equation (2.7.2). The input autocorrelation matrix may also be viewed as

$$\underline{\phi}_{xx} + \mu I \tag{5.4.5}$$

where I is the identity matrix. The autocorrelation matrix now has a smallest eigenvalue of greater than μ, thus favourably conditioning the input. For finite precision implementation, the LMS algorithm may be redefined as

$$\underline{c}(k+1) = \underline{c}(k) - 2\mu . f[\underline{x}(k)] . f[e(k)] \tag{5.4.6}$$

where

$$f[x] = sgn[x] . 2^{[[\log_2 |x|]]}$$

and $[[x]]$ denotes the greatest integer less than or equal to the argument.

A number of simplifications are possible to the basic LMS algorithm in equation (5.4.1), leading to reduced complexity at the expense of some performance degradation. Simplification is commonly through using only the sign information from signal inputs e.g. the clipped LMS algorithm [125]

$$\underline{c}(k+1) = \underline{c}(k) - 2\mu.sgn[\underline{x}(k)]e(k) \tag{5.4.7}$$

The sign function, $sgn[x]$, is defined by

$$sgn[x] = \begin{cases} 1 & x \geq 0 \\ -1 & x < 0 \end{cases} \tag{5.4.8}$$

Steady state performance is compatible with the linear LMS algorithm, while convergence is approximately 25% slower [125]. Implementation of the update product no longer requires full multiplication, as the error term, $e(k)$, is now either inverted or unaltered conditional on the sign of $x(k)$. This is the logical equivalent to an EXOR function. Multiplication of the convergence factor is by scaling by a factor of two, equivalent to a binary right shift by simply misaligning the bits of the parallel data word.

The ZF algorithm is an iterative solution, minimising the equalised peak distortion, and not MSE. From equation (2.8.5) in chapter 2, the ZF algorithm is recursively described by

$$\underline{c}(k+1) = \underline{c}(k) - \mu_{ZF}.sgn[\underline{y}(k)]e(k) \tag{5.4.9}$$

where $\underline{y}(k)$ is the output from the decision device after equalisation. Implementation requirements for the ZF algorithm will be similar to those for the clipped LMS algorithm. Reported simulation results have indicated that a word length of 10 provides sufficient internal resolution, together with an 8 bit ADC [131].

5.4.3 The Block LMS Algorithm

The block LMS (BLMS) algorithm may be viewed in one sense as an extension of the LMS algorithm, where the update product, $\mu\underline{x}(k)e(k)$, is replaced by a time averaged value. Adaptation with the BLMS algorithm is performed according to

$$\underline{c}(k+1+L) = \underline{c}(k) - 2\mu_L \frac{1}{L}\sum_{m=0}^{L-1} \underline{x}(k+L-m)e(k+L-m) \tag{5.4.10}$$

where L corresponds to the block length. By setting $L=1$, equation (5.4.10) reduces to (5.4.1), the conventional LMS algorithm. The LMS algorithm thus may in fact be considered as a special case of the BLMS algorithm with a block length, $L=1$. To ensure BLMS convergence, μ_L should be bounded by [136]

$$0 < \mu_L < \frac{L}{(L+2).N.E[x^2(n)]} \tag{5.4.11}$$

where N is the number of equaliser taps. Setting $L=1$, (5.4.11) reduces to the equivalent bound for the LMS algorithm given by equation (2.8.10) in chapter 2.

The BLMS algorithm is valid for any block length, L, greater than or equal to 1, where L is greater than the equaliser time span, N, tap adaptation is performed with more information than required by the FIR filter, implying additional hardware and inefficiency. For $L \leq N$, the filter length is longer than the input block, also implying inefficiency. With the following results, for a tapped delay line of length 7, the block length is taken as $L=8$, such that L is an integer power of 2. This results in straightforward implementation of the time averaging operation (an arithmetic shift left corresponding to division). Simplification of the algorithm is possible by using only sign information when calculating the update product, in a similar manner to the clipped LMS algorithm. Results with the clipped BLMS (CBLMS) algorithm are given in section 5.5, and the algorithm may be recursively described by

$$\underline{c}(k+1+L) = \underline{c}(k) - 2\mu_L \frac{1}{L} \sum_{m=0}^{L-1} sgn[\underline{x}(k+L-m)]e(k+L-m) \qquad (5.4.12)$$

A major motivation in the development of block adaptive algorithms is the reduction in computation through using fast convolution techniques in the frequency domain [137]. Frequency domain implementation is however only efficient for block lengths of greater than 64 [63] i.e. considerably longer than the time span of microwave digital radio equalisers.

Analogous to the relationship between the recursive descriptions of LMS and BLMS algorithms are the applicable Wiener filter solutions. The solution to the block Wiener filter is given by [63]

$$\underline{c}_{opt,L} = \underline{\phi}^{-1}_{xx,L} \underline{\phi}_{xy,L} \qquad (5.4.13)$$

where notation is defined in a similar manner to equation (3.3.3), except now over the block input case. Under stationary conditions, the block MSE is equivalent to the conventional MSE [63]. Care should however be taken in generalised BLMS performance for all applications. BLMS and LMS algorithm performance has been shown to be similar for channel equalisation, however when applied to system identification with a highly ill-conditioned input, BLMS performance was generally inferior [21] .

When considering analogue or infinite precision time domain implementation, there is no advantage in using the BLMS algorithm, hence it's omission from earlier chapters. For practical finite precision implementation, results in section 5.5 will demonstrate that the BLMS algorithm converges to a lower steady state solution than

the LMS algorithm, and this may be translated into a reduction in required bit lengths. Recent analysis on LMS/BLMS performance appears contradictory, and requires careful interpretation with the physical implementation. Panda et al [138] suggest that a possible saving of around 2-3 bits is possible with the BLMS algorithm, however this analysis neglects the saturation problem. Bershad does include this saturation problem, concluding that the BLMS algorithm actually requires $\frac{1}{2}\log_2 L$ more bits for the same steady state (or stalling) performance [139]. In fact, with careful design, results compatible with those of Panda are possible. This is in agreement with work applying the BLMS algorithm to echo cancellers [140, 141].

Two solutions to the problem of BLMS saturation are proposed. Saturation may be avoided with careful use of scaling during the design stage. Simulations play an important role in quantifying the required dynamic ranges. Secondly, a novel solution is to switch from LMS to BLMS algorithms after an initial fixed training period. This switched algorithm approach combines the advantages of both algorithms, namely faster convergence and improved steady state MSE performance. In terms of implementation, the additional hardware would consist of switching circuitry plus a counter/control to achieve the switching after a fixed time period of say 50-100 iterations. Performance results from both solutions to the BLMS saturation problem will be discussed in section 5.5.

5.5 ADAPTIVE ALGORITHM PERFORMANCE - A COMPARATIVE STUDY

Of the adaptive algorithms introduced in section 5.4, only the ZF and LMS algorithms have found serious application to microwave digital radio equalisers. Given the effect of quantisation error in the adaptation process, it is perhaps surprising that alternative, computationally simple algorithms have not received consideration. A comparative study now follows, with the objective of evaluating a number of adaptive algorithms to update a 7-tap symbol spaced transversal equaliser in a 34 Mbit/s 4-QAM microwave digital radio system.

Five algorithms are now considered: (1) least means squares (LMS), (2) clipped least mean squares (CLMS), (3) block least mean squares (BLMS), (4) clipped block least mean squares (CBLMS), and (5) zero forcing (ZF). Block algorithms are implemented in the time domain with block length $L = 8$. For ease of implementation convergence factors were chosen to be an integer power of 2 i.e.

$$\mu_L = 2^{-n} \tag{5.5.1}$$

where L denotes the block length and the maximum value for n is dictated by the available arithmetic precision. Setting $L = 1$ implies the convergence factor for the

LMS algorithm (block length = 1). To ensure similar convergence rates, the convergence factors is set according to the following ratio

$$\mu_L = L\,\mu_1 \tag{5.5.2}$$

For the simulation study, the following convergence factors were used

$$LMS:\ \mu_1 = 0.015625 = 2^{-6} \quad BLMS:\ \mu_8 = 0.125 = 2^{-3} \tag{5.5.3}$$

The ZF and LMS convergence factors were taken to be the same. Table 5.1.1, compiled from section 5.4, provides recursive descriptions for each algorithm.

Algorithm	Recursive Update
LMS	$\underline{c}(k+1) = \underline{c}(k) - 2\mu.\underline{x}(k)e(k)$
Clipped LMS	$\underline{c}(k+1) = \underline{c}(k) - 2\mu.sgn[\underline{x}(k)]e(k)$
BLMS	$\underline{c}(k+1+L) = \underline{c}(k) - \frac{2}{L}.\mu_L.\sum_{m=0}^{L-1}\underline{x}(k+L-m)e(k+L-m)$
Clipped BLMS	$\underline{c}(k+1+L) = \underline{c}(k) - \frac{2}{L}.\mu_L.\sum_{m=0}^{L-1}sgn[\underline{x}(k+L-m)]e(k+L-m)$
Zero Forcing	$\underline{c}(k+1) = \underline{c}(k) - \mu.\underline{y}(k)e(k)$

Table 5.5.1 Adaptive Algorithm Definitions

The presented results are not exhaustive instead emphasis is on comparative performance of the algorithms, and results are presented where neccessary, illustrating major points. Specific acceptable performance levels will inevitably be specified by the particular application. With the emphasis on algorithm performance, results are presented for a a 7-tap symbol spaced transversal equaliser operating with a 34 Mbit/s 4-QAM system and a receiver SNR of 50 dB. Specific assumptions regarding the implementation of the multi-level decision device are thereby avoided. The LMS algorithm is taken as the performance benchmark, since it's performance is well known and finite precision analysis already provides an indication of required word lengths [142, 143]. Figures 5.5.1 to 5.5.3 illustrate the effects of implementations with different word lengths, on the convergence properties of the three main algorithm types (LMS, BLMS and ZF) with an ensemble average length of 100. Results were obtained from a receiver with automatic gain control and MEO timing. In a similar manner to chapters 3 and 4, simulations were performed at baseband with carrier recovery

assumed ideal. Specific equaliser internal arithmetic arrangements are defined by table 5.5.2, while the equaliser is retraining on Channel A in table 5.5.3.

	Word Lengths			
Configuration	ADC	FIR Filter	Updating	DAC
A	8	8	8	8
B	8	10	12	8
C	8	8	14	8
D	8	10	14	8
E	8	14	16	8

Table 5.5.2 Equaliser Internal Arithmetic

	Channel A	**Channel B**
Notch Depth	5 dB	15 dB
Phase Type	MP	MP
Frequency Offset	0 MHz	0 MHz
Min. Eigenvalue	0.8924	0.3295
Max. Eigenvalue	1.1620	2.0114
Eigenvalue Ratio	1.3021	6.1050
Optimum Wiener MSE	-49.92 dB	-37.39 dB

Table 5.5.3 Channel Specifications

For simplification, ADC and DAC word lengths were fixed at 8 bits, in keeping with current practical resolution. The effects of different ADC/DAC resolution are assessed elsewhere [58, 144]. Section 5.4 discussed two means of limiting the problem of

BLMS saturation during the initial retraining stage. Figure 5.5.2 is obtained from the scaled solution, consistent with the definitions given in table 5.5.1 and equation (5.4.10). The switched BLMS solution, along with the clipped algorithms, will shortly be examined. Results in figure 5.5.1 are fairly consistent with existing published work on the LMS algorithm [125, 142], the major observation being that coefficient resolution of greater than 10 bits is required for acceptable performance. Where sufficient lengths are not available (e.g. configurations **A** and **B**), adaptation stalling follows and the equaliser coefficients remain close to the forced values at reset. These convergence curves were obtained with decision-directed operation, where the equaliser output is assumed correct, and then used to calculate the error term. For a relatively shallow fade, the reset condition corresponds closely to the final tap setting. The resulting convergence curve is initially very steep, while further convergence is dependant on the convergence and the available arithmetic precision. Figures 5.5.1 to 5.5.3 also provide the first indication that the LMS algorithm may not be the ideal algorithm for implementation at high data rates where scope for high arithmetic accuracy is limited. Both ZF and BLMS algorithms offer improved steady state performance, the BLMS algorithm, more so. For practical implementation, the required word lengths indicated by figures 5.5.1 to 5.5.3 may not be practical, hence for further results fixed internal bit lengths were set. Configuration **B** provides realistic bit lengths for high speed implementation, and this arrangement provided the remaining simulation results in this section.

Figures 5.5.4 to 5.5.10 illustrate convergence of the 5 algorithms in table 5.5.1 with the addition of the switched BLMS algorithm, during conditions specified by channels **A** and **B** in table 5.5.3. Channel **A** is representative of a shallow MP fade, while a more severe fade is represented by channel **B** . Figure 5.5.4 is an infinite precision benchmark with the LMS algorithm converging close to the optimum Wiener solutions of -49.92 dB and -37.39 dB for channels **A** and **B**, respectively. When implemented according to configuration **B**, the LMS algorithm suffers greatest degradation. Improved performance is obtained with greater word lengths as indicated by figure 5.5.1. Use of sign information in the clipped LMS algorithm, requires less overall precision and resulted in the improved convergence curves in figure 5.5.2. The zero forcing algorithm, with similar implementation requirements to the clipped LMS algorithm, produced still better convergence, at the expense of increased steady state error variance. The three block algorithms all produced MSE results typically better than the ZF algorithm. The clipped BLMS algorithm resulted in the lowest overall MSE, however a degree of noise is introduced to the the steady state MSE, increasing the variance in a similar manner to the clipped LMS algorithm.

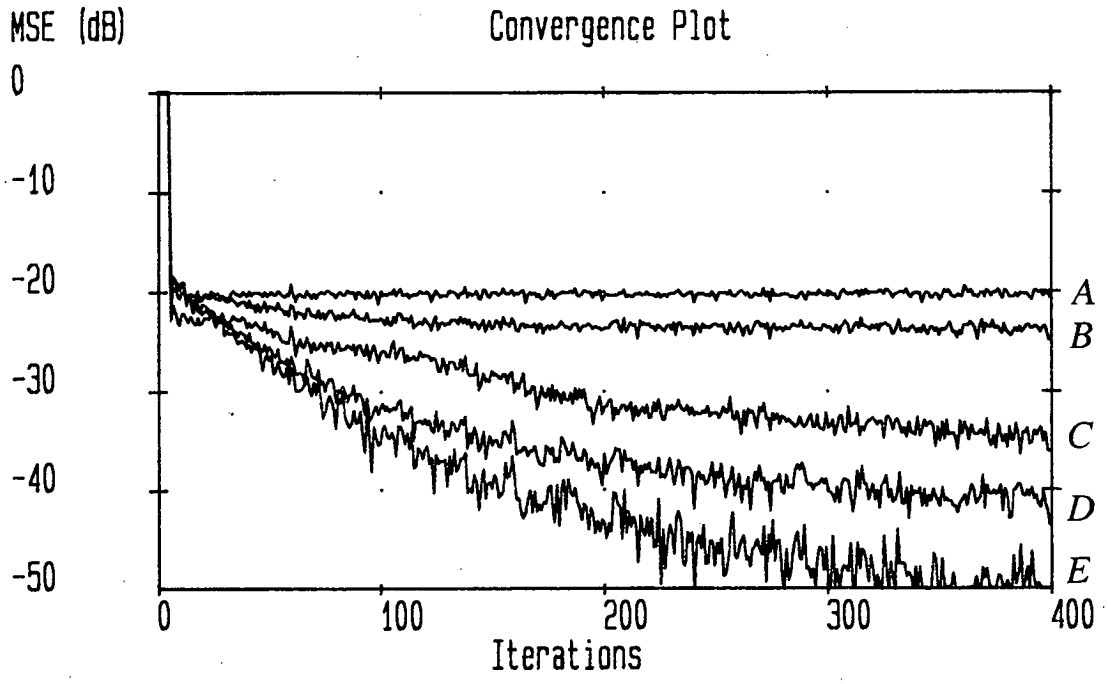

Figure 5.5.1 Finite Precision LMS Performance

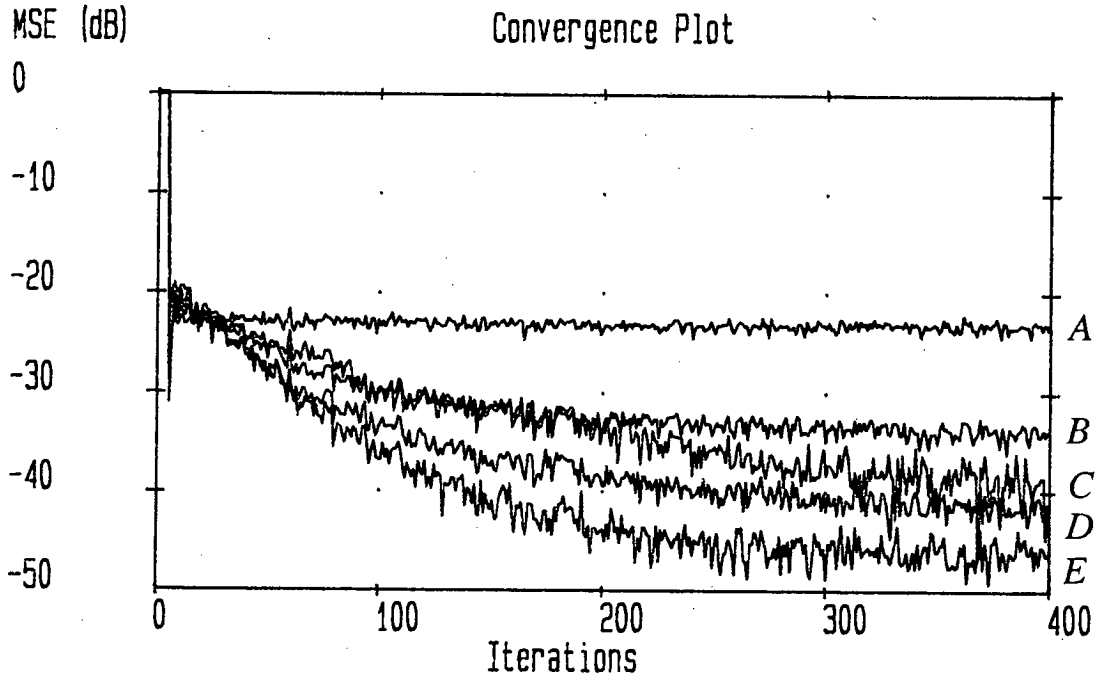

Figure 5.5.2 Finite Precision BLMS Performance

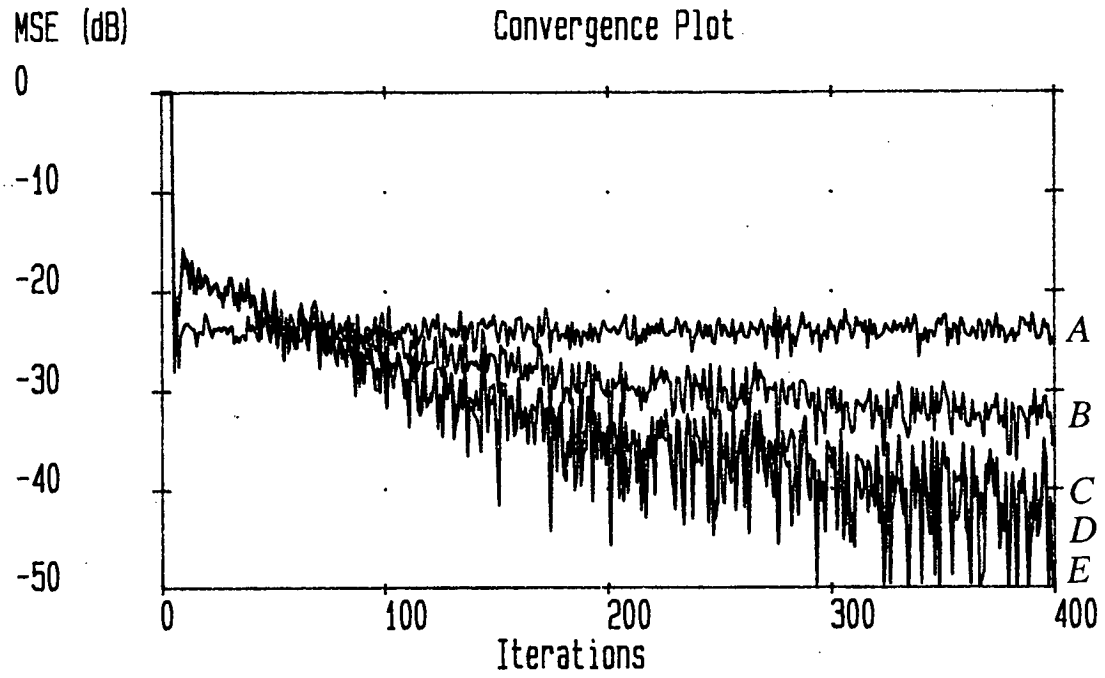

Figure 5.5.3 Finite Precision ZF Performance

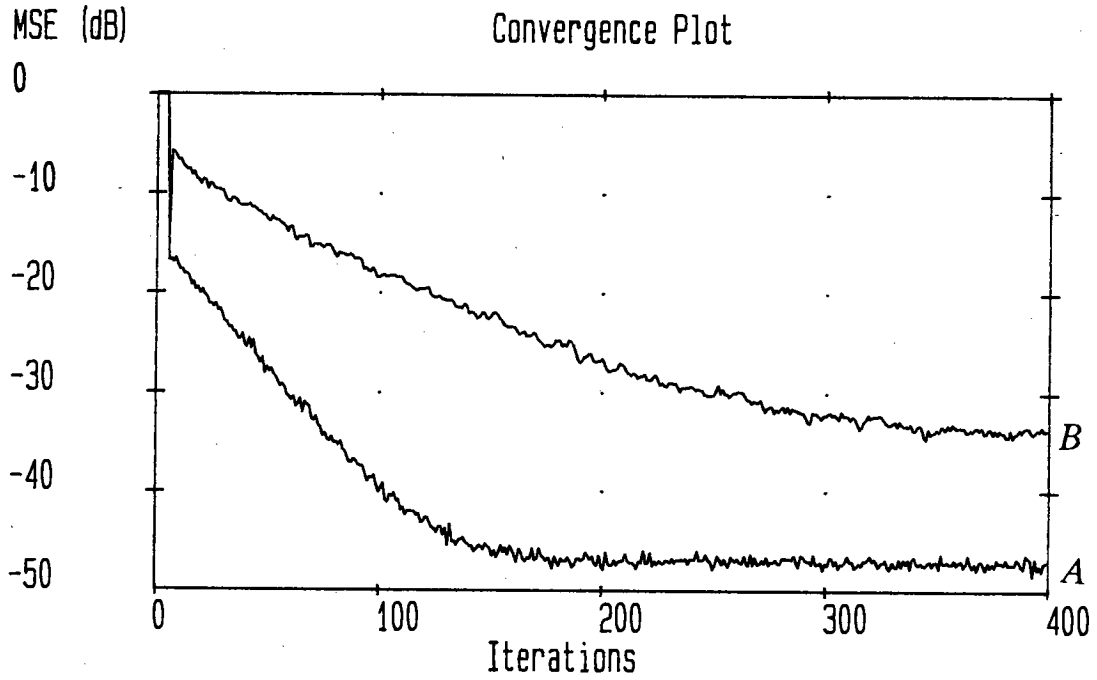

Figure 5.5.4 Infinite Precision LMS Performance. Channels A and B

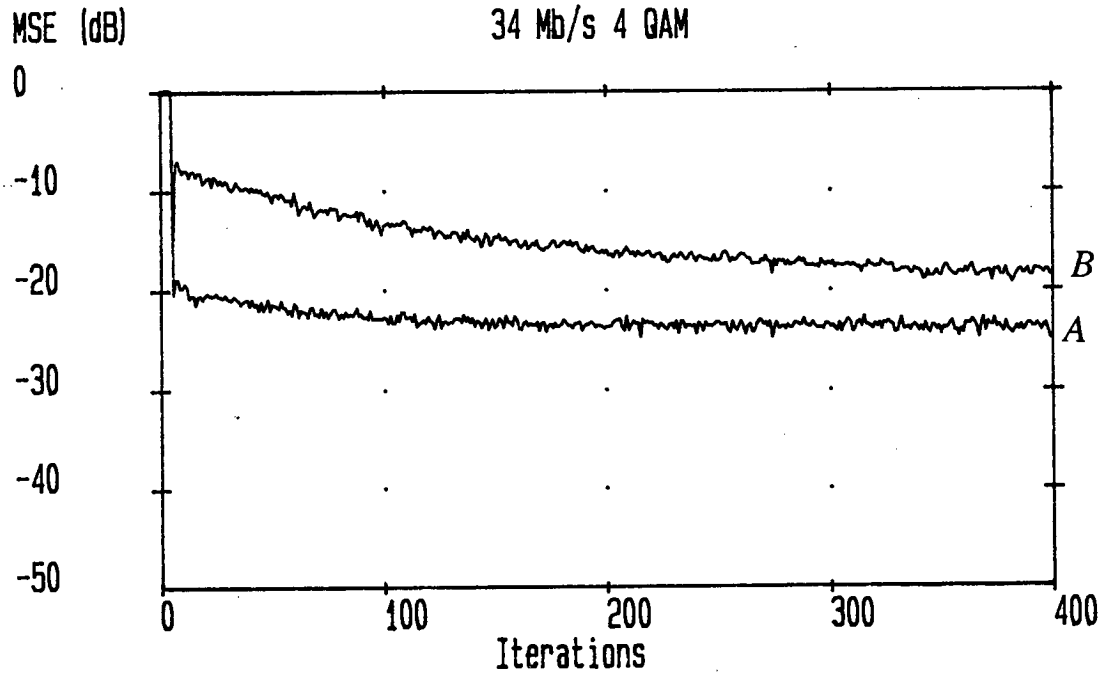

Figure 5.5.5 Finite Precision LMS Performance. Channels **A** and **B**

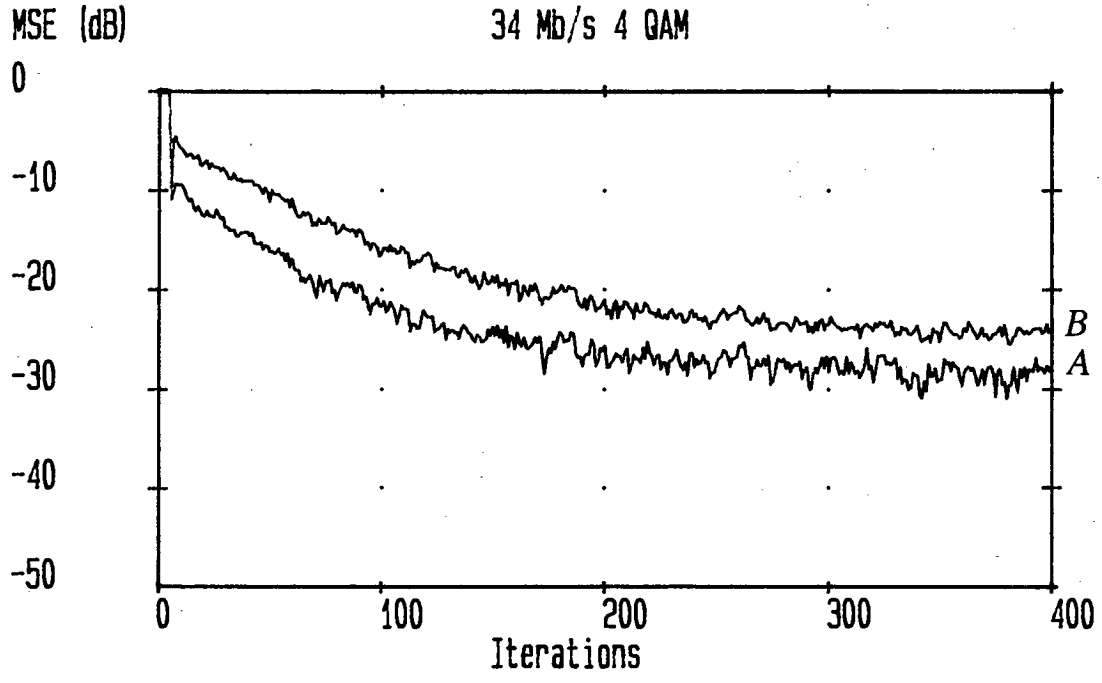

Figure 5.5.6 Finite Precision CLMS Performance. Channels **A** and **B**

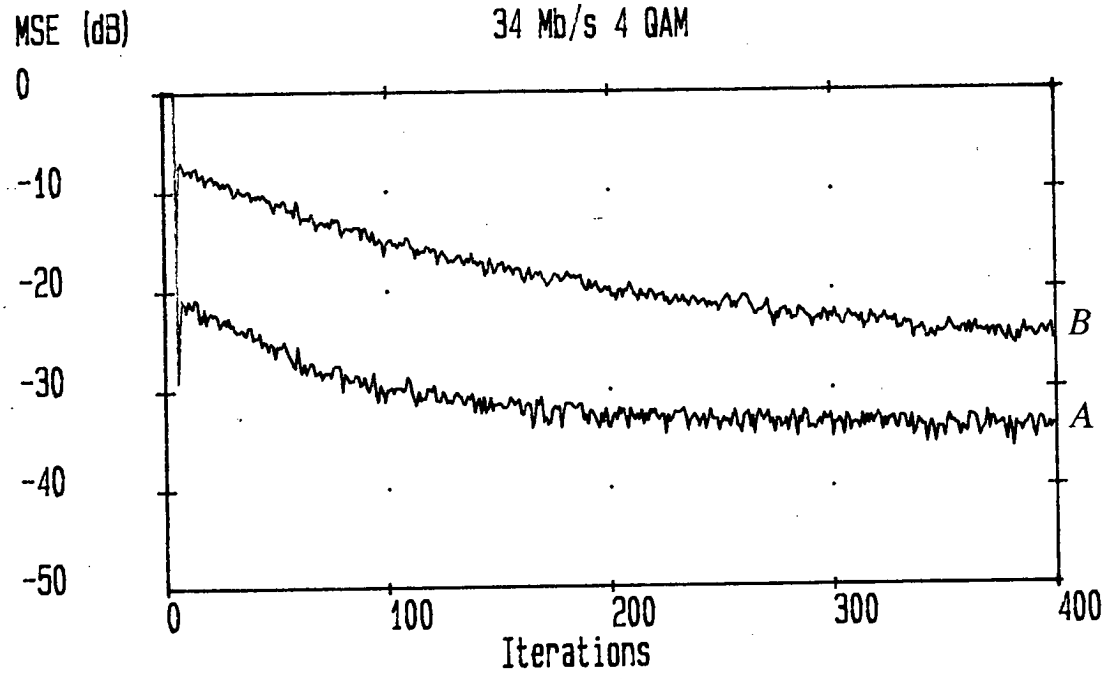

Figure 5.5.7 Finite Precision Scaled BLMS Performance. Channels **A** and **B**

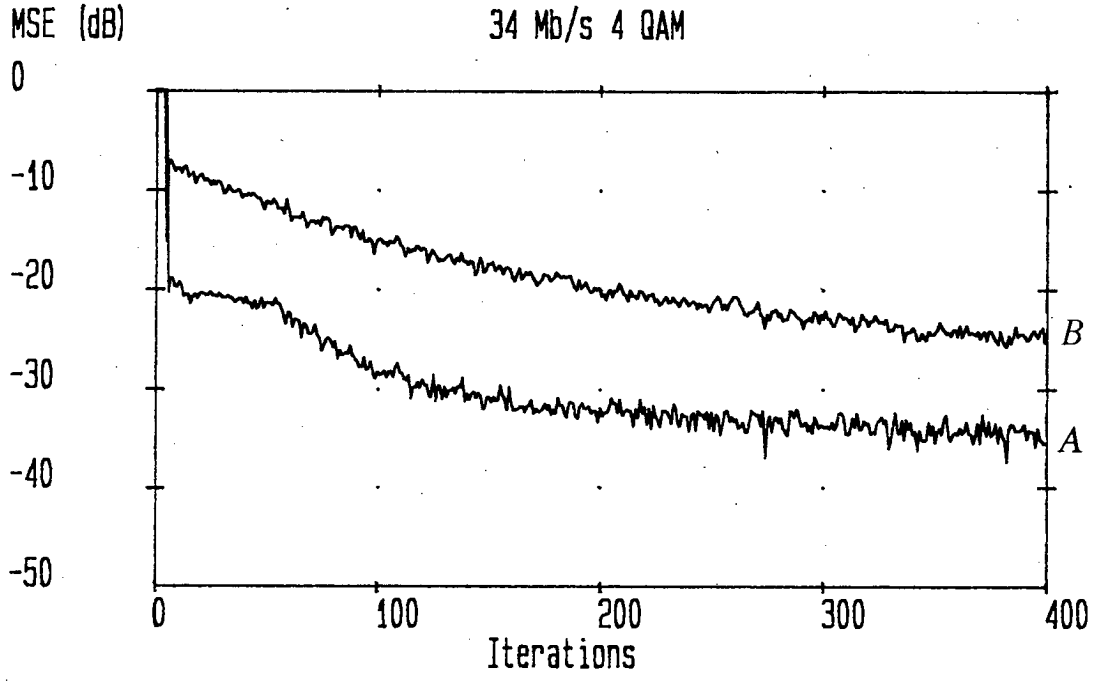

Figure 5.5.8 Finite Precision Switched BLMS Performance. Channels **A** and **B**

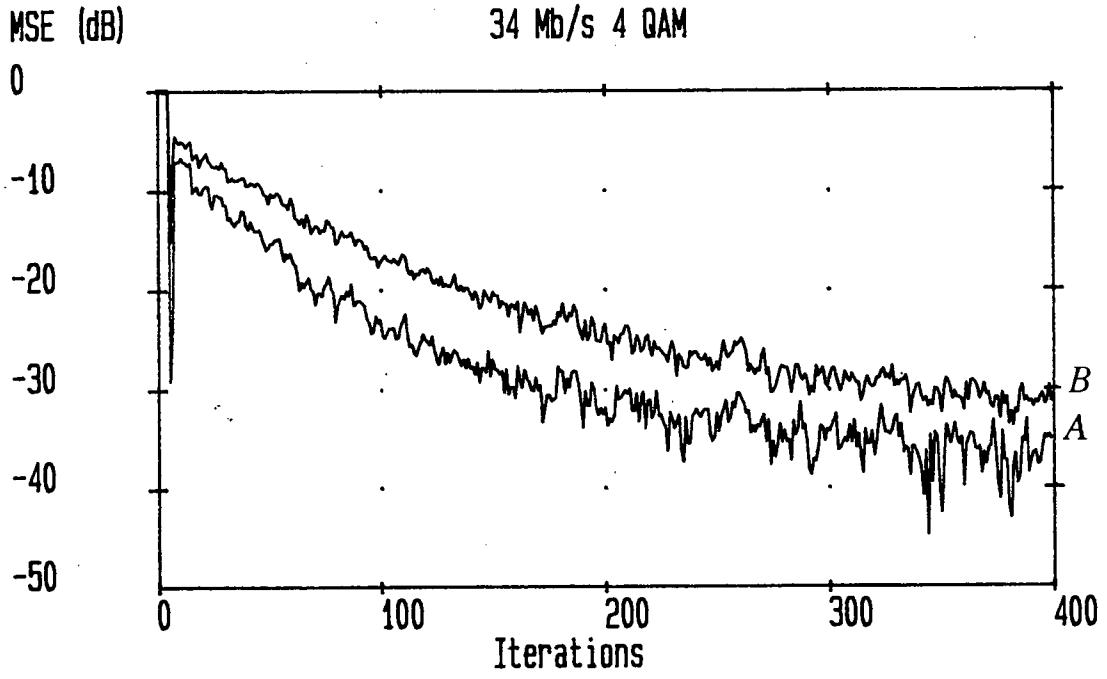

Figure 5.5.9 Finite Precision CBLMS Performance. Channels **A** and **B**

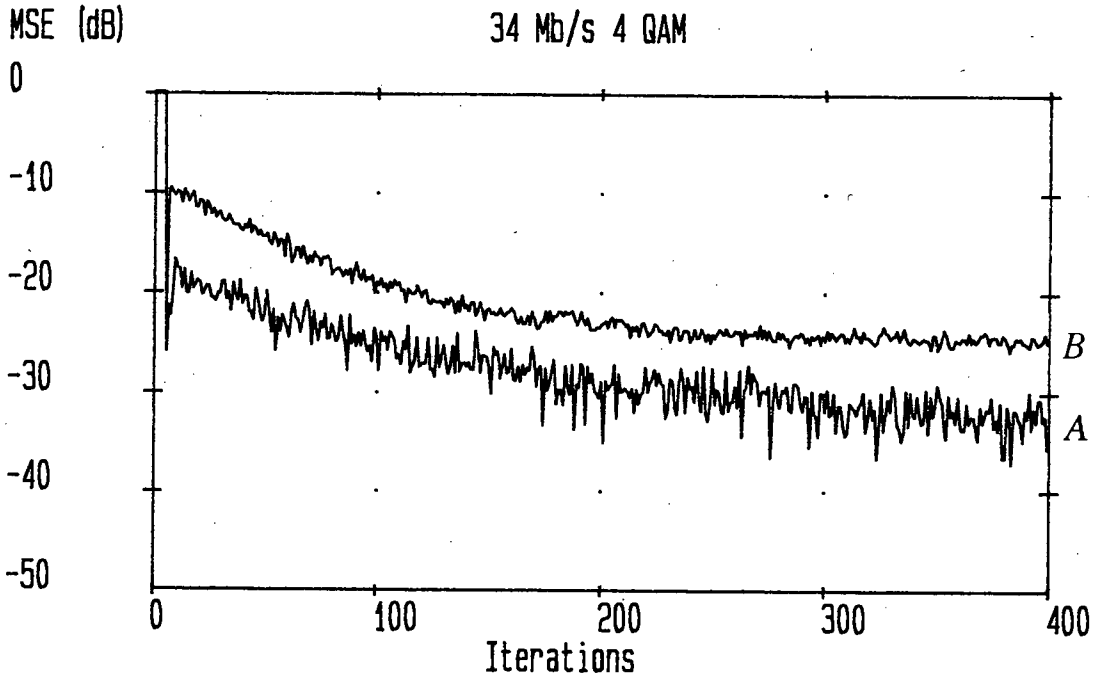

Figure 5.5.10 Finite Precision ZF Performance. Channels **A** and **B**

Table 5.5.4 summarises results from the preceeding discussion. While not intended to be conclusive, the table does give an indication of the comparative algorithm performance within the constraints of relatively short lengths.

Rating	Algorithm	Comments
1	BLMS (Switched)	*Best steady state performance. Requires some additional control logic.*
2	Clipped BLMS	*Similar complexity to LMS. Good performance at expense of increased error variance.*
3	BLMS (Scaled)	*Similar performance to ZF, but more complex. Loss in dynamic range due to scaling.*
4	ZF	*Good performance when noise and distortion are initially low. Simpler than BLMS*
5	Clipped LMS	*Similar in complexity to ZF. Performance not as good, but likely to be more robust.*
6	LMS	*Performance benchmark. Not ideal for high speed implementation unless high precision available.*

Table 5.5.4 Algorithm Performance

With the simulated word lengths, results indicate the performance gain through using block adaptation. With increasing word length, the gain will diminish as results tend to approximate those obtained with infinite precision. Table 5.5.4 is arranged in terms of steady state MSE performance, with the switched BLMS algorithm rated first. Implementation requirements vary from the clipped LMS and ZF algorithms, to the switched BLMS algorithm. Table 5.5.5 summarises the implementation requirements for each algorithm with a transversal equaliser of length N. Factors such as operating speeds, convergence/update rates, and implementation difficulty should be also considered prior to implementation.

To conclude, this section has indicated the suitability of time domain block algorithms for the adaptation of microwave digital radio equalisers. This conclusion is not intended as general, but specific to the special characteristics and requirements of microwave digital radio.

	Operation		
Algorithm	Multiply	Add	Shift/Invert
ZF	-	*N*	*2N*
CLMS	-	*N*	*2N*
LMS	*N*	*N*	*N*
CBLMS	-	*2N*	*2N*
BLMS (Scaled)	*N*	*2N*	*N*
BLMS (Switched)	*N*	*2N*	*N*

Table 5.5.5 Algorithm Complexity

5.6 CHANNEL SIMULATOR DESIGN

A means of testing the constructed hardware described in section 5.7, was required. The following section covers potential simulator designs and the approach actually taken.

5.6.1 Channel Simulator Implementations

Channel simulators provide a means of assessing equaliser hardware under controlled fading conditions. Field testing, while still ultimately necessary, is by comparison time consuming, expensive, and is without the advantage of a priori channel knowledge. To assess the performance of the equaliser implementation described in section 5.7, a channel simulator was required. The following brief discussion covers possible simulator designs, leading to a description of the hardware design actually employed.

Generally, simulators are designed for the IF or RF operation of a complete radio system [145-147]. For testing a baseband equaliser , such elaboration is not essential, and a baseband channel simulator is permissible. IF/RF simulators generally implement the two path, three path or 'Rummler' models directly through an arrangement similar to figure 5.6.1. The relative time delay, τ, may be introduced by a length of coaxial cable, either switchable in length or fixed according to a set delay e.g. 6.3 ns. Attenuators and a phase shifter control the fading parameters. Computer

control is desirable, providing dynamic control and ease of use [146, 147].

For testing a 'stand alone' equaliser, a slightly different solution was taken in designing the channel simulator. Since the required data rate was relatively low and the equaliser was to be tested at baseband, the equivalent baseband channel response was modelled by a programmable FIR filter. This approach is now discussed.

5.6.2 A Practical Channel Simulator

Figure 5.6.2 is a block diagram of the constructed channel simulator. This structure offered a straightforward solution to hardware testing, and while only applicable to static channel conditions, the design has sufficient flexibility to ultimately include dynamically varying fading conditions. Appendix E includes circuit diagrams for the construction used to produce the convergence results in section 5.7. The overall structure is very similar to the simulated multipath channel, allowing straightforward calculation of the binary channel coefficients for manual setting on the board. Factors such as timing phase and automatic gain control are taken into account in the simulation program. The programmable FIR filter is based around a TRW TMC2243 IC, implementing the FIR in a distributed manner similar to figure 5.3.1(b) and offering a potential clock rate of 20 MHz. This high rate made the TMC2243 suitable for inclusion in the channel simulator and the equaliser design. The FIR output is passed directly to the output port as an 8 bit 2's complement parallel word. The 10 bit FIR output is truncated to 8 bits. Data and noise sources are provided by pseudo random binary sequence generators [148].

To assess equaliser performance during dynamic (slowly-varying) conditions, the switch bank in figure 5.6.2 would be replaced by an EPROM/PROM arrangement, for the storage of the channel coefficients corresponding to various degrees of fading. Accessing channel coefficients would be under the control of two counter circuits, one to generate the next sequential memory address, and the second to control the rate of memory access i.e. the rate of dynamic change.

5.7 A DIGITAL EQUALISER DESIGN

The survey in sections 5.3 and 5.4, and the results from 5.5, revealed that considerable complexity and effort is required to satisfy the performance standards of modern microwave digital radio. Any reduction in processing and hardware complexity is highly desirable, allowing the use of more complex techniques. A structure is now proposed based on 'off-line' equaliser adaptation, and results are presented from the implementation of the adaptation section.

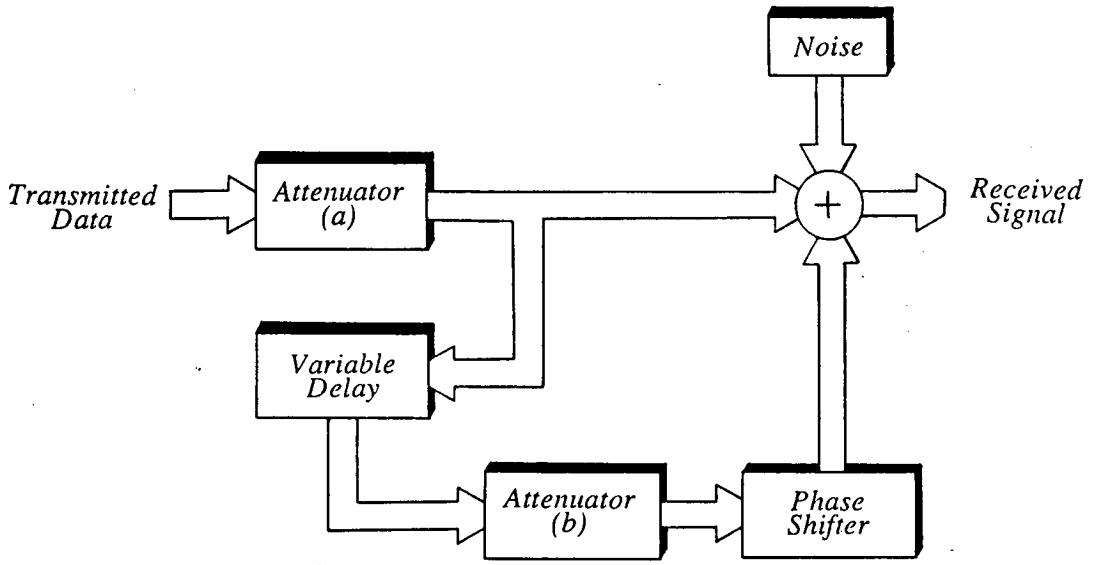

Figure 5.6.1 General Three Path Simulator

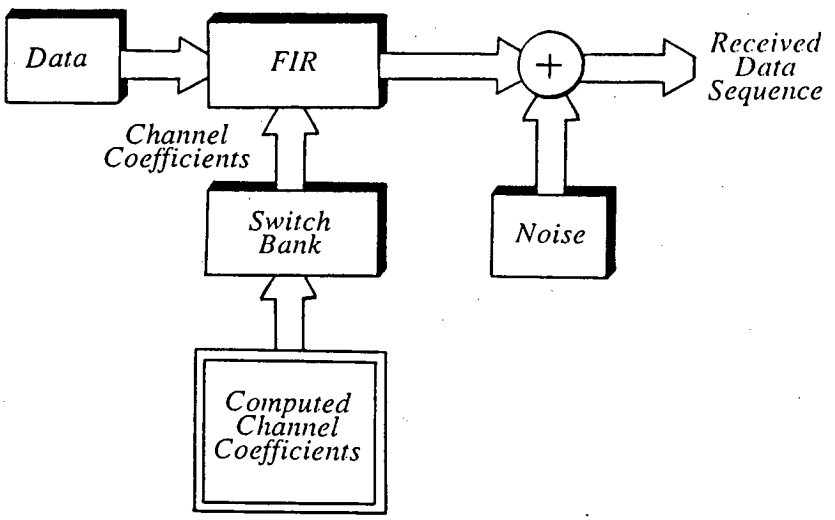

Figure 5.6.2 Channel Simulator Block Diagram

5.7.1 An Off-Line Approach

While the FIR filter section of the adaptive equaliser must still run at the symbol rate, the relative channel stationarity may be exploited by off-line processing to update at less than the symbol rate. The construction is an initial feasibility study and was designed to equalise the real channel of an 8 Mbit/s QPSK digital radio system. Full operation would require careful PCB construction in place of the current wire-wrap connected Eurocards.

The proposed equaliser structure is illustrated in figure 5.7.1, and differs from figure 5.1.1 in the requirement for buffering to pass data and updated coefficients between the programmable FIR filter and adaptation sections. The FIR filter is based on a cascade of the same TMC2243 device used in the channel simulator. Buffering is accomplished by fast access RAMs with over all control provided by the adaptation board. Transfer of data blocks is possible with the RAMs, rendering the overall structure particularly suitable for implementing the BLMS algorithm. Off-line adaptation permits the direct use of DSPs in the adaptation process, with the benefits of flexibility and compact design. DSP designs have other advantages when compared to hardwired implementations, for example, optimisation in performing certain arithmetic functions and relatively long computational word lengths. The consequences of DSP implementation of the adaptive algorithms is discussed, together with hardware results, in the next section. Selection of a Texas Instruments TMS32010 DSP was based on cost and the backup/support facilities available. Future designs could operate faster and more efficiently with one of the so-called 'third generation' DSPs e.g. the TMS320C30 (the TMS32010 ranks as a 'first generation' DSP).

Hardware results are given only from the DSP adaptation board. The FIR filter board was constructed, and the correct logical operation of control signals and data transfer via the buffering RAMs, confirmed. Complete testing has not been possible and as such, the FIR board is discussed no further. Sufficient versatility was incorporated into the design to allow direct connection of the channel simulator to the coefficient adaptation board, rather than indirectly through the FIR board.

5.7.2 Hardware Results

Some results are now presented illustrating real and simulated convergence of the adaptive algorithm hardware. The hardware test arrangement in figure 5.7.2, essentially consists of the channel simulator and algorithm adaptation blocks, with analogue outputs obtained via DACs. TMS32010 code for implementing the test structure is included in appendix F.

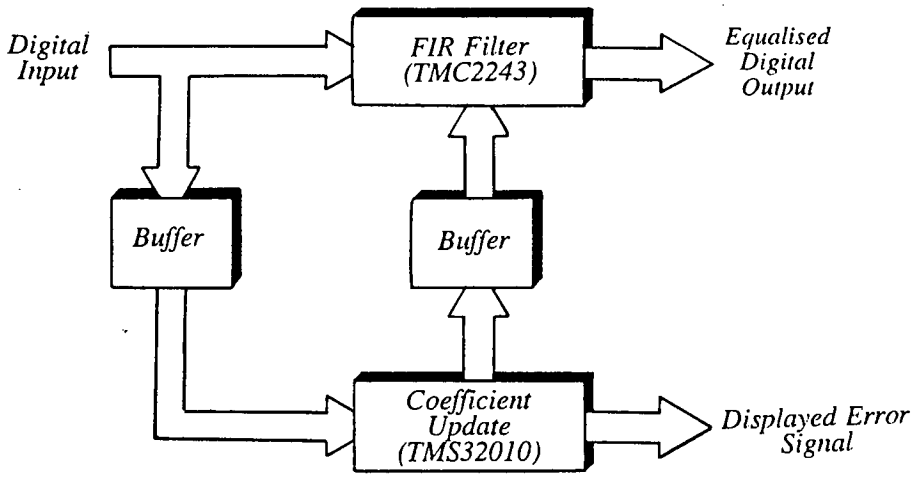

Figure 5.7.1 Proposed Equaliser Design

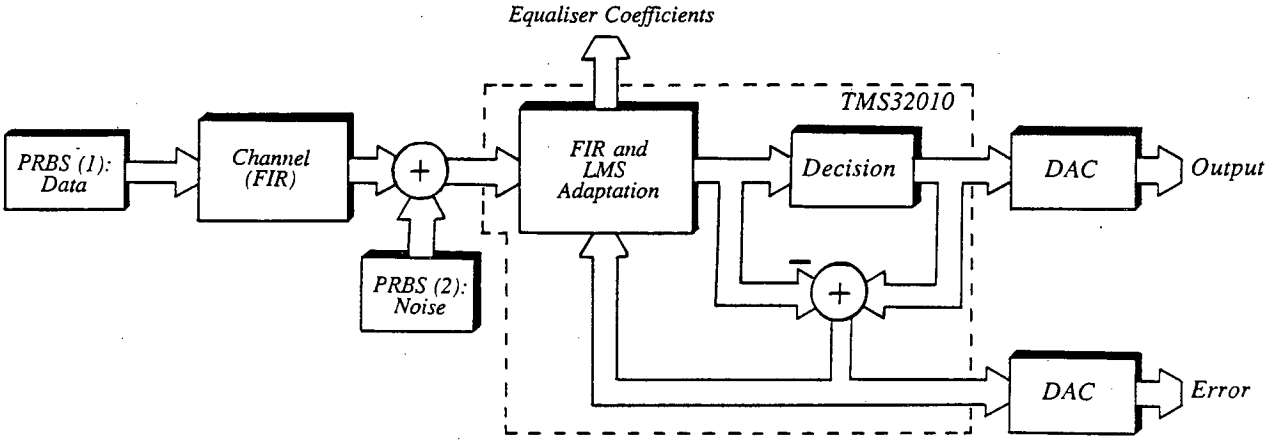

Figure 5.7.2 Hardware Test Arrangement

The simplest structure was initially examined: a (7 tap) symbol spaced transversal equaliser, along with LMS and BLMS adaptive algorithms. Clipped adaptation algorithms were not included because the computational saving for DSP implementation will be minimal. Convergence factors were set according to equations (5.5.1) and (5.5.2) and values of 0.125 and 0.015625 were adopted for the LMS and BLMS algorithms, respectively.

Figures 5.7.3 and 5.7.4 represent convergence curves obtained with retraining on channels **A** and **B** in table 5.5.3. Individual photographs represent the decision-directed convergence of the error magnitude from a reset condition (center coefficient set to one, all others zero). Two observations are readily made. Firstly, with increased signal coloration, the error mean and variance, not unexpectedly, increase. Ensemble averaging would be required to produce results for comparison with simulations. The second observation is that there is actually little observable performance difference between the LMS and BLMS algorithm implementations. Results from section 5.5 would appear to contradict this statement, however relatively high arithmetic accuracy is available with the DSP (16 bit data words, 32 bit ALU). When implemented with infinite precision, both algorithms should yield comparable results [63]. Shorter and more practical word lengths for a hardwired design were considered in section 5.5. Figure 5.7.5 provides simulated finite precision ensemble averaged curves for the same channel conditions as figures 5.7.3 and 5.7.4, and with similar arithmetic precision to the DSP. The similarity in performance is apparent.

5.8 FURTHER DESIGN CONSIDERATIONS

A number of design issues have been addressed so far in this chapter. Inevitably many questions remain unsolved and new ones arise. With application to higher level modulation formats, even further demands will be placed on the adaptive equaliser to counter multipath channel distortion and nonlinearities in the transmitter amplifier. Potential developments of the two main ideas proposed in this chapter will now be assessed.

Application of block adaptation is highly dependant on the implementation approach. High speed operation invariably limits the amount of feasible processing and the results in section 5.5 were derived under this assumption. Given that word lengths may be limited, the performance improvement from block adaptation should be weighted against the additional hardware required to implement the algorithm. In the case of the simplest block algorithm, the clipped BLMS, the additional hardware would consist of another add/register plus control logic to initiate the averaging (a

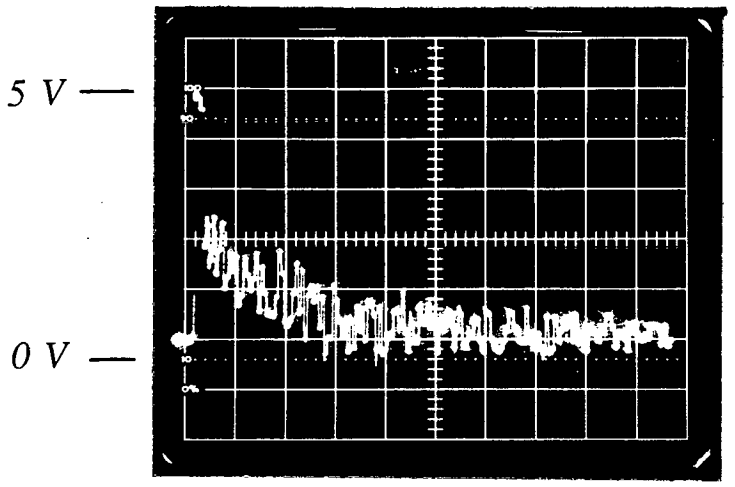

(a) 5 dB MP Bandcentred Fade

Scales:
1 V/div
1 ms/div

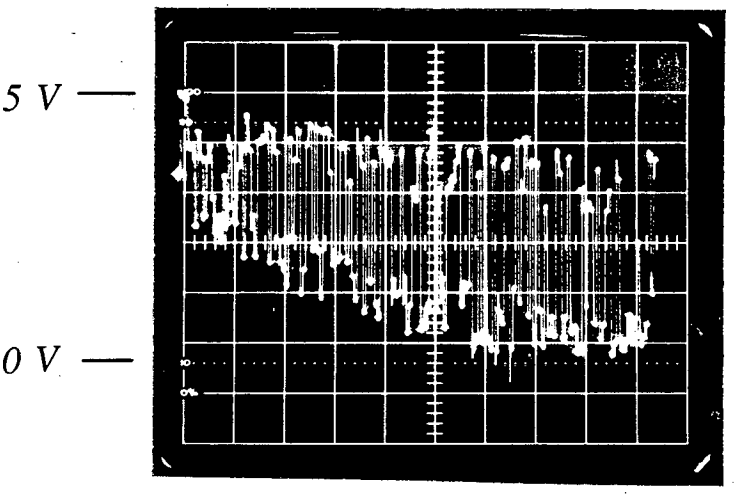

(b) 15 dB MP Bandcentred Fade

Figure 5.7.3 Implemented LMS Convergence

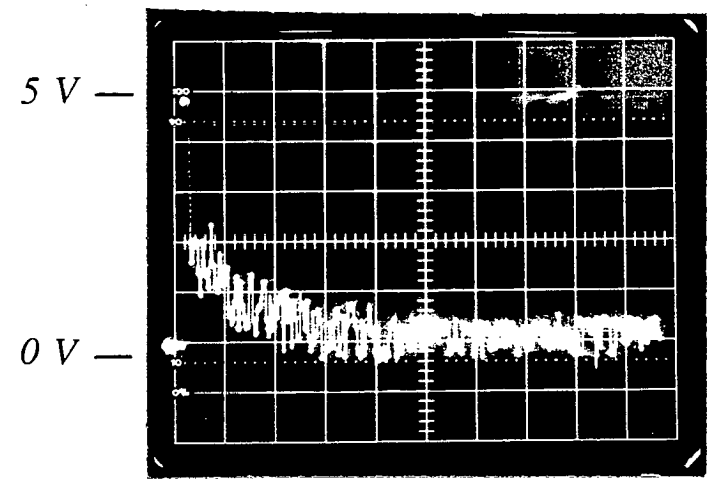

(a) 5 dB MP Bandcentred Fade

Scales:
1 V/div
1 ms/div

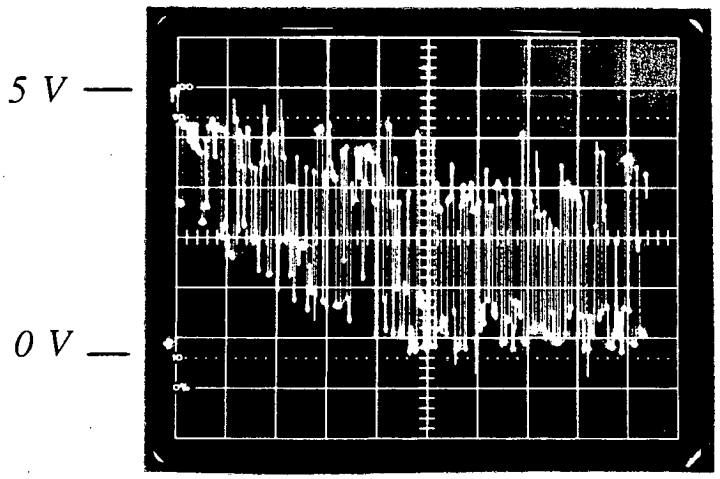

(b) 15 dB MP Bandcentred Fade

Figure 5.7.4 Implemented BLMS Convergence

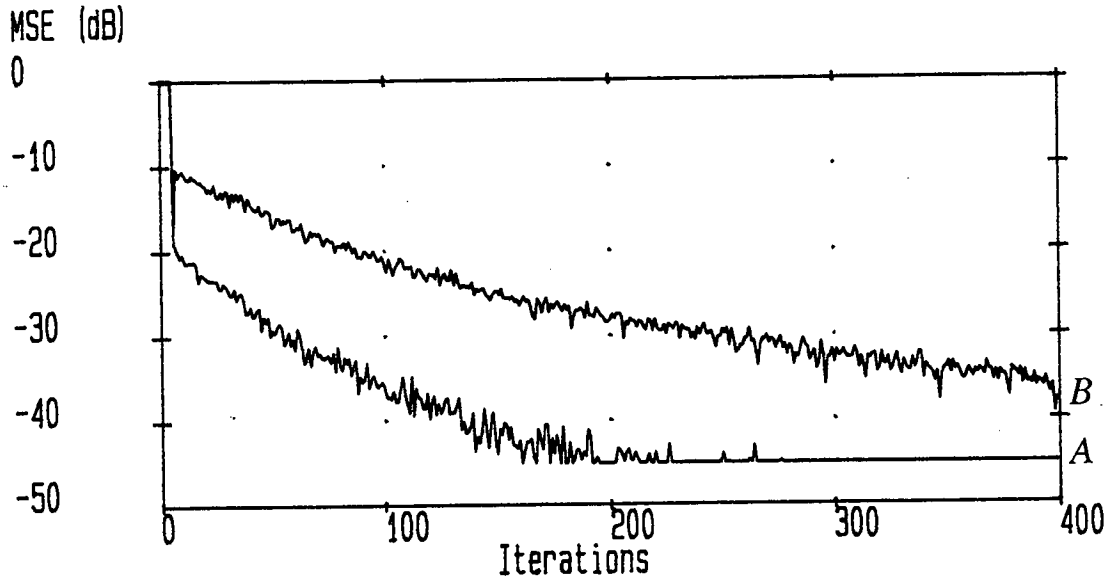

(a) LMS Algorithm

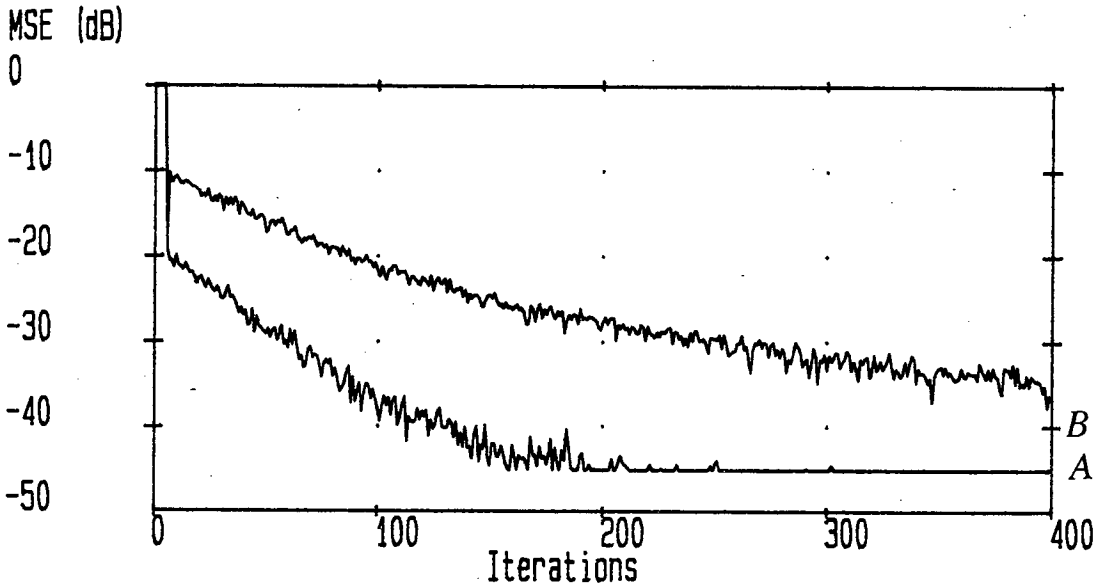

(b) BLMS Algorithm

Figure 5.7.5 Finite Precision Comparative Simulations

right shift if the block length, L, is an integer power of 2) and reset the storage register. The problem of BLMS saturation [139] is avoided with suitable scaling in the design or switching from LMS to BLMS algorithms after an initial retraining period. Further work is required to to evaluate block adaptation for higher modulation formats.

The second design proposal is for off-line adaptation with a DSP. This approach has a number of advantages including relatively high arithmetic precision for coefficient adaptation and storage. Off-line processing also permits the use of more complex algorithms, however the sampling update rate should not be reduced such that the channel appears non-stationary. A DSP solution may be less attractive for a single chip LSI implementation, although the data buffers may be incorporated into the LSI design so that a DSP would additionally only require RAM/ROM blocks. For a full 'complex' equaliser, some hardware duplication will be unavoidable, unless the DSP is operating sufficiently fast to allow updating of more than one FIR structure. For the 8 Mbit/s QPSK system this would be feasible with newer DSP designs e.g. the TMS 320C25. Another means of increasing the update rate is to feedback, when required, the error calculated at the FIR output. The error is calculated at the symbol rate and additional buffering would be required for the transfer to the DSP. With the present arrangement, the error term in the update product is calculated from within the DSP.

Preceeding comments have applied to work performed with symbol spaced transversal equalisers. Similar analysis applies to symbol and fractionally spaced DFEs to realise the potential performance gain and implement the proposed receiver structure in chapter four. One assumption is that sufficiently fast operation is possible to calculate the feedback term. Further work is required on equalisers with fractionally spaced taps, to evaluate long term numerical instability problems and the requirements for the introduction of leakage in the adaptation process.

5.9 SUMMARY

This chapter has considered a number of important aspects of receiver implementation. Two fundamental design considerations are the high data rates involved and the relative stationarity of the chanel during fading conditions. With current technology, only linear transversal equalisers are currently in commercial use, and only a handful of high speed DFEs have been implemented for research purposes. Fractionally spaced equaliser implementations have generally been for lower data rate modems. The high sampling rates and throughput provide a fundamental problem for

microwave digital radio applications, although the fractionally spaced DFE proposed in chapter 4 effectively operates at the symbol rate. For these reasons, the chapter emphasis has been on transversal equaliser implementation. The same techniques may be applied to other equalisation structures and higher modulation formats.

As a consequence of the slowly fading channel, the adaptive algorithm is not required to adapt quickly, and may be relatively simple. This is fortunate because implementation is dictated by the high data rate. For high speed implementation, practical word lengths will be limited. Section 5.5 provided a comprehensive examination of adaptive algorithms suitable for high speed use, including the ZF, LMS, and BLMS algorithms, and simplifications where applicable. Results indicated that for limited arithmetic precision, the BLMS algorithm may result in some performance gain over the ZF and LMS algorithms, at the expense of only a slight increase in complexity. The BLMS algorithm employing only sign information from the received signal, requires no multiplication operations and has similar complexity to the LMS algorithm.

Another consequence of the slowly varying channel is that it is not neccessary to update the channel at the symbol rate. Section 5.8 presented a novel means of equaliser adaptation involving an 'off-line' DSP. DSPs offer high performance at relatively low cost and considerable flexibility during the design stage. Currently DSPs find most application in voiceband modems [65]. With increasing clock rates and computational power, DSPs should find greater application in microwave digital radio, both 'on-' and 'off-line'.

Chapter 6

DISCUSSION AND CONCLUSIONS

Work presented in earlier chapters may be broadly classed under theoretical and practical studies. Chapters 3 and 4 presented results for linear and nonlinear equalisation, while chapter 5 covered practical aspects of equaliser design. This closing chapter summarises the thesis and suggests future research directions in keeping with current and future trends in communications by microwave digital radio.

6.1 EQUALISATION TECHNIQUES

Chapter 3 examined the ability of linear transversal equalisers to compensate against severe fading conditions. Linear equalisation in isolation was found to provide insufficient compensation if high level modulation is used. The use of other compensation measures e.g. diversity and coding, may help rectify this situation, however research in these areas is outwith the scope of this text. Initial investigations into timing phase recovery indicated that during a deep fade, the recovery circuit would be liable to loose lock. This suggested placing less emphasis on recovering timing information, and more on the equaliser operating at sufficiently high sampling rate i.e. a FSE, to overcome the sensitivity of symbol spaced equalisers to inaccurate timing information. This concept was exploited for a receiver structure proposed in chapter 4. In terms of system planning, very deep fades are more likely to occur on long hops, possibly over water. Linear equalisers may therefore find application to short to medium length links. On longer links or where high modulation techniques are employed, the increased sensitivity to multipath fading requires a more powerful equalisation approach.

Decision feedback equalisers formed the basis for chapter 4 on nonlinear equalisation. Other nonlinear equalisation techniques exist, however they are generally too complex to operate at the high data rates required for microwave digital radio. A

DFE with symbol spaced forward taps was able to maintain acceptable performance during a deepening MP fade to a notch depth of 40 dB. At the transition between MP to NMP phase types, DFE performance rapidly breaks down due to error propagation in the feedback section. When the forward DFE taps are spaced by half the symbol period ($T/2$), acceptable performance may be maintained providing that the timing phase is held constant relative to that obtained during normal channel conditions i.e. no attempt is made to track any changes in timing phase due to fading. This apparently simple timing recovery technique would be difficult to obtain in practice, therefore a novel technique was proposed in chapter 4 based on an estimate of the channel impulse response. For correct operation, the channel estimator theoretically requires knowledge of the transmitted data. In practice this is not available at the receiver, however the DFE output is sufficiently accurate to be used instead. The proposed receiver structure appears capable of dealing with the most severe frequency selective fades described by the simplified three path (Rummler) channel model. The timing phase would not have to be updated at the symbol rate rendering the algorithm suitable for off-line DSP implementation.

6.2 HARDWARE DESIGN AND DSP APPLICATIONS

Chapter 5 covered practical aspects of equaliser design. Emphasis was on the adaptation process, with a survey of potential algorithms for high speed implementation and an investigation into off-line adaptation. Analogue technology may still be used in certain parts of the equaliser design i.e. the tapped delay line of the FIR filter, which must be implemented at the symbol rate. A literature survey revealed widespread use of digital technology in current research designs.

The requirement for the high speed operation of microwave digital radio equalisers will limit the available word lengths and the ADC resolution in any digital design. When implemented (or simulated) with floating point arithmetic, the LMS algorithm provides a straightforward solution to equaliser adaptation, or alternatively the zero-forcing algorithm provides a simpler solution at the expense of some performance degradation. Results presented in chapter 5 indicated that the finite precision BLMS algorithm offers increased steady state performance at the expense of a modest increase in hardware relative to the LMS algorithm. Saturation in the BLMS algorithm may be prevented by either suitable scaling at the design stage or by switching between LMS and BLMS algorithms.

The relative stationarity of the microwave channel during fading permits the equaliser coefficients to be updated at less than the symbol rate. The proposed hardware implementation in chapter 5 employs a DSP to perform the required

computation. When required data is transferred to and from the FIR filter via fast-access buffer RAMs. The system accommodates both LMS and BLMS algorithms, the arithmetic operations required by the latter being particularly suited to DSP calculation. DSP designs offer powerful performance at economic cost, and with the advent of new technology, DSPs are likely to find greater application within future high speed receiver designs. The timing recovery technique based on the channel estimator output is also suitable for DSP implementation, particularly where time averaging is required for the power terms (table 4.9.1).

6.3 FUTURE TRENDS IN MICROWAVE DIGITAL RADIO

The following section places the work presented in this thesis within the context of the rapidly developing microwave communications environment. In short, a key part of the further development of spectrally efficient radio communications will be the advancement in effective equalisation techniques.

6.3.1 System Design

Current trends in microwave radio are towards the replacement of analogue by digital systems and the consequent need for greater spectral efficiency to increase transmission capacity. Such trends are likely to continue as greater demands are placed on radio network infrastructures and finite transmission bandwidth. Digital radio systems will complement as well as compete with optical fibres depending on the nature of the route type and terrain.

Increased network capacity on microwave links will be possible by increased spectral efficiency on existing frequency allocations or through the use of frequency bands above 15 GHz e.g. the 18, 23, 28 and 38 GHz bands [4]. Higher frequencies permit the design of compact equipment and antennas (within the limitations of prevailing RF technologies). A potential major outage source at high frequency bands is attenuation due to rain. Further work is required to optimise digital radio operation at these higher frequencies.

Increased spectral efficiency may be achieved by dual polarisation operation and higher level modulation formats. Modulation complexity of the order of 256-QAM is currently under test, while the application of 1024-QAM is likely. Cross polarisation interference cancellers will have to be further developed for the satisfactory operation of dual polarisation techniques with high level modulation. Technological advances should lead to greater monitoring and maintenance capabilities, and expert systems may provide receiver control during adverse conditions. Other advances in radio design are likely to occur at the transmitter and antenna stages. Predistortion

techniques will allow transmitter power amplifiers to operate at higher power levels with less distortion [115], and advances in antenna design will permit the incorporation of aperture diversity.

6.3.2 Equalisation and Other Compensation Measures

Diversity systems provided one of the first means of multipath compensation, and their continued use is likely in the near future. Recent results have demonstrated the effectiveness of space diversity with linear equalisation [17] and angle diversity may potentially be more effective. Future diversity developments may include ECC/diversity combinations [115] and adaptive techniques for the combination of main and diversity signals [4]. Error correction coding should find greater application within the constraints imposed by limited frequency overheads. High coding gains may also be derived from combined modulation and coding, and near maximum-likelihood (Viterbi) methods. An interesting conjecture from Meyers and Prabhu [115] is that future compensation techniques will be designed for immunity from interference in an increasingly crowed (and limited) transmission spectrum.

Equalisation to some degree is now a standard on most current microwave radio receivers. The increased sensitivity of high level modulation formats to multipath fading requires greater compensation from the adaptive equaliser, and in turn advances in the basic equalisation concept. Techniques proposed in this thesis should help reduce outage time by keeping the equaliser in lock for as long as possible. Ideally, the adaptive equaliser will maintain acceptable performance during all fading conditions.

6.4 FURTHER RESEARCH

A number of research directions may be developed from work reported in this thesis. Research effort may be directed towards refining the new ideas, and practical applications to microwave and other communications systems. An initial comment concerns the adoption of the MSE performance measure. BER measurements provide the standard means of assessing equaliser performance, however MSE calculations are computationally faster and given the comparative nature of the results, MSE is an acceptable means of comparing relative equaliser performance. Future results would be envisaged to consider BER as well as MSE performance.

Simulation results from chapters 3 and 4 were performed with floating point arithmetic. Finite precision simulations would be required to evaluate practical performance and highlight any stability problems due to limited arithmetic precision. With the use of numerically robust adaptive algorithms (e.g. LMS) and inherently

stable filter structures, significant changes between floating and fixed point simulation results would not be expected. Finite precision simulations would precede practical hardware implementation, possibly involving techniques examined in chapter 5. Practical hardware realisations allow the possibility of field trials. Results from real systems would help substantiate a number of assumptions made in the course of simulations, particularly regarding channel stationarity and the nature of the channel transfer function during phase transitions.

Ideas arising from this thesis may be applied to other communications systems. For example, the concept behind the receiver structure proposed in chapter 4 may be applied to HF and mobile radio channels, where changes in the channel response are nonstationary. Attempting to track changes in the optimum choice of timing phase may be difficult or impossible. One solution would be to hold the timing phase fixed relative to a predetermined value i.e. the receiver proposed in chapter 4. The technique of offline adaptation may also find application in other communications systems or any high speed adaptive systems with a slowly time varying input.

Future receiver designs based on the offline approach are required to examine applications to higher modulation formats and data rates. Newer DSP products offer greater processing power and throughput compared with the design presented in chapter 5. Ultimately complete receivers may be implemented with DSPs. In the more immediate future, high speed digital operation will limit practical word lengths and consequently, arithmetic precision. The BLMS algorithm is one means of obtaining greater performance from limited precision or alternatively reducing word length requirements for a given level of performance. Again, such techniques may be applied to other communications systems.

REFERENCES

1. R.C. Kirby, "Radio Relay Systems in International Telecommunications," *Proceedings of the European Radio Relay Conference*, pp. 13-21, Munich, November 1986.
2. N.F. Dinn, "Digital Radio: It's Time Has Come," *IEEE Communications Magazine*, vol. 18, pp. 6-12, Nov. 1980.
3. R.L. Freeman, *Radio System Design For Telecommunications (1-100 GHz)*, J. Wiley & Sons, 1987.
4. G. Hart and J.A. Steinkamp, "Future Trends in Microwave Digital Radio: A View from Europe," *IEEE Communications Magazine*, vol. 25, pp. 49-52, Feb. 1987.
5. "Microwave and Optical Communications Systems," *Electronic Engineering (U.K.)*, pp. 165-170, Nov. 1984.
6. M. Borgne, "A New Class of Adaptive Cross-Polarization Interference Cancellers for Digital Radio Systems," *IEEE Journal on Selected Areas in Communications*, vol. SAC-5, pp. 484-492, April 1987.
7. K. Feher, *Digital Communications: Microwave Applications*, Prentice-Hall, 1981.
8. H. Sari and G. Karam, "Cancellation of Power Amplifier Nonlinearities in Digital Radio Receivers," *IEEE Proceedings of ICC '87*, pp. 1809-1814, Seattle, USA, June 1987.
9. H. Kostal, "Annual and Seasonal Variability in the Occurence of Multipath Fading," *IEEE Proceedings of ICC '86*, pp. 15.4.1-15.4.5, 1986.
10. A. Ranade, "Frequency and Duration of Dispersive Fades at 6 GHz," *IEEE Proceedings of ICC '87*, pp. 10.7.1-10.7.5, Seattle, June 1987.
11. J.A. Schiavone, "Predicting the Geographical Distribution of Microwave Fading from Ground- Based Climatological Measurements," *IEEE Proceedings of ICC '86*, 1986.
12. W.D. Rummler, "A New Selective Model: Application to Propagation Data," *Bell System Techical Journal*, vol. 58, pp. 1037-1071, May-June 1979.

13. M. Emshwiller, "Characterisation of the Performance of PSK Digital Radio in the Presence of Interference," *IEEE Proceedings of ICC '78*, pp. 47.3.1.-47.3.6, June 1978.

14. E. Vilar, A. Burgueno, M. Puigcerver, and J. Austin, "Analysis of Joint Rainfall Rate and Duration Statistics: Microwave System Design Implications," *IEEE Transactions on Communications*, vol. 36, pp. 650-661, June 1988.

15. A.R. Webster and W.I. Lim, "Microwave Multipath from Sea Reflections - The Bay of Fundy," *Proceedings of URSI Com. F Symp.*, vol. ESA SP-194, pp. 25-30, Louvain, Belgium, June 1983.

16. R.G. McKay and M. Shafi, "Multipath Propagtion Measurements on an Overwater Path in New Zealand," *IEEE Proceedings of ICC '87*, pp. 23.1.1-23.1.5, Seattle, June 1987.

17. S.H. Lin, T.C. Lee, and M.F. Gardina, "Diversity Protections for Digital Radio - Summary of Ten-Year Experiments and Studies," *IEEE Communications Magazine*, vol. 26, pp. 51-64, February 1988.

18. P. Hartmann and B. Bynum, "Adaptive Equalisation for Digital Microwave Radio Systems," *IEEE Proceedings of ICC '80*, pp. 8.5.1-8.5.6, June 1980.

19. N. Wiener, *The Extrapolation, Interpolation, and Smoothing of Stationary Time Series*, John Wiley & Sons, New York, 1962.

20. R. E. Kalman, "A New Approach to Linear Filtering and Prediction Problems," *ASME Transactions, Journal of Basic Engineering*, pp. 35-45, March 1960.

21. B. Mulgrew and C.F.N. Cowan, *Adaptive Filters and Equalisers*, Kluwer Academic Publishers, 1988.

22. J. Makhoul, "Linear Prediction a Tutorial Review," *Proceedings IEEE*, vol. 63, no. 4, pp. 561-580, April 1975.

23. B. Widrow and S. D. Stearns, *Adaptive Signal Processing*, Prentice-Hall, Englewood Cliffs, N.J., 1985.

24. R. W. Lucky, "Techniques for Adaptive Equalisation of Digital Communications Systems," *Bell System Technical Journal*, vol. 45, no.2, pp. 255-286, February 1966.

25. J. G. Proakis, *Digital Communications*, McGraw-Hill, 1983.

26. S. Benedetto, E. Biglieri, and V. Castellani, B.W. Kernighan, and D.M. Ritchie, *The 'C' Programming Language*, Prentice-Hall, 1978.

27. M.S. Roden, *Digital Communication Systems Design*, Prentice-Hall, 1988.

28. F.G. Stremler, *Introduction to Communications Systems,* Addison-Wesley, 1982.

29. J.A.C. Bingham, *The Theory and Practice of Modem Design,* J. Wiley & Sons, 1988.

30. G.C. Clark and J. Bibb-Cain, *Error-Correction Coding for Digital Communications,* Plenum Press, 1981.

31. E.R. Berlekamp, R.E. Peile, and S.P. Pope, "The Application of Error Control to Communications," *IEEE Communications Magazine*, vol. 25, pp. 44-57, April 1987.

32. S. Bellini and G. Tartara, "Coding for Error Correction in High Capacity Digital Radio: An Application to 64-QAM Systems," *Proceedings of the European Radio Relay Conference*, pp. 166-172, Munich, November 1986.

33. S.B. Aftelak and A.P. Clarke, "Adaptive Reduced-State Viterbi Algorithm Detector," *IERE Journal*, vol. 56, pp. 197-206, May 1986.

34. R.D. Gitlin and J.F. Hayes, "Timing Recovery and Scramblers in Data Transmission," *Bell System Technical Journal*, vol. 54, pp. 569-593, March 1975.

35. B.P. Lathi, *Modern Digital and Analogue Communications Systems,* Holt-Saunders, 1983.

36. T. Noguchi, Y. Daido, and J.A. Nossek, "Modulation Techniques for Microwave Digital Radio," *IEEE Communications Magazine*, vol. 24, pp. 21-30, October 1986.

37. G. Hart, B. Humphries, and M. Relph, and J.E. Doble, "A Flexible Digital Radio System Outage Model Based on Measured Propagation Data," *Proc. European Radio Relay Conference*, pp. 64-74, Munich, Nov. 1986.

38. A. Chouly and H. Sari, "Application of Trellis Coding to Digital Microwave Radio," *IEEE Proceedings of ICC 88*, pp. 468-472, Philadelphia, USA, June 1988.

39. Y. Nakamura, Y. Saito, and S. Aikawa, "256 QAM Modems for Multicarrier 400 Mbits/s Digital Radio," *IEEE Journal on Selected Areas in Communications*, vol. SAC-5, pp. 329-335, April 1987 .

40. K. Feher, "1024-QAM and 256-QAM Coded Modems for Microwave and Cable System Applications," *IEEE Journal on Selected Areas in Communications*, vol. SAC-5, pp. 357-368, April 1987 .

41. K. Kohiyama and O. Kurita, "Future Trends in Microwave Digital Radio: A View from Asia," *IEEE Communications Magazine*, vol. 25, pp. 41-46, February 1987.

42. S. Haykin, *Communication Systems*, J. Wiley and Sons, 1978.

43. R.W. Lucky, J. Salz, and E.J. Weldon Jr., *Principles of Data Communication*, McGraw-Hill, 1968.

44. M. D. Srinath and P. K. Rajasekaron, *An Introduction to Statistical Processing with Applications*, John Wiley & Sons, New York, 1979.

45. B. Sklar, "A Structured Overview of Digital Communications - a Tutorial Review - Part 2," *IEEE Communications Magazine*, pp. 6-21, October 1983.

46. M.H. Meyers and L.E. Franks, "Joint Carrier Phase and Symbol Timing Recovery for PAM systems," *IEEE Transactions on Communications*, vol. COM-28, pp. 1121-1129, August 1980.

47. G.R. McMillen , M. Shafi, and D.P. Taylor, "Simultaneous Adaptive Equalisation of Carrier Phase, Symbol Timing and Data for a 49-QPRS DFE Radio Receiver," *IEEE Transactions on Communications*, vol. COM-32, no. 4, pp. 429-443, April 1984.

48. J.K. Chamberlain , F.M. Clayton, H. Sari, and P. Vandamme, "Receiver Techniques for Microwave Digital Radio," *IEEE Communications Magazine*, vol. 24, pp. 43-54, November 1986.

49. A. Leclert and P. Vandamme, "Timing Synchronisation in Digital Radio Systems with Multipath Propagation," *IEEE Proceedings of ICC '83*, pp. 530-533, 1983.

50. K.H. Mueller and M. Muller, "Timing Recovery Techniques in Digital Synchronous Data Receivers," *IEEE Transactions on Communications*, vol. COM-24, pp. 561-531, October 1982.

51. A. Jennings and B.R. Clarke, "Data-Sequence Timing Recovery for PAM Systems," *IEEE Transactions on Communications*, vol. COM-33, pp. 729-731, July 1985.

52. H. Kobayashi, "Simultaneous Adaptive Estimation and Decision Algorithm for Carrier Modulated Data Transmission Systems," *IEEE Transactions on Communications Technology*, vol. COM-19, pp. 268-280, June 1971.

53. H. Sari , L. Desperben, and S. Moridi, "Minimum Mean Square Error Timing Recovery Schemes for Digital Equalisers," *IEEE Transactions on Communications*, vol. COM-34, pp. 694-702, July 1986.

54. N. Amitay and L.J. Greenstein, "Multipath Outage Performance of Digital Radio Receivers using Finite-Tap Adaptive Equalisers," *IEEE Tranactions on Communications*, vol. COM-32, pp. 597-608, May 1984.

55. MacNally and J.C.Y. Huang, "Propagation Protection Techniques for High Capacity Digital Radio Systems," *IEEE Proceedings of ICC 84*, pp. 1007-1010, Amsterdam, Holland, June 1984.

56. R. Merwin, "IF Amplitude Adaptive Filtering," *RF Design*, pp. 54-59, January 1986.

57. G. Sebald, B. Lankl, and J.A. Nossek, "Advanced Time and Frequency Domain Adaptive Equalisation in Multilevel QAM Digital Radio Systems," *IEEE Journal on Selected Areas in Communications*, vol. SAC-5, pp. 448-356, April 1987.

58. W.K. Wong , B. Williamson, P.M. Grant, and C.F.N. Cowan, "Adaptive Transversal Filters for Multipath Compensation in Microwave Digital Radio," *IEEE Proceedings of 'ICC 84'*, pp. 989-992, Amsterdam, June 1984.

59. D.D. Falconer, "Bandlimited Digital Communications - Recent Trends and Applications to Voiceband Modems and Digital Radio," *Digital Communications*, North Holland, Amsterdam, 1986.

60. C.F. Weaver and D.P. Taylor, "The Implementation of Adaptive Decision Feedback Equalisation of Multipath Distortion in Microwave Digital Radio," *IEEE Proceedings of Globecom '84*, pp. 1548-1552, Atlanta,USA, 1984.

61. G. Ungerboeck, "Theory on the Speed of Convergence in Adaptive Equalisers for Digital Communication," *IBM Journal of Research and Development*, vol. 16, no. 6, pp. 546-555, November 1972.

62. A. Feuer and E. Weinstein, "Convergence Analysis of LMS Filters with Uncorrelated Gaussian Data," *IEEE Transactions on Acoustics Speech and Signal Processing*, vol. ASSP-33, no. 1, pp. 220-230, February 1985.

63. G. A. Clark, S. K. Mitra, and S. R. Parker, "Block Implementations of Adaptive Digital Filters," *IEEE Transactions on Circuits and Systems*, vol. CAS-28, pp. 584-592, June 1981.

64. C.F.N. Cowan, "Performance Comparison of Finite Linear Adaptive Filters," *IEE Proceedings Part F*, vol. 134 (3), pp. 211-216, June 1987.

65. S.U.H. Qureshi, "Adaptive Equalisation," *Proceedings IEEE*, vol. 73, no. 9, pp. 1349-1387, September 1985.

66. B. Widrow, J. McCool, and M. Ball, "The Complex LMS Algorithm," *Proceedings IEEE*, vol. 63, no. 4, pp. 719-720, April 1975.

67. C.W. Lundgren and W.D. Rummler, "Digital Radio Outage Due to Selective Fading - Observation vs Prediction From Laboratory Simulation," *Bell System*

Technical Journal, vol. 58, pp. 1073-1100, May-June 1979.

68. M. Shafi, "Statistical Analysis/Simulation of a Three Ray Model for Multipath Fading with Applications to Outage Prediction," *IEEE Journal on Selected Areas in Communications*, vol. SAC-5, pp. 389-401, April 1987.

69. M. Shafi and D. Moore, "Further Results on Adaptive Equaliser Improvements for 16-QAM and 64-QAM Digital Radio," *IEEE Transactions on Communications*, vol. COM-34, pp. 59-66, January 1986.

70. K. Metzger, "On the Probability Density of Intersymbol Interference," *IEEE Transactions on Communications*, vol. COM-35, pp. 396-402, April 1987.

71. L.J. Greenstein and B.A. Czekaj-Agun, "A Polynomial Model for Multipath Fading Channel Responses," *Bell System Technical Journal*, vol. 64, pp. 885-905, April 1985.

72. W.D. Rummler, R.P. Coutts, and M. Liniger, "Multipath Fading Models for Microwave Digital Radio," *IEEE Communications Magazine*, vol. 24, no. 11, pp. 30-42, November 1986.

73. L.J. Greenstein and M. Shafi, "Outage Calculation Methods for Microwave Digital Radio," *IEEE Comms. Mag.*, vol. 25, pp. 30-39 , Feb. 1987.

74. G. Waters, "Digital Radio Measurement Techniques," *Telecommunications Measurements, Analysis, and Instrumentation*, Prentice-Hall, 1987.

75. M.C. Jeruchim, "Techniques for Estimating the Bit Error Rate in the Simulation of Digital Communications Systems," *IEEE Journal on Selected Areas in Communications*, vol. SAC-2, pp. 153-170, January 1984.

76. M. Liniger and D. Vergeres, "Field Test Results for a 16-QAM and a 64-QAM Digital Radio, compared with the Prediction based on Sweep Measurements," *Technische Mitteilungen PTT (Switzerland)*, vol. 64, no. 7, pp. 346-353, 1986.

77. R.A. Roberts and C.T. Mullis, *Digital Signal Processing*, Addison-Wesley, 1987.

78. A.P. Clark, *Equalisers for Digital Modems*, Pentech Press, 1985.

79. R.D. Gitlin and S.B. Weinstein, "Fractionally-Spaced Equalisation: An Improved Digital Transversal Equaliser," *Bell System Technical Journal*, vol. 60, pp. 275-296, February 1981.

80. G. Long, F. Ling, and J.G. Proakis, "Fractionally Spaced Equalisers Based on Singular Value Decomposition," *Proceedings of ICASSP 88*, vol. 4, pp. 1514-1517, New York, USA, April 1988.

81. G. Ungerboeck, "Fractional Tap-Spacing and Consequences for Clock Recovery in Data Modems," *IEEE Transactions on Communications*, vol. COM-24, pp.

856-864, August 1976.

82. W.K. Wong, "Adaptive Equalisers for Multipath Compensation in Digital Microwave Communications," PhD Thesis, University of Edinburgh, September 1987.

83. I. Korn, "Effect of Adjacent Channel Interference and Frequency Selective Fading on Outage of Digital Radio," *IEE Proceedings, Part F*, vol. 132, pp. 604-612, December 1986.

84. B. Widrow, J. M. McCool, M. G. Larimore, and C. R. Johnson, "Stationary and Nonstationary Learning Characteristics of the LMS Adaptive Filter," *Proceedings IEEE*, vol. 64, no. 8, pp. 1151-1162 , August 1976.

85. W. Grafinger, J.A. Nossek, and G. Sebald, "Design and Realisation of a High Speed Multilevel QAM Digital Radio Modem with Time-Domain Equalisation," *IEEE Proceedings of ICC 85*, pp. 971-976, Chicago, USA, June, 1985.

86. P.A. Kennard, J.D. McNicol, and M.D. Caskey, "Fading Dynamics in High Spectral Efficiency Digital Radio," *IEEE Proceedings of 'ICC 86'*, pp. 1487-1492, June 1986.

87. E.W. Allan, "Digital Radio Propagation - Long Term Test and Nonminimum Phase," *IEEE Proceedings of ICC 87*, pp. 23.3.1-23.3.6, Seattle, June 1987.

88. R.H. Lahlum, M.H. Meyers, G.W. Miller, and R.B. Ward, "Digital Radio Receiver Dynamics: A New Robust Receiver," *IEEE Proceedings of 'Globecom 87'*, pp. 1212-1216, Tokyo, November 1987.

89. O. Macchi, "Adaptive Equalisation of Time Varying Channels: What is Meant by Slow Variations," *IEEE Proceedings of ICC 84*, pp. 1247-1249, Amsterdam, Holland, 1984.

90. S.L. Wood, M.G. Larimore, and J.R. Treichler, "The Impact of an Adaptive Equaliser's Behavior at Symbol Error Rate in a Nonstationary Environment," *Proceedings of ICAASP 88*, pp. 1608-1611, New York, U.S.A., May 1988.

91. K.S. Shanmugan and A.M. Breipol, *Random Signals: Detection, Estimation and Data Analysis*, J. Wiley & Sons, 1988.

92. E.W. Allan, "Angle Diversity Test Using a Single Aperture Dual Beam Antenna," *Proceedings of ICC 88*, vol. 3, pp. 1626-1632, Philadelphia, U.S.A., June 1988.

93. C.F. Weaver, "A High-Capacity Terrestrial Digital Microwave Radio Employing Adaptive Techniques," PhD Thesis, McMaster University, Hamilton, Ontario, Canada, October 1985.

94. R. Valentin and K. Metzger, "An Analysis of the Sensitivity of Digital Modulation Techniques to Frequency Selective Fading," *IEEE Transactions on Communications*, vol. COM-33, no. 9, pp. 986-992, September 1985.

95. O. Macchi and E. Eweda, "Convergence Analysis of Self-Adaptive Equalisers," *IEEE Transactions on Information Theory*, vol. IT-30, pp. 161-176, March 1984.

96. Y. Sato, "A Method of Self-recovering Equalisation for Multilevel Amplitude Modulation Schemes," *IEEE Transactions on Communications*, vol. COM-23, pp. 679-682, June 1975.

97. D.N. Godard, "Self-Recovering Equalisation and Carrier Tracking in Two-Dimensional Data Communication Systems," *IEEE Transactions on Communications*, vol. COM-28, pp. 1867-1875, November 1980.

98. A. Benveniste and M. Goursat, "Blind Equalisers," *IEEE Transactions on Communications*, vol. COM-32, pp. 871-883, August 1984.

99. G.J. Foschini, "Equalising Without Altering or Detecting Data," *AT&T Technical Journal*, vol. 64, pp. 1885-1911, October 1985.

100. G. Picchi and G. Prati, "Blind Equalisation and Carrier Recovery Using a "Stop-and-Go" Decision- Directed Algorithm," *IEEE Transaction on Communications*, vol. COM-35, pp. 877-887, September 1987.

101. C. A. Belfiore and J. H. Park, "Decision Feedback Equalisation," *Proceedings IEEE*, vol. 67, no. 8, pp. 1143-1156, August 1979.

102. J. Salz, "Optimum Mean-Square Decision Feedback Equalisation," *Bell System Technical Journal*, vol. 52, no. 8, pp. 1341-1373, October 1973.

103. A. Leclert and P. Vandamme, "Decision Feedback Equalisation of Dispersive Radio Channels," *IEEE Transactions on Communications*, vol. COM-33, no. 7, pp. 676-684, July 1985.

104. J.J. Olmos, R. Agusti, and F. Casadevall, "Decision Feedback Equalisation and Carrier Recovery in 140 Mbit QAM Digital Radio Systems," *IEEE Proceedings of ICC 88*, pp. 1336-1342, Philadelphia, USA, June, 1988.

105. K. Watanabe, K. Inoue, and Y. Sato, "A 4800 Bit/s Microprocessor Data Modem," *IEEE Transactions on Communications*, vol. COM-26, no. 5, pp. 493-499, May 1978.

106. P. Herbig, "Adaptive Time Domain Equalisation for LOS Channels," *Proceedings of 'European Conference on Radio-Relay Systems' (ECRR)*, pp. 182-189, Munich, W. Germany, November 1986.

107. D.L. Duttweiler, J.E. Mazo, and D.G. Messerschmitt, "An Upper Bound on the Error Probability in Decision-Feedback Equalisation," *IEEE Transactions on Information Theory*, vol. IT-20, no. 4, pp. 490-497, July 1974.

108. J. J. O'Reilly and A. M. de Oliveira Duarte, "Error Propagation in Decision Feedback Receivers," *IEE Proceedings Part F*, vol. 132, no. 7, pp. 561-566, Dec. 1985.

109. R.A. Kennedy and B.D.O. Anderson, "Error Recovery of Decision Feedback Equalisers on Exponential Impulse Response Channels," *IEEE Transactions on Communications*, vol. COM-35, no. 8, pp. 846-848, August 1987.

110. D.P. Taylor and M. Shafi, "Decision Feedback Equalisation for Microwave Induced Interference in Digital Microwave LOS Links," *IEEE Transactions on Communications*, vol. COM-32, no. 3, pp. 267-279, March 1984.

111. M.S. Mueller and J. Salz, "A Unified Theory of Data-Aided Equalisation," *Bell System Technical Journal*, vol. 60, no. 9, pp. 2023-2038, November 1981.

112. D.D. Falconer, A.U.H. Sheikh, E. Eleftheriou, and M. Tobis, "Comparison of DFE and MLSE Receiver Performance on HF Channels," *IEEE Proceedings of 'Globecom 83'*, pp. 13-18, San Diego, USA, 1983.

113. J. Salz, "On Mean-Square Decision-Feedback Equalisation and Timing Phase," *IEEE Transactions on Communications*, vol. COM-25, pp. 1471-1476, June 1975.

114. E. Dahlman and B. Gudmundson, "Performance Improvement in Decision Feedback Equalisers by Using 'Soft Decision'," *Electronics Letters*, vol. 24, no. 17, pp. 1084-1085, 18 August 1988.

115. M.H. Meyers and V.K. Prabhu, "Future Trends in Microwave Digital Radio: A View from North America," *IEEE Communications Magazine*, vol. 25, pp. 46-49, February 1987.

116. G.K. Kaleh and V. Kumar, "Compensation for the Time Synchronisation Error in Data Modems," *Signal Processing IV: Proceedings of EUSIPCO 88*, pp. 207-210, Elsevier (North Holland), September 1988.

117. R.D. Gitlin and H.C. Meadors, "Centre-Tap Tracking Algorithms for Timing Recovery," *AT&T Technical Journal*, vol. 66, no. 6, pp. 63-78, November/December 1987.

118. A.P. Clark and F. McVerry, "Time Synchronisation of an HF Radio Modem," *IEE Proceedings Part F,*, vol. 129, no. 6, pp. 403-410, December 1982.

119. W. Hodgkiss and L.F. Turner, "Practical Equalisation and Synchronisation Strategies for use in Serial Data Transmission over HF Channels," *The Radio and*

Electronic Engineer, vol. 53, no. 4, pp. 141-146, April 1983.

120. H. Sari, S. Moridi, L. Desperben, and P. Vandamme, "Baseband Equalisation and Carrier Recovery in Digital Radio Systems," *IEEE Transactions on Communications*, vol. COM-35, no. 3, pp. 319-327, March 1987.

121. S.L. Freeny, "Special-Purpose Hardware for Digital Filtering," *Proceedings IEEE*, vol. 63, no. 4, pp. 633-648, April 1975.

122. G.L. Fenderson, J.W. Parker, P.D. Quigley, S.R. Shepard, and C.A. Siller Jr., "Adaptive Transversal Equalisation of Multipath Propagation for 16-QAM, 90-Mb/s Digital Radio," *AT&T Bell Labs. Technical Journal*, vol. 63, pp. 1447-1463, October 1984.

123. C.P. Bates, W.G. Robinson, and M.A. Skinner, "Very High Capacity Digital Radio Systems Using 64-State Quadrature Amplitude Modulation," *IEE Proceedings of 'Telecommunications Transmission 85'*, pp. 48-51, London,UK, 1985.

124. E. Fukuda, N. Iizuka, M. Minowa, Y. Daido, and H. Nakamura, "A New 90 Mbps 68 ASK Modem with a Honeycomb Constellation for Digital Radio Systems," *IEEE Proceedings of Globecom '88*, pp. 1490-1494, Tokyo,Japan, Nov. 1987.

125. C.F.N. Cowan and P.M. Grant, "Survey of Analogue and Digital Adaptive Filter Realisations," in *Adaptive Filters*, ed. C. F. Cowan P. M. Grant, Prentice-Hall, 1985.

126. W. Wang, B. Auld, and J. Liu, "Design and Analysis of a New Structured Adaptive SAW Filter," *IEEE Proceedings of International Symposium on Circuits and Systems*, pp. 1405-1408, Espoo, Finland, June 1988.

127. G. Riha, "SAW Filters for Radio Communication Systems," *IEEE Proceedings of International Symposium on Circuits and Systems*, pp. 1389-1394, Espoo, Finland, June 1988.

128. K. Otremba, J. Steinkamp, H.-J. Thaler, and K. Vogel, "High Capacity Digital Radio System Familly for the 18 GHz Band," *IEEE Proceedings of Globecom '88*, pp. 1485-1489, Tokyo, Japan, November 1987.

129. B. Baccetti, S. Bellini, G. Filiberti, and G. Tartara, "Full Digital Adaptive Equalisation in 64-QAM Radio Systems," *IEEE Journal on Selected Areas in Communications*, vol. SAC-5, pp. 466-475, April 1987.

130. L.E. Larson, "High-Speed Analogue-to-Digital Conversion with GaAs Technology: Prospects, Trends and Obstacles," *IEEE Proceedings of International Symposium on Circuits and Systems*, pp. 2871-2878, Espoo, Finland, June 1988.

131. A. Nist, T.Noll, J.A. Nossek, and C. Sebald, "Fully Digital Implementation of Adaptive Time-Domain Equalisation for Multilevel QAM Digital Radio Systems," *IEEE Proceedings of 'Globecom 87'*, pp. 1212-1216, Tokyo, November 1987.

132. H. Matsue, T. Shirato, and K. Watanabe, "256QAM 400 Mb/s Microwave Radio System with DSP Fading Countermeasures," *IEEE Proceedings of ICC 88*, pp. 1362-1367, Philadelphia, USA, June, 1988.

133. C. Caraiscos and B. Liu, "A Roundoff Errors Analysis of the LMS Adaptive Algorithm," *IEEE Transactions on Acoustics, Speech and Signal Processing*, vol. ASSP-32, no. 1, pp. 34-41, Febuary 1984.

134. J.M. Cioffi, "Limited-Precision Effects in Adaptive Filtering," *IEEE Transactions on Circuits and Systems*, vol. CAS-34, no. 7, pp. 821-833, July 1987.

135. R.D. Gitlin , H.C. Meadors, and S.B. Weinstein, "The Tap-Leakage Algorithm: An Algorithm for the Stable Operation of a Digitally Implemented, Fractionally Spaced Adaptive Equaliser," *Bell System Technical Journal*, vol. 61, pp. 1817-1839, October 1982.

136. A. Feuer, "Performance Analysis of the Block Least Mean Square Algorithm," *IEEE Transactions on Circuits and Systems*, vol. CAS-32, no. 9, September 1985.

137. G. Panda, B. Mulgrew, C. F. N. Cowan, and P. M. Grant, "A Self Orthogonalised Efficient Block Adaptive Filter," *IEEE Transactions on Acoustics Speech and Signal Processing*, vol. ASSP-34, pp. 1573-1582, December 1986.

138. G. Panda, C.F.N. Cowan, and P.M. Grant, "Assessment of Finite Precision Limitations in LMS and BLMS Adaptive Algorithms," *IEEE Proceedings of ICAASP '87*, pp. 137-140, Tokyo, Japan, May 1987.

139. N.J. Bershad, "Nonlinear Quantisation Effects in the LMS and Block LMS Adaptive Algorithms -A Comparison," *IEEE Proceedings of ICAASP '88*, pp. 1491-1494, New York, USA, May 1988.

140. J.M. Cioffi, "Precision-Efficient Use of Block Adaptive Algorithms in Data-Driven Echo Cancellers," *IEEE Proceedings of ICC '88*, pp. 355-359, Philadelphia, USA, June 1988.

141. C.R. Cole, A. Haoui, and P.L. Winship, "A High-Performance Digital voice Echo Canceller on a Single TMS32020," *IEEE Proceedings of ICAASP '86*, pp. 429-432, Tokyo, Japan, April 1986.

142. R.D. Gitlin and S.B. Weinstein, "On the Required Tap-Weight Precision for Digitally Implemented, Adaptive Mean-Squared Equalisers," *Bell System*

Technical Journal, vol. 58, no. 2, pp. 301-321, February 1979.

143. R.D. Gitlin, J.E. Mazo, and M.G. Taylor, "On the Design of Gradient Algorithms for Digitally Implemented Adaptive Filters," *IEEE Transactions on Circuit Theory*, vol. CT-20, no. 2, pp. 125-136, March 1973.

144. M. Bolla, L. Rossi, A. Spalvieri, and A. D'Andrea, "Design of a Fully Digital Adaptive Equaliser for a 256QAM Modem," *IEEE Proceedings of ICC 88*, pp. 1368-1373, Philadelphia, USA, June, 1988.

145. K. Aamo, "An Experimental Test Loop to Assist in Designing Digital Radio Microwave Radio Systems," *IEEE Transactions on Communications*, vol. COM-27, no. 12, pp. 1968-1971, December 1979 .

146. A.J. Rustako, Jr., C.B. Woodworth, R.S. Roman, and H.H. Hoffman, "A Laboratory Simulation Facility for Multipath Fading Microwave Radio Channels," *AT&T Technical Journal*, vol. 64, no. 10, December 1985 .

147. R.N. Kolte, S.C. Kwatra, and G.H. Stevens, "Computer Controlled Hardware Simulation of Fading Channel Models," *IEEE Proceedings of ICC '88*, pp. 1646-1650, Philadelphia, USA, June 1988.

148. P. Horowitz and W. Hill, *The Art of Electronics,* Cambridge University Press, 1980.

149. B.W. Kernighan and R. Pike, *The UNIX Programming Environment,* Prentice-Hall, 1984.

150. A.T. Kerr, "Adaptive Filter Based on TMS32010 Digital Signal Processor," BSc Hons. Project Report HSP 457, University of Edinburgh, May 1985.

151. *TMS32010 User's Guide,* Texas Instruments.

Appendix A

The Baseband Channel Model

The following appendix describes modeling the sampled channel response by a FIR filter. Consider a linear analogue system with output

$$x(t) = \int_{n=-\infty}^{\infty} a(n).h_N(t-n)\,dn \tag{A.1}$$

where $a(n)$ is the transmitted data sequence and the overall convolved impulse response is given by

$$h_N(t) = h_T(t)*h_C(t)*h_R(t) \tag{A.2}$$

If the $x(t)$ is sampled every kT seconds, where T is the time period

$$x(k) = \int_{n=-\infty}^{\infty} a(n).h_N(k-n)\,dn \tag{A.3}$$

The input is a train of impulses such that

$$a(n) = \sum_{i=-\infty}^{\infty} a(i)\delta(n-i) \tag{A.4}$$

where $\delta(n)$ is an impulse function. Equation (A.3) may be rewritten as

$$x(k) = \int_{n=-\infty}^{\infty} \sum_{i=-\infty}^{\infty} a(i).\delta(n-i).h_N(k-n)\,dn \tag{A.5}$$

Changing the order of integration and summation

$$x(k) = \sum_{i=-\infty}^{\infty} a(i) \int_{n=-\infty}^{\infty} \delta(n-i).h_N(k-n)\,dn \tag{A.6}$$

The impulse is non-zero when $(n-i)=0$, thus $n=i$. Substituting yields

$$x(k) = \sum_{i=-\infty}^{\infty} a(i).h_N(k-i) \tag{A.7}$$

If $h_N(t)$ has a finite response, (A.7) may be rewritten as a FIR filter of length N (neglecting noise)

$$x(k) = \sum_{i=0}^{N-1} h_N(i).a(k-i) \tag{A.8}$$

Appendix B

Simulation Software - Structure and Examples

The general structure of the main program kernel, providing many of the simulation results, is now described. Extensive use was made of UNIX shell programming [149] to control the simulation functions written in 'C' [26]. Figure B.1 illustrates the hierarchy of the simulation approach.

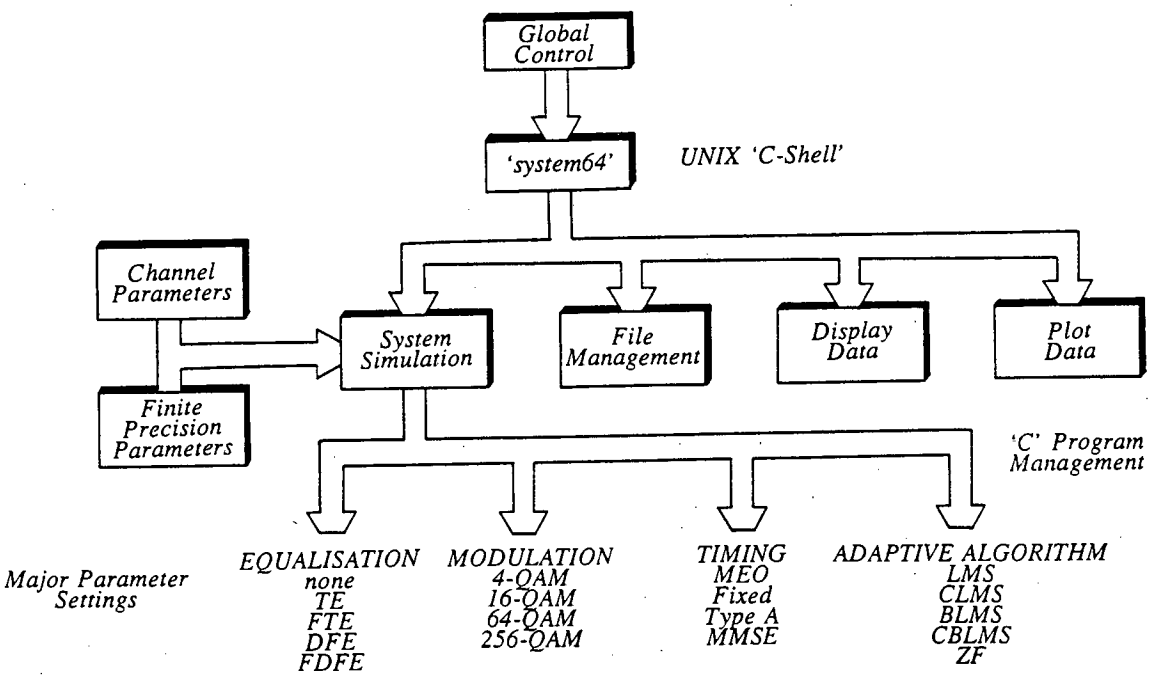

Figure B.1 Simulation Structure

Passing suitable parameters with *system64* allows highly flexible simulation of many of the required receiver configurations e.g. calling

system64 simulate sig 64QAM dfe typeA ZF

would initiate the simulation of a signature curve for a 64-QAM radio system with type A timing recovery and a decision feedback equaliser updated with the zero forcing algorithm. Further flexibility is achieved by calling system64 commands from within the global control file.

In total, the main 'C' program and associated functions required over 4200 lines of code, and therefore only a number of key functions are now included. Simulation of symbol spaced transversal and decision feedback equalisers is by *equaliser_te()* and

equaliser_dfe(), respectively. Adaptation by the LMS algorithm is with *lms()*, while data generation and detection for a 64-QAM system is with *data64()* and *decision64()*.

```
/*-------------------------------------------------------------------------
VARIABLES: Global arrays used for 2 FIR model of T/2 FSE, and symbol spaced
equalisers requiring only a single forward FIR filter.
*/
double Cr1[15],Ci1[15],Cr2[15],Ci2[15]; /* Equaliser coefficient vectors */
double Sr1[15],Si1[15],Sr2[15],Si2[15]; /* Equaliser delay lines */
double Br[15],Bi[15];                   /* DFE Feedback coefficients */
double x2r[15],x2i[15];         /* Feedback delay lines */
double YDr[15],YDi[15];         /* Equaliser output vector */


/*-------------------------------------------------------------------------
FUNCTION: equaliser_te()
Performs equaliser operations. Simulates a symbol spaced transversal
equaliser, although parameters are also passed allowing a second
FIR filter for a T/2 spaced equaliser.
*/
equaliser_te(nF1taps,nF2taps,nBtaps,yor1,yoi1,yor2,yoi2,Yr,Yi,ar,ai)
int nF1taps,nF2taps,nBtaps;          /* Equaliser tap lengths */
double yor1,yoi1,yor2,yoi2,*Yr,*Yi,ar,ai; /* Input variables */
{
int i,j;          /* Counters */
/*
Input new data to forward filter, FIR1 and calculate response
*/
for (i=nF1taps-1;i>0;i--) {    /* Shift real and imaginary delay lines */
      Sr1[i]=Sr1[i-1];
      Si1[i]=Si1[i-1];
}
Sr1[0]= yor1;                  /* Add new received data */
Si1[0]= yoi1;

*Yr= *Yi=0;
for (i=0;i<nF1taps;i++) {      /* Form complex equaliser outputs */
      *Yr += (Sr1[i]*Cr1[i] - Si1[i]*Ci1[i]);
      *Yi += (Sr1[i]*Ci1[i] + Si1[i]*Cr1[i]);
}
}


/*-------------------------------------------------------------------------
FUNCTION: equaliser_dfe()
Decision feedback equaliser
*/
equaliser_dfe(nF1taps,nF2taps,nBtaps,yor1,yoi1,yor2,yoi2,Yr,Yi,ar,ai)
int nF1taps,nF2taps,nBtaps;
double yor1,yoi1,yor2,yoi2,*Yr,*Yi,ar,ai;
{
int i;            /* Counter */
double Xr,Xi;           /* Feedback summation terms */

/*
```

```
Shift backward stage
*/
for (i=nBtaps;i>0;i--) {
      x2r[i]=x2r[i-1];
      x2i[i]=x2i[i-1];
}
/*
DFE: Add decision to feedback filter array
*/
x2r[1]=ar;
x2i[1]=ai;

/*
Input new data to forward filter, FIR1 and calculate response
*/
for (i=nF1taps-1;i>0;i--) {    /* Shify delay lines */
      Sr1[i]=Sr1[i-1];
      Si1[i]=Si1[i-1];
}
Sr1[0]= yor1;                  /* Add new data */
Si1[0]= yoi1;

*Yr= *Yi =0.0;                 /* Reset summation terms */
for (i=0;i<nF1taps;i++) {
      *Yr += (Sr1[i]*Cr1[i] - Si1[i]*Ci1[i]);
      *Yi += (Sr1[i]*Ci1[i] + Si1[i]*Cr1[i]);
}

/*
Calculate backward filter section
*/
Xr=Xi=0.0;
for (i=1;i<= nBtaps;i++) {
      Xr += (x2r[i]*Br[i] - x2i[i]*Bi[i]);
      Xi += (x2r[i]*Bi[i] + x2i[i]*Br[i]);
}

/*
Subtract ISI calculated from previously detected symbols
*/
*Yr= *Yr-Xr;
*Yi= *Yi-Xi;

}


/*-------------------------------------------------------------------------
FUNCTION: lms()
Performs conventional lms update. Update rate may be changed with
appropriate value for 'update_rate', default=1. Updates two forward FIR
filters if required for T/2 spaced operation.
*/
lms(mu,er,ei,nF1taps,nF2taps,nBtaps,update_rate,update_count)
double mu,er,ei;
int nF1taps,nF2taps,nBtaps,
    update_rate,*update_count;
{
```

```
int i;
int temp_update_count;

temp_update_count= *update_count;
temp_update_count++;
if(temp_update_count==update_rate) {
      for (i=0;i<nF1taps;i++) {      /* Update FIR1 taps */
                  Cr1[i]= Cr1[i] +
                      mu*( Sr1[i]*er + Si1[i]*ei);
                  Ci1[i]= Ci1[i] +
                      mu*( Sr1[i]*ei - Si1[i]*er);
      }
      for (i=0;i<nF2taps;i++) {      /* Update FIR2 taps */
                  Cr2[i]= Cr2[i] +
                      mu*( Sr2[i]*er + Si2[i]*ei);
                  Ci2[i]= Ci2[i] +
                      mu*( Sr2[i]*ei - Si2[i]*er);
      }
      for (i=1;i<=nBtaps;i++) {      /* Update feedback taps */
            Br[i]= Br[i] -
                mu*( x2r[i]*er + x2i[i]*ei);
            Bi[i]= Bi[i] -
                mu*( x2r[i]*ei - x2i[i]*er);
      }
temp_update_count=0;
}
*update_count=temp_update_count;
}


/*-------------------------------------------------------------------------
FUNCTION: data64()
Generates multilevel data for 64QAM modulation. Output may take values from
the set {-7,-5,-3,-1,1,3,5,7}
*/
double data64()
{
 double digit1,digit2,digit3,digit64;

 /* Generate random numbers. 'Randomness' increased by using only
 every tenth number generated */
 for(i=0;i<10;i++) {
      digit1=random()&01;
      digit2=random()&01;
      digit3=random()&01;
 }
 if (digit1==1) {
      if (digit2==1) {
            if (digit3==1)
                  digit64=1;
            else
                  digit64= -1;
      }
      else {
            if (digit3==1)
                  digit64=3;
            else
```

```
                digit64= -3;
        }
}
else {
        if (digit2==1) {
                if (digit3==1)
                        digit64= 5;
                else
                        digit64= -5;
        }
        else {
                if (digit3==1)
                        digit64=7;
                else
                        digit64= -7;
        }
}
/* Return normalised data i.e. all returned values are scaled for
fractional representation */
 return(digit64/7.0);
}


/*-------------------------------------------------------------------------
FUNCTION: decision64()
Multilevel decision device at the receiver. Decisions may be made from the
set {-7,-5,-3,-1,1,3,5,7}. The returned value is normalised.
*/
double decision64(y)
double y;    /* Input */
{
double Y;    /* Output decision */

y*= 7.0;            /* Scale input */
if (y< -6.0)
        Y= -7.0;
if ((y>= -6.0) && (y< -4.0))
        Y= -5.0;
if ((y>= -4.0) && (y< -2.0))
        Y= -3.0;
if ((y>= -2.0) && (y< 0.0))
        Y= -1.0;
if ((y>= 0.0) && (y< 2.0))
        Y= 1.0;
if ((y>= 2.0) && (y< 4.0))
        Y= 3.0;
if ((y>= 4.0) && (y< 6.0))
        Y= 5.0;
if (y>= 6.0)
        Y= 7.0;

return(Y/7.0);
}
```

Appendix C

Optimum Finite Length DFE Performance

An optimum solution to a linear transversal equaliser is obtained by direct application of Wiener filter theory (chapter 2). This solution may be extended to the nonlinear decision feedback equaliser (DFE) since only the decision process is nonlinear. Final decisions are assumed correct. The output of a symbol spaced DFE with N forward and M feedback taps may be expressed as the summation of forward and feedback terms

$$\hat{y}(k-d) = \sum_{i=0}^{N-1} c_i x(k-i) + \sum_{i=1}^{M} b_i y(k-d-i) \tag{C.1}$$

where d is the delay through the equaliser. For a normal DFE configuration, with the reference tap set as the last forward filter position, $d=N$. Equation (C.1) may be expressed as vector inner products

$$\hat{\underline{y}}(k) = \underline{c}^T \underline{x}(k) + \underline{b}^T \underline{y}(k-d-1) \tag{C.2}$$

$$= [\underline{c}^T \underline{b}^T(k)] \begin{bmatrix} \underline{x}(k) \\ \underline{y}(k-d-1) \end{bmatrix} \tag{C.3}$$

$$= \underline{g}^T \underline{z}(k) \tag{C.4}$$

Equation (C.4) is equivalent to a linear combiner. The set of optimum coefficients, $\underline{g}_{opt}$, may now be derived in a similar manner to the derivation in section 2.7 of chapter 2. Replacing the terms in equation (2.7.9) by those defined by (C.4) gives

$$E[\underline{z}(k)y(k-d)] = E[\underline{z}(k)\underline{z}^T(k)]\underline{g}_{opt} \tag{C.5}$$

Replacing $\underline{z}(k)$ and $\underline{g}_{opt}(k)$ by the appropriate definition from (C.3) yields

$$E\left\{ \begin{bmatrix} \underline{x}(k) \\ \underline{y}(k-d-1) \end{bmatrix} y(k-d) \right\} = E\left\{ \begin{bmatrix} \underline{x}(k) \\ \underline{y}(k-d-1) \end{bmatrix} [\underline{x}^T(k)\ \underline{y}^T(k-d-1)] \right\} \begin{bmatrix} \underline{c}_{opt} \\ \underline{b}_{opt} \end{bmatrix} \tag{C.6}$$

Expanding (C.6) results in

$$\underline{b}_{opt} = -E[\underline{y}(k-d-1)\ \underline{x}^T(k)]\underline{c}_{opt} \tag{C.7}$$

Substituting (C.7) back into the expanded form of (C.6) provides an expression for the optimum forward filter, c_{opt}. This is defined in a similar manner to the optimum linear Wiener filter in equation (2.7.11), where now the autocorrelation matrix, $\underline{\phi}_{xx}$ is defined by

$$\underline{\phi}_{xx} = E[\underline{x}(k)\underline{x}^T(k)] - E[\underline{x}(k)\underline{y}^T(k-d-1)].E[\underline{y}(k-d-1)\underline{x}^T(k)] \tag{C.8}$$

While similar to the definition in (2.7.11), (C.8) now excludes the span of the

feedback filter. The cross-correlation vector is defined by

$$\underline{\phi}_{xy} = E[\underline{x}(k)y(k-d)] \tag{C.9}$$

A expression for the output MSE is derived from equation (C.4), thus

$$\xi(k) = E[(y(k-d) - \underline{g}^T \underline{z}(k))^2] \tag{C.10}$$

Expanding (C.10), differentiating with respect to $\underline{g}^T$ and equating to zero results in the minimum MSE

$$\xi_{opt}(k) = E[y^2(k-d)] - \underline{c}_{opt}{}^T \underline{\phi}_{xy} \tag{C.11}$$

Appendix D

Finite Precision Simulation

The following set of functions written in 'C' provide some of the finite precision routines required for the simulation of digital equaliser implementations. Functions return double precision floating point value permitting simple incorporation into the overall 'C' program structure. Notation is assumed to be fractional as defined in chapter 5. Application of these functions is illustrated by two functions simulating a finite precision FIR filter and finite precision implementation of the clipped LMS algorithm.

```
/*-----------------------------------------------------------------
FUNCTION:  saturate()
Saturates passed value to bounds defined by fractional 2's compliment
notation
*/
double saturate(x,nbits)
double x;
int nbits;
{
if (x> 1.0- 1.0/( (double)(1<<(nbits-1)) ));
      x=1.0- 1.0/( (double)(1<<(nbits-1)) );     /* Set upper bound */
if (x< -1.0)
      x= -1.0;                          /* Set lower bound */
return(x);
}


/*-----------------------------------------------------------------
FUNCTION:  truncate()
Truncates infinite precision floating input to n bit floating
representation. Incorporates saturation. All inputs are converted
firstly to integer form by suitable scaling according to the
required precision. Truncation is achieved by this scaling operation.
The operand is then converted back to fractional representation for
further operations.
*/
double truncate(frac,nbits)
double frac;
int nbits;
{
int sign;               /* Sign of input */
int nfrac;              /* Integer representation of input */
double dfrac;                 /* Result of reconverting integer i/p */
sign=sgn(frac);               /* Take sign of input */
frac=saturate(frac,nbits);    /* Saturate input */
frac= fabs(frac);       /* Take modulus of input */
frac*= (double)(1<<(nbits-1));/* Convert to integer form */
```

```
nfrac =(int)frac;       /* Cast from double to integer type */
if(sign) {              /* Covert to 2's complement form if negative */
      nfrac= ~nfrac;          /* 1's complement negation */
      nfrac++;          /* Add one */
      nfrac &= (1<<nbits)-1;  /* Mask unwanted bits */
}

/* Input now in integer representation. Now required to convert back to
a fractional number   */

dfrac= (double)nfrac / ((double)(1<<(nbits-1)));
if(sign) {              /* If negative, convert to sign and magnitude
                           format then convert */
      nfrac= ~nfrac;
      nfrac++;
      nfrac &= (1<<nbits)-1;
      dfrac= -1.0 * (double)nfrac / ((double)(1<<(nbits-1)));
}
return(dfrac);
}


/*-------------------------------------------------------------------
FUNCTION:  sgn2()
Returns sign of n bit hex number. Effectively returns MSB of passed value.
A value of 1 corresponds to a negative number in Q15 notation.
*/
sgn2(x,nbits)
int x,nbits;
{
x >>= (nbits-1);
x &= 1;                 /* Mask MSB */
return(x);
}


/*-------------------------------------------------------------------------
FUNCTION:  invert()
Performs bitwise inversion of input
*/
double invert(x,nbits)
double x;
int nbits;
{
 int nx;
 x= saturate(x,nbits);
 x *= (double)(1<<(nbits-1));
 nx= (int)x;
 nx= ~nx;          /* 1's complement negation */
 nx++;             /* Add one */
 x= (double)nx/((double)(1<<(nbits-1)));
 return(x);
}


/*-------------------------------------------------------------------------
FUNCTION:  add()
```

```
Adds y to x
*/
double add(x,y,nbits)
double x,y;
int nbits;
{
double sum;
x= truncate(x,nbits);
y= truncate(y,nbits);
sum = x+y;
sum=saturate(sum,nbits);
sum= truncate(sum,nbits);
return(sum);
}


/*---------------------------------------------------------------------------
FUNCTION:  multiply()
Multiplies x by y
*/
double multiply(x,y,nbits)
double x,y;
int nbits;
{
double prod;
x= truncate(x,nbits);
y= truncate(y,nbits);
prod= x*y;
prod= truncate(prod,nbits);
return(prod);
}


/*---------------------------------------------------------------------------
FUNCTION:  multiply_sgn()
Multiplies y by the sign of x. Equivalent to inverting y if the sign
is negative. If x is positive, y is unaffected.
*/
double multiply_sgn(x,y,nbits)
double x,y;
int nbits;
{
 x= dsgn(x);
 if (x>=0.0) {
      return(y);
 }
 else {
      y=invert(y,nbits);
      y=saturate(y,nbits);
      return(y);
 }
}


/*---------------------------------------------------------------------------
FUNCTION:  shift_r()
Performs right shift with sign extension
```

```
*/
double shift_r(x,ny,nbits)
double x;
int ny,nbits;
{
int nx,nprod;
double prod;

nx= normalise_data(x,nbits);  /* Convert to integer format */
if (sgn2(nx,nbits)) {         /* If negative, extend sign to MSB */
      nprod= nx >>ny;         /* Right shift */
      nprod |= ~(((1<<nbits)-1)>>ny);
}
else
      nprod= nx >>ny;
prod= denormalise_data(nprod,nbits); /* Convert back to fractional number */
return(prod);
}


/*-------------------------------------------------------------------------
FUNCTION:  shift_l()
Performs left shift. Operates in overflow mode i.e. if an overflow is
detected, the output saturates to the appropriate maximum or minimum
value. Three test are required to ensure that sign information is not lost
during the simulation.
*/
double shift_l(x,ny,nbits)
double x;
int ny,nbits;
{
int nx,nprod,sign1,sign2;
int OVRFLOW=false;
double prod;
if((x*(double)pow(2.0,(double)ny)) >=1.0) {
      nprod= (1<<(nbits-1))-1;
      OVRFLOW=true;
}
if((x*(double)pow(2.0,(double)ny)) < -1.0) {
      nprod= (1<<(nbits-1));
      OVRFLOW=true;
}
if (OVRFLOW==false) {
      sign1=sgn(x);
      nx= normalise_data(x,nbits);
      if (sign1)
            nx |= ~((1<<nbits)-1);
      nprod= nx <<ny;
}
prod= denormalise_data(nprod,nbits);
return(prod);
}
```

The following two functions illustrate application of the finite precision functions to simulating a symbol spaced transversal equaliser updated by the clipped LMS algorithm. Notation is defined in Appendix **B.**

```
/*-------------------------------------------------------------------------
FUNCTION: EQ_te_finite()
Finite precision complex symbol spaced transversal equaliser.
*/
EQ_te_finite(nF1taps,nF2taps,nBtaps,yor1,
                yoi1,yor2,yoi2,Yr,Yi,ar,ai,nbits)
int nF1taps,nF2taps,nBtaps;
double yor1,yoi1,yor2,yoi2,*Yr,*Yi,ar,ai;
int nbits;              /* Arithmetic Precision */
{
int i;                  /* Counter */
double temp1,temp2,temp3;     /* Temporary variables */
/*
Input new data to forward filter, FIR1 and calculate response
*/
for (i=nF1taps-1;i>0;i--) {   /* Shift delay lines */
      Sr1[i]=Sr1[i-1];
      Si1[i]=Si1[i-1];
}
Sr1[0]=saturate(yor1,nbits);  /* Add new data */
Si1[0]=saturate(yoi1,nbits);

*Yr= *Yi=0.0;
for (i=0;i<nF1taps;i++) {
      temp1= multiply(Sr1[i],Cr1[i],nbits);
      temp2= multiply(Si1[i],Ci1[i],nbits);
      temp3= subtract(temp1,temp2,nbits);
      *Yr= add(*Yr,temp3,nbits);
      temp1= multiply(Sr1[i],Ci1[i],nbits);
      temp2= multiply(Si1[i],Cr1[i],nbits);
      temp3= add(temp1,temp2,nbits);
      *Yi= add(*Yi,temp3,nbits);
}
/* Two bit coefficient headroom, so scale output */
*Yr= shift_l(*Yr,2,nbits);
*Yi= shift_l(*Yi,2,nbits);
}


/*-------------------------------------------------------------------------
FUNCTION: clms_finite()
Performs Clipped lms update for symbol spaced transversal equaliser. Update
rate may be changed with appropriate value for 'update_rate', default=1.
*/

clms_finite(mu,er,ei,nF1taps,nF2taps,nBtaps,update_rate,
                        update_count,nbits)
double mu;              /* Convergence factor */
double er,ei;                 /* Errors (real and imaginary) */
int nF1taps,nF2taps,nBtaps,
```

```
    update_rate,*update_count,nbits;
{
int i;                  /* Counter */
int temp_update_count;
double temp1,temp2,temp3;

temp_update_count= *update_count;
temp_update_count++;
if(temp_update_count==update_rate) {
      for (i=0;i<nF1taps;i++) {
            temp1= multiply_sgn(Sr1[i],er,nbits);
            temp2= multiply_sgn(Si1[i],ei,nbits);
            temp1= multiply(mu,temp1,nbits);
            temp2= multiply(mu,temp2,nbits);
            temp3= add(temp1,temp2,nbits);
            Cr1[i]= add(Cr1[i],temp3,nbits);    /* Update real coef. */

            temp1= multiply_sgn(Sr1[i],ei,nbits);
            temp2= multiply_sgn(Si1[i],er,nbits);
            temp1= multiply(mu,temp1,nbits);
            temp2= multiply(mu,temp2,nbits);
            temp3= subtract(temp1,temp2,nbits);
            Ci1[i]= add(Ci1[i],temp3,nbits);    /* Update imag. coef. */
      }
temp_update_count=0;
}
*update_count=temp_update_count;
}
```

Appendix E

Hardware Design

The hardware demonstration system consisted of three extended double Eurocards: the channel simulator, the programmable FIR filter and the DSP update board. Sufficient flexibility was incorporated into the design to allow the channel simulator to be connected directly to either the FIR filter or DSP boards.

E.1 Channel Simulator

The channel simulator design may be broken down into three stages: (1) FIR filter, (2) control and (3) data and noise generation. The FIR filter is implemented by a TRW TMC2243 device (figure E.1). Two's complement data is input and output in parallel, at a potential clocking rate of 20 MHz. A single TMC2243 provides 3 filter taps and longer designs are possible by cascading the devices. Coefficients are stored sequentially, and the three storage registers must be addressed by the 2-bit write enable control (CW_{1-0}). Coefficient storage and transfer are accomplished by the circuit in figure E.2. Transfer is initiated by a negative edge on $\overline{load}$. Data and noise generation are provided by two feedback shift register PRBS generators (figure E.3). Suitably long sequences, of different length to decorrelate data and noise, were selected [148].

E.2 FIR Filter

As stated in chapter 5, this board although logically tested, was not incorporated into the test system. Consequently only an outline of the basic operation is provided here. The FIR filter board consists of two TMC2243s in series plus suitable buffering and control to interface with the DSP board. Buffering is with TTL 74LS189 64-bit RAMs, each with as access time of 25 ns. Block lengths (in the BLMS algorithm) of up to 16 may be accommodated, although hardware reduction would be possible for a purely LMS implementation (block length = 1). Figure E.4, obtained from a Tekronix DAS logic analyser, illustrates the timing requirements for the transfer updated coefficients from the DSP board. A similar arrangement is required when transferring data to the DSP. To initially simplify the design, both DSP and FIR clocks were assumed to be the same. Once the newly updated coefficients are stored in RAM (DSP control lines not shown), the coefficients are sequentially addressed and read, with FIR control provided by lines CW_{00-11}.

E.3 DSP Board

The DSP board containing the TMS32010 was taken from part of an Edinburgh University project design. A full description may be found in the relevant report [150]. Interfacing the TMS32010 to the channel simulator or the FIR filter is through two independent strobes, data enable $\overline{DE}$ and write enable $\overline{WE}$, controlling data on a 16-bit data bus. Full details of the TMS32010 may be found in the users guide [151]. Code required to implement the adaptive algorithms is contained in appendix F.

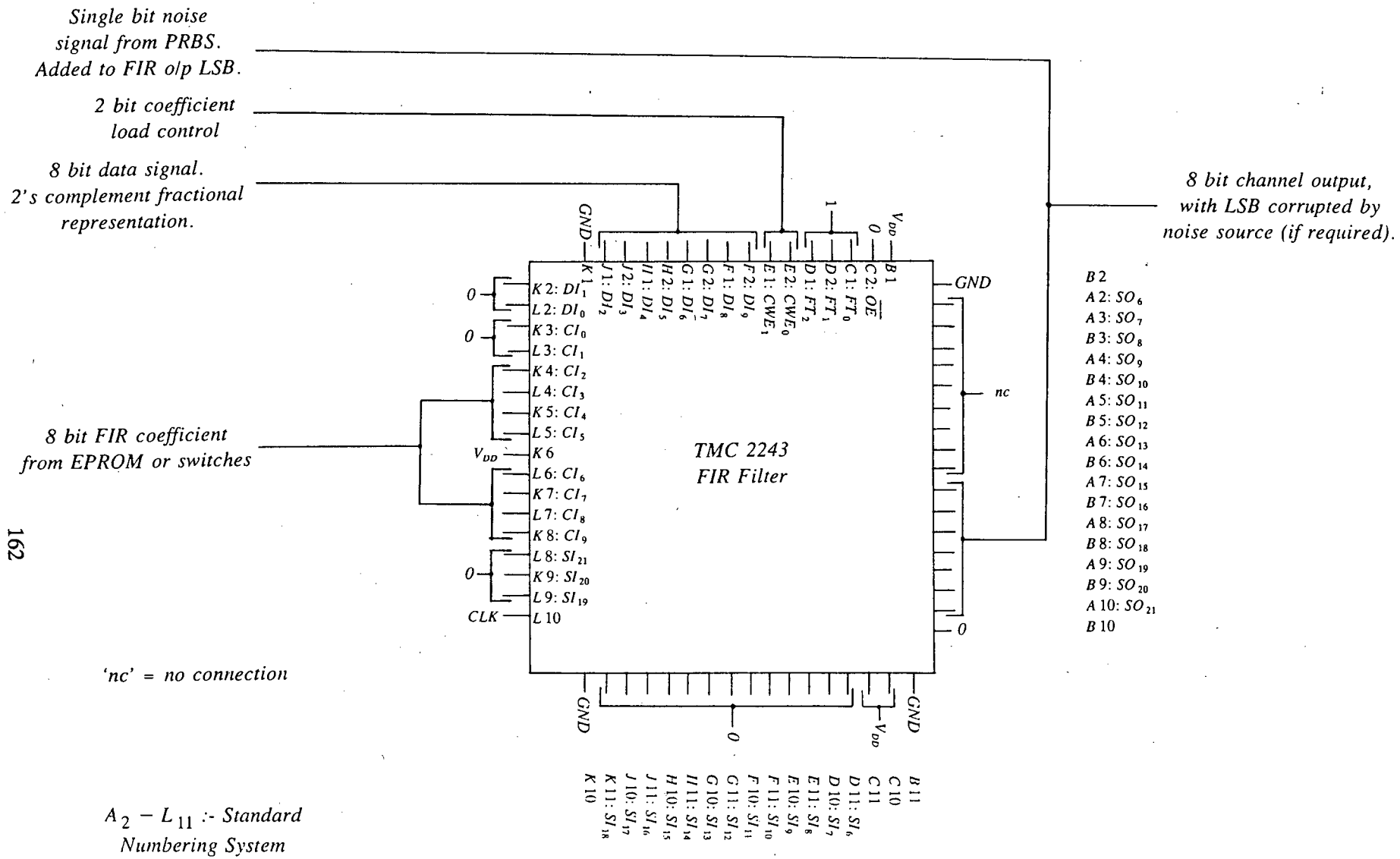

Figure E.1 Channel Simulator: FIR Filter

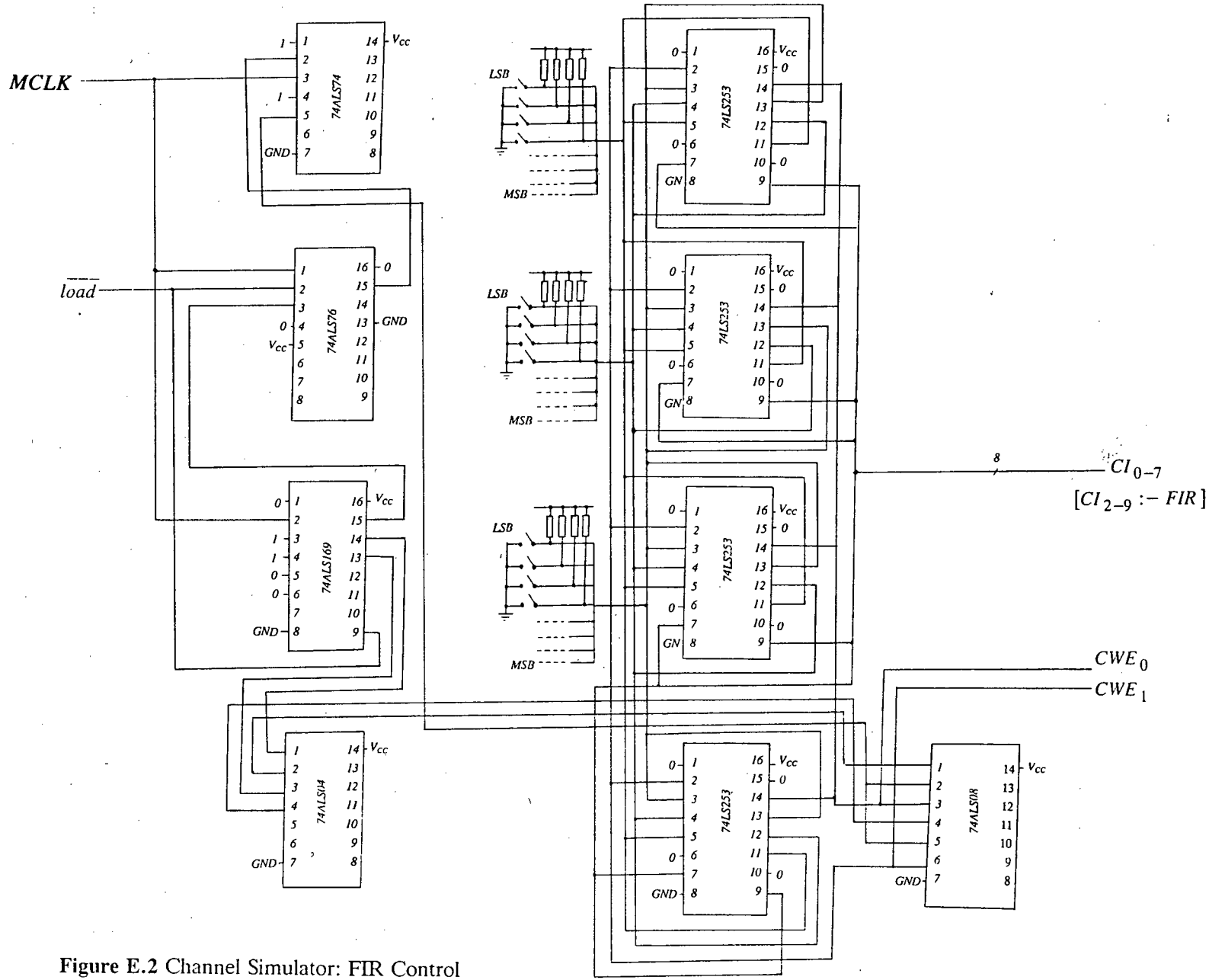

Figure E.2 Channel Simulator: FIR Control

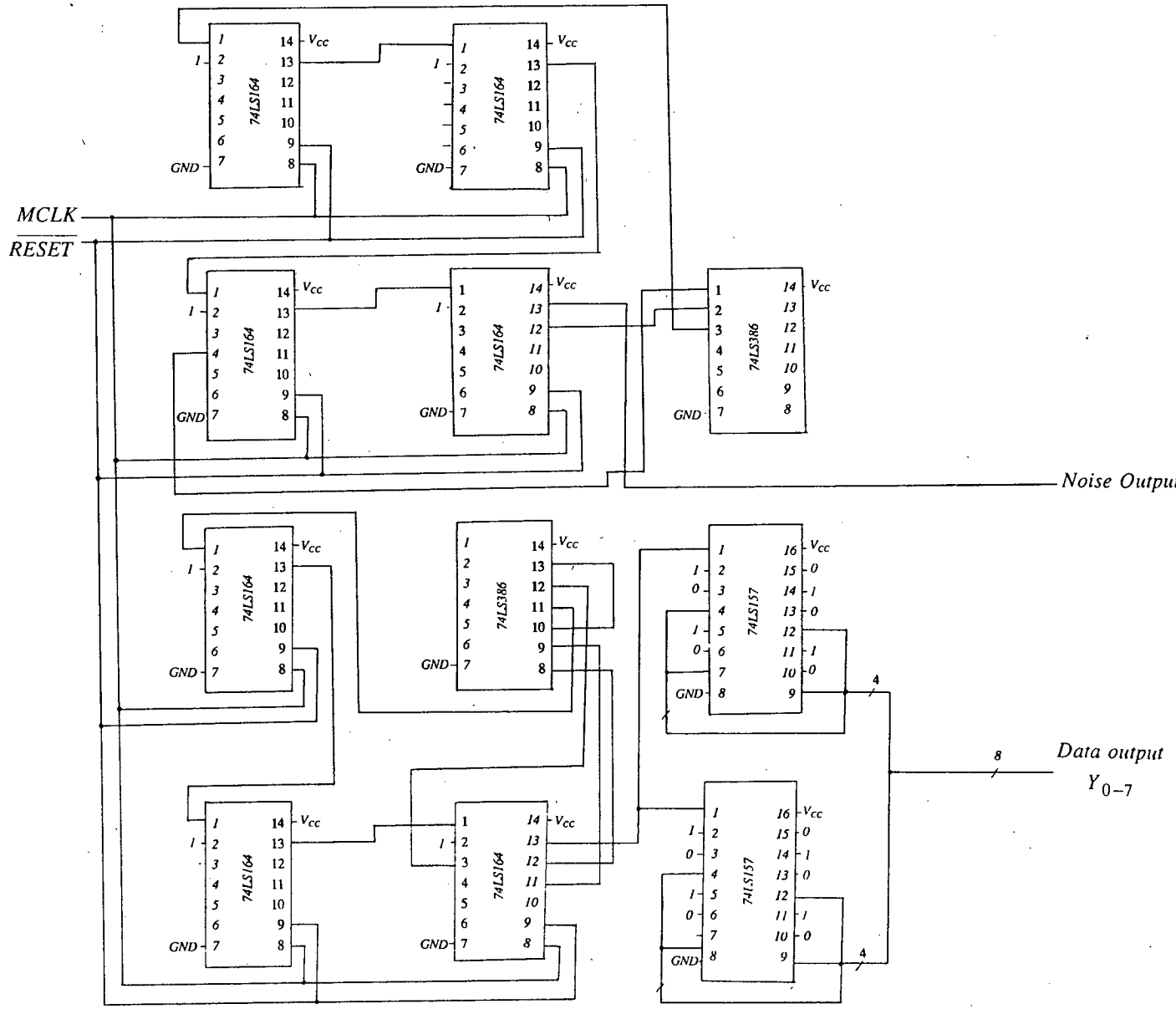

Figure E.3 Channel Simulator: Data/Noise Generation

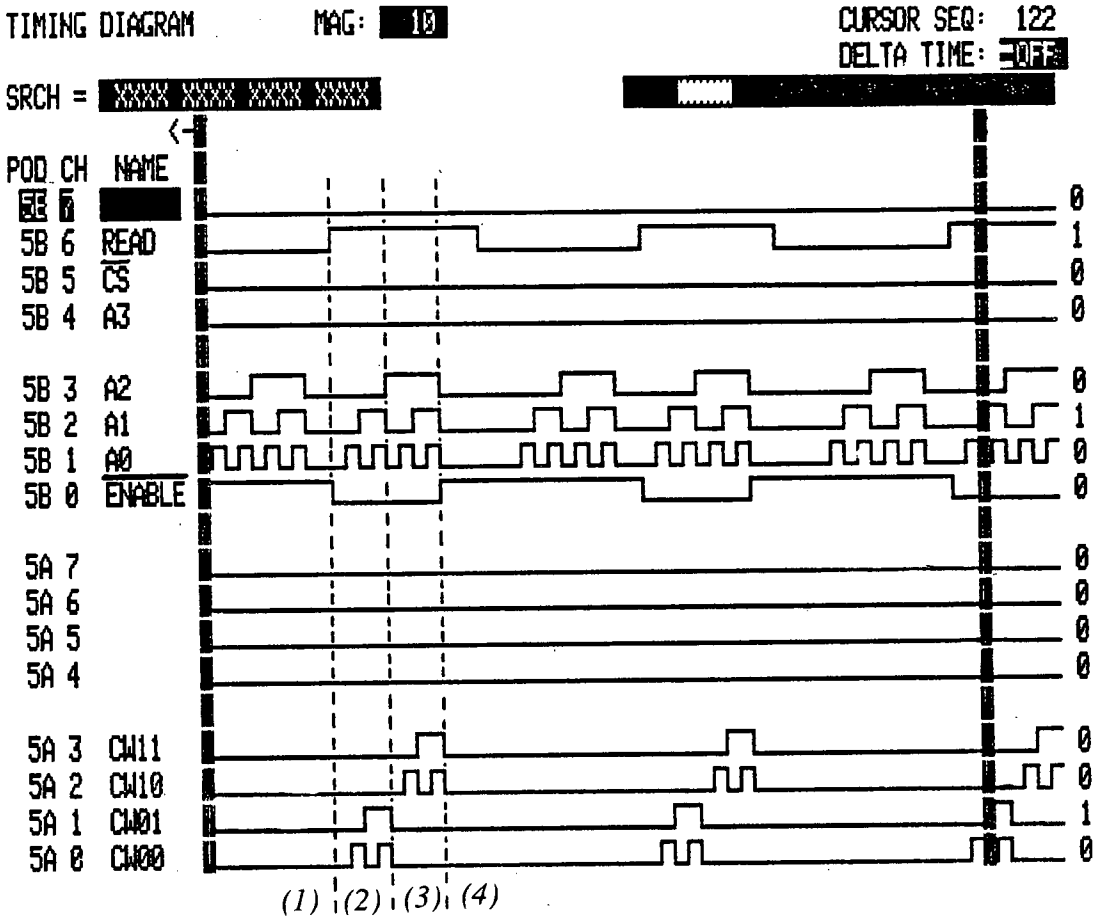

Transfer Type:

Coefficient transfer from RAM to FIR filters.

Timing Sequence

(1) RAM disabled. Address generator counters in free run.

(2) Start read cycle. Counters reset. Address lines *CW*00 and *CW*01 used for first TMC2243.

(3) Load coefficients into second TMC2243.

(4) Load new coefficients from DSP to RAM when ready.

Key:

*CW*00–11: TMC2243 write enable control - address of coefficient storage registers.

*A*0–*A*3: RAM address lines.

READ: RAM read/write select

$\overline{CS}$: RAM chip select.

$\overline{ENABLE}$: Enables coefficient transfer

Figure E.4 Data Transfer Timing Sequence

Appendix F

TMS32010 Code

Hardware results in chapter 5 were generated from the following assembly code. Code is given for the full off-line equaliser implementation, however modifications are included allowing stand-alone operation with the channel simulator. Extra code is also included to generate the error modulus term for the convergence curves. Although the overall program appears long, considerable initialisation is required, and potential savings are possible within the main program block e.g. omitting rounding operations. Faster operation is also possible by calculating the error at the symbol rate, and passing values, via buffering, as required by the TMS32010. The DSP would no longer be required to perform FIR filtering to generate the error term, only coefficient adaptation.

```
; Include required files

changequote({,})
include(defs.i)                    ; basic definitions file
include(FIR.m)
include(DECISION.m)
include(BLKSUM.m)              ; x(t)*e(t) summation
include(BLKLMS.m)              ; lms macro file
include(BLKRST.m)              ; reset x(t)*e(t) products

;-----------------------------------------------------------------

; Program constant definitions

      Ntaps equ   7            ; Number of filter taps
      blockMequ   8            ; Block length
      sftM  equ   16-3         ; 2**shiftM = blockM

; Data memory labels

      ONE   equ   0            ; Location contains x'0001
      TMP   equ   1            ; Temporary Location
      YF    equ   2            ; Filter output
      YD    equ   3            ; Desired input
      ERROR equ   4            ; Error output
      ERR_SUM     equ   5      ; Sum of ERROR*YF product
      ERR_AVE     equ   6      ; Average of ERROR*YF product
      MU2   equ   7            ; Initialised to 2*mu
      DUMMY equ   8            ; Dummy variable
      MIN   equ   9            ; Minimum input value (-1)
      MAX   equ   10           ; Maximum input value (+1)
      REF   equ   11
      TMP2    equ 12
```

```
XB      equ   13           ; Start of input vector
XE      equ   XB+Ntaps     ; End of input vector
HB      equ   XE+1         ; Start of tap weight vector
HE      equ   HB+Ntaps-1   ; End of tap weight vector
ERR_PDB equ HE+1           ; Start of x(t)*e(t) sum.
ERR_PDE     equ   ERR_PDB+Ntaps     ; End of x(t)*e(t) sum

;-----------------------------------------------------------------------

; Reset and interupt vectors

      org   x'0000

      b     pstart           ; Reset vector
      ret                    ; Interrupt vector, return

      org   x'0008

;-----------------------------------------------------------------------

; Data stored in program memory

MU:   data  x'0100           ; Convergence factor, mu
MAXDAT:     data  x'7FFF           ; Input data = 1.0 (approx.)
MINDAT:     data  x'8000           ; Input data = -1.0
REFDAT:     data  x'07FF

;-----------------------------------------------------------------------

; Main program initialisation - read value of mu from memory, and
; initialise tap vectors cf. 'C' program.

pstart:     ldpk   DP0             ; Use data page zero
      sovm                   ; Set accumulator overflow mode

      lack  1                ;
      sacl  ONE              ; Init. ONE to x'0001  ??

; Read value of mu from program memory

      lack  MU
      tblr  TMP              ; TMP <- mu
      zalh  TMP
      sach  MU2,1            ;MU2 <- mu*2  (Shift left)

; Read decision constants from memory

      lack  MINDAT
      tblr  MIN              ;load value of MINDAT into MIN
      lack  MAXDAT
      tblr  MAX              ;load value of MAXDAT into MAX
      lack  REFDAT
      tblr  REF


; Initialise input data and tap weight vectors
```

```
local
      $XC   set   XE
      $HC   set   HE
      zac                     ;Zero last Ntaps words of each vector

rept Ntaps
      sacl  $XC
      sacl  $HC
      $XC   set   $XC-1
      $HC   set   $HC-1
endr

      sacl  XB                ;Zero first word of x()
local

      lac   REF
      sacl  HB+((Ntaps-1)/2)  ; Set center tap to 1

;-----------------------------------------------------------------------

; Continious update of adaptive equaliser taps with Block lms algorithm

update:

;l1:  bioz  p1
;     b     l1
;p1:

;read:in    DUMMY,PA1          ; Read in dummy variable. This
                              ; causes PDR1 to be active for
                              ; use by external circuitry
;     nop

; Wait for two clock cycles and start reading data from dual-port RAM
; Not yet decided if true data should be read in as well. Originally
; planned to run in decision-directed mode
; Repeat this blockM times (lms block length)

rept  blockM

local
      in    XB,PA2            ; Read filter input
$l2:  bioz  $p2
      b     $l2
$p2:
      in    YD,PA3            ; Read desired input (optional)
local

; Calculate the filter output

      FIR( Ntaps , XB , HB )        ; Calculate output

      add   ONE,14            ; Round LSB
      sach  YF,1              ; Save filter output
      lac   YF,4
      sacl  YF
```

```
; Make decision on filter output

      DECISION( YF , YD )

; Calculate error

      zalh  YD                ; Use top half of acc. so that
      subh  YF                ; overflow will be detected
      sach  ERROR             ; ERROR = YD - YT

; Multiply and accumulate YF*ERR product for use in update calculation

      BLKSUM( Ntaps , XB , ERR_PDB , ERROR , MU2  )

; THE FOLLOWING HAVE BEEN INSERTED/ DELETED FOR TESTING
local
      lac   ONE,15            ; set MSB mask
      and   ERROR
      bnz   $neg
$plus:zac
      sub   ERROR
      sacl  ERROR
$neg: out   ERROR,PA1
;     out   YF,PA5
;     out   YD,PA6
local

endr

; End of block summation.

;-------------------------------------------------------------------------

; Average ERR_PD over block length by right shifting by sftM
; where, 2**sftM = blockM

local

      $EPC  set   ERR_PDE

 rept Ntaps
                              ; Right shift to perform division
      zac
      lac   $EPC,sftM         ; Left shift by 16- (block length)
      sach  $EPC              ; Store upper 16 bits in acc

      $EPC  set   $EPC-1
 endr

local

; Update filter weights

      BLKLMS( Ntaps , XB , HB , ERR_PDB , MU2 )

; Reset filter weights
```

```
      BLKRST( Ntaps , ERR_PDB )

;-------------------------------------------------------------------------

; Output updated taps to data memory. Memory address generated by external
; counter circuitry.

local

      $H    set   HB

rept  Ntaps

      out   $H,PA4
      $H    set   $H+1

endr

local

; Read dummy variable from peripheral address line 4. This causes
; PDR4 to be active. External circuit generates addresses and a BIO
; signal to put TMS320 into a 'wait' state. BIO is normally low
; and will go high during coefficient transfer.
; Wait for taps to be transfered from data memory to filter

      b     update
;     in    DUMMY,PA4
;write:    bioz  update                ; Transfer complete
;     b     write                 ; Not finished - wait


; defs.i  ---------------------------------------------------------------

      DP0   equ   0           ; Data Memory Page Pointers
      DP1   equ   1

      PA1   equ   1           ; Port Addresses
      PA2   equ   2
      PA3   equ   3
      PA4   equ   4
      PA5   equ   5
      PA6   equ   6
      PA7   equ   7
      PA8   equ   8

; Macro: 'fir filter' ---------------------------------------------------

define(FIR,{

local

; Rename passed parameters

      $NT   equ   $1          ; Number of taps
      $X    equ   $2          ; Input vector address
      $H    equ   $3          ; Tap weight address
```

```
; Initialise local variables

      $XC   set   $X+$NT-1     ; End of input address
      $HC   set   $H+$NT-1     ; End of tap weights address

; Initialise accumulator

      ltd   $XC                ; T=x(t-(N-1)), x(t-N)=x(t-(N-1))
      zac                      ; Zero sum
      mpy   $HC                ; p=x(t-(N-1))*h(N-1)

; Calculate sum of products

rept $NT-1

      $XC   set   $XC-1
      $HC   set   $HC-1

      ltd   $XC
      mpy   $HC

endr

      apac                     ; Accumulate last product

local})

;Macro:  'decision' ------------------------------------------------------------

define(DECISION,{

local
      $YF   equ   $1
      $YD   equ   $2

      lac   ONE,15       ; Set mask for MSB
      and   $YF                ; Check if MSB is set
      bz    $ldmx              ; If acc. 0, then YF positive

$ldmn:lac   MIN                ; Decision = 1
      b     $ld
$ldmx:lac   MAX                ; Decision = -1
$ld:  sacl  $YD                ; Store decision

local})

; Macro: 'Block lms sum' --------------------------------------------------

define(BLKSUM,{

local

      $N    equ   $1           ; Tap No.
      $X    equ   $2           ; I/p vector start address
      $EP   equ   $3           ; Error-product start address
      $ERR  equ   $4           ; Error address
      $MU2  equ   $5           ; Convergence factor
```

```
      $XC   set   $X+$N
      $EPC  set   $EP+$N


      lt    $ERR
      mpy   $MU2              ; Multiply convergence factor
      pac
      sach  TMP2,1
      lt    TMP2              ; Error constant for update period

rept $N

      mpy   $XC               ; T=x(t)*(e(t)*mu)
      pac
      add   ONE,14      ; Round accumulator
      sach  TMP,1             ; Convert to Qbits notation

      zalh  TMP
      addh  $EPC              ; Add error-product to TMP
      sach    $EPC            ; Save error-product summation

      $XC   set   $XC-1
      $EPC  set   $EPC-1

endr

local))

; Macro: 'block lms update' ------------------------------------------------

define(BLKLMS,(

local

      $N    equ   $1          ; Tap No.
      $X    equ   $2          ; I/p vector start address
      $H    equ   $3          ; Tap vector start address
      $EP   equ   $4          ; Error start address
      $MU2  equ   $5          ; Address of value of 2*mu


; Initialise for tap weight update

      $EPC  set   $EP+$N
      $HC   set   $H+$N-1

; Update (Ntaps) filter weights. h(Ntaps-1) is updated first, h(0) last

rept $N

      zalh  $EPC              ; Load 2*mu*E[e(t)*x(t)]
      addh  $HC               ; Add filter weights to TMP
      sach    $HC             ; Save updated filter weight

      $EPC  set   $EPC-1
      $HC   set   $HC-1
```

```
endr

local})

; Macro: 'Reset block lms sum' ------------------------------------------------

define(BLKRST,{

local

      $N    equ   $1          ; Tap No.
      $EP   equ   $2          ; Error-product start address


      $EPC  set   $EP+$N

      zac                     ; zero accumulator

rept $N

      sacl  $EPC              ; Store 0 from acc. in EP addr.

      $EPC  set   $EPC-1

endr

local})
```

Appendix G

Relevant Publications

Reprints are included from the following publications:

[1] M.C.S. Young, P.M. Grant and C.F.N. Cowan, "Equaliser Timing Considerations for Microwave Digital Radio", *IEEE Proceedings of the 'International Conference on Communications (ICC) 88'*, Philadelphia, USA, pp. 488-492, June 1988.

[2] M.C.S. Young, P.M. Grant and C.F.N. Cowan, "Block LMS Adaptive Equaliser Design for Digital Radio", *Signal Processing IV: Proceedings of the Fourth European Signal Processing Conference*, Grenoble, France, North-Holland, pp. 1349-1352, September 1988.

EQUALISER TIMING CONSIDERATIONS FOR MICROWAVE DIGITAL RADIO DURING DEEP MULTIPATH FADING

M.C.S. Young, P.M. Grant, and C.F.N. Cowan

Department of Electrical Engineering, University of Edinburgh,
King's Buildings, Mayfield Road, Edinburgh. EH9 3JL. Scotland

ABSTRACT

This paper examines a high level 64-QAM modulation system operating in conjunction with digital linear and non-linear equalisers; and digital timing recovery techniques. Results illustrate the difficulty of maintaining acceptable performance during fading. The problem of timing recovery during deep minimum and non-minimum phase fades is discussed, along with means of limiting the tracking ability of a timing circuit during a deep fade.

1. INTRODUCTION

The trend in communication networks towards digital hardware has resulted in the subsequent development of the digital radio relay line-of-sight (LOS) system. The greater bandwidth requirements of digital compared to analogue transmission are motivating development of digital M-ary QAM systems with similar bandwidths to their analogue equivalents. Channel distortion due to multipath fading still remains the principle source of outage for high capacity digital radio. The effects become more pronounced with high level modulation schemes and the accuracy requirements for timing recovery become increasingly severe.

Multipath compensation techniques have concentrated on diversity and equalisation. Many systems use a combination of both, however redundancy is associated with diversity systems. Equalisers implemented at IF usually perform only amplitude compensation, while baseband equalisers are able to perform amplitude and group delay compensation.

This paper presents results on the use of baseband equalisers and timing recovery techniques for microwave digital radio receivers, and in particular examines the effects of sampling phase on equaliser performance.

2. MULTIPATH FADING CHANNELS

Under certain atmospheric conditions, two or more, slightly out of phase, signals may be received. This results in pulse smearing of the received pulses (designed to have Nyquist characteristics), known as inter-symbol interference (ISI). A frequency selective fade follows, where a notch of variable fade depth, sweeps across the transmitted bandwidth, as the multipath delay and amplitude vary. Measurements have indicated fade depths changing by up to 100 dB/s, with a notch sweeping across the bandwidth at rates up to 600 MHz/s [1], however fade rates are slow relative to the symbol rate. Dependant upon the phase delay, the multipath channel impulse response may be of minimum or non-minimum phase type.

Radio system performance in the presence of multipath fading may be predicted from a model characterising the channel under fading conditions. If H(f) is the complex frequency response of a microwave LOS path, H(f) may be written as

$$H(f) = \begin{cases} 1+j0. & \textit{normal conditions} \\ H_c(f) & \textit{during fading} \end{cases} \qquad (1)$$

The most commonly used model for $H_c(f)$ is the three path model developed by Rummler [2] from measurements taken on a 25 MHz bandwidth link centred at 6 GHz:

$$H_c(f) = a.[\,1 - b.e^{-j.2.\pi f.\tau}.e^{j.2.\pi(f_c-f_0).\tau}] \qquad (2)$$

where: a = flat fade margin, b = relative magnitude of received signals, f_0 = notch offset from band-centre, f_c = carrier frequency and τ = relative delay between received signals. The relative fade depth is related to 'b' by: $A = -20.log(1-b)$. A value of b=0 corresponds to an unfaded channel, while b=1.0 corresponds to a fade of infinite notch depth. The channel is minimum phase if b<1.0, and non-minimum phase if b>1.0. The phase transition occurs at b=1.0.

3. DIGITAL RECEIVER STRUCTURE

Figure 1 illustrates the digital radio system examined. Carrier phase and symbol timing are assumed to be recovered in a two stage process, and to simplify simulations, carrier recovery is assumed optimal and

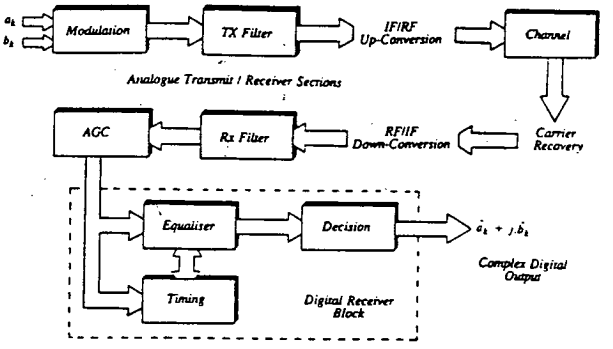

Figure 1. 64-QAM Digital Radio System

0488 CH2538-7/88/0000-0488 $1.00 © 1988 IEEE

calculations are performed at baseband. Some performance improvement may be gained by the joint recovery of the two parameters [3].

For a general M-QAM system the transmitted signal may be written as $c_k = a_k + j.b_k$ where a_k and b_k take values from the set $\{ \pm 1, \pm 3, .., (\pm M^{\frac{1}{2}}-1) \}$, so that adjacent symbols are separated by a distance of 2.0. Transmitted symbols are assumed equi-probable and uncorrelated. Both real and imaginary parts have zero mean and variance, q = (M-1)/3. Higher modulation formats have greater spectral efficiency, at the expense of increased sensitivity to degradations.

The received complex baseband signal envelope may be written as

$$y(t) = \sum_{n=-\infty}^{\infty} (a_n + j.b_n).h_N(t - nT - \tau) + n(t) \quad (3)$$

where τ is the sampling phase offset determined by the timing recovery circuit, and $h_N(t)$ is the combined response of the channel and transmit and receive filters, given by

$$h_N(t) = h_c(t) * h_T(t) * h_R(t) \quad (4)$$

with * denoting convolution. The combined response of the transmit and receive filters is the raised cosine response with roll-off factor, $\beta = \frac{1}{2}$. Noise at the receiver, n(t), is complex and shaped by the receiver filter. At symbol rate sampling, noise is assumed to be white zero-mean Gaussian. Neglecting noise, multipath fading effects a single transmitted pulse is shown in figure 2. Fading varies from unfaded conditions, through an increasingly severe MP fade and phase transition at b=1.0, to a NMP fade.

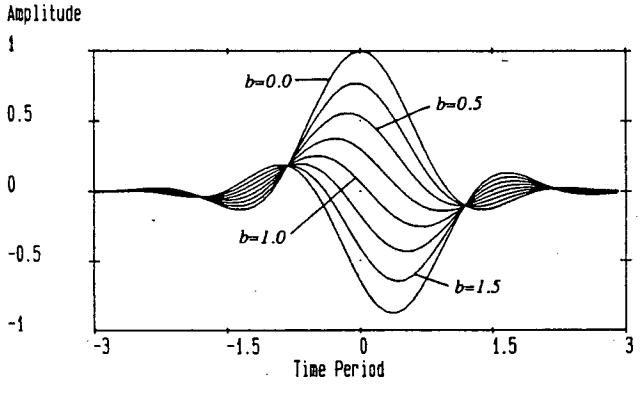

Figure 2. Effect of Multipath Fading on a Single Transmitted Pulse

At the receiver input, the AGC normalises the received signal power. Ideally, unity power is received under all conditions. Performance improvement could obviously be gained by increasing the signal power, however a unity power level provides a performance standard.

Mean square error (MSE), $\zeta(t)$, is the criteria used in assessing equaliser performance. The complex error may be expressed as

$$\epsilon_I(t) = y_I(t) - \hat{y}_I(t) \quad (5)$$
$$\epsilon_Q(t) = y_Q(t) - \hat{y}_Q(t)$$

where $\hat{y}(t)$ is the correct decision, I is the in-phase or real channel, and Q, the quadrature or complex channel. Then

$$\zeta(t) = E[\epsilon^2(t)] = E[\epsilon_I^2(t) + \epsilon_Q^2(t)] \quad (6)$$

Time averaging, over typically 100 samples, is performed to estimate the MSE.

Minimising MSE is used as the basis of one timing recovery method and updating the equaliser tap coefficients, with the least mean squares (LMS) algorithm providing a stochastic gradient approximation to the Wiener-Hopf LMS result [4].

3.1 Adaptive Equalisation

This paper concerns the performance of transversal (linear) and decision- feedback (non-linear) equalisers [5] (Figure 3). Structures are complex, i.e. consist of four real equalisers; the real parts reducing ISI, while cross-coupling is reduced by the imaginary equalisers. Known training sequences are assumed unavailable, and the equaliser must retrain with the LMS algorithm, in decision-directed mode. If an equaliser looses lock while tracking a deepening fade, retaining cannot occur until channel conditions have improved considerably or a 'blind convergence' method is employed [6].

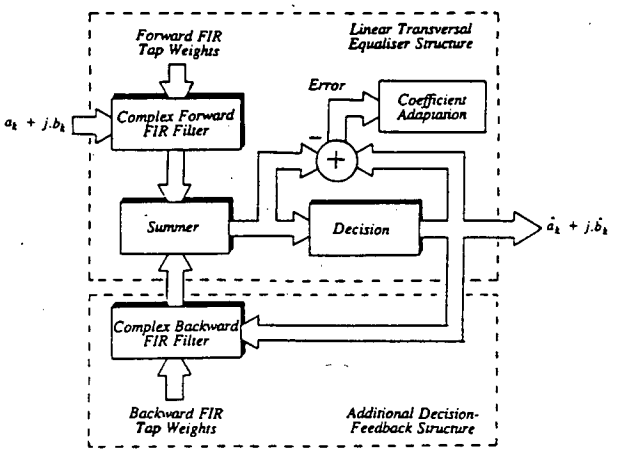

Figure 3. General Equaliser Structure

Tap lengths have been taken as 7 for transversal structures, and 4 forward and 3 feedback for decision-feedback structures. Fractionally spaced equalisers (FSE) are the general equaliser type where the forward tap spacing is less than the symbol period, T. Most commonly this is T/2. While more complex to implement, FSE's may suffer from a finite-precision ill-conditioning problem. This may however be reduced by modifying the MSE cost function with the so-called 'tap-leakage' algorithm [7].

3.2 Timing Recovery

Proper detection of the received data signal requires a clock accurately time aligned with the incoming pulses. The problem of timing recovery in a baseband QAM system is to determine the proper sampling instant, while minimising ISI. The timing recovery circuit attempts to

counter two main problems during multipath fading (1) shifts in the optimum sampling phase due to multipath distortion, and (2) timing jitter. This paper addresses only the former.

Synchronisation of the received signal may be obtained by multiplexing special timing signals onto the transmitted signal, at the expense of extra bandwidth. Timing information is usually extracted directly from the received signal. This paper examines the performance of the following digital timing recovery schemes during fading:

Type A: First reported in [8], the simulation approach taken was suggested in [9]. Type A timing recovery exploits the symmetry of the received pulse, and the timing function may be written

$$U(\tau) = \tfrac{1}{2}.[h_N(\tau+kT) - h_N(\tau-kT)] \qquad (7)$$

When reduced to digital form, type A timing has a very simple implementation, lending itself for use with high data rates.

MMSE: This approach minimises the MSE at the receiver output with respect to timing phase. The timing phase may be tracked by the stochastic gradient algorithm

$$\tau_{k+1} = \tau_k + \alpha.\frac{\partial|\epsilon^2(t)|}{\partial\tau} \qquad (8)$$

The implemented approach is that of [11]. This method offers digital implementation, and is insensitive to carrier phase. A disadvantage is the relatively slow convergence time.

Optimal Timing Recovery: Assuming that the optimal sampling instant occurs at the peak eye opening, the timing phase was calculated by a gradient search routine, converging to the peak eye opening.

Other Timing Recovery Methods: More complex timing recovery techniques do exist, for example, methods based on maximum likelihood estimation theory [3] or where multi-sampling per symbol is available. However the high data rates used in microwave radio limit implementation in most cases. The most common analogue implementation is based on a 'square-law' non-linear device and a band-pass filter tuned to 1/T [11].

4. RESULTS AND DISCUSSION

Figures 4 to 10 illustrate 64-QAM MSE tracking performance with different equaliser/ timing recovery combinations. The graph notation is - *TE:* T-spaced transversal equaliser, *FTE:* T/2 -spaced transversal equaliser, *DFE:* decision-feedback equaliser (T-spaced forward filter) *FDFE:* fractionally spaced decision-feedback equaliser (T/2 -spaced forward filter). All simulation results are for a fade at bandcentre, deepening at 100 dB/s. The unfaded signal to noise ratio (SNR) was set at 50 dB. The results highlight the problems encountered during deep multipath fading with high level M-QAM systems, and a number of points for discussion arise.

Two main equaliser/ timing combinations are apparent (1) symbol spaced systems, with T-spaced equalisers and more precise timing recovery schemes, and (2) systems sampling at greater than the sampling rate, exploiting the timing phase insensitivity of FSE's. Such an approach may employ relatively simple timing recovery e.g. based on equaliser tap values [12].

4.1 Deep MP Fading

Figure 4 illustrates equaliser performance with the timing instant calculated to occur at the peak eye opening, during an MP fade sweeping from ideal conditions to a 40 dB deep fade. A high MSE implies poor equaliser performance and it is apparent that the DFE performance is considerably better than that of linear structures. However, at the transition between MP and NMP fades, DFE performance rapidly diverged (Figure 8). Hysteresis effects would inevitably result in a delay before the equaliser could be retrained (at a considerably shallower fade depth), so ideally the equaliser would remain in lock even if BER performance was unacceptable.

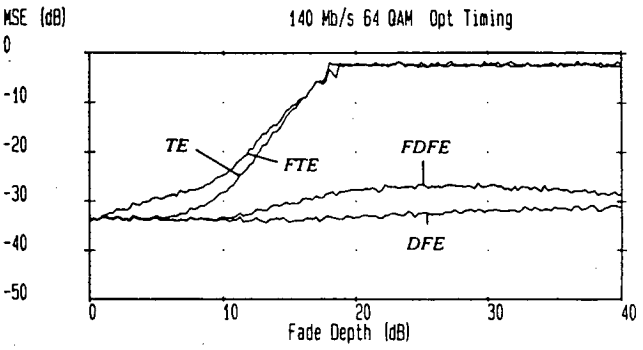

Figure 4. Optimum Equaliser Performance During MP Fading

Figures 5 and 6 show the problem of obtaining the correct timing phase during a deep fade, with 'type A' and 'MMSE' timing tracking a deepening MP fade in conjunction with symbol-spaced transversal and decision-feedback equalisers. While the DFE appears to suffer the greatest performance degradation, the TE performance is already poor. Both timing schemes had poor performance, in particular 'type A' timing which, in this simulation diverged at a 16 dB deep fade.

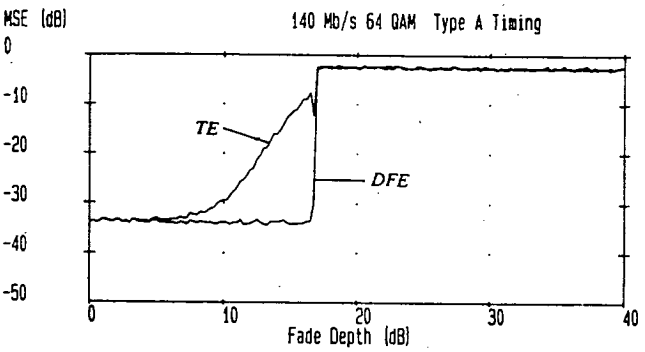

Figure 5. T-Spaced Equaliser Performance with Type A Timing During MP Fading

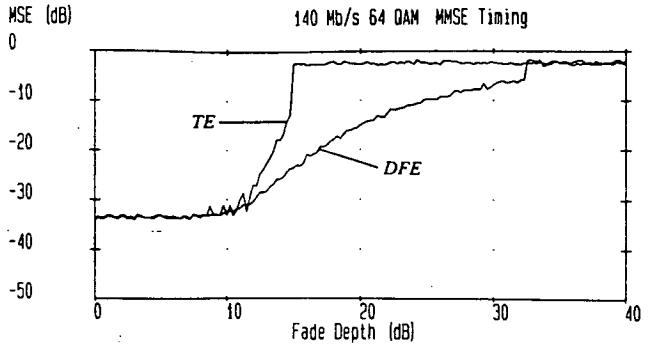

Figure 6. T-Spaced Equaliser Performance with MMSE Timing During MP Fading

4.2 Timing Recovery and Phase Transitions

Referring to figure 2, if a timing recovery circuit attempts to track the peak of the received pulse, then a timing phase shift occurs as the fade deepens. During a deep MP fade, this shift is approximately 180 ° relative to non-fading conditions. While in general rigorous timing requirements apply to symbol sampled systems, particularly transversal equalisers, timing phase sensitivity does tend to increase with higher modulation formats.

Figure 7 indicates the potential of fractionally spaced DFE's with only limited timing. Tracking performance of symbol spaced and T/2 spaced DFE's is compared in the situation where no attempt is made to track the phase shift due to the deepening fade. While unrealistic to hold the timing phase fixed over a period of possibly seconds, figure 7 points to possible performance gain if the timing circuit is sufficiently damped. The problem of the MP/NMP fade transitions remains.

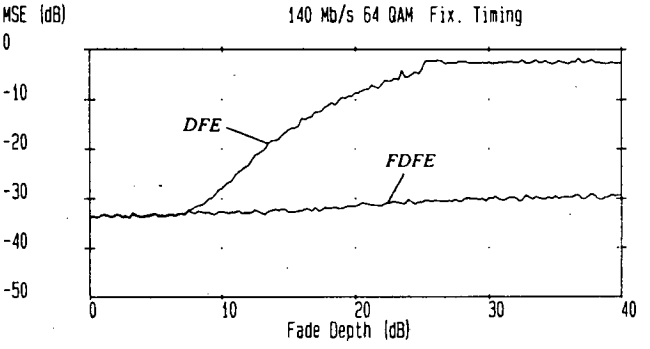

Figure 7. DFE Performance with no Timing Phase Tracking

A phase transition corresponds to a 360 ° phase shift in the optimum timing scheme. Such a non-stationarity is not directly trackable. Two possible solutions to the timing problem are suggested.

Firstly, when adaptively updated, the timing phase for deep MP fading may be tracked with the following algorithm

$$\tau_{k+1} = \beta.(\tau_k + \alpha.U(t,\tau)) \qquad (9)$$

where $U(t,\tau)$ is the timing phase detector algorithm and β a convergence factor, inversely proportional to the fade depth. During a period of very deep fading when a transition may occur, timing would be effectively locked. The timing 'freeze' would be accommodated by stable timing references obtained during non-fading conditions. Timing recovery may be made more accurate, at the expense of tracking speed, by limiting the data used by the circuit with an approach similar to [6].

Secondly, for linear T-spaced equalisers and low-level modulation where the equalisers may have a chance to recover, a 'dual-equaliser' approach may be taken with equalisers configured for MP and NMP type fades. The change between fade types corresponds to the time reversal of tap values in a linear T-spaced equaliser. This is similar to an idea proposed in [13].

If the equaliser could track a fade changing in one direction, say from a MP to a NMP fade, tracking must still occur in the reverse direction, compounding the problem. This problem was addressed in [14].

4.3 NMP Fading

Figure 8 further illustrates the performance of the four equaliser structures as a fade sweeps through a MP to NMP transition. MSE is plotted against relative amplitude for convenience. As expected none recover from the catastrophic channel conditions.

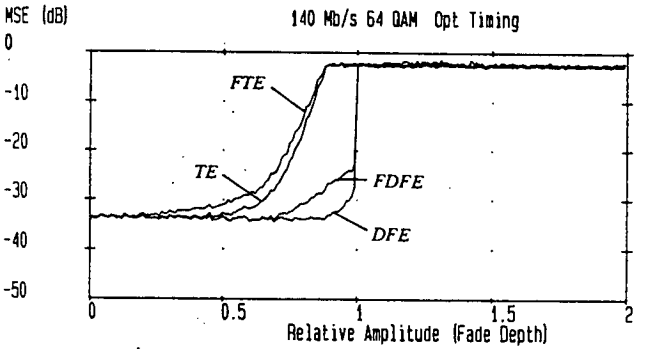

Figure 8. Equaliser Performance Tracking Through a MP/NMP Fade

Figures 4 and 7 suggested the potential of DFE structures for compensating for deep fading. It has been shown that DFE structures are inherently less sensitive to timing phase degradation than linear structures [15]. The

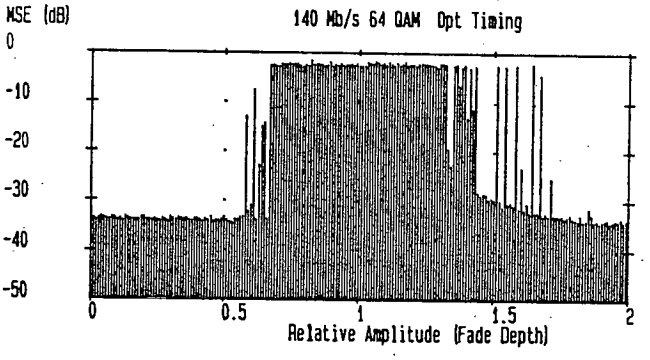

Figure 9. T-Spaced DFE Retraining at Discrete Intervals

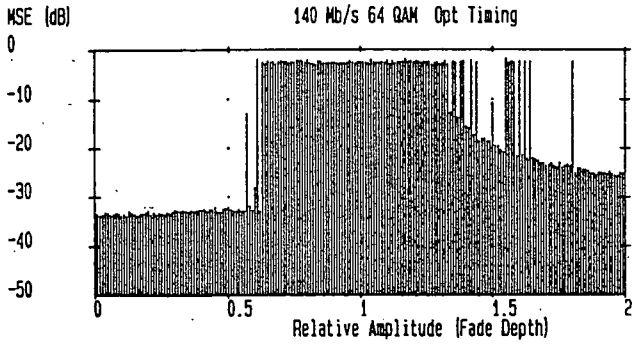

Figure 10. T/2 -Spaced DFE Retraining at Discrete Intervals

problem of MP/NMP fade transitions remains, and the DFE's would require retraining. Figures 9 and 10 plot the MSE as symbol and T/2 spaced DFE's retrain at discrete intervals over the fade depth range. Two points are highlighted here (1) the problem of retraining during non-ideal conditions, and (2) the performance degradation due the NMP fade. Unlike transversal equalisers, DFE performance is not transparent to fade type.

The question must arise over the significance of NMP fading. It has been found [16] that for fades greater than 10 dB, only 0.29% are NMP type, rising to ~ 50% for fades greater than 45 dB. The average fade duration was found to be 1.4 seconds, the shortest 200 ns and the longest 12.4 seconds. The conclusion here being that deployment of high level M-QAM systems must take into account the likelihood of NMP fades on the transmission path.

4.4 Other Compensation Techniques

Results would indicate that equalisation alone will not result in acceptable performance (i.e. bit error rate < 10^{-3}) with a deep band-centred fade. The joint recovery of equaliser taps, timing and carrier phases is one possible solution [17]. Other compensation methods, in particular diversity and forward error correcting coding, when used in conjunction with equalisation, may improve overall performance.

5. CONCLUSIONS

This paper has addressed the problem of equalisation and timing recovery during a multipath fading environment. The severe problems encountered during deep fading with a fade transition have been highlighted, as have the limitations of equalisation/timing recovery schemes. These limitations become increasingly severe with higher level M-QAM systems. Determining the correct timing phase has been shown to be difficult during a very deep fade, and superior performance may be obtained using a fractionally spaced decision-feedback equaliser with less emphasis on exact choice of timing phase. The digital timing circuits considered were found to be unstable during deep fading or tracking through a fade transition, and suggestions for limiting tracking have been discussed.

ACKNOWLEDGEMENTS

The funding of the Science and Engineering Research Council and Ferranti Industrial Electronics, Dalkeith, Edinburgh, is gratefully acknowledged.

REFERENCES

[1] W.D.RUMMLER, 'A New Selective Fading Model: Application to Propagation Data', BSTJ Vol.58, May-June 1979, pp 1037-1071

[2] L.MARTIN, 'Rates of Change of Propagation Medium Transfer Functions during Selective Fadings', Proc. URSI Com. F Symp., Louvain, Belgium, June 1983 (ESA SP-194), pp. 31-35

[3] L.E. FRANKS, 'Carrier and Bit Synchronisation in Data Communications - A Tutorial Review', IEEE Trans. Comms., Vol. COM-28, Aug. 1980, pp. 1107-1121

[4] C.F.N. COWAN, P.M. GRANT, 'Adaptive Filters', Prentice Hall, 1985

[5] S.U.H.QURESHI, 'Adaptive Equalisation', Proc. IEEE, Vol.73, Sept. 1985, pp 1349-1387.

[6] Y.SATO, "A Method of Self-recovering Equalisation for Multilevel Amplitude- Modulation Systems",IEEE Trans. Comms., Vol. COM-23, June 1975, pp. 679-682

[7] R.D.GITLIN et al, 'The Tap-Leakage Algorithm: An Algorithm for the Stable Operation of a Digitally Implemented, Fractionally Spaced Adaptive Equaliser', B.S.T.J., Vol. 61, October 1982, pp 1817-1839

[8] K.H. MUELLER, M.MULLER, 'Timing Recovery Techniques in Digital Synchronous Data Receivers',IEEE Trans. Comms, Vol. COM-24, May 1976, pp. 561-531

[9] M.SHAFI, D.MOORE, 'Further Results on Adaptive Equaliser Improvements for 16-QAM and 64-QAM Digital Radio', IEEE Trans. Comms., Vol. COM-34, Jan. 1986, pp. 59-66

[10] H. SARI et al, 'Minimum Mean Square Error Timing Recovery Schemes for Digital Equalisers', IEEE Trans. Comms., Vol. COM-34, July 1986, pp. 694-702

[11] N.AMITAY,L.J.GREENSTEIN, 'Multipath Outage Performance of Digital Radio Receivers using Finite-Tap Adaptive Equalisers',IEEE Trans. Comms., Vol. COM-32, May 1984, pp 597-608.

[12] G. UNGERBOECK, 'Fractional Tap-Spacing Equaliser and Consequences for Clock Recovery in Data Modems', IEEE Trans. Comms., Vol COM-24, August 1976, pp. 856-864

[13] H. SARI, 'Baseband Equaliser Performance in the Presence of Selective Fading', IEEE GLOBECOM 83, San Diego, pp 1.1.1-1.1.7

[14] A.LECLERT, P.VANDAMME, 'Decision Feedback Equalisation of Dispersive Radio Channels', IEEE Trans. Comms., Vol. COM-33, July 1985, pp 676-683.

[15] J.SALZ, 'On Mean-Square Decision-Feedback Equalisation and Timing Phase', IEEE Trans. Comms. Vol. COM-25, June 1975, pp. 1471-1476

[16] E.W. ALLAN, 'Digital Radio Propagation - Test Long Term and Nonminimum Phase', ICC 87, Seattle, 1987, pp. 23.3.1-23.3.6

[17] G.R. McMILLAN et al, 'Simultaneous Adaptive Equalisation of Carrier Phase, Symbol Timing and Data for a 49-QPRS DFE Radio Receiver', IEEE Trans. Comms., Vol. COM-32, April 1984, pp.429-443

SIGNAL PROCESSING IV: Theories and Applications
J.L. Lacoume, A. Chehikian, N. Martin, and J. Malbos (Editors)
Elsevier Science Publishers B.V. (North-Holland)

BLOCK LMS ADAPTIVE EQUALISER DESIGN FOR DIGITAL RADIO

M.C.S. Young, P.M. Grant, and C.F.N. Cowan

Department of Electrical Engineering, University of Edinburgh,
King's Buildings, Mayfield Road, Edinburgh. EH9 3JL. Scotland

ABSTRACT

The wide-sense stationarity of a microwave communications channel during multipath fading is exploited with an approach allowing a linear equaliser to be adaptively updated with a TMS32010 digital signal processor (DSP), at less than the symbol rate. The high data rates involved with microwave transmission limit equaliser adaptation techniques, most commonly to the LMS algorithm. The hardware for the DSP board has been extended to evaluate the potential use of the Block LMS algorithm, and examples of convergence are given.

1. INTRODUCTION

Many radio systems experience performance degradation due to multipath fading, where multiple replicas of the transmitted signal are captured at the receiver. This paper addresses one such system: digital microwave line-of-sight (LOS) links. Such a medium is interesting for two reasons: (1) the channel characteristics change slowly during fading, and may be considered wide-sense stationary over a limited time period, and (2) the high data rates involved (8-140 Mb/s) preclude complex compensation techniques.

With the trend in communications networks towards digital technology, come additional problems due to multipath fading. Digital microwave systems are not only more sensitive to multipath fading than their analogue predecessors, but modern digital radios are designed using increasingly complex signaling sets. Systems have been implemented with 256 and 1024 phase/amplitude states (256/1024 QAM).

One of the most effective measures for reducing distortion due to multipath, is adaptive equalisation. If equaliser adaptation is performed at the transmitted data rate, the resulting structure may be complex and difficult to implement. This paper presents a novel and relatively simple means of equaliser adaptation, employing 'off-line' processing to exploit the 'stationarity' of the channel during fading.

2. FADING CHANNEL MODEL

Extensive measurements of microwave LOS links have resulted in a number of models characterising fading channels. The most commonly used, and the one used here, was proposed by Rummler [1]. This model introduces a ripple distortion or notch into the channel passband, with the notch period inversely related to the differential path delay. The depth and spacing of the notch change as the multipath parameters change over time. Attenuation due to the notch is generally known as the fade depth. The power transfer function for a 20 dB deep band-centred fade is shown in figure (1).

For analysis, a digital communications channel may be represented by a discrete-time model [2]. The cascade of transmitter filter, channel, matched filter, sampler, and discrete-time noise whitening filter, may be modelled by a FIR filter of sufficient length to span the overall impulse response. White Gaussian noise is added to the filter output. Under ideal conditions, the transmitted pulse will typically have raised cosine Nyquist characteristics; and the optimum decision instants will be uncorrupted by past or future symbols. Multipath fading introduces pulse smearing, producing inter-symbol interference (ISI) between successive pulses.

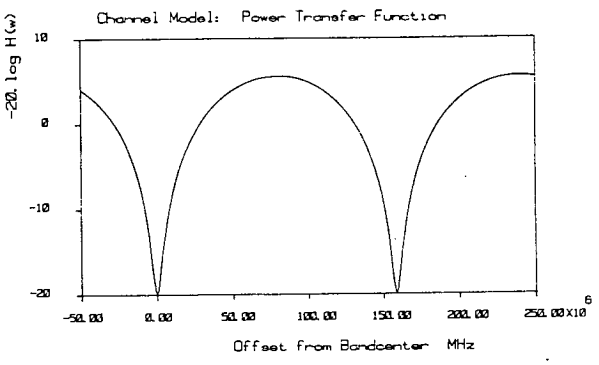

Figure 1. Channel Model: Power Transfer Function

3. ADAPTIVE EQUALISATION

An adaptive equaliser is an adaptive filter performing inverse system modelling. The adaptive equaliser attempts to reconstruct the transmitted sequence before a final decision is made at the receiver output. The simplest of the many adaptive equaliser structures and the one considered here, is the transversal equaliser. This is essentially an adaptively updated FIR filter of order N-1, where N current and past data samples are linearly combined to produce the output. Thus

$$\hat{y}(n) = \sum_{k=o}^{N-1} h_k . x(n-k) \qquad (3.1)$$

where $h_k(n)$ are the equaliser tap weights (impulse response) and x(n) the data sequence. This finite sum of products may be written more compactly as a vector inner product

$$\hat{y}(n) = \mathbf{h}^T . \mathbf{x}(n) \qquad (3.2)$$

where h is a column vector containing the N elements of the equaliser impulse response, and $\mathbf{x}(n)$ is a column vector containing the last N elements of the input sequence x(n)

The optimum FIR filter is one minimising a given cost function, usually mean square error (MSE), where the error is the difference between known and estimated data. The optimum impulse response $\mathbf{h}_{opt}$ minimising the MSE is given by the solution to the classical Wiener filter

$$\mathbf{h}_{opt} = \mathbf{R}^{-1}\mathbf{P} \qquad (3.3)$$

where **R** and **P** are the auto-correlation and cross-correlation matrices, respectively.

In practice, data sequences are known, rather than the second order statistics **R** and **P** , so requiring an adaptive algorithm to converge to and track the optimum impulse response. The most commonly used means of adaptation used in high data rate radio systems is the least mean squares (LMS) algorithm. This, and the block LMS algorithm, are discussed in the next section.

With certain radio systems, a known data sequence is available during the training period. Microwave systems are required to retrain and adapt in a decision-directed manner. The error signal is now derived from the (not necessarily correct) filter estimate. At the start of retraining, the centre tap is set to 1.0 and the remainder reset to 0.0.
The decision-directed equaliser structure examined in this paper is shown in figure 2.

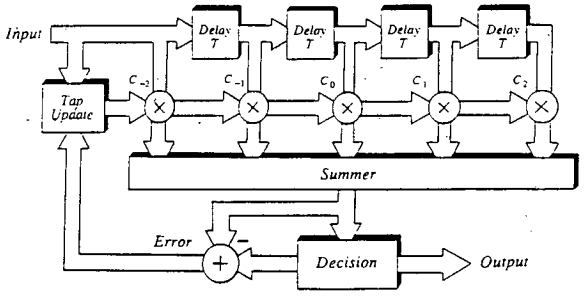

Figure 2. Decision-Directed Linear Equaliser Structure

Other adaptive equaliser structures and multipath compensation techniques are in use or under investigation. This area can be pursued further in the papers by Qureshi [3] on adaptive equalisers, and Stein [4] on general fading issues.

4. THE BLOCK LMS ALGORITHM

Adaptation with the BLMS algorithm may be implemented in both time and frequency domains. For long filter lengths, a major motivation behind frequency domain implementation is the potential complexity reduction through using fast convolution techniques [5]. With the hardware approach taken, little additional hardware is required to convert from LMS to BLMS systems. The relatively short filter length involved makes only a time-domain realisation practical.

The LMS algorithm may be considered to be a stochastic gradient search solution to the Wiener FIR filter. It has been shown that where the Wiener filter is extended to the block input case, then the block mean square error is equal to the conventional mean square error, if inputs are stationary [6]. Thus the optimum set of filter weights $\mathbf{W}^*$, for the block Wiener filter is the same as the Wiener filter i.e.

$$\mathbf{W}^* = \mathbf{R}^{*-1}\mathbf{P}^* \qquad (4.1)$$

where $\mathbf{R}^*$ and $\mathbf{P}^*$ are the block auto-correlation and cross-correlation matrices, respectively. The Wiener filter solution may thus be considered a special case of the block Wiener filtering problem.

Analogous to the relationship between Wiener filtering and block Wiener filtering, the LMS algorithm may be considered to be a special case of the BLMS algorithm (block length=1). Tap adaptation with the BLMS algorithm may be written as

$$h_k(n+M+1) \qquad (4.2)$$
$$= h_k(n) + 2.\beta_M . \frac{1}{M} \sum_{m=0}^{M-1} e(n+M-m).x(n+M-m-k)$$

where h_k is the k^{th} filter coefficient, x(n) is the input signal, e(n) is the error between the input and the desired signals, and β_M is the convergence factor. When M=1, the BLMS algorithm reduces to the conventional LMS algorithm

$$h_k(n+1) = h_k(n) + 2.\beta_1 . e(n).y(n-k) \qquad (4.3)$$

BLMS convergence may be ensured if [6]

$$0 \le \beta_M < \frac{M}{(M+N+1)} \qquad (4.4)$$

The BLMS algorithm is valid for any block length M, greater than or equal to one. Where M is greater than N, tap adaptation is performed with more information than is used by the FIR filter. For M less than N, the filter length is longer than the input block also implying inefficiency.

A block approach may also be advantageous for finite precision implementations. Potentially this may offer a saving of 2-3 bits in arithmetic accuracy requirements when compared with the LMS algorithm [7].

5. DEMONSTRATION SYSTEM

A system has been constructed to examine the performance of the BLMS algorithm, for use in conjunction with a high data rate baseband equaliser. Figure 3. illustrates the hardware design, where the equaliser is sub-divided into FIR filter and tap adaptation sections. Initially, the system has been designed for the real channel of an 8 Mb/s QPSK receiver. A full equaliser implementation would require duplication of the hardware design.

The FIR design is based on a cascade of TRW TMC2243 I.C.'s, with an 8-bit two's complement input. Tap adaptation is performed 'off-line' by a TMS32010 digital signal processor (DSP). Buffering is accomplished with RAM's temporarily storing data and coefficients. Finite precision corruption of the coefficient weights is minimised by exploiting the full 16-bit word-length of the DSP for storage. The stationary discrete-time model of the

fading channel is implemented by another TMC2243. Computer simulations of the fading channel calculate the channel coefficients and these may be easily set through a switch-bank.

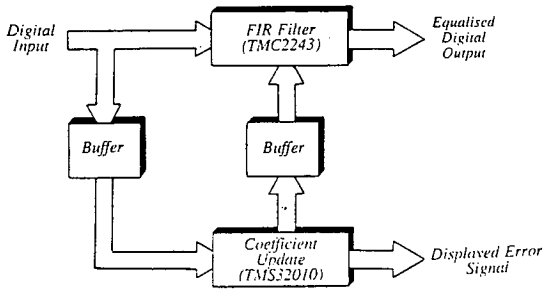

Figure 3. Equaliser Hardware: Block Diagram

An indication of BLMS efficiency on the TMS32010, may be obtained by considering the DSP instruction cycle count over a block length of 8. The BLMS requires a total of 776 cycles, while LMS adaptation would have required 1208 cycles. This is important - if adaptation is too slow, the channel may no longer be considered stationary.

Some initial results from a storage scope, illustrate convergence of the TMS32010 error signal magnitude under different fading conditions. Figures 4 to 6 illustrate convergence with the LMS (block length = 1) and BLMS (block length = 8) algorithms for (1) ideal conditions, (2) a relatively shallow 5dB fade, and (3) a moderately deep 15 dB deep fade. Figures 4 to 6 represent the error magnitude on a linear scale. Figure 7 is included to make a comparison against a logarithmic scale. This is the instantaneous MSE output from a TMS32010 simulator under the same channel conditions as figure 5, with simulated 8-bit ADC and DAC's. In an attempt to ensure similar convergence rates, the convergence factor, β , was set according to

$$\beta_M = M.\beta_1 \qquad (5.1)$$

Values were taken as 0.1875 and 0.0234 for the BLMS and LMS algorithms, respectively. Scope settings are 1V/cm and 1mS/cm. Under ideal conditions, the error signal converges from a maximum value (0 dB) to approximately the noise floor (-36 dB). Convergence during the 5 dB fade was close to the ideal, however as the fade deepens, the mean value and the variance of the error signal increase. Under all channel conditions, performance between BLMS and LMS algorithms was very similar, with the BLMS algorithm offering marginally better error variance performance.

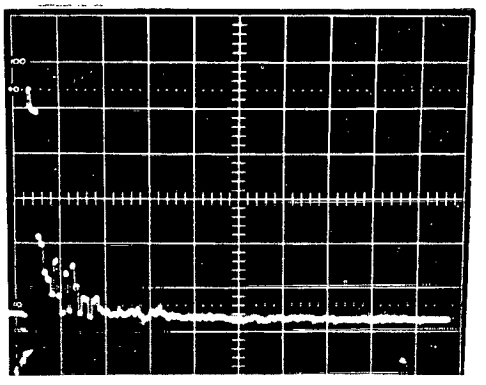

Figure 4(a). LMS Convergence During Ideal Conditions

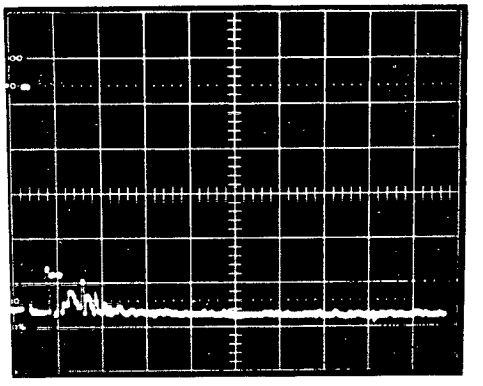

Figure 4(b). BLMS Convergence During Ideal Conditions

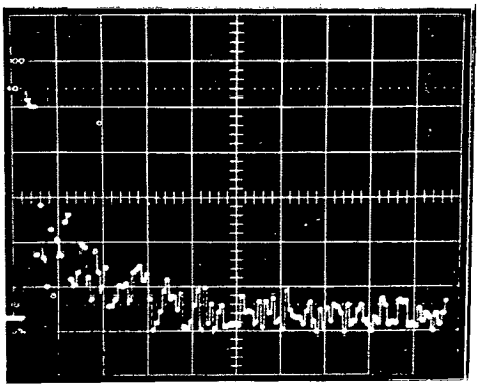

Figure 5(a). LMS Convergence During 5 dB Fade

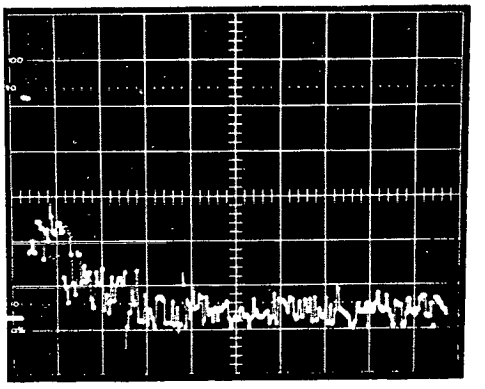

Figure 5(b). BLMS Convergence During 5 dB Fade

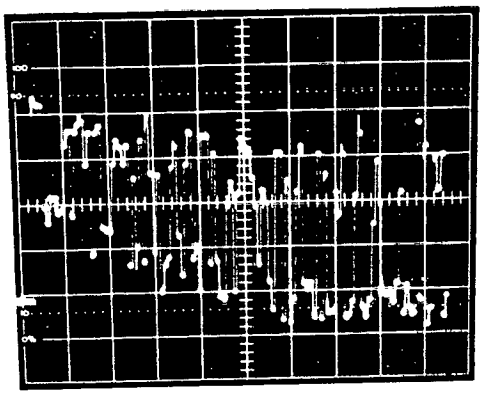

Figure 6(a). LMS Convergence During 15 dB Fade

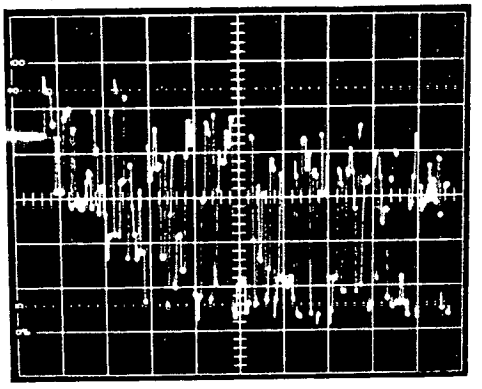

Figure 6(b). BLMS Convergence During 15 dB Fade

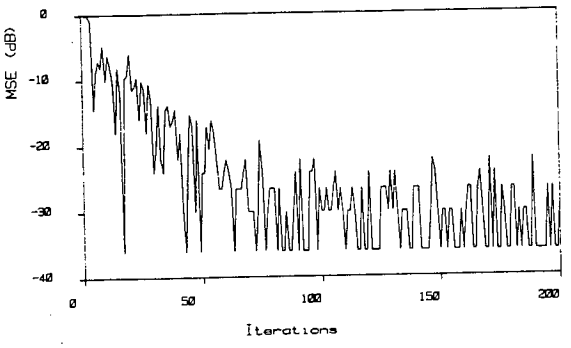

Figure 7(a). TMS32010 Simulator: LMS Convergence During 5 dB Fade

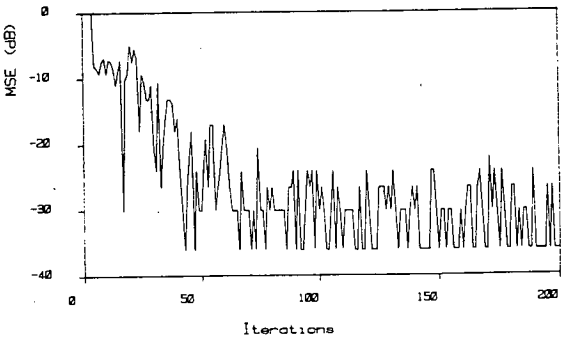

Figure 7(b). TMS32010 Simulator: BLMS Convergence During 5 dB Fade

6. DISCUSSION AND CONCLUSIONS

A literature survey reveals little information on BLMS algorithm implementations. Use of the BLMS algorithm is system dependent. The efficiency of the multiply-accumulate (MAC) instruction cycle on the TMS32010 results in a simple implementation, with some overall complexity reduction. A hardwired approach would require an additional MAC block to perform time averaging. Given the use of finite arithmetic, it might be expected that a BLMS approach would have some performance advantage over the LMS algorithm. While this was not great with the results presented here, it must be remembered that relatively high accuracy is available with the TMS32010 (16 bit data words, 32 bit ALU). Performance gains may only be obvious on (faster) fully hardwired systems, where less accuracy is available (e.g. 8-10 bits).

This work may be extended in a number of ways. Given the lack of BLMS literature, further finite precision simulations would be useful in assessing performance. The hardware may be further developed for a full QPSK system, higher modulation levels, and increased data rates. Faster adaptation would be possible with newer DSP's e.g. TMS320C25 or a chip count reduction with the TMS320E15. The channel simulator may be further developed to deal with slowly changing fades, employing EPROM's and additional address/counter circuitry.

To conclude, a relatively simple means of equaliser adaptation with a DSP has been discussed, and the BLMS algorithm assessed to be a useful alternative for equaliser adaptation with the LMS algorithm.

ACKNOWLEDGEMENTS

The funding of the Science and Engineering Research Council and Ferranti Industrial Electronics, Dalkeith, Edinburgh, is gratefully acknowledged.

REFERENCES

[1] W. RUMMLER, "Time and Frequency Domain Representation of Multipath Fading on Line-of-Sight Microwave paths", Bell Sys. Tech. J., Vol. 59, pp 763-796, May-June 1980

[2] J.G. PROAKIS, "Digital Communications", McGraw-Hill, 1983

[3] S.U.H. QURESHI, "Adaptive Equalisation", Proc. IEEE, Vol. 73, pp. 1349-1387, Sept. 1985

[4] S. STEIN, "Fading Channel Issues in System Engineering", IEEE Trans. Comms., Vol. SAC-5, pp. 68-89, Feb. 1987

[5] G. PANDA et al, "A Self-Orthogonalizing Efficient Block Adaptive Filter", IEEE Trans. ASSP, Vol. ASSP-34,pp. 1573-1582, Dec. 1986

[6] G.A. CLARK et al, "Block Implementation of Adaptive Digital Filters", IEEE Trans. ASSP, Vol. ASSP-29, pp. 744-752, June 1981

[7] G. PANDA et al, "Assessment of Finite Precision Limitations in LMS and BLMS Adaptive Algorithms", Proc. ICASSP 1987, Dallas, pp. 4.10.1-4.10.4